uOttawa

L'Université canadienne
Canada's university

FACULTÉ DES ÉTUDES SUPÉRIEURES ET POSTOCTORALES

uOttawa

L'Université canadienne
Canada's university

FACULTY OF GRADUATE AND POSDOCTORAL STUDIES

Guohua Qi

AUTEUR DE LA THÈSE / AUTHOR OF THESIS

Ph.D. (Electrical Engineering)

GRADE / DEGREE

School of Information Technology and Engineering

FACULTÉ, ÉCOLE, DÉPARTEMENT / FACULTY, SCHOOL, DEPARTMENT

Optical Generation and Distribution of Millimeter-Wave Signals and Optical Up-Conversion for Radio-Over-Fiber Applications

TITRE DE LA THÈSE / TITLE OF THESIS

Jianping Yao

DIRECTEUR (DIRECTRICE) DE LA THÈSE / THESIS SUPERVISOR

CO-DIRECTEUR (CO-DIRECTRICE) DE LA THÈSE / THESIS CO-SUPERVISOR

EXAMINATEURS (EXAMINATRICES) DE LA THÈSE / THESIS EXAMINERS

Xavier Fernando

Tet H. Yeap

Jacques Albert

Mustapha C.E. Yagoub

Gary W. Slater

Le Doyen de la Faculté des études supérieures et postdoctorales / Dean of the Faculty of Graduate and Postdoctoral Studies

Optical Generation and Distribution of Millimeter-Wave Signals and Optical Up-Conversion for Radio-Over-Fiber Applications

By

Guohua Qi

A thesis submitted in partial fulfillment of the
requirements for the degree of

Doctor of Philosophy

Ottawa-Carleton Institute of Electrical and Computer Engineering
School of Information Technology and Engineering
Faculty of Engineering
University of Ottawa

January 2008

Your file Votre référence
ISBN: 978-0-494-48417-3
Our file Notre référence
ISBN: 978-0-494-48417-3

ABSTRACT

This thesis presents a theoretical and experimental study of two techniques used in radio-over-fiber applications. The first technique is concerned with the optical generation and distribution of microwave and millimeter-wave signals. The second is concerned with the optical up-conversion of an electrical subcarrier signal from a low-frequency band to the millimeter-wave band.

The thesis consists of two parts: In the first, three approaches to generating frequency-tunable, high spectral-purity microwave and millimeter-wave signals in the optical domain are proposed and experimentally demonstrated. These approaches are based on external optical modulation using an optical intensity modulator or an optical phase modulator. The key advantage of these approaches is that high spectral purity, frequency-tunable microwave and millimeter-wave signals can be generated using a simple configuration with no tunable optical filter. In addition, optical carrier recovery at a radio-over-fiber base station is also experimentally demonstrated. A detailed theoretical study on the spectral purity of the optically generated and distributed microwave or millimeter-wave signals based on external optical modulation techniques is also conducted. These theoretical results are verified by experiments.

In the second part of the thesis, an approach to optically up-converting an electrical subcarrier signal from a low-frequency band to a millimeter-wave band is proposed. In this approach, two phase-correlated optical waves, which are separated by a frequency difference in the millimeter-wave frequency band, are directly modulated by an electrical subcarrier using an optical intensity modulator. Theoretical analysis shows that the information carried by the low-frequency electrical subcarrier is up-converted to a subcarrier in the millimeter-wave band. Transmission of BPSK and QPSK signals is conducted to validate the proposed approach. In addition, nonlinearities caused by the optical intensity modulator in realizing optical up-conversion are analyzed and discussed. Harmonic distortions and inter-modulation distortions are also analyzed. One-tone and two-tone measurements are performed to validate the analysis.

ACKNOWLEDGMENTS

First, I owe a deep sense of gratitude to my Ph.D. supervisor, Professor Jianping Yao. He has been a source of constant motivation, encouragement and enthusiasm. I thank him for providing strong support and valuable directions throughout this work and my Ph.D. program.

I also own a deep sense of gratitude to my Ph.D. co-supervisor, Joe Seregelyi of the Advanced Radio Systems, Communications Research Centre, Canada, for his support and generous help while I stayed at the Communications Research Centre to conduct my Ph.D. research and through my Ph.D. program.

I would like to thank my colleague researchers, Stéphane Paquet, Claude Bélisle, John Oldham and David Barlow of the Advanced Radio Systems, Communications Research Centre, Canada, for the fruitful collaborations.

I would like to thank Dr. Fei Zeng for his valuable suggestions and generous help when he was a Ph.D. student at the Microwave Photonics Research Laboratory, School of Information Technology and Engineering, University of Ottawa.

I would like to thank Dr. Xiangfei Chen, Dr. Hao Chi, and Dr. Yitang Dai of the Microwave Photonics Research Laboratory, School of Information Technology and Engineering, University of Ottawa, for their help and support.

I would also like to thank my colleague students, Jun Wang, Sebastien Blais, and Quan Li for their help and support.

Lastly, I will thank my wife Jie Chen and my daughter Xin Qi for their understanding, support, and encouragement.

TABLE OF CONTENTS

CHAPTER 1
INTRODUCTION

In this Chapter, an overview on radio-over-fiber technology is performed. First, the concept of radio-over-fiber is presented. Then, the necessity of radio-over-fiber systems for wireless communications systems is detailed. This begins with an introduction to the cost and performance factors of a wireless communication system. Then the advantages of optical fiber as a transmission medium are introduced. A discussion on the use of radio-over-fiber systems to improve performance and reduce the cost of wireless communication systems is presented. A few radio-over-fiber system architectures are also reviewed.

Finally, the objectives of the thesis are defined, the major contributions are summarized, and the organization of this thesis is outlined.

1.1 Concept of Radio-over-fiber systems

Broadly speaking, a radio-over-fiber system is a means of information transportation with the characteristic of transmitting radio-frequency signals over an optical fiber. The goal of distributing radio signals over fiber in an information transportation system is to improve the ratio of performance over cost. Numerous techniques have been proposed in the past for achieving this goal.

In this sense, conventional cable television (CATV) over fiber systems are radio-over-fiber systems since the frequency of analog CATV falls in the traditional radio frequency band. However, people usually do not consider a CATV-over-fiber system as a radio-over-fiber system because, first, the distribution of CATV signals in an optical fiber is a unilateral broadcast, not a bi-directional communication. Second, a CATV-over-fiber system is fully wire connected, i.e., the CATV signals are confined in the optical fiber and the coaxial cable from

the source to the destination. There is no radio radiation and reception in a CATV-over-fiber system.

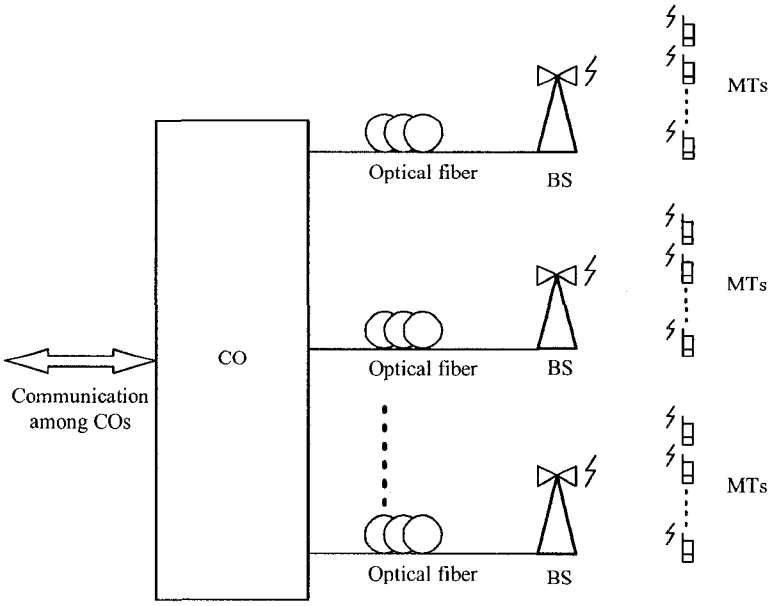

(a)

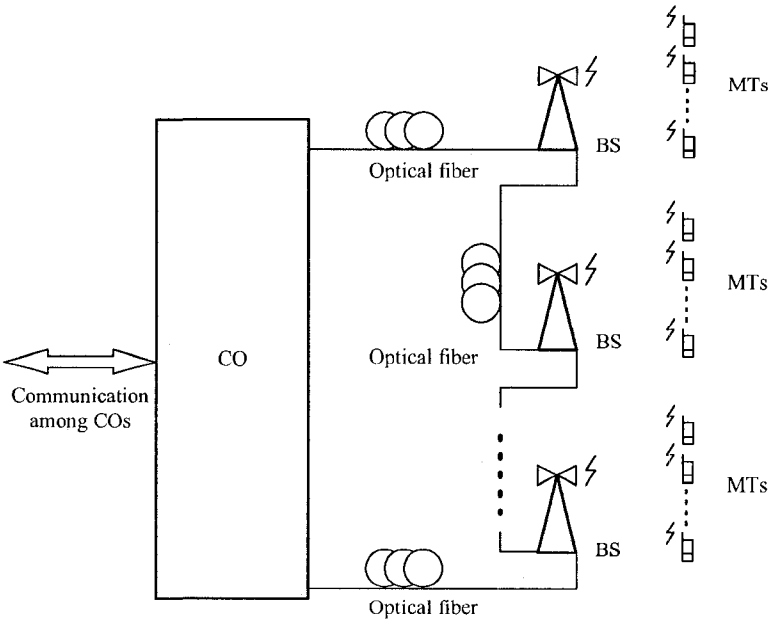

(b)

Fig. 1.1. Schematic diagrams of two basic radio-over-fiber configurations. (a) Radio-over-fiber system in star structure. (b) Radio-over-fiber system in loop structure. (CO: central office, BS: base station, MT: mobile terminal)

The generally accepted concept of a radio-over-fiber system is a communication system in which radio frequency signals are transmitted over optical fiber to enhance the performance of a wireless communication system. Alternatively, a radio-over-fiber system is a communication network that consists of high-frequency analog optical fiber communication systems and wireless communication systems.

Fig. 1.1 shows the schematic diagrams of two basic radio-over-fiber configurations with a star structure and a ring structure. An important characteristic in these two radio-over-fiber configurations is that RF subcarriers are modulated on an optical carrier for distribution over an optical fiber. The baseband data signals are modulated on the subcarriers. A key feature of this arrangement is that the subcarrier signals can be easily recovered by direct photo-detection at base stations. The recovered subcarrier signals are ready to feed an antenna to be radiated to free space after appropriate amplification.

In the remainder of this thesis, this generally accepted concept is adopted.

1.2 Necessity of radio-over-fiber systems

A discussion on the necessity of radio-over-fiber systems has to involve both wireless communication systems and optical fiber technology. In the former, wireless communication systems have attracted significant attention in the communications field due to the fact that they offer convenient connectivity amongst users for transmitting and receiving voice, video and data signals. This attention has lead to an explosive development in wireless communication systems, with a continuous requirement for improved performance and cost reduction. This is the fundamental reason for the deployment of radio-over-fiber systems in wireless communications systems.

On the optical side, in the past decade optical fiber technology has matured in the development of digital optical communication systems, primarily for long-haul applications. This is the basic physical foundation making radio-over-fiber systems possible.

The motivation for building radio-over-fiber systems is to improve the performance and lower the cost of wireless communication systems by making use of optical fiber technology. In the

following Subsections, the necessity of radio-over-fiber is discussed. Specifically, in Subsection 1.2.1, the performance factors and the costs of a wireless communication system are introduced. In Subsection 1.2.2, a comparison is made between the optical fiber technology and the conventional transmission lines. In Subsection 1.2.3, how a radio-over-fiber system helps improve the performance and reduce the cost of a wireless communication system is presented. In Subsection 1.2.4, a few radio-over-fiber system configurations are reviewed.

1.2.1 Performance factors and costs of wireless communication systems

A typical wireless communication system consists of a large number of widely distributed base stations and numerous mobile terminals. All base stations are connected by transmission lines, and all mobile terminals are connected to a base station wirelessly. The performance of a wireless communication system can be evaluated by their capability of supporting a reliable and broadband wireless connectivity between a base station and a mobile terminal.

For a wireless communication system, this capability can be evaluated by the coverage and the capacity of the system. According to the propagation property of an electromagnetic wave, a low-frequency radio signal covers a larger area than a high-frequency radio signal, provided that the same transmitted power level and receiver sensitivity are used. This is given by the Friis transmission equation [1]

$$P_R = P_T G_T G_R \left(\frac{\lambda}{4\pi R}\right)^2$$

$$= P_T G_T G_R \left(\frac{c}{4\pi R}\right)^2 \left(\frac{1}{f}\right)^2, \qquad (1.1)$$

where P_T is the transmitted power from the transmitter, P_R is the power received at the receiver, G_T is the gain of the transmitting antenna, G_R is the gain of the receiving antenna, λ is the wavelength of the electromagnetic wave in free space, R is the distance between transmitting and receiving antennas, c is the light speed in free space, and f is the frequency of the electromagnetic wave. Signal power attenuation is proportional to the inverse of the square of the signal frequency. This means that the use of a low frequency will improve the coverage and

the system connectivity of a wireless communication system if, like in rural areas, the system capacity is not a concern. However, in an area with high population density, this is not true since the available effective electrical bandwidth in a wireless communication system is usually a few to a few tens percentage of the carrier frequency. This is due to the bandwidth limitations of the associated radio frequency circuits and antennas for efficient power transmission. The available bandwidth of a wireless communication system is the physical foundation of the system capacity. If low-frequency radio frequency signals are deployed, narrow bandwidth is obtained which, in turn, means a reduced system capacity. This means that lowering the carrier frequency to cover a large area does not always guarantee an improvement of connectivity in highly populated areas. Therefore, to increase the system capacity and the connectivity, one must use a higher carrier frequency with a smaller area of coverage. To cover a larger area, more base stations are needed. It is commonly believed that the use of a higher carrier frequency is the most efficient solution to improve the connectivity of a wireless communication system.

It is a key requirement of future wireless communication systems to support broadband wireless connectivity, such as mobile interactive multimedia connectivity between a base station and a mobile terminal. This capability requires that future wireless communication systems must have abundant bandwidth. As discussed before, the available bandwidth of a radio frequency signal is proportional to the carrier frequency. Therefore, increasing the carrier frequency of a radio frequency signal is an efficient way to increase the capacity of a future wireless communication system, which further allows the system to further support broadband wireless connectivity.

An increase in the carrier frequency of a wireless communication system is an effective solution to improve system performance; however, wireless spectrum below 18 GHz is very crowded and it appears that there is little possibility of obtaining new licensed bands in this range. Therefore, the use of higher-frequency bands, up to the millimeter-wave band, is an obvious choice and a key measure that will greatly improve the performance of future wireless communication systems.

In addition to the system performance, the costs of a wireless communication system should also be investigated. Only a reasonably priced and high-performance wireless communication

system can be put into service. The costs can be classified as a one-time equipment cost and a daily operating cost and minimizing both of these is crucial for the practical application of these systems.

In addition, the transmission of millimeter-wave signals in free space not only experiences large transmission loss, as shown in Friis transmission equation in (1.1), but also suffers from large absorption loss caused by water molecules in the air. On one hand, this characteristic helps to limit a wide effective bandwidth to a small area. In this way the capacity of a millimeter-wave wireless communication system is increased. In addition, attenuation reduces cross-talk with adjacent cells allowing more efficient spectrum reuse. However, this also requires the communication system to have more millimeter-wave base stations, which will increase cost. New technology to reduce these costs is required.

In the next Subsections, we will discuss how the costs of a wireless communication system can be reduced by applying optical fiber technology to wireless communications.

1.2.2 Advantages of optical fiber as a transmission medium

In the previous Subsection, the performance and costs of a wireless communication system were discussed. A solution to improve performance and reduce costs is to incorporate radio-over-fiber technology into a wireless communication system, in which the base stations are connected through optical fibers. In this Subsection, conventional electrical transmission lines are reviewed and compared with optical fibers. The advantages of using optical fiber for signal transmission are discussed.

Many electrical transmission lines have been widely used in the last few decades for communications Among them, only parallel lines and coaxial cables can operate over a relatively long distance. Parallel lines work well at low frequency from a few kHz to a few MHz. A typical application of parallel lines is in a telephony system where they are used to distribute voice signals. Parallel lines are not appropriate to work at high frequency bands because, when the signal frequency increases, radiation effects become prominent and the attenuation of the lines increases. Coaxial cables have been widely used for signal distribution when the signal frequency is in the low GHz range. Typical applications of coaxial cables

include the distribution of CATV signals to residential areas, and the transmission of intermediate frequency (IF) signals in conventional wireless communication systems. The attenuation of a coaxial cable increases when the signal frequency increases due to skin effect in the conductors. Even when a coaxial cable is operating at a frequency below 1 GHz, its attenuation is still high and cannot be neglected. This is why there are many in-line amplifiers in a CATV distribution network.

In addition to the attenuation, dispersion is also an important characteristic of a transmission line. For a parallel or a coaxial line, they operate in a transverse electromagnetic (TEM) mode, the radio signals traveling in the two types of transmission lines do not suffer from any dispersion. Other transmission lines, such as waveguides and microstrip lines, are mainly for signal processing purposes. For example, a waveguide can be used to make low loss, highly selective filters; a microstrip line can be used to make planar circuits for amplifiers, mixers, and oscillators.

Optical fiber is considered a promising transmission medium for the distribution of high frequency electrical signals in the optical domain. The state-of-the-art optical fibers bear the following advantages [2]: low signal attenuation: 0.2 dB/km in the 1550-nm band; huge bandwidth: around 50 THz, low dispersion: $\leq$ 17 ps/km·nm at 1550 nm; low power requirement; low material usage; light weight; low cost; and electromagnetic interference free. It should be noted that although optical fibers have low chromatic dispersion comparing with a rectangular waveguide, this dispersion factor has to be taken into account when a millimeter-wave signal is transmitted over the optical fiber, or a special arrangement has to be made to eliminate the dispersion-induced power fading. Thanks to the numerous advantages, state-of-the-art optical fibers have laid a solid foundation for making radio-over-fiber systems possible.

1.2.3 Merits of radio-over-fiber systems

In a radio-over-fiber system, optical fibers are employed as the transmission medium for radio signal transmission between a central office and base stations, or between base stations, to take advantage of the low loss and wide bandwidth offered by modern optical fibers. By

incorporating radio-over-fiber technology into a wireless communication system, the performance of the system can be greatly improved and the cost can be significantly reduced.

First, the use of radio-over-fiber systems can increase the capacity of present and future wireless communication systems. For current wireless communication networks, base stations are always located outside buildings to cover designated areas according to the network plan. This arrangement works well for wireless communications outside the buildings. However, it significantly reduces the communication quality for wireless communications inside buildings because of large signal attenuation inherently present in these structures. Airports, shopping malls and office buildings have a dense mobile communications requirement. These places suffer from signal blockage problems and require indoor base stations. The number of base stations installed depends on the demand. It may be one for the whole building, for one floor, or for one office. Base stations inside buildings use distributed microcells to provide a relatively uniform coverage. This type of indoor wireless network always uses high-frequency transmission lines to distribute the wireless signals from a centralized base station to microcell locations. Among the numerous transmission lines, optical fiber is an ideal candidate to be used in this distribution network because of the low attenuation, small size, and light weight. Although conventional coaxial cables used in the distribution network are an option due to its current low cost, optical fiber is a competitive alternative for in-building wireless networks [3]. Right now about 10 to 20% of the in-building installations are done with radio-over-fiber techniques.

As discussed in Subsection 1.2.1, future broadband wireless communication systems will operate in the millimeter-wave band. If these systems deploy heterodyne techniques, as in conventional millimeter-wave systems, the connection between the central office and the base stations will use coaxial cables to carry intermediate-frequency signals or base-band signals to lower the transmission losses. In this scenario, the electrical components at a base station typically includes a millimeter-wave synthesizer working as a local oscillator for millimeter-wave up-conversion and down-conversion, millimeter-wave up-converters and down-converters, millimeter-wave power amplifiers and low noise amplifiers, filters and duplexers. Because of the limitation of the speed of electron mobility of semiconductor material and the process ability of semiconductor equipment, the yield and performance of millimeter-wave devices and

millimeter-wave monolithic microwave integrated circuits (MMICs) are limited, making millimeter-wave communications very expensive. More millimeter-wave components in base stations will make the system equipment more expensive. Further more, if the millimeter-wave base stations are located outside of a building, all the electronic circuits would experience a wide range of temperature change, typically from -40 to +80°C. Some components are temperature insensitive but others, like millimeter-wave synthesizers, are no longer functional at extreme environmental temperatures. The elimination of local oscillators from a millimeter-wave base station is highly desirable for the practical applications.

Based on radio-over-fiber technology, a base station can be simplified by directly transmitting millimeter-wave signals between a central office and base stations or between two base stations. In this way, temperature sensitive circuits and local synthesizers can be eliminated at a base station, hence makes the network more reliable, cost effective and practical.

The above discussion shows that with the radio-over-fiber technology, the one-time equipment cost of the base station can be reduced. The use of radio-over-fiber technology can also reduce the everyday operating cost [3], [4]. For example, due to the high losses of the coaxial cables, 100 base stations are connected currently to one central office in a conventional wireless communication system. With the radio-over-fiber technology, 1000 base stations could be connected to one central office. In this way, the everyday operating cost can be greatly reduced. Temperature sensitive circuits, like high-frequency electrical sources, are located inside the central office, where the ambient temperature could be controlled. Then the reliability of these sources is ensured. In addition, these sources could be shared by remote base stations. Therefore, the radio-over-fiber technology provides the possibility of dynamic management of network resources.

In addition to the above-mentioned applications, radio-over-fiber systems can also find applications in defense systems, such as antenna remoting, phased array antenna, and radar signal transmission [5]-[7]. In these applications, high-frequency analog signals with a frequency ranging from L band to the millimeter-wave band can be transmitted over optical fiber without up-conversion or down-conversion of these signals at the antenna sites.

1.2.4 Review of radio-over-fiber system development

In 1990, Cooper demonstrated the first fiber-radio system [8]. In his report, a four-channel, second-generation, cordless telephony system was demonstrated over single-mode fiber by using subcarrier multiplexing techniques. In his system, the RF carriers were located in the frequency band of 864-868 MHz. The optical transmitters employed 1300 nm multi-longitudinal mode laser diodes. These laser diodes were directly modulated by the RF carriers. Under small-signal modulation conditions, the laser diodes have a relative intensity noise of -134 dB/Hz. To lower the level of in band third-order inter-modulation products the laser diodes were biased to give a mean output power of -3 dBm and a 1 dB power compression point of 2.6-2.9 dBm. The optical link was 0.5 km single-mode fiber. The optical receivers were PIN photodetectors with amplifiers. This system exhibited an electrical dynamic range of 70 dB for one channel and 50 dB for four channels.

Since then, radio-over-fiber systems and associated techniques have become an attractive topic for analog optical fiber communications and wireless communications. Different radio-over-fiber techniques for present and future wireless communication systems have been reported.

Radio-over-fiber network architectures employing subcarrier multiplexing and wavelength division multiplexing were reported in [9]-[12]. Star-tree, radio-over-fiber network configurations were proposed for building a wireless local area network [9], [10]. Techniques of subcarrier multiplexing and optical wavelength division multiplexing were applied for increasing the system capacity and realizing a full-duplex function [9], [11]. A radio-over-fiber network having a ring architecture was proposed to construct a wireless local area network using dense wavelength division multiplexing and optical add-drop multiplexing in 1999 [12].

Radio-over-fiber systems operating in millimeter-wave band for future wireless communication systems were widely reported in [13]-[18]. In 1992, Ogawa proposed a conceptual configuration with possible architectures for a fiber-optic millimeter-wave subcarrier transmission link [13]. He evaluated these architectures with experiments for an IF and RF links by using 70 MHz, 300 MHz and 26 GHz subcarriers, with either FM or QPSK data modulations. In 1997, Goloubkoff et al. reported outdoor and indoor applications of a broadband local loop with fiber-supported millimeter-wave radio system [14]. Noel et al. showed a 60-GHz fiber-

radio transmission system in 1997 [15] in which the fiber span was 13 km and the wireless communication distance was 5 m. In the down-stream path, a radio signal composed of a 120 Mb/s QPSK data and 20-channel TV signals was distributed to the base station. In the up-stream path, a 120 Mb/s QPSK data signal was transmitted to the central office. A bit error rate (BER) of the QPSK signal better than 10^{-9} was achieved. The quality of the TV signals received at the terminal was maintained, with no significant degradation being observed. In 1998, Kitayama et al. reported an error-free 156 Mb/s optical millimeter-wave wireless transport system [16], in which a 60-GHz external modulation technique was deployed. Recently, Olmos et al. proposed and demonstrated a dynamic reconfigurable wavelength-division-multiplexed millimeter-wave-over-fiber system [17]. Four 155-Mb/s radio-over-fiber channels were generated and transmitted through 25-km fiber, then switched and transmitted again over a 2-km fiber. Its BER was reported below 10^{-10}. In 2007, Nkansah et al. proposed a cost-effective, star-tree architecture for millimeter-wave over fiber applications based on a low-cost vertical-cavity surface-emitting laser (VCSEL) [18]. Signals with QPSK, 16-QAM, and 64-QAM formats at 20 and 6 MS/s were successfully transmitted.

Radio-over-fiber systems operating in the conventional RF frequency bands for present wireless communication systems were also widely studied [19]-[25]. Radio-over-fiber systems based on multimode optical fibers with a reduced cost were also widely investigated [26]-[32]. Demonstrations of the co-existence of analog radio-over-fiber systems and digital fiber-to-the-home systems with dense wavelength division multiplexed technology were reported [33]-[34].

The techniques reviewed above were concerned with system architectures of radio-over-fiber systems. Other techniques to develop subsystems for radio-over-fiber applications have also been extensively studied, which include optical generation of microwave and millimeter-wave signals [35]-[42], optical up-conversion of a microwave signal [43]-[46], and distortion analysis of optical up-conversion [47]-[51].

In industry, engineers have developed transceivers using optical fiber technology for present wireless communication systems. Now the majority of the currently deployed wireless communication systems still employ coaxial cables for radio signal distribution because of the low one-time equipment cost. In recent years, the wireless market has pushed the working

frequency of silicon components to the edge of X band. The large wafers used in silicon process, 8 to 12 inches in diameter, have greatly reduced the cost of the electronic circuits. By taking advantage of the break-through in silicon semiconductor fabrication, conventional coaxial cable wireless communication systems has a competitive price over optical fiber-supported wireless communication systems in one-time system equipment cost. As discussed in the previous Subsection, when the number of base stations reaches a certain quantity in a wireless communication network, there is a balance point between the one-time system equipment cost and the daily system operating cost. Therefore, radio-over-fiber technology can still find applications in the present wireless communication systems. In the past decade, successful applications of CATV-over-fiber and the maturity of long-haul digital optical communications have made electrical techniques and optical techniques ready for application in radio-over-fiber systems. In current radio-over-fiber systems, direct intensity modulation of a semiconductor laser is usually employed in a transmitter, and direct detection using a PIN photodiode is used in a receiver, for simplifying system and lowering cost [3]. These commercially available fiber-radio systems can be classified in three categories: RF over single mode fiber, IF over multimode fiber, and digital over single mode fiber [3].

1.3 Objectives of the study

As discussed above, radio-over-fiber systems have many advantages over conventional wireless communication systems. They are especially suitable for future generations of wireless communication systems operating in the millimeter-wave band. Compared with techniques that are widely deployed in conventional digital optical communication systems, radio-over-fiber techniques have their own specialty. In a digital optical communication system, high-speed digital signal processing is one of the key techniques. There are many unique techniques, which need to be studied in a radio-over-fiber system. For example: network architecture, system configuration, new photonic components, the generation of optical signals for millimeter-wave generation or optical generation of millimeter-wave signals, optical up-conversion, and optical carrier recovery at remote sites.

Among the above-mentioned techniques, this thesis focuses on two techniques for radio-over-fiber applications, the technique for optically generating millimeter-wave signals and the technique for optical up-conversion. Optical carrier recovery is also demonstrated within an optical millimeter-wave generation technique.

1.4 Major contributions

The major contributions of this thesis:

1) Techniques to optically generate microwave and millimeter-wave signals

Three approaches, based on optical external modulation techniques, are proposed and demonstrated to generate wideband, continuously tunable, millimeter-wave signals. In the first, a technique, which uses an optical intensity modulator and an optical notch filter, is detailed. The frequency of the optically generated millimeter-wave signal can be continuously tuned from 32 GHz to 50 GHz. In the second, an optical phase modulator and an optical notch filter are used to generate two bands of millimeter-wave signals. The frequency ranges of the two bands are continuously tunable from 37.6 GHz to 50 GHz and from 75.2 GHz to 100 GHz, respectively. Finally, the third approach details a single-longitudinal-mode, fiber ring laser that incorporates an optical intensity modulator for millimeter-wave signal generation. This approach can generate a continuously tunable, millimeter-wave signal from 32 GHz to 50 GHz. The power level of the recovered optical carrier is approximately -5 dBm.

The spectral purity of an optically generated millimeter-wave signal is studied in two ways. In the first, the phase noise performance of the signal is investigated both theoretically and experimentally. Mathematical models are developed to represent perturbations on the transmitted optical signal caused by the phase fluctuations of the electrical drive signal and the phase fluctuations of the optical carrier. Closed form expressions of the power spectral density for the optically generated electrical signals are derived.

In the second analysis, the degradation due to the optical amplifier's amplified spontaneous emission noise is theoretically studied. This analysis is required since it is inevitable that an erbium-doped fiber amplifier or semiconductor optical amplifier will be used in the signal

generation techniques mentioned above. The result of the analysis explains the results observed in earlier experimental studies of this subject.

2). Techniques for optical up-conversion

An optical approach to up-converting a subcarrier from a low-frequency band to the millimeter-wave band is proposed. In the proposed approach, two phase-correlated optical carriers and a series of optical sidebands, generated with an optical phase modulator and an optical notch filter, are directly modulated by a low-frequency subcarrier signal in an optical intensity modulator. Analyses show that the up-converted millimeter-wave signals bears the information carried by the low-frequency subcarrier after photodetection. Data transmission experiments and simulations of BPSK and QPSK signals are conducted to validate the proposed approach.

General nonlinearities caused by the optical intensity modulator used for optical up-conversion are studied and analyzed. Electrical fields of the up-converted optical signal are expressed in power series form, which are widely used in electronics in expressing memoryless nonlinearity. Harmonic distortion and inter-modulation distortion generated in the above-proposed optical up-conversion approach are analyzed in detail for the up-converted millimeter-wave signal. Characterization with a one-tone measurement and a two-tone measurement are performed to validate the analysis results.

1.5 Organization of this thesis

This thesis consists of two parts in six chapters. In Chapter 1, the necessity of radio-over-fiber systems is discussed. This leads to the objectives of the study. The first objective of the study is to investigate techniques to optically generate microwave and millimeter-wave signals, and to perform optical carrier recovery. The second objective is to investigate techniques for optical up-conversion. Contributions to the study are also summarized in this Chapter.

In Chapter 2, a review on the techniques for optically generating microwave and millimeter-wave signals and techniques of optical up-conversion for radio-over-fiber applications is provided. Radio-over-fiber techniques are classified and compared with their advantages and disadvantages outlined. Then the need of the present study is drawn.

In Chapter 3, three new approaches for generating wideband, continuously tunable, millimeter-wave signals based on optical external modulation techniques are proposed and demonstrated. One of the three proposed approaches realizes the function of optical carrier recovery at the same time as millimeter-wave signal generation.

In Chapter 4, the spectral purity of the optically generated electrical signals are analyzed using a phase noise analysis with respect to: the spectral purity of the optical source, the spectral purity of the electrical source, the transmission effect of standard single-mode fiber, and the amplified spontaneous emission of optical amplifiers.

In Chapter 5, techniques of optical up-conversion for radio-over-fiber systems are discussed. An approach to up-converting a subcarrier signal from a low-frequency band to the millimeter-wave band based on optical techniques is proposed. Principle analyses show that information carried by the low-frequency subcarrier signal is up-converted to the millimeter-wave band with the proposed approach. Data transmission experiments and simulations of BPSK and QPSK signals are conducted to validate the proposed approach. Nonlinearities caused by the optical intensity modulator used for optical up-conversion are analyzed and discussed. Harmonic distortion and inter-modulation distortion generated in the proposed optical up-conversion scheme are analyzed in detail. Experimental characterization with a one-tone and a two-tone measurement are performed to validate the analysis result.

In Chapter 6, a summary is drawn and a recommendation for the future work is proposed.

References

[1] C. A. Balanis, *Antenna Theory Analysis and Design*, 2nd ed., John Wiley & Sons, Inc., 1997, pp. 86-88.

[2] B. Mukherjee, "WDM optical communication networks: progress and challenges," *IEEE J. Select. Areas Commun.*, vol. 18, no. 10, pp. 1810-1824, Oct. 2000.

[3] D. Wake, "Trends and prospects for radio over fiber picocells," in *Proc. Microwave Photonics*, Nov. 2002, pp. 21-24.

[4] E. V. Mooney, "Hybrid fiber radio replaces traditional cable solutions," *Radio Communications Report*, wireless news, Aug. 2002.

[5] J. E. Román, L. T. Nichols, K. J. Williams, R. D. Esman, G. C. Tavik, M. Livingston, and M. G. Parent, "Fiber-optic remoting of an ultrahigh dynamic range radar," *IEEE Trans. Microwave Theory Tech.*, vol. 46, no. 12, pp. 2317-2323, Dec. 1998.

[6] E. C. Niehenke and P. Hercafeld, "An optical link for W-band transmit/receive applications," in *Tech. Dig. IEEE MTT-S Int. Microwave Symp.*, Jun. 1997, vol. 1, pp. 35-38.

[7] J. L. Corral, J. Marti, J. M. Fuster, R. Laming, and M. J. Cole, "Continuously variable true time-delay optical feeder for phased-array antenna employing chirped fiber gratings," *IEEE Trans. Microwave Theory Tech.*, vol. 45, no. 8, pp. 1531-1536, Aug. 1997.

[8] A. J. Cooper, "Fiber/radio for the provision of cordless/mobile telephony services in the access network," *Electron. Lett.*, vol. 26, no. 24, pp. 2054-2056, Nov. 1990.

[9] G. H. Smith, D. Novak, and C. Lim, "A millimeter-wave full-duplex radio-over-fiber star-tree architecture incorporating WDM and SCM," *IEEE Photon. Tech. Lett.*, vol. 10, no. 11, pp. 1650-1652, Nov. 1998.

[10] A. Nkansah, A. Das, N. J. Gomes, P. Shen, and D. Wake, "VCSEL-based single-mode and multimode fiber star/tree distribution network for millimeter-wave wireless systems," in *Proc. Microwave Photonics,* Oct. 2006, pp. 1-4.

[11] A. Kaszubowska, P. Anandarajah, and L. P. Barry, "Multifunctional operation of a fiber Bragg grating in a WDM/SCM radio over fiber distribution system," *IEEE Photon. Tech. Lett.*, vol. 16, no. 2, pp. 605-607, Feb. 2004.

[12] A. Stöhr, K. Kitayama, and D. Jäger, "Full-duplex fiber-optic RF subcarrier transmission using a dual-function modulator/photodetector," *IEEE Trans. Microwave Theory Tech.*, vol. 47, no. 7, pp. 1338-1341, Jul. 1999.

[13] H. Ogawa, D. Polifko, and S. Banba, "Millimeter-wave fiber optics Systems for Personal radio communication," *IEEE Trans. Microwave Theory Tech.*, vol. 40, no. 12, pp. 2285-2293, Dec. 1992.

[14] M. Goloubkoff, E. Penard, D. Tanguy, P. Legaud, D. Mathoorasing, F. Devaux, and C. Minot, "Outdoor and indoor applications for broadband local loop with fibre supported mm-wave radio systems," in *Tech. Dig. IEEE MTT-S Int. Microwave Symp.*, Jun. 1997, vol. 1, pp. 31-34.

[15] L. Noel, D. Wake, D. G. Moodie, D. D. Marcenac, L. D. Westbrook, and D. Nesset, "Novel techniques for high-capacity 60 GHz radio-over-fiber transmission systems," *IEEE Trans. Microwave Theory Tech.*, vol. 45, no. 8, pp. 1416-1423, Aug. 1997.

[16] K. Kitayama, T. Kuri, and Y. Ogawa, "Error-free optical 156-Mbit/s millimeter-wave wireless transport through 60-GHz external modulation," *OFC '98 Technical Digest*, Feb. 1998, pp. 14-15.

[17] J. J. Vegas Olmos, T. Kuri, and K. Kitayama, "Dynamic reconfigurable WDM 60-GHz millimeter-waveband radio-over-fiber access network: architectural considerations and experiment," *J. Lightwave Technol.*, vol. 25, no. 11, pp. 3374-3380, Nov. 2007.

[18] A. Nkansah, A. Das, N. J. Gomes, and P. Shen, "Multilevel modulated signal transmission over serial single-mode and multimode fiber links using vertical-cavity surface-emitting lasers for millimeter-wave wireless communications," *IEEE Trans. Microwave Theory Tech.*, vol. 55, no. 6, pp. 1219-1228, Jun. 2007.

[19] B. L. Dang and I. Niemegeers, "Analysis of IEEE 802.11 in radio over fiber home networks," *IEEE Conference on Local Computer Networks*, Nov. 2005, pp. 744-747.

[20] Y. Horiuchi, "ROF application to 3G mobile systems in offices and outdoors," in *Proc. Microwave Photonics,* Oct. 2005, pp. 3-3.

[21] M. J. Crisp, L. Sheng, A. Wonfor, R.V. Penty, and I. H. White, "Demonstration of a radio over fibre distributed antenna network for combined in-building WLAN and 3G coverage," *OFC/NFOEC 2007*, Mar. 2007, pp. 1-3.

[22] A. Brizido, M. Lima, R. Nogueira, P. Andre, and A. Teixeira, "3G radio distribution based on directly modulated lasers over passive transparent optical networks," *Microwave and Optoelectronics Conference*, 2007, pp. 658-661.

[23] H. Kosek, Y. He, X. Gu, and X. N. Fernando, "All-optical demultiplexing of WLAN and cellular CDMA radio signals," *J. Lightwave Technol.*, vol. 25, no. 6, pp. 1401-1409, Jun. 2007.

[24] M. J. Crisp, L. Sheng, A. Watts, R.V. Penty, and I. H. White, "Uplink and downlink coverage improvements of 802.11g signals using a distributed antenna network," *J. Lightwave Technol.*, vol. 25, no. 11, pp. 3388-3395, Nov. 2007.

[25] M. Mjeku and N. J. Gomes, "Performance analysis of 802.11e transmission bursting in fiberfed networks," *Radio and Wireless Symposium*, Jan. 2008, pp. 133-136.

[26] C. Lethien, J. -P. Vilcot, S. McMurtry, J. -F, Lampin, D. Vignaud, P. Miska, D. Decoster, and F. Mollot, "Characterisation of SiO_2 transferred GaAs electroabsorption modulator for 850 nm radio over fibre systems based on multimode fibre," *Electron. Lett.*, vol. 40, no. 17, pp. 1075-1076, Aug. 2004.

[27] C. Loyez, C. Letien, N. Deparis, J. P. Vilcot, D. Decoster, N. Rolland, and P. A. Rolland, "A radio over multimode system based on a LO phase-noise cancellation for 60-GHz WLAN," *European Microwave Conference,* Oct. 2005, vol. 1, pp. 3 pp.

[28] A. Nkansah and N. J. Gomes, "Characterization of radio over multimode fiber links using coherence bandwidth," *IEEE Photon. Tech. Lett.*, vol. 17, no. 12, pp. 2694-2696, Dec. 2005.

[29] A. Nkansah, A. Das, C. Lethien, J. -P. Vilcot, N. J. Gomes, I. J. Garcia, J. C. Batohelor, and D. Wake, "Simultaneous dual band transmission over multimode fiber-fed indoor wireless network," *IEEE Microw. Wireless Compon. Lett.*, vol. 16, no. 11, pp. 627-629, Nov. 2006.

[30] J. D. Ingham, R.V. Penty, and I. H. White, "Bidirectional multimode-fiber communication links using dual-purpose vertical-cavity devices," *J. Lightwave Technol.*, vol. 24, no. 3, pp. 1283-1294, Mar. 2006.

[31] I. Gasulla and J. Capmany, "Transmission of high-frequency radio over fibre signals through short and middle reach multimode fibre links using a low-linewidth laser," in *Proc. Microwave Photonics,* Oct. 2007, pp. 116-119.

[32] M. Sauer, A. Kobyakov, and J. George, "Radio over fiber for picocellular network architectures," *J. Lightwave Technol.*, vol. 25, no. 11, pp. 3301-3320, Nov. 2007.

[33] K. Kitayama, T. Kuri, H. Toda, and J. J. V. Olmos, "Radio over fiber: DWDM analog/digital access network and its enabling technologies," *Lasers and Electro-Optics Society, LEOS 2007*, Oct. 2007, pp. 794-795.

[34] T. Kuri, H. Toda, and K. Kitayama, "Radio over fiber: DWDM-based analog/digital access networking and its enabling technologies," *Radio and Wireless Symposium,* Jan. 2008, pp. 137-140.

[35] R. Gindera and D. Jager, "Remote optoelectronic microwave generation in fiber radio systems using a ring oscillator," *European Microwave Conference*, Sept. 2006, pp. 1115-1117.

[36] C. Lin, W. Peng, P. Peng, C. Peng, C. Chiang, J. chen, B. Chiou, and S. Chi, "Simultaneous baseband and RF signal generation using only one single-electrode MZM based on double-sideband with optical carrier suppression," in *Proc. Microwave Photonics,* Oct. 2006, pp. 1-4.

[37] J. Yu, Z. Jia, L. Yi, Y. Su, G. Chang, and T. Wang, "Optical millimeter-wave generation or up-conversion using external modulators," *IEEE Photon. Tech. Lett.*, vol. 18, no. 1, pp. 265-267, Jan. 2006.

[38] Z. Deng, and J. P. Yao, "Photonic generation of microwave signal using a rational harmonic mode-locked fiber ring laser," *IEEE Trans. Microwave Theory Tech.*, vol. 54, no. 2, pp. 763-767, Feb. 2006.

[39] J. Yu, Z. Jia, L. Xu, L. Chen, T. wang, and G. Chang, "DWDM optical millimeter-wave generation for radio-over-fiber using an optical phase modulator and an optical interleaver," *IEEE Photon. Tech. Lett.*, vol. 18, no. 13, pp. 1418-1420, Jul. 2006.

[40] M. Mohamed, X. Zhang, B. Hraimel, and K. Wu, "Efficient photonic generation of millimeter-waves using optical frequency multiplication in radio-over-fiber systems," in *Proc. Microwave Photonics,* Oct. 2007, pp. 179-182.

[41] J. Zhang, H. Chen, M. Chen, T. Wang, and S. Xie, "A photonic microwave frequency quafrupler using two cascaded intensity modulators with repetitious optical carrier suppression," *IEEE Photon. Tech. Lett.*, vol. 19, no. 14, pp. 1057-1059, Jul. 2007.

[42] J. Yu, Z. Jia, T. wang, and G. Chang, "Centralized lightwave radio-over-fiber system with photonic frequency quadrupling for high-frequency millimeter-wave generation," *IEEE Photon. Tech. Lett.*, vol. 19, no. 19, pp. 1499-1501, Oct. 2007.

[43] H. -J. Song, J. S. Lee, and J. -I. Song, "All-optical frequency upconversion of radio over fibre signal with optical heterodyne detection," *Electron. Lett.*, vol. 40, no. 5, pp. 330-331, Mar. 2004.

[44] J. S. Lee, H. -J. Song, W. B. Kim, M. Fujise, Y. -H. Kim, and J. -I. Song, "All-optical harmonic frequency upconversion of radio over fibre signal using cross-phase modulation in semiconductor optical amplifier," *Electron. Lett.*, vol. 40, no. 19, pp. 1211-1213, Sept. 2004.

[45] H. Song, J. S. Lee, and J. Song, "Simultaneous all-optical frequency upconversion for WDM radio over fiber applications," in *Tech. Dig. IEEE MTT-S Int. Microwave Symp.*, Jun. 2005, pp. 4 pp.

[46] M. Shin and P. Kumar, "1.25 Gbps optical data channel up-conversion in 20 GHz-band via a frequency-doubling optoelectronic oscillator for radio-over-fiber systems," in *Tech. Dig. IEEE MTT-S Int. Microwave Symp.*, Jun. 2007, pp. 63-66.

[47] S. Yaalob, W. R. Wan Abdullah, M. N. Osman, A. K. Zamzuri, R. Mohamad, M. R. Yahya, A. F. Awang Mat, M. R. Mokhtar, and H. A. Abdul Rashid, "Effect of laser bias current to the third order intermodulation in the radio over fibre system," *RF and Microwave Conference,* Sept. 2006, pp. 444-447.

[48] L. Rosa, S. Selleri, G. Tartarini, P. Faccin, and E. M. Fabbri, "Distortion performance prediction in multi-band radio over fiber systems exploiting direct laser modulation," *European Microwave Conference,* Sept. 2006, pp. 1292-1295.

[49] B. Hraimel, M. O. Twati, and K. Wu, "Closed-form dynamic range expression of dual-electrode Mach-Zehnder modulator in radio-over-fiber WDM system," *J. Lightwave Technol.*, vol. 24, no. 6, pp. 2380-2387, Jun. 2006.

[50] K. Uegaki, K. Kumamoto, K. Yasukawa, K. Inagaki, T. Higashino, K. Tsukamoto, and S. Komkj, "A novel nonlinear distortion suppression method in RoF systems using optical filter," in *Proc. Microwave Photonics,* Oct. 2007, pp. 33-36.

[51] J. Zhang and T. E. Darcie, "Two-tone analysis of distortion suppression in microwave-photonic links using phase modulation and fiber-Bragg grating filters," *International Symposium on Signals, Systems and Electronics*, 2007, pp. 621-624.

CHAPTER 2

BACKGROUND REVIEW

In this Chapter, a literature review of optical techniques for high-frequency electrical signal generation and for carrier up-conversion is performed with respect to the objectives of the study. Techniques of earlier works are classified and compared. Their advantages and disadvantages are outlined.

2.1 Optical techniques for high-frequency electrical signal generation

A. Principle of electrical signal generation with optical techniques

Optical high-frequency electrical signal generation is actually based on an optical heterodyne technique, i.e. beating two optical carriers, separated by the desired millimeter-wave frequency, on a square-law photodetector. Here the optical carrier refers to an un-modulated laser light. The optical heterodyne technique can be shown in Fig. 2.1.

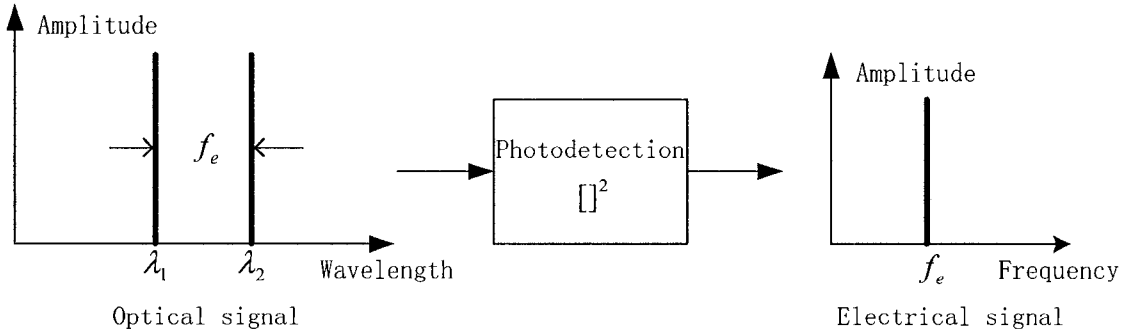

Fig. 2.1. Schematic diagrams of optical heterodyne technique in generating electrical signals.

In communications systems, the amplitude and phase noise quality of the optically generated electrical signal must meet system requirements. This is because the signal is always used as a carrier for up-conversion in a transmitter, or a local oscillator for down-conversion in a receiver.

In order to establish appropriate criteria for these signals, the requirements of the two optical carriers need to be discussed.

Generally, an optical carrier transmitting in a homogeneous media can be expressed in wave form as

$$\overrightarrow{E(t)} = \overrightarrow{E_o(t)}\cos(2\pi f_o t - \overrightarrow{k_o}\cdot\vec{z} + \phi_o(t)), \quad (1)$$

where $\overrightarrow{E(t)}$ is the electric field of the optical carrier in vector form, $\overrightarrow{E_o(t)}$ is the amplitude of the electric field of the optical carrier (the vector shows its polarization state and the time variation shows the amplitude fluctuation), f_o is the frequency of the optical carrier, $\overrightarrow{k_o}$ is the propagation constant of the optical carrier (the vector shows the propagation direction; $\vec{z}$ is one direction of a coordination system in evaluating the phase delay of the optical carrier with respect to this direction) and, finally, $\phi_o(t)$ is the phase fluctuation of the optical carrier which determines the spectral width of the optical carrier. Equation (1) shows that an optical carrier is characterized by five parameters: polarization, amplitude, frequency, propagation constant, and phase variation.

I will assume that the discussion of the requirements of is limited to fiber optics, which is the most likely scenario in a radio-over-fiber system. In addition, the two optical carriers are generated by modern laser diodes having a relative stable frequency offset and a correlated phase fluctuation. Finally, that the polarization state of the two optical carriers are aligned in the same direction. Under these circumstances the electric fields of the two optical carriers can be simply expressed as

$$E_1(t) = E_{o1}\cos(2\pi f_o t), \quad (2)$$

$$E_2(t) = E_{o2}\cos[2\pi(f_o + f_e)t], \quad (3)$$

where $E_1(t)$ and $E_2(t)$ is the electric field of each optical carrier in scalar form, E_{o1} and E_{o2} are the electric field amplitude of the two optical carriers and, f_o and f_e are the frequency of one optical carrier and the offset frequency of the other optical carrier, respectively.

When the two optical carriers expressed in (2) and (3) are fed into a square-law photodetector, electrical signals will be generated. The generated high-frequency electrical signal, $V(t)$, can be written as

$$V(t) = C\cos(2\pi f_e t), \tag{4}$$

where C is a constant related to the values of E_{o1}, E_{o2}, and the responsivity of the photodetector. Other output components at DC and twice the optical frequency are ignored due to AC coupling and the bandwidth limitation of the photodetector. Equation (4) clearly indicates that an ideal electrical signal is generated. It must be emphasized that any approach that uses optical carriers to generating high quality electrical signals must adhere to the signal conditions described above.

In the past, extensive investigations on optical generation of microwave or millimeter-wave signals have led to a variety of methods. They can be classified into two categories: single or multiple optical sources.

B. Electrical signal generation with more than one optical sources

One method for optically generating millimeter-wave signals employs an automatic frequency control (AFC) loop, a common technique widely used in frequency stabilizing high-frequency oscillators. It can also be used in the optical band to obtain frequency stabilized electrical signals. In 1996 Braun et al. generated a 60 GHz millimeter-wave signal with this technique [1]. The schematic diagram of this method is shown in Fig. 2.2. Two distributed feedback (DFB) laser diodes (GEC-Marconi LD4804, λ=1540 nm) were used. The optical signals from the two DFB laser diodes were combined on a photodetector and a millimeter-wave signal was generated at the output of the photodetector. This was then mixed with an offset millimeter-wave reference signal in a mixer to generate an intermediate frequency signal. Part of the intermediate frequency signal is fed back to drive one DFB laser diode. Using this technique a frequency stabilized, millimeter-wave signal was generated. The linewidth of the generated signal was about 4 MHz, which was caused by the phase noise of laser diodes.

In this technique, a high spectral purity millimeter-wave reference signal is required and the spectral purity of the generated millimeter-wave signal is limited by the linewidth of the DFB laser diodes. High spectral purity laser diodes are required in this technique.

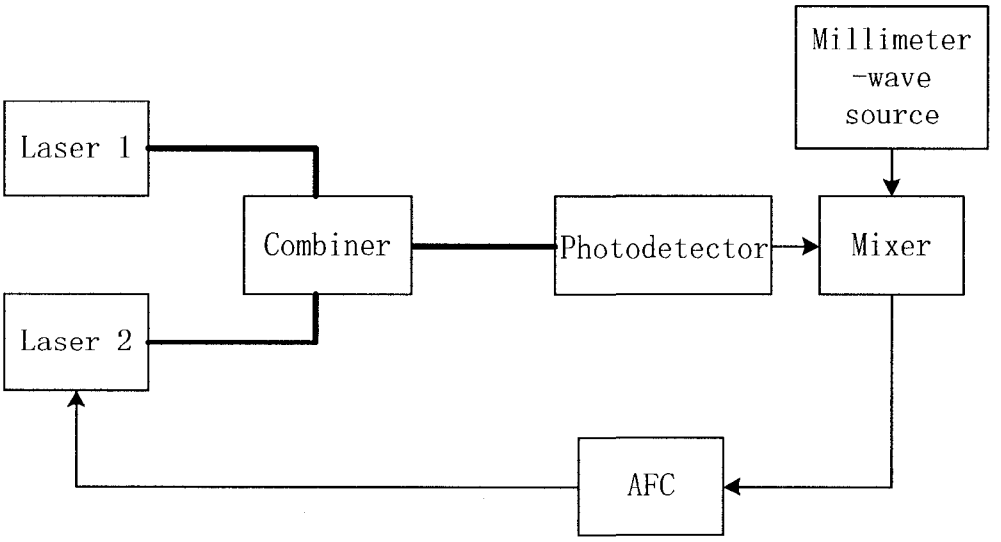

Fig. 2.2. Schematic diagram of millimeter wave generation based on the AFC technique. Thick lines indicate optical path.

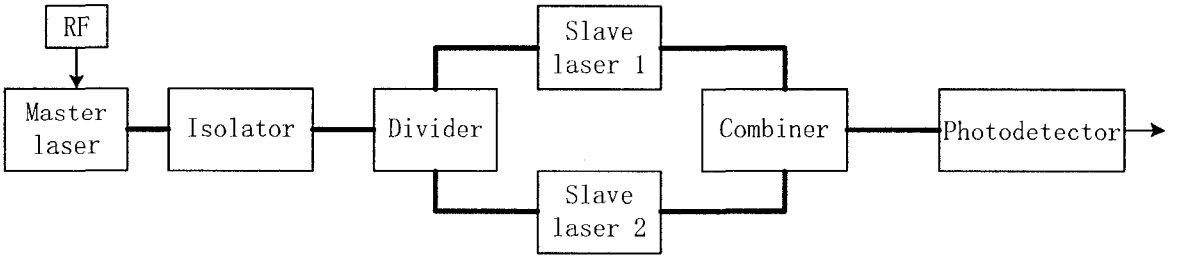

Fig. 2.3. Schematic diagram of millimeter wave generation based on optical sideband injection locking technique.

Optical sideband injection locking can also be used to generate a high-frequency electrical signal. In 1983, Goldberg, et al. reported using a modulated master laser diode to injection lock two slave laser diodes [2]. The beating of the two lasers in a photodetector led to the generation of a 10.5 GHz electrical signal. It was reported that the generated electrical signal had a linewidth of less than 5 kHz and a frequency jitter of about 20 kHz. A general schematic description of this method is shown in Fig. 2.3. Due to the discrete mode nature of the two slave lasers, this method is apt to support fixed-frequency electrical signal generation.

Applying the concept of phase lock loop (PLL), which is widely used in electrical domain, to the optical domain is another method of generating millimeter-wave signals of high spectral purity. Fig. 2.4 shows a general setup of this method. In 1992, Ramos et al. proposed a fast heterodyne optical phase lock loop using double quantum well laser diodes [3]. In 1999, Langley et al. demonstrated a packaged semiconductor laser optical phase-locked loop for photonic generation, processing and transmission of microwave signals [4]. In 2000 Hyodo et al. generated a millimeter wave signal of high spectral purity by heterodyning optical phase locked external-cavity semiconductor lasers [5]. The pair of grating-extended external-cavity semiconductor lasers operated around 1530 nm. The frequency of the generated millimeter-wave signal was determined by the wavelength difference between the two diodes. The millimeter-wave signal was phase-locked to a low-frequency reference source. A portable spectrum analyzer is used as a harmonic mixer. In their experiment the spectrum of the generated 70.5 GHz signal clearly showed that the phase noise in the near carrier frequency range was highly suppressed. However, this technique could not suppress the phase noise of the generated millimeter-wave signal outside of the phase lock bandwidth. Therefore, high spectral purity laser diodes have to be used.

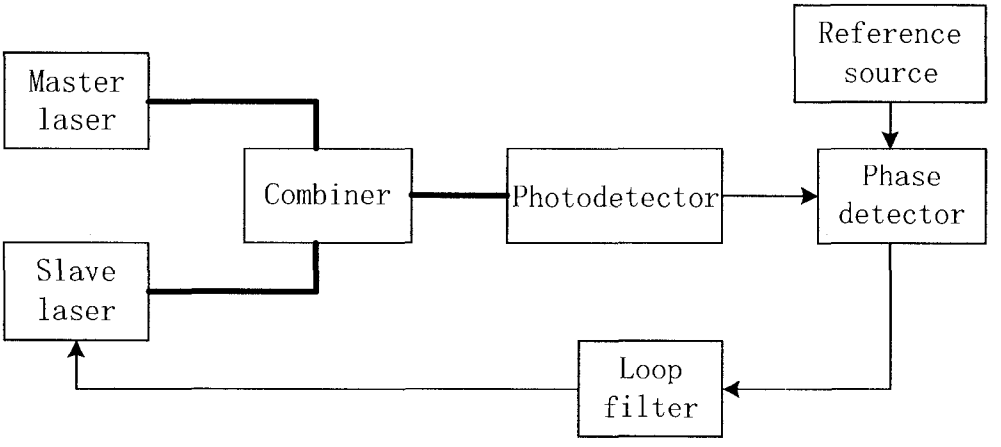

Fig. 2.4. Schematic diagram of millimeter wave generation based on an optical phase lock loop technique. Thick lines indicate optical path.

In 2001 Johansson et al. combined the technique of optical injection locking and the technique of optical phase lock loop and generated a 36 GHz signal [6].

C. Electrical signal generation with one optical source

The above methods of optical signal generation are based on two controlled optical sources. A second group of techniques use only one optical source plus some form of external modulation, either in the form of optical intensity or phase modulation.

In 1992 O'Reilly et al. proposed a scheme of generating electrical signals by externally modulating an optical intensity modulator [7]. The schematic diagram of this method is shown in Fig. 2.5. A Mach-Zehnder modulator was DC biased at the V_π point and driven by an 18 GHz microwave signal. Under these circumstances, the optical modulator suppressed the optical carrier and all even-order optical sidebands. After the optical signal was fed into a photodetector, a narrow linewidth 36 GHz signal was obtained at the output of the photodetector both locally and after passing through several kilometers of optical fiber. This method doubles the frequency of the electrical drive signal.

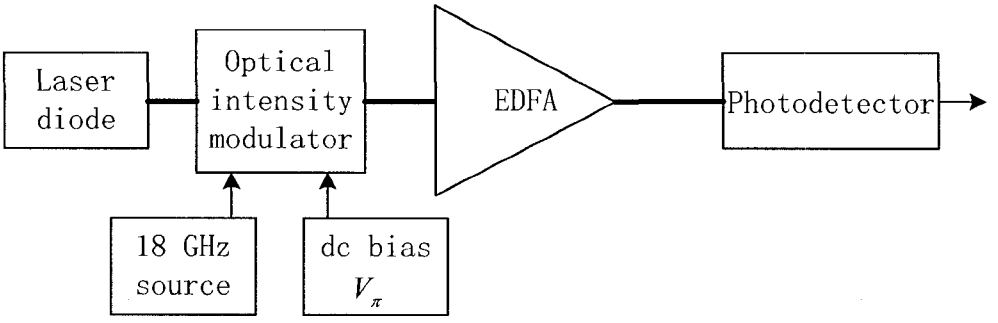

Fig. 2.5. Schematic diagrams of millimeter wave generation based on external intensity modulation technique. Thick lines indicate optical path.

In 1994, O'Reilly et al. proposed another method to generate a frequency-quadrupled electrical signal using an optical intensity modulation technique [8]. The schematic diagram of this method is shown in Fig. 2.6. Instead of biasing the Mach Zehnder modulator to suppress the even-order optical sidebands, this method was based on the quadratic response of an optical intensity modulator. The optical carrier, the first- and the third-order optical sidebands were suppressed by adjusting the power level of the microwave drive signal. A 60 GHz millimeter-wave signal was generated when a 15 GHz drive signal was applied to the Mach Zehnder modulator. However, to ensure a clean spectrum at the output of a photodetector, an imbalanced Mach-Zehnder filter with a free spectral range (FSR) equal to the spacing of the two second-order optical sidebands was used to suppress the unwanted optical components.

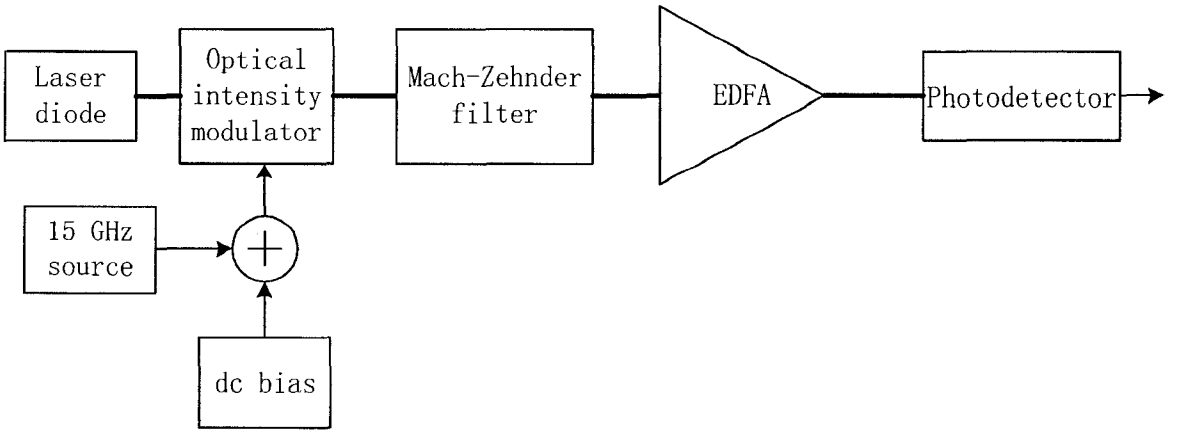

Fig. 2.6. Schematic diagram of millimeter wave generation based on an external intensity modulation technique. Thick lines indicate optical path.

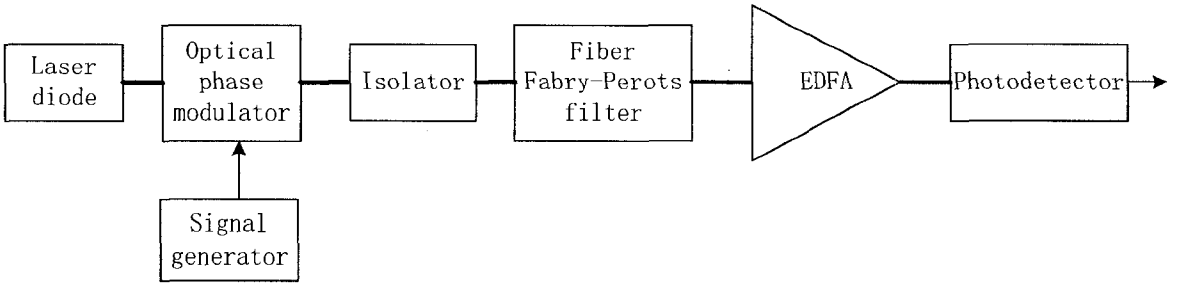

Fig. 2.7. Schematic diagrams of millimeter wave generation based on external phase modulation technique. Thick lines indicate optical path.

A few additional methods were proposed based on this optical phase modulation technique. For example, Shen, et al. in 2003 proposed an approach using an optical phase modulator to generate a frequency-quadrupled electrical signal [9]. The schematic diagram of this method is shown in Fig. 2.7. In this approach, a Fabry-Perot filter was used to select the two second-order optical sidebands. An electrical signal that has four times the frequency of the electrical drive signal was generated by beating the two second-order sidebands in a photodetector. Obviously, the fixed FSR of the Fabry-Perot filter makes this method difficult to use when generating a frequency tunable electrical signal. In 2003, Hedekvist, et al. also proposed harmonic generation of microwave frequency signals [10].

Recently, new approaches to the optical generation of microwave and millimeter-wave signals for radio-over-fiber applications have been proposed based on the basic techniques described above [11]-[18].

D. Discussion

Optical carriers in the optical signals generated with methods based on external optical modulation techniques with one optical source naturally meet the requirements of polarization, phase correlation, and frequency stability discussed in Section 2.1. In addition, these methods are based on the inherent non-linearity of the optical modulator. Taking advantage of this property dramatically lowers the bandwidth requirements of the optical modulator and allows the use of a much lower frequency electrical drive signal. This greatly reduces the cost of the system and makes it more practical for real-world applications.

Most of the methods mentioned above generate an electrical signal with a fixed frequency. For many applications - such as wideband surveillance radar, distributed antenna remoting network, spread-spectrum, and software-defined radio - systems are expected to be frequency reconfigurable and continuously tunable electrical signals are required. Under these circumstances, a very complicated and costly tunable optical filter is required to select the two second-order sidebands in the output spectrum. A means of generating a wideband, continuously tunable, millimeter-wave signal using fixed optical filters and narrow bandwidth optical modulators would be very attractive.

In addition, reusing the down-stream optical carrier for up-stream purposes at the base stations is also important for radio-over-fiber systems since this eliminates the need to place an optical source at these locations. Approaches of optical carrier recovery were reported by Nirmalathas et al. in 2001 [19]. Two configurations of the optical carrier reuse were proposed and are schematically shown in Fig. 2.8. One was the application of an FBG with a 3 dB optical power splitter; another was the application of an FBG with an optical circulator.

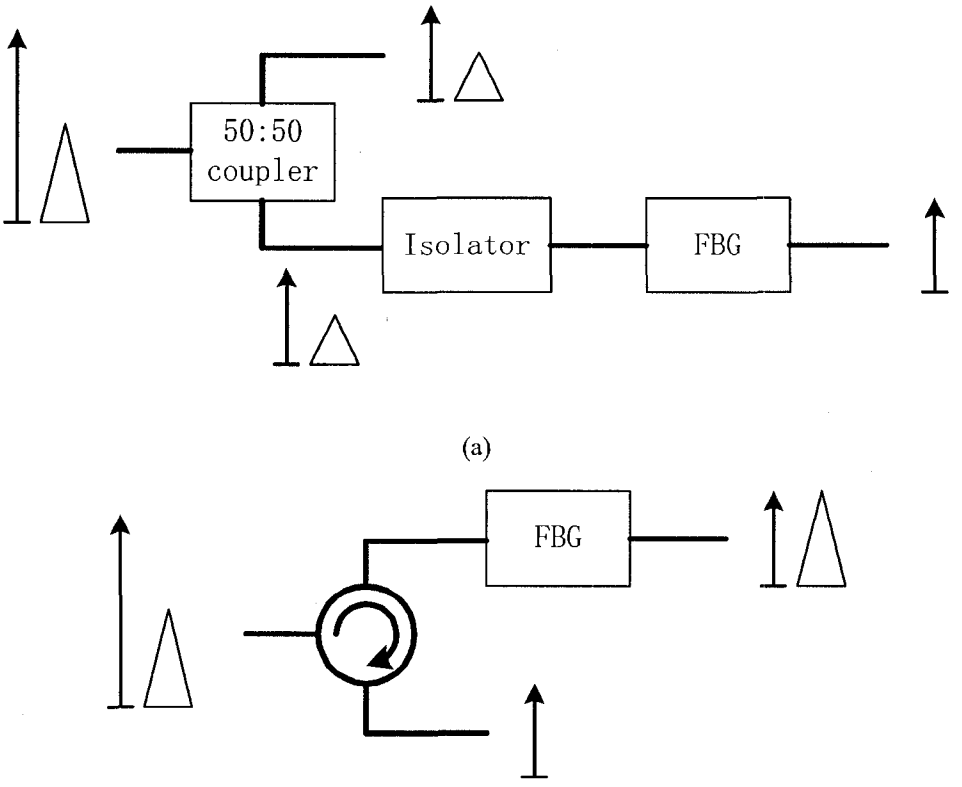

Fig. 2.8. Configurations for optical carrier recovery. (a) An FBG with an optical power splitter. (b) An FBG with an optical isolator.

2.2 Optical techniques for up-conversion

A. Fundamentals of optical up-conversion

Optical up-conversion can have two meanings. The first meaning is the up-conversion of an electrical signal from the electrical band to the optical band. The second meaning is the up-conversion of an electrical signal from a low-frequency electrical band to a high-frequency electrical band using an optical technique. In radio-over-fiber systems the second meaning of optical up-conversion is required, so in this thesis this meaning of is used.

Optical up-conversion of an electrical signal, from a low-frequency electrical band to a high-frequency electrical band, is actually based on techniques of up-converting an electrical signal from an electrical band to an optical band. The most widely used technique to do this is optical

intensity modulation. Optical intensity modulation can be realized by using an electrical signal to directly modulate a laser diode, or externally modulate an optical intensity modulator. The conversion spectra of these two typical schemes of optical intensity modulation are shown in Fig. 2.9.

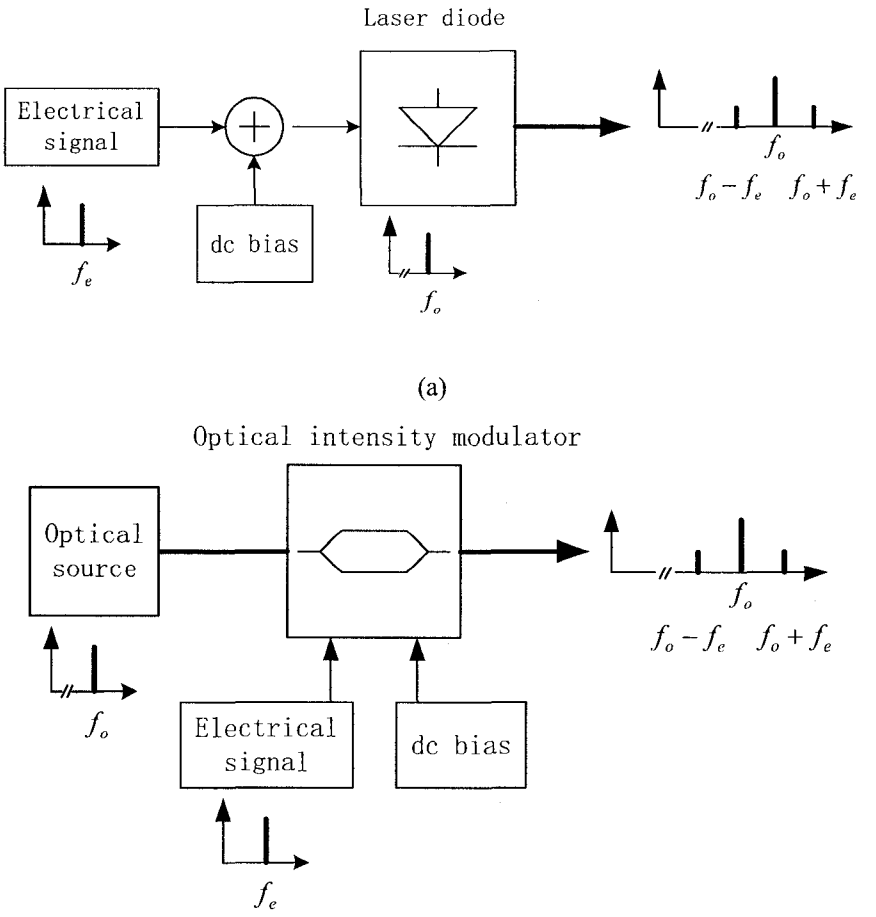

Fig. 2.9. Schematic diagrams of optical intensity modulation. Thick line indicates optical path. (a) Direct modulation of a laser diode. (b) External modulation with an optical intensity modulator.

In Fig. 2.9 the optical spectrum of the up-converted optical signal bears the characteristic of amplitude modulation. With an envelope detector - like a square law photodetector - the electrical signal can be recovered. From a communications point of view, information carried by the electrical signal can be distributed with this optical technique. However, during this process there is no optical up-conversion, i.e. up-converting an electrical signal from a low-frequency electrical band to a high-frequency electrical band.

In addition, the optical intensity modulation shown in Fig. 2.9 is widely used for low-frequency electrical signals; however, it becomes impractical when the frequency of the electrical signal is high as, for example, in the millimeter-wave band. There are many problems, which need to be overcome, such as the power penalty caused by the chromatic dispersion of the single-mode fiber after transmission [20], the relaxation oscillation frequency limitation of a laser diode in direct modulation [21], or the high half-wave voltage of a Mach-Zehnder modulator in an external modulator [21].

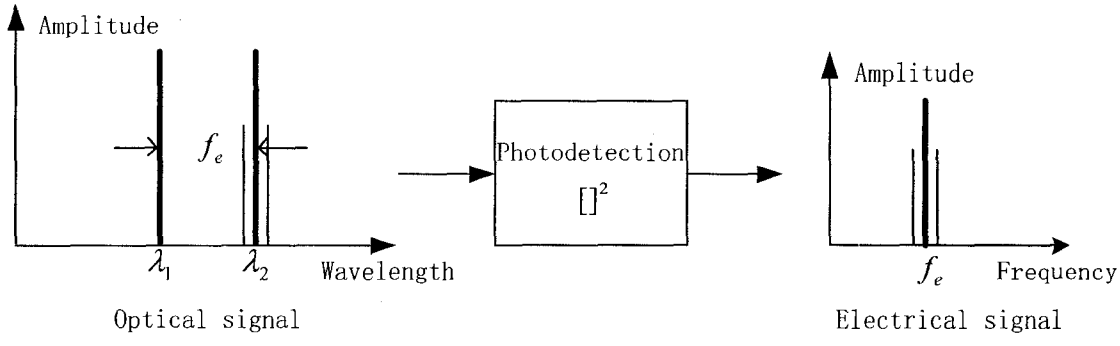

Fig. 2.10. Diagrams of spectra of the ideal optical signal and the up-converted electrical signal.

In radio-over-fiber applications, optical heterodyne technique has to be deployed to realize the required optical up-conversion. That means the optical signal distributed from a central office to various base stations contains two optical carriers which are: phase correlated, polarization aligned, separated by the desired frequency and, in addition, information is superimposed on one optical carrier. The spectra of an ideal optical signal and the up-converted electrical signal are shown in Fig. 2.10. This allows for easy generation of a millimeter-wave electrical signal and simple direct-detection of the information at remote base stations. After appropriate electrical amplification, this millimeter-wave signal is ready to be feed to an antenna for radiation. Hence, there is no need to have a high-quality local oscillator at each base station.

B. Optical up-conversion techniques

Different techniques have been reported to generate the optical signal shown in Fig. 2.10.

Fig. 2.11 shows the reported optical up-conversion configuration for electrical signal generation using automatic frequency control [1]. Since the optical carriers are generated by two separate

laser sources, information can be directly superimposed onto one of these optical carriers using an external optical intensity modulator. Then the modulated optical carrier combines with the un-modulated optical carrier to form the spectrum shown in Fig. 2.10. The feedback control would be used to keep the carrier at its proper operating frequency.

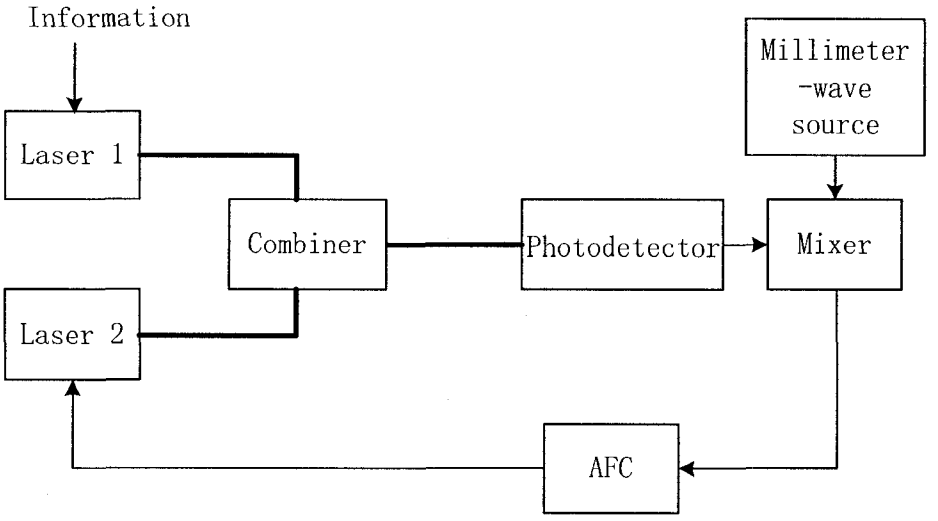

Fig. 2.11. Optical up-conversion based on millimeter wave generation with AFC technique. Thick lines indicate optical path.

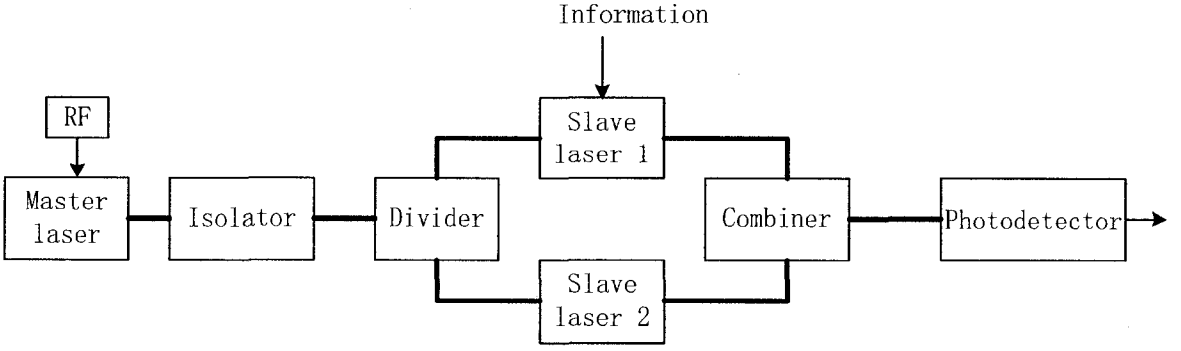

Fig. 2.12. Optical up-conversion based on millimeter wave generation with optical sideband injection locking technique. Thick lines indicate optical path.

Fig. 2.12 shows an optical up-conversion configuration using optical sideband injection locking [22]. Again, it is also possible to use external optical intensity modulation technique after either Slave laser 1 or Slave laser 2 to superimpose information.

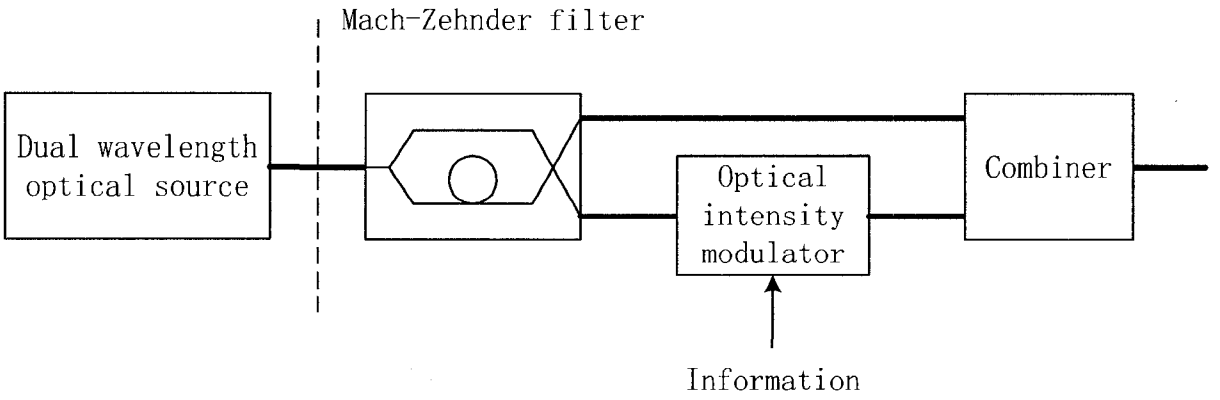

Fig. 2.13. Optical up-conversion with dual wavelength optical source. Thick lines indicate optical path.

In other electrical signal generation approaches - such as an optical phase lock loop, optical injection phase-lock loop and external optical modulation - optical up-conversion is usually based on external optical intensity modulation [20], [21]. The simplified configuration diagram of this method is shown in Fig. 2.13. It can be seen that a Mach-Zehnder filter is used to separate the two optical carriers. Then the information signal externally modulates one optical carrier and the two optical carriers are combined for fiber transmission. This separation complicates the system and limits its versatility.

Recently, based on the above basic techniques, new approaches of optical up-conversion for radio-over-fiber applications have been proposed [23]-[26].

Another important topic in this area is the nonlinear distortion of direct laser modulation and external Mach-Zehnder intensity modulation [27]-[30]. Theoretical analysis of the optical crosstalk in fiber-radio WDM networks was made by Castleford et al. in 2001 [31]. The significant nonlinear impairments: the second harmonic distortion and the wavelength division multiplexing crosstalks were studied by Funk et al. in 2002 [32]. Using a predistortion linearization method to modify the nonlinearity of a MZM in order to improve the system performance was first reported in 2003 [33]. Based on a two-tone analysis, using phase modulation and fiber-Bragg grating filters to suppress distortion for microwave-photonic links was proposed in 2007 [34]. These nonlinearity analyses and approaches to reducing optical up-conversion distortion are crucial to the performance of radio-over-fiber systems.

References

[1] R.P. Braun, G. Grosskopf, D. Rohde, and F. Schmidt, "Optical millimetre-wave generation and transmission experiments for mobile 60 GHz band communications," *Electron. Lett.*, vol. 32, no. 7, pp. 626-628, Mar. 1996.

[2] L. Goldberg, H. F. Taylor, J. F. Weller, and D. M. Bloom, "Microwave signal generation with injection-locked laser diodes," *Electron. Lett.*, vol. 19, no. 13, pp. 491-493, Jun. 1983.

[3] R. T. Ramos and A. J. Seeds, "Fast heterodyne optical phase-lock loop using double quantum well laser diodes," *Electron. Lett.*, vol. 28, no. 1, pp. 82-83, Jan. 1992.

[4] L. N. Langley, M. D. Elkin, C. Edge, M. J. Wale, U. Gliese, X. Huang, and A. J. Seeds, "Packaged semiconductor laser optical phase-locked loop (OPLL) for photonic generation, processing and transmission of microwave signals," *IEEE Trans. Microwave Theory Tech.*, vol. 47, no. 7, pp. 1257-1264, Jul. 1999.

[5] M. Hyodo, A. Sarwar, and N. Onodera, "High-purity, optoelectronic millimeter-wave signal generation by heterodyne optical phase-locking of external-cavity semiconductor lasers," *Lasers and Electro-Optics Europe*, Sept. 2000, pp. 1 pp.

[6] L.A. Johansson, D. Wake, A. J. Seeds, "Millimetre-wave over fibre transmission using a BPSK reference-modulated optical injection phase-lock loop," *Optical Fiber Communication Conference and Exhibit*, OFC 2001, vol. 3, pp. WV3-1-WV3-3, Mar. 2001.

[7] J. J. O'Reilly, P. M. Lane, R. Heidemann, and R. Hofstetter, "Optical generation of very narrow linewidth millimetre wave signals," *Electron. Lett.*, vol. 28, no. 25, pp. 2309-2311, Dec. 1992.

[8] J. J. O'Reilly and P. M. Lane, "Fibre-supported optical generation and delivery of 60 GHz signals," *Electron. Lett.*, vol. 30, no. 16, pp. 1329-1330, Aug. 1994.

[9] P. Shen, N. J. Gomes, P. A. Davies, W. P. Shillue, P.G. Huggard, and B. N. Ellison, "High-purity millimetre-wave photonic local oscillator generation and delivery," in *Proc. Microwave Photonics*, Sept. 2003, pp. 189-192.

[10] P. O. Hedekvist, B. E. Olsson, and A. Wiberg, "Harmonic generation of photonic microwave frequencies utilizing the properties of a phase modulator," in *Proc. Microwave Photonics,* Sept. 2003, pp. 193-196.

[11] R. Gindera and D. Jager, "Remote optoelectronic microwave generation in fiber radio systems using a ring oscillator," *European Microwave Conference,* Sept. 2006, pp. 1115-1117.

[12] C. Lin, W. Peng, P. Peng, C. Peng, C. Chiang, J. chen, B. Chiou, and S. Chi, "Simultaneous baseband and RF signal generation using only one single-electrode MZM based on double-sideband with optical carrier suppression," in *Proc. Microwave Photonics,* Oct. 2006, pp. 1-4.

[13] J. Yu, Z. Jia, L. Yi, Y. Su, G. Chang, and T. Wang, "Optical millimeter-wave generation or up-conversion using external modulators," *IEEE Photon. Tech. Lett.*, vol. 18, no. 1, pp. 265-267, Jan. 2006.

[14] Z. Deng, and J. P. Yao, "Photonic generation of microwave signal using a rational harmonic mode-locked fiber ring laser," *IEEE Trans. Microwave Theory Tech.*, vol. 54, no. 2, pp. 763-767, Feb. 2006.

[15] J. Yu, Z. Jia, L. Xu, L. Chen, T. wang, and G. Chang, "DWDM optical millimeter-wave generation for radio-over-fiber using an optical phase modulator and an optical interleaver," *IEEE Photon. Tech. Lett.*, vol. 18, no. 13, pp. 1418-1420, Jul. 2006.

[16] M. Mohamed, X. Zhang, B. Hraimel, and K. Wu, "Efficient photonic generation of millimeter-waves using optical frequency multiplication in radio-over-fiber systems," in *Proc. Microwave Photonics,* Oct. 2007, pp. 179-182.

[17] J. Zhang, H. Chen, M. Chen, T. Wang, and S. Xie, "A photonic microwave frequency quafrupler using two cascaded intensity modulators with repetitious optical carrier suppression," *IEEE Photon. Tech. Lett.*, vol. 19, no. 14, pp. 1057-1059, Jul. 2007.

[18] J. Yu, Z. Jia, T. wang, and G. Chang, "Centralized lightwave radio-over-fiber system with photonic frequency quadrupling for high-frequency millimeter-wave generation," *IEEE Photon. Tech. Lett.*, vol. 19, no. 19, pp. 1499-1501, Oct. 2007.

[19] A. Nirmalathas, D. Novak, C. Lim, and R. B. Waterhouse, "Wavelength reuse in the WDM optical interface of a millimeter-wave fiber-wireless antenna base station," *IEEE Trans. Microwave Theory Tech.* , vol. 49, no. 10, pp. 2006-2012, Oct. 2001.

[20] J. O'Reilly and P. Lane, "Remote delivery of video services using mm-waves and optics," *J. Lightwave Technol.*, vol. 12, no. 2, pp. 369-375. Feb. 1994.

[21] R. Hofstetter, H. Schmuck, and R. Heidemann, "Dispersion effects in optical millimeter-wave systems using self-heterodyne method for transport and generation," *IEEE Trans. Microwave Theory Tech.*, vol. 43, no. 9, pp. 2263-2269, Sept. 1995.

[22] R. P. Braun and G. Grosskopf, "Optical millimeter-wave systems for broadband mobile communications, devices and techniques," in *Proc. Broadband Communications*, Feb. 1998, pp. 51-58.

[23] H. -J. Song, J. S. Lee, and J. -I. Song, "All-optical frequency upconversion of radio over fibre signal with optical heterodyne detection," *Electron. Lett.*, vol. 40, no. 5, pp. 330-331, Mar. 2004.

[24] J. S. Lee, H. -J. Song, W. B. Kim, M. Fujise, Y. -H. Kim, and J. -I. Song, "All-optical harmonic frequency upconversion of radio over fibre signal using cross-phase modulation in semiconductor optical amplifier," *Electron. Lett.*, vol. 40, no. 19, pp. 1211-1213, Sept. 2004.

[25] H. Song, J. S. Lee, and J. Song, "Simultaneous all-optical frequency upconversion for WDM radio over fiber applications," in *Tech. Dig. IEEE MTT-S Int. Microwave Symp.*, Jun. 2005, pp. 4 pp.

[26] M. Shin and P. Kumar, "1.25 Gbps optical data channel up-conversion in 20 GHz-band via a frequency-doubling optoelectronic oscillator for radio-over-fiber systems," in *Tech. Dig. IEEE MTT-S Int. Microwave Symp.*, Jun. 2007, pp. 63-66.

[27] S. Yaalob, W. R. Wan Abdullah, M. N. Osman, A. K. Zamzuri, R. Mohamad, M. R. Yahya, A. F. Awang Mat, M. R. Mokhtar, and H. A. Abdul Rashid, "Effect of laser bias current to the third order intermodulation in the radio over fibre system," *RF and Microwave Conference,* Sept. 2006, pp. 444-447.

[28] L. Rosa, S. Selleri, G. Tartarini, P. Faccin, and E. M. Fabbri, "Distortion performance perdiction in multi-band radio over fiber systems exploiting direct laser modulation," *European Microwave Conference,* Sept. 2006, pp. 1292-1295.

[29] B. Hraimel, M. O. Twati, and K. Wu, "Closed-form dynamic range expression of dual-electrode Mach-Zehnder modulator in radio-over-fiber WDM system," *J. Lightwave Technol.*, vol. 24, no. 6, pp. 2380-2387, Jun. 2006.

[30] K. Uegaki, K. Kumamoto, K. Yasukawa, K. Inagaki, T. Higashino, K. Tsukamoto, and S. Komkj, "A novel nonlinear distortion suppression method in RoF systems using optical filter," in *Proc. Microwave Photonics,* Oct. 2007, pp. 33-36.

[31] D. Castleford, A. Nirmalathas, D. Novak, and R. S. Tucker, "Optical crosstalk in fiber-radio WDM networks," *IEEE Trans. Microwave Theory Tech.*, vol. 49, no. 10, pp. 2030-2035, Oct. 2001.

[32] E. E. Funk, A. L. Campillo, and D. A. Tulchinsky, "Nonlinear distortion and crosstalk in microwave fiber-radio links," in *Tech. Dig. IEEE MTT-S Int. Microwave Symp.*, Jun. 2002, vol. 3, pp. 1691-1693.

[33] A. Katz, W. Jemison, M. Kubak, and J. Dragone, "Improved radio over fiber performance using pre-distortion linearization," in *Tech. Dig. IEEE MTT-S Int. Microwave Symp.,* Jun. 2003, vol. 2, pp. 1403-1406.

[34] J. Zhang and T. E. Darcie, "Two-tone analysis of distortion suppression in microwave-photonic links using phase modulation and fiber-Bragg grating filters," *International Symposium on Signals, Systems and Electronics*, 2007, pp. 621-624.

PART 1

CHAPTER 3
OPTICAL GENERATION AND DISTRIBUTION OF MILLIMETER-WAVE SIGNALS

This Chapter focuses on techniques to optically generating millimeter-wave signals for radio-over-fiber systems. As reviewed in Chapter 2, most of the reported approaches usually generated a fixed frequency electrical signal. However, there are many system applications, which require a reconfigurable electrical signal. Under these circumstances, the prospect of generating a wideband, continuously tunable, millimeter-wave signal of high spectral purity becomes very attractive. Also, as reviewed in Chapter 2, external optical modulation techniques have shown great potential for generating electrical signals with high spectral purity and for realizing frequency multiplication. Using fixed optical filters and narrow bandwidth optical modulators to generate wideband, continuously tunable millimeter-wave signal is the emphasis of this Chapter.

In this Chapter, three new approaches based on optical external modulation techniques are proposed and demonstrated for generating wideband, continuously tunable, millimeter-wave signals. In Sec. 3.1, the first proposed approach based on the modulation of an optical intensity modulator plus an optical notch filter is detailed. This method generates a single-frequency millimeter-wave signal tunable from 32 to 50 GHz. In Sec. 3.2, the second proposed approach is described. This approach is based on the modulation of an optical phase modulator and an optical notch filter. It can generate two bands of millimeter-wave signals. One band is from 37.6

to 50 GHz; and another band is from 75.2 to 100 GHz. In Sec. 3.3, the third proposed approach is presented. This approach is based on the incorporation of an optical intensity modulator into a single-longitudinal-mode, fiber ring laser. This approach can generate a continuously tunable millimeter-wave signal with frequency from 32 GHz to 50 GHz; and this approach also has a function to recover an optical carrier at remote sites simultaneously.

3.1 Millimeter-wave signal generation using an optical intensity modulator

In this Section, an approach to generating and distributing a wideband, continuously tunable millimeter-wave signal using an optical intensity modulator and a wavelength-fixed optical notch filter is proposed. A millimeter-wave signal tunable from 32 GHz to 50 GHz is obtained by tuning the microwave drive signal from 8 GHz to 12.5 GHz. The generated millimeter-wave signal is stable and of high spectral purity. The integrity of the generated millimeter-wave signal maintains after transmission over a 25-km standard single-mode optical fiber.

Generation and distribution of a wide-band continuously tunable millimeter-wave signal with an optical external modulation technique [1]

Guohua Qi, Jianping Yao, *Senior Member, IEEE*, Joe Seregelyi*, Stéphane Paquet* and Claude Bélisle*

Microwave Photonics Research Laboratory

School of Information Technology and Engineering

University of Ottawa, Ottawa, Ontario, Canada K1N 6N5

(Email: jpyao@site.uottawa.ca)

* Communications Research Centre

Ottawa, Ontario, Canada K2H 8S2

Abstract

A new technique to generate and distribute a wideband, continuously tunable millimeter-wave signal using an optical external modulator and a wavelength-fixed optical notch filter is proposed. The optical intensity modulator is biased to suppress the odd-order optical sidebands. The wavelength-fixed optical notch filter is then used to filter out the optical carrier. Two second-order optical sidebands are obtained at the output of the notch filter. A millimeter-wave signal that has four times the frequency of the microwave drive signal is generated by beating the two second-order optical sidebands at a photodetector. Since no tunable optical filter is used, the system is easy to implement. A system using a LiNbO3 intensity modulator and a fiber Bragg grating filter is built. A stable and high spectral purity millimeter-wave signal tunable from 32 GHz to 50 GHz is observed on an electrical spectrum analyzer by tuning the microwave drive signal from 8 GHz to 12.5 GHz. The integrity of the generated millimeter-wave signal is maintained after transmission over a 25-km standard single-mode fiber. Theoretical analysis on the harmonic suppression with different modulation depths and filter attenuations is also discussed.

[1] Published in *IEEE Trans. Microwave Theory Tech.*, vol. 53, no. 10, pp. 3090-3097, Oct. 2005.

Index terms: Electro-optic modulator, fiber Bragg grating (FBG), microwave photonics, millimeter-wave generation, optical heterodyne.

1. Introduction

Generation and transmission of microwave and millimeter-wave signals over optical fibers are of great interest for applications such as broad-band wireless access networks operating at the millimeter-wave band, antenna remoting, phased-array antennas, optical sensors, and radars [1]-[5]. Optical generation and transmission of electrical signals have been extensively investigated with most work to date focused on high-frequency signals, especially millimeter-wave signals. This is because there are fewer difficulties with conventional electronic techniques or optical techniques in generating and distributing lower-frequency electrical signals. Furthermore, the low-frequency modulated double-sideband (DSB) optical signal suffers less from the chromatic dispersion of the fiber than that of the high-frequency modulated signal when transmitting over standard single-mode fiber (SSMF) [6]-[8].

Therefore, the highest frequency of the signal produced by these DSB techniques is limited by the bandwidth of the laser or the external modulator and the fiber chromatic dispersion. To overcome these limitations, an optical generation scheme that uses narrow bandwidth optical components to generate high-frequency electrical signals becomes attractive.

Optical microwave or millimeter-wave signal generation is usually based on heterodyne techniques by beating two optical carriers separated by the desired frequency in a square-law photodetector (PD). If the offset frequency of the two optical carriers is stable and their phases are correlated, a high spectral purity electrical signal will be generated. However, after the transmission of the two optical carriers over an SSMF, the quality of the generated microwave or millimeter-wave signal will be deteriorated because of the fiber chromatic dispersion [9].

Electrical signal generation based on optical heterodyning can be achieved by using either two stabilized lasers or one laser with an external optical modulator. The quality of the electrical signal produced by beating two free-running lasers rarely meets application specifications. Methods to further improve the signal quality, such as optical injection locking [10], [11] and optical phase-locked loop (OPLL) [12], [13], have been proposed. The OPLL techniques allow

the suppression of the low-frequency components of the phase noise that deteriorate the generated signal. However, it is difficult to suppress the high-frequency components of the phase noise unless very narrow linewidth (in kilohertz) optical sources are used [14].

Methods using a laser with an external optical modulator, such as an optical intensity modulator or optical phase modulator, have shown great potential for producing high-purity high-frequency millimeter-wave signals. These approaches are based on the inherent nonlinearity of the response of the optical modulator for generating high-order optical sidebands. Taking advantage of this property can dramatically lower the bandwidth requirements for the optical modulator and allows the use of a much lower frequency electrical drive signal. This can greatly reduce the cost of the system and makes it more practical to use.

A method to generate millimeter-wave signals using an external optical modulation technique was proposed by O'Reilly *et al.* in 1992 [15]. A frequency-doubled electrical signal was optically generated by biasing the Mach–Zehnder modulator (MZM) to suppress even-order optical sidebands. A 36-GHz millimeter-wave signal was generated when the MZM was driven by an 18-GHz microwave signal. Such a system was employed for a remote delivery of video services [16].

In 1994, O'Reilly *et al.* proposed another method to generate a frequency-quadrupled electrical signal [17]. Instead of biasing the MZM to suppress the even-order optical sidebands, this method was based on the quadratic response of an optical intensity modulator. The optical carrier, the first and third-order optical sidebands were suppressed by adjusting the drive signal level. A 60-GHz millimeter-wave signal was generated when a 15-GHz drive signal was applied to the MZM. However, to ensure a clean spectrum at the output of a PD, an imbalanced Mach–Zehnder filter with a free spectral range (FSR) equal to the spacing of the two second-order optical sidebands are used to suppress the unwanted optical components. Recently, an approach using an optical phase modulator to generate a frequency-quadrupled electrical signal was proposed [18]. In this approach, a Fabry–Perot filter was used to select the two second-order optical sidebands. An electrical signal that has four times the frequency of the electrical drive signal was generated by beating the two second-order sidebands at a PD. A key advantage of these approaches is that an optical modulator with a maximum operating frequency of 15

GHz can generate a millimeter-wave signal up to 60 GHz. However, since both approaches rely on the optical filter to select the two optical sidebands to generate tunable millimeter-wave signals, a tunable optical filter must be used, which significantly increases the complexity and the cost of the system.

For system applications with frequency reconfigurability, such as a wide-band surveillance radar, spread-spectrum or software-defined radio (SDR), continuously tunable millimeter-wave signals are highly desired. The prospect of generating a wide-band continuously tunable single-frequency millimeter-wave signal using fixed optical filters and narrow bandwidth optical modulators becomes very attractive. In this Section, we propose a new approach that can optically generate a wide-band continuously tunable millimeter-wave signal without using a tunable optical filter. The system employs an optical intensity modulator, which is biased to suppress the odd-order optical sidebands. A fiber Bragg grating (FBG) serving as a wavelength fixed notch filter is then used to filter out the optical carrier. A stable low-phase noise millimeter-wave signal at four times the frequency of the electrical drive signal is generated at the output of a PD. A 32–50-GHz millimeter-wave signal is observed on an electrical spectrum analyzer (ESA) when the electrical drive signal is tuned from 8 to 12.5 GHz. The spectral purity of the generated millimeter-wave signal is maintained after transmission over a 25-km SSMF.

2. Analysis

A. Principle of the Proposed Approach

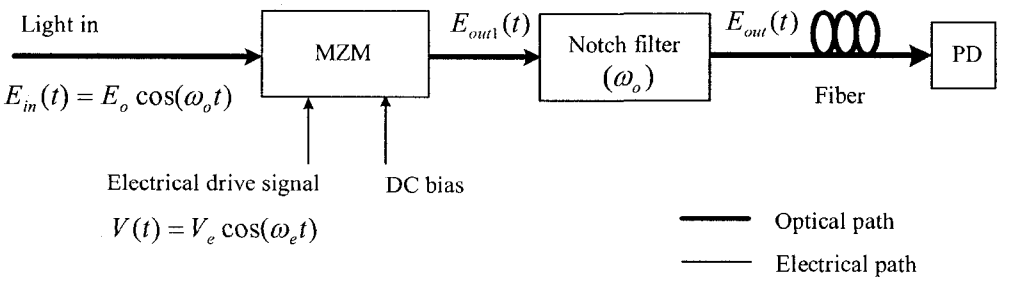

Fig. 1. Diagram of the proposed microwave signal generation system.

The proposed millimeter-wave signal generation system is shown in Fig. 1. An electrical drive signal is applied to an MZM. The MZM is biased to suppress the odd-order optical sidebands. An optical notch filter is connected at the output of the MZM to remove the optical carrier. Two

second-order optical sidebands are obtained at the output of the notch filter. A beat signal with four times the frequency of the electrical drive signal is generated at a PD.

It is known that the electric field at the output of a lithium niobate MZM, $E_{out1}(t)$, can be approximately expressed by

$$E_{out1}(t) = E_o \cos[\frac{\Phi[V(t)]}{2}] \cdot \cos(\omega_o t), \tag{1}$$

where E_o and ω_o are respectively the electric field amplitude and angular frequency of the input optical carrier, $V(t)$ is the applied electrical drive voltage, $\Phi[V(t)]$ is the optical phase difference caused by $V(t)$ between the two arms of the MZM. If the MZM is driven by a sinusoidal electrical signal and biased with a constant DC voltage, $\Phi[V(t)]$ is expressed as

$$\Phi[V(t)] = \phi_0 + \frac{\pi}{V_\pi} \cdot V_e \cos(\omega_e t), \tag{2}$$

where ϕ_0 is a constant phase shift determined by the constant DC bias voltage, V_π is the half-wave voltage at high frequency and V_e and ω_e are the amplitude and angular frequency of the electrical drive signal respectively. Substituting Eq. (2) into Eq. (1), the electric field of the output optical signal can be written as

$$E_{out1}(t) = E_o \cos(\frac{\phi_0}{2}) J_0(\beta) \cos(\omega_o t)$$

$$+ E_o \cos(\frac{\phi_0}{2}) \left\{ \sum_{n=1}^{\infty} J_{2n}(\beta) [\cos(\omega_o t - 2n\omega_e t + n\pi) + \cos(\omega_o t + 2n\omega_e t - n\pi)] \right\}$$

$$- E_o \sin(\frac{\phi_0}{2}) \left\{ \sum_{n=1}^{\infty} J_{2n-1}(\beta) \left[\sin(\omega_o t - (2n-1)\omega_e t + n\pi - \frac{\pi}{2}) - \sin(\omega_o t + (2n-1)\omega_e t - n\pi + \frac{\pi}{2}) \right] \right\}, \tag{3}$$

where J_n is the Bessel function of the first kind of order n, and $\beta = \frac{V_e}{V_\pi} \cdot \frac{\pi}{2}$ is the phase modulation index.

When the MZM is driven by an electrical signal with adequate power, a large value of β is obtained. In this case, Eq. (3) shows that the power in the input optical carrier will be spread out among the first-, second-, third-, and higher-order optical sidebands. The amplitude distribution of these sidebands is governed by the variation of Bessel functions parameterized by β. Their amplitude is also affected by ϕ_0. If all these optical sidebands are fed to a square-law photodetector, harmonics of the electrical drive signal will be generated. From the point of view of obtaining higher-order electrical harmonics and maximizing its conversion efficiency, the parameters β and ϕ_0 can be optimized. For example, ϕ_0 is tuned to suppress all even-order optical sidebands, so that the power of all even-order sidebands is transferred to the odd-order ones [15]. An efficiency-improved, frequency-doubled electrical signal is then obtained.

In our proposed method, the DC bias of the MZM is tuned to have $\phi_0 = 0, 2\pi, 4\pi, \ldots..$ Then, all the odd-order optical sidebands associated with the term $\sin(\phi_0/2)$ vanish, as indicated in Eq. (3). Only the even-order optical sidebands are kept. The power in the odd-order optical sidebands is transferred to the even-order sidebands, improving the signal generation efficiency. If the electrical drive signal is applied to the MZM with an appropriate power level, optical sidebands up to the second-order is generated and all optical sidebands above the second-order have an amplitude low enough to be ignored. But the optical carrier, represented by the term with the zero-order Bessel function (J_0) in Eq. (3), is still part of the spectrum. Then the optical signal can be approximately expressed as

$$E_{out1} \cong E_o k J_0(\beta)\cos(\omega_o t) - E_o J_2(\beta)\cos(\omega_o t - 2\omega_e t) - E_o J_2(\beta)\cos(\omega_o t + 2\omega_e t). \quad (4)$$

When this optical signal is fed to a photodetector, a strong frequency-doubled electrical signal and a weaker frequency-quadrupled electrical signal will be generated. However, when this optical signal that is composed of two second-order sidebands and one optical carrier transmits over a long span of optical fiber, the frequency-doubled electrical signal suffers from the chromatic-dispersion-induced power penalty [6]-[8], which limits its applications. And the presence of the frequency-doubled electrical signal will cause interference to the operation of the frequency-quadrupled electrical signal in a wideband system application. To eliminate the frequency-doubled electrical signal, we propose to use a wavelength-fixed optical notch filter to

filter out the optical carrier, as shown in Fig. 1. Then the electric field of the optical signal at the output of the optical notch filter can be approximately expressed as

$$E_{out} \cong -E_o J_2(\beta)\left[\cos(\omega_o t - 2\omega_e t) + \cos(\omega_o t + 2\omega_e t)\right]. \quad (5)$$

Therefore, at the output of the FBG filter, only two optical sidebands separated by four times the frequency of the drive signal are present. Applying this optical signal to a photodetector, an electrical signal that has four times the frequency of the electrical drive signal will be generated. The generated electrical signal, V_{out}, can be written as

$$V_{out} = CJ_2{}^2(\beta)\cos(4\omega_e t), \quad (6)$$

where C is a constant that is related to the responsivity of the photodetector. Since the two optical sidebands originate from the same optical source, the frequency stability and the phase noise of the generated signal are predominately determined by the electrical drive signal. Eq. (6) also shows that the amplitude of the generated electrical signal can be maximized by optimizing the value $J_2(\beta)$.

It is important to note that the DC bias level for which the odd-order optical sidebands are eliminated is not dependent on the frequency of the electrical drive signal. In addition, the optical carrier has a fixed wavelength; therefore the FBG notch filter does not need to be tunable. These characteristics ensure that the proposed approach can generate a frequency-tunable electrical signal by simply tuning the frequency of the electrical drive signal at a low frequency band.

B. Electrical harmonic suppression analysis

Usually in a wideband electrical heterodyne system, especially when the system operates over an octave bandwidth, an electrical tuned band-pass filter is always inserted between the local oscillator and the mixer to suppress the unwanted harmonics of the local carrier, to prevent the needed receive signal from the interferences caused by the harmonics of the local oscillator at the intermediate frequency (IF) when the local oscillator has poor harmonic suppression performance. But the use of an electrically tunable filter makes the system very complicated. A

direct solution to this problem is to use a highly harmonic-suppressed local oscillator. In the following we will analyze the harmonic-suppression characteristics of the proposed approach.

Assume that all odd-order optical sidebands generated by the modulation of the MZM by a sinusoidal signal can be completely suppressed by using an appropriate DC bias voltage. That means that the condition of $\phi_0 = 0, 2\pi, 4\pi, ...$ is satisfied with a constant DC bias. Assume also that the attenuation of the optical notch filter at its center notch wavelength is α dB. Based on the above assumptions, from Eq. (3) the optical signal at the output of the optical notch filter can be written as

$$E_{out1} = E_o k J_0(\beta)\cos(\omega_o t) + E_o\left\{\sum_{n=1}^{\infty} J_{2n}(\beta)[\cos(\omega_o t - 2n\omega_e t + n\pi) + \cos(\omega_o t + 2n\omega_e t - n\pi)]\right\}, \quad (7)$$

where k is the optical electrical field attenuation factor, which is related to α by $\alpha = -20\log_{10} k$.

Usually, for a commercially available MZM the maximum available phase modulation index, $\beta_{\max}$ is 2. When $0 \le \beta \le 2$, Bessel functions J_{2n} for $n > 1$ are all monotonically increasing with respect to β and monotonically decreasing with respect to the order of Bessel function n. And $J_2(2) = 0.35283$, $J_4(2) = 0.033996$, $J_6(2) = 0.0012024$. So it is reasonable to ignore the optical sidebands with Bessel coefficient higher than $J_4(\beta)$ in our discussion. Therefore, Eq. (7) can be further simplified to

$$E_{out1} \cong E_o k J_0(\beta)\cos(\omega_o t) - E_o J_2(\beta)\cos(\omega_o t - 2\omega_e t) - E_o J_2(\beta)\cos(\omega_o t + 2\omega_e t)$$

$$+ E_o J_4(\beta)\cos(\omega_o t - 4\omega_e t) + E_o J_4(\beta)\cos(\omega_o t + 4\omega_e t). \quad (8)$$

Eq. (8) shows that the optical signal consists of an attenuated optical carrier and 4 optical sidebands. The spectrum of this optical signal is illustrated as in Fig. 2. The arrow direction shows their initial phase with respect to the phase of the optical carrier before transmission.

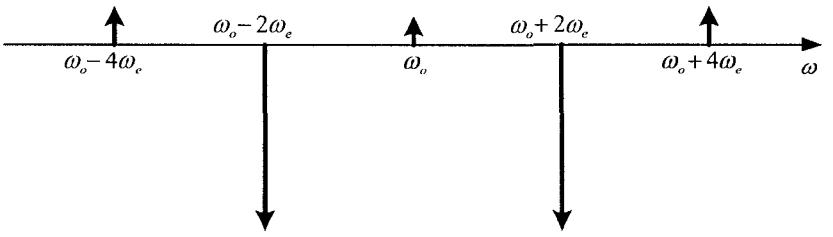

Fig. 2. Illustration of the optical spectrum at the output of the optical notch filter.

When the optical signal shown in Fig. 2 transmits over a single mode fiber, the chromatic dispersion of the fiber will cause an extra phase shift to each optical sideband compared to the optical carrier. By expanding the propagation constant $\beta(\omega)$ of the fiber for each optical sideband to a Taylor series around the angular frequency of the optical carrier, i.e. [19]

$$\beta(\omega_o \pm 2n\omega_e) = \beta(\omega_o) + \beta'(\omega_o)(\pm 2n\omega_e) + \frac{1}{2}\beta''(\omega_o)(\pm 2n\omega_e)^2 + ..., \tag{9}$$

where $\beta'(\omega_o)$ and $\beta''(\omega_o)$ is the first- and second-order derivative of the propagation constant $\beta(\omega)$ at the angular frequency ω_o, respectively. The effect of higher-order dispersion is neglected for the single mode fiber at 1550 nm band [20]. And $\beta''(\omega_o)$ can be expressed by the chromatic dispersion parameter D as

$$\beta''(\omega_o) = -\frac{c}{2\pi f_o^{\,2}} D \quad , \tag{10}$$

where c is the speed of light in free space and f_o is the frequency of the optical carrier.

The electric field representing the optical signal at the end of the transmission over a single mode fiber of length L can be obtained by adding the transmission phase delay, $\beta(\omega_o \pm 2n\omega_e)L$, to the corresponding optical sideband shown in Eq. (8). Electrical harmonics will be generated by applying this optical signal to a photodetector. The output voltage of the generated high-frequency electrical signal is

$$V_{out} \propto -2E_o^{\,2}\left\{kJ_0(\beta)J_2(\beta)\cos\left[4\pi cDL\left(\frac{f_e}{f_o}\right)^2\right]+J_2(\beta)J_4(\beta)\cos\left[12\pi cDL\left(\frac{f_e}{f_o}\right)^2\right]\right\}\cos[2\omega_e t-2\omega_e\beta'(\omega_o)L]$$
$$+E_o^{\,2}\left\{J_2^{\,2}(\beta)+2kJ_0(\beta)J_4(\beta)\cos\left[16\pi cDL\left(\frac{f_e}{f_o}\right)^2\right]\right\}\cos[4\omega_e t-4\omega_e\beta'(\omega_o)L]$$
$$-2E_o^{\,2}\left\{J_2(\beta)J_4(\beta)\cos\left[12\pi cDL\left(\frac{f_e}{f_o}\right)^2\right]\right\}\cos[6\omega_e t-6\omega_e\beta'(\omega_o)L]\text{,} \tag{11}$$

where f_e is the frequency of the electrical drive signal. The electrical spectrum of the generated signal expressed by Eq. (11) is illustrated as in Fig. 3.

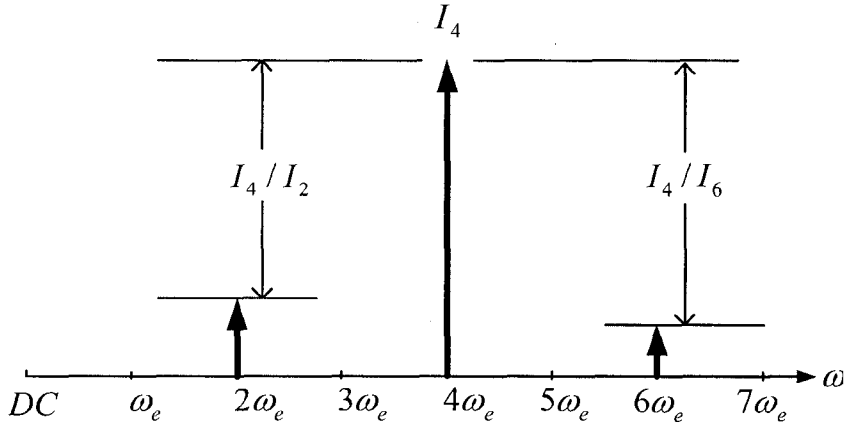

Fig.3. Illustration of the electrical spectrum at the output of a photodetector.

From Eq. (11), the power intensity of the fourth-order electrical harmonic I_4 is proportional to the coefficients of optical sidebands

$$I_4 \propto \frac{E_o^{\,4}}{2}\left\{J_2^{\,2}(\beta)+2kJ_0(\beta)J_4(\beta)\cos\left[16\pi cDL\left(\frac{f_e}{f_o}\right)^2\right]\right\}^2. \tag{12}$$

The power intensities of the second- and sixth-order electrical harmonics,, I_2, I_6 are

$$I_2 \propto 2E_o^{\,4}\left\{kJ_0(\beta)J_2(\beta)\cos\left[4\pi cDL\left(\frac{f_e}{f_o}\right)^2\right]+J_2(\beta)J_4(\beta)\cos\left[12\pi cDL\left(\frac{f_e}{f_o}\right)^2\right]\right\}^2, \tag{13}$$

$$I_6 \propto 2E_o^{\,4}\left\{J_2(\beta)J_4(\beta)\cos\left[12\pi cDL\left(\frac{f_e}{f_o}\right)^2\right]\right\}^2. \tag{14}$$

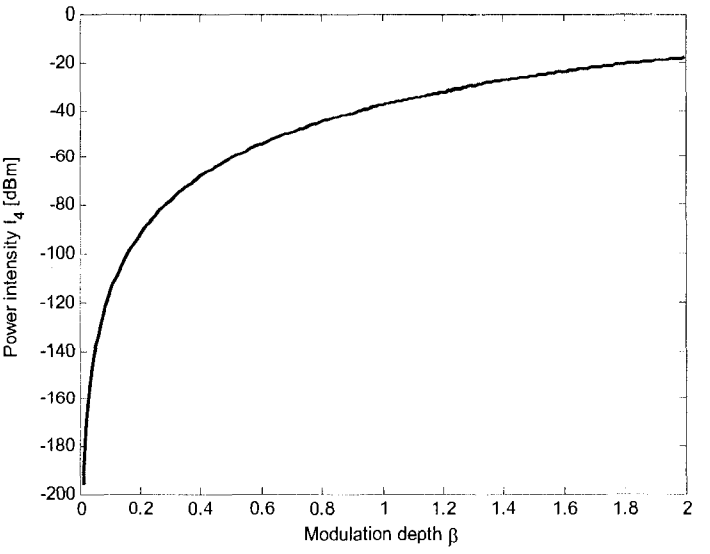

(a)

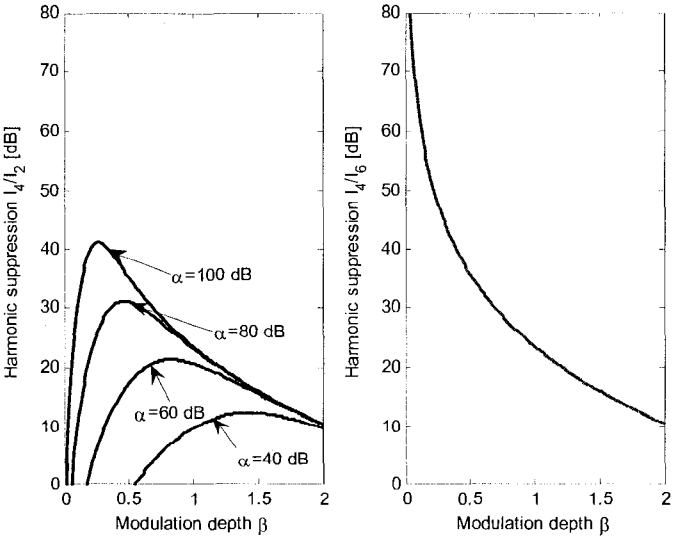

(b)

Fig. 4. Power intensity and harmonic suppressions vs. modulation depth. (a) Power intensity I_4 of the fourth-order harmonic. (b) Harmonic suppressions I_4 / I_2 and I_4 / I_6. (Frequency of the electrical drive signal f_e =12.5 GHz)

For a distribution system that operates at 1550 nm with a transmission distance of 25 km over standard single mode fiber with $D = 17 ps/(nm \cdot km)$, the power intensity I_4 and the harmonic suppressions of I_4 / I_2 and I_4 / I_6 versus the modulation depth β ($0 \le \beta \le 2$) are plotted in Fig. 4.

Fig. 4 (a) shows that the power intensity I_4 is monotonically increasing for $0 \le \beta \le 2$, and Fig. 4 (b) shows that the harmonic suppression I_4/I_2 is monotonically decreasing for $0.5 \le \beta \le 2$ and $\alpha \ge 80$ dB, and for $0.25 \le \beta \le 2$ and $\alpha \ge 100$ dB; the harmonic suppression I_4/I_6 is monotonically decreasing for $0 \le \beta \le 2$, which is independent of the attenuation α of the optical notch filter. With a large attenuation of the optical notch filter, a lower modulation depth corresponds to an improved harmonic suppression. As can be seen from Fig. 4 (b), for $\alpha = 100$ and $0.25 \le \beta \le 2$, the lower the modulation depth the higher the harmonic suppression. However, lower modulation depth leads to a lower output power of the fourth-order electrical harmonic, as shown in Fig. 4 (a). This problem can be solved at low cost by using erbium doped fiber amplifiers (EDFAs) at 1550 nm band. Note that a lower modulation depth means a less power requirement for the electrical drive signal.

Fig. 5 shows the power variation of the generated electrical signal I_4, which is caused by the combined effects of the limited attenuation of the optical carrier and the chromatic dispersion of the fiber, when tuning the frequency of the electrical drive signal from 8 GHz to 15 GHz. It is clearly seen that when $\alpha \ge 40$ dB, this power variation is smaller than 0.03 dB. That means the amplitude of the frequency-quadrupled electrical signal is stable over the tuning band when β is a constant and $\alpha \ge 40$ dB. Small ripples found in Fig. 5 are caused by the chromatic dispersion of the 25-km single mode fiber.

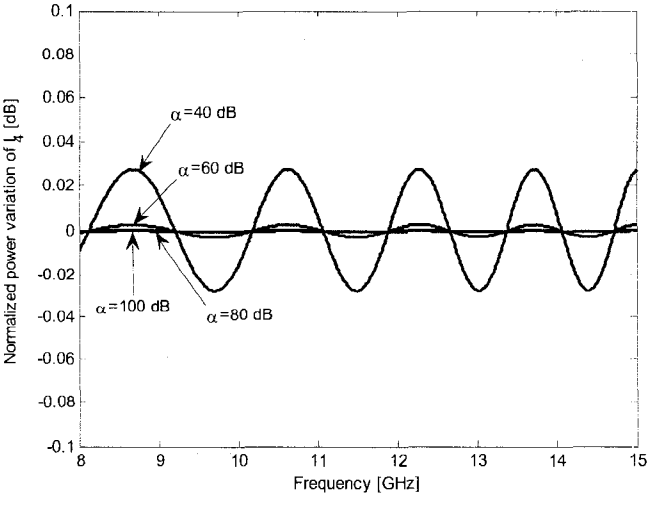

Fig. 5. Power variation of I_4 vs. frequency of the electrical drive signal. (Modulation depth β =0.6)

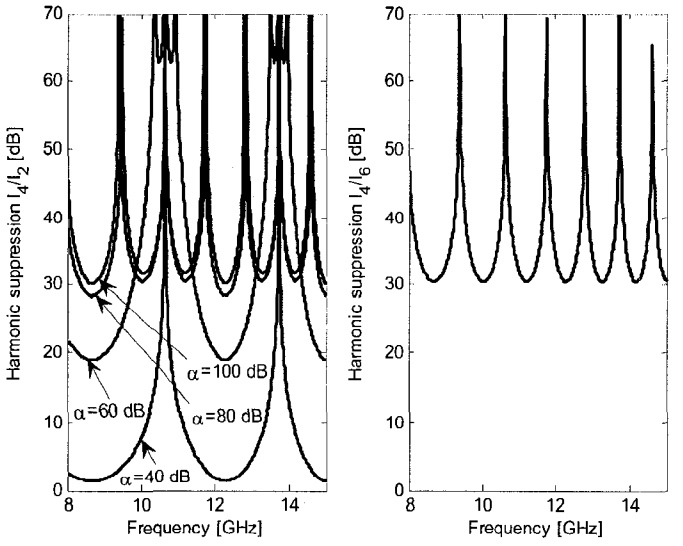

(a)

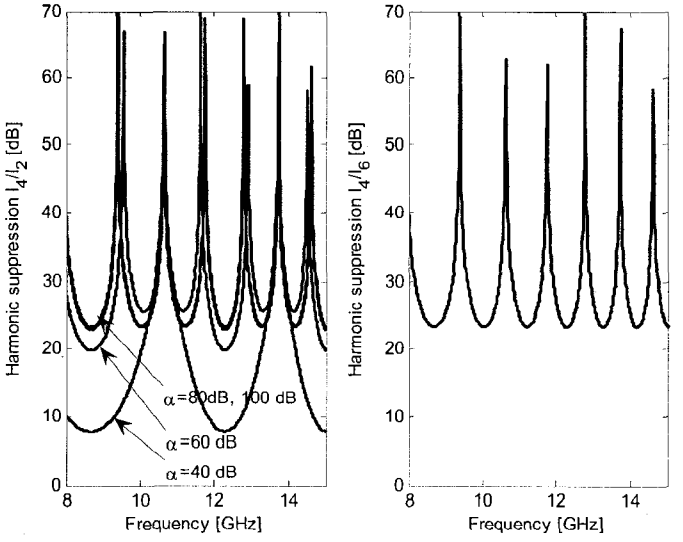

(b)

Fig. 6. Harmonic suppressions vs. frequency of the electrical drive signal. (a) Modulation depth β =0.6. (b) Modulation depth β =0.9.

Fig. 6 (a) shows that when the modulation depth $\beta = 0.6$, minimum value of I_4 / I_2 is around 2 dB with α=40 dB, greater than 18.5 dB with $\alpha = 60$ dB, 28.3 dB with $\alpha = 80$ dB and 30 dB with $\alpha = 100$ dB; minimum value of I_4 / I_6 is greater than 30 dB and is independent of α. That means with a small value of modulation depth the harmonic suppression is mostly affected by the attenuation of the optical notch filter. Fig. 6 (b) indicates that with a small value of the

attenuation of the optical notch filter, increasing the modulation depth of the MZM from 0.6 to 0.9 improves the harmonic suppression. The minimum value of I_4/I_2 has increased from 2 dB to 7.7 dB for α=40dB case, 18.5 dB to 19.7 dB for $\alpha = 60$ dB case.

3. Experiment

In order to validate the proposed method and verify the analysis, an experimental setup shown in Fig. 7 is built. The spectral purity of the generated mm-wave signal is evaluated both before (local signal) and after (remote signal) propagation over 25 km of standard single-mode fiber. Light from a tunable laser source (TLS) is applied to the MZM via a polarization controller (PC). The MZM is a commercially available lithium niobate modulator, which is biased to suppress all the odd-order optical sidebands. An FBG filter with a central wavelength equal to the wavelength of the optical carrier is used as an optical notch filter. The optical carrier is removed at the output of the FBG filter. The transmission spectrum of the FBG filter is shown in Fig. 8. The bandwidth from the minimum attenuation point at lower wavelengths to the minimum attenuation point at longer wavelengths is about 0.3 nm (≈37.5 GHz).

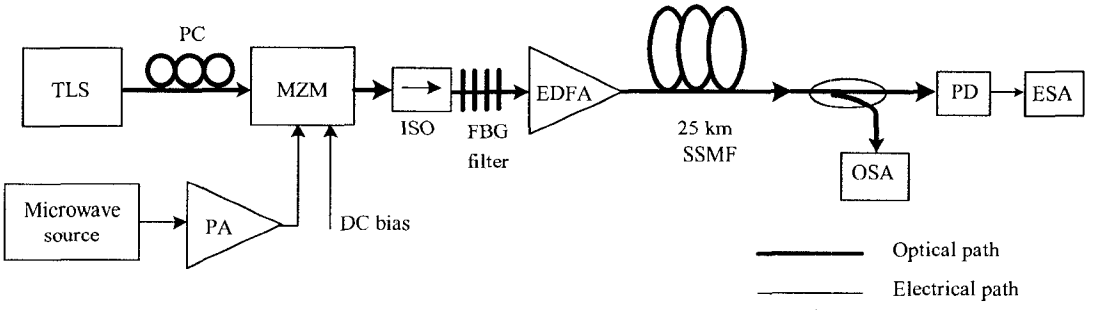

Fig.7. Experimental setup for optical generation and transmission of mm-wave signals. (TLS: tunable laser source, MZM: Mach-Zehnder modulator, EDFA: erbium-doped fiber amplifier, PA: power amplifier, OSA: optical spectrum analyzer, PD: photodetector, ESA: electrical spectrum analyzer, SSMF: standard single mode fiber)

A 25-dBm microwave signal with frequencies tunable from 8 GHz to 15 GHz is used to drive the MZM. By appropriately adjusting the DC bias voltage of the MZM, the odd-order optical sidebands are suppressed as indicated by Eq. (3). The optical spectrum at the output of the MZM is shown in Fig. 9 (a). The optical carrier is then suppressed by the FBG filter. The optical spectrum is shown in Fig. 9 (b).

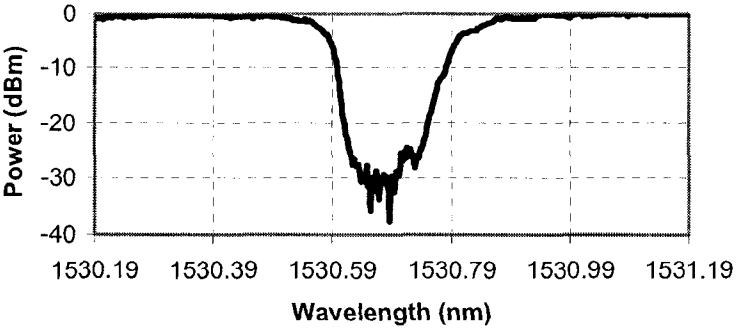

Fig. 8. Transmission spectrum of the FBG filter.

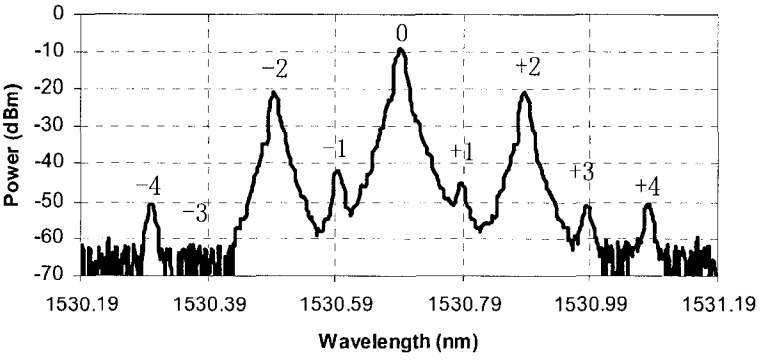

(a)

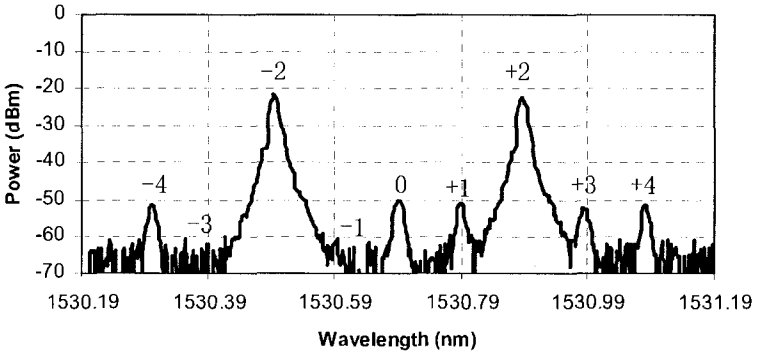

(b)

Fig. 9. Optical spectra before transmission. (a) Before the FBG filter. (b) After the FBG filter.

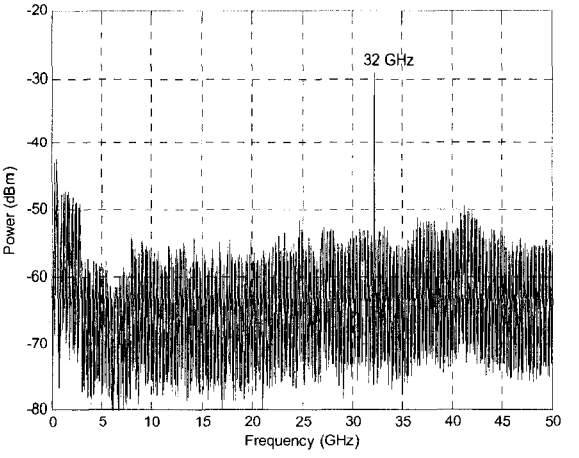

(a)

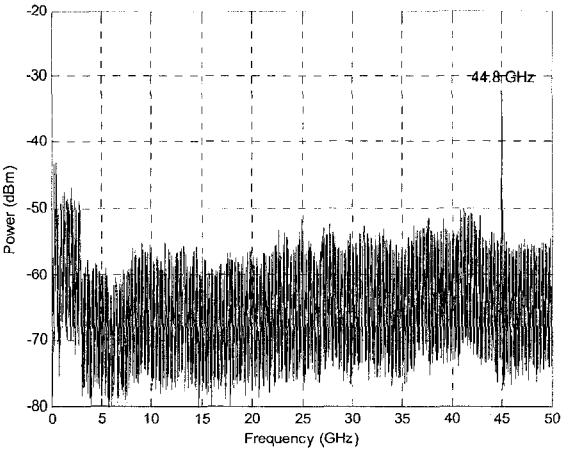

(b)

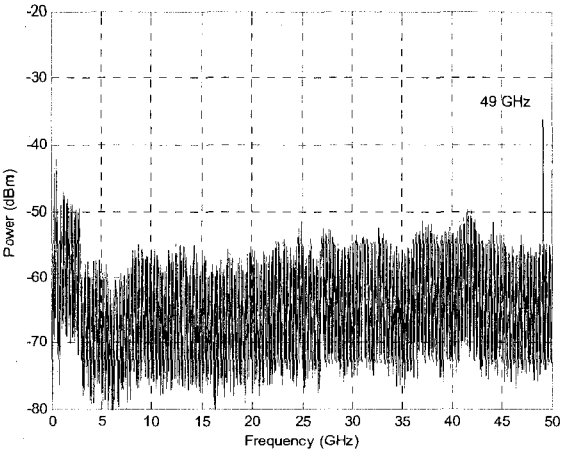

(c)

Fig. 10. The spectra of the generated mm-wave signals. (a) 32 GHz. (b) 44.8 GHz. (c) 49 GHz.

Fig. 10 shows the spectra of the generated electrical signals when the microwave drive signal is tuned at 8 GHz, 11.2 GHz and 12.25 GHz. Beating signals with frequencies four times of the drive signals are generated. It can be seen from Fig. 10 that mm-wave signals at the frequency of 32 GHz, 44.8 GHz, and 49 GHz are generated. The spectra are very clean, no other beating signals can be observed across the 50 GHz band.

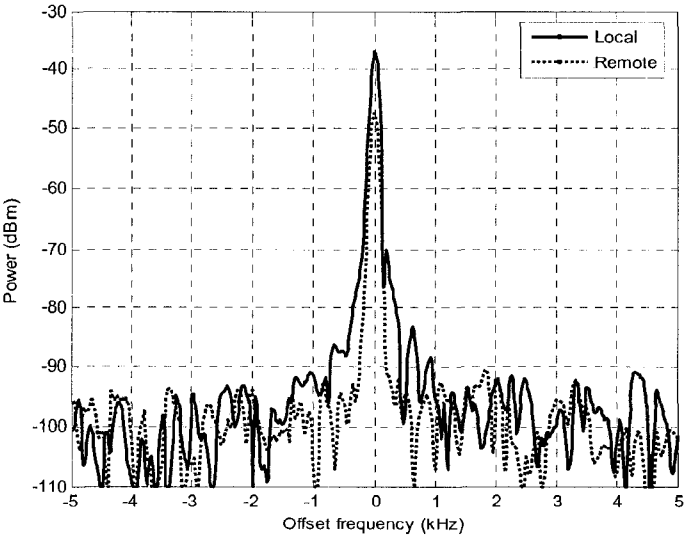

(a)

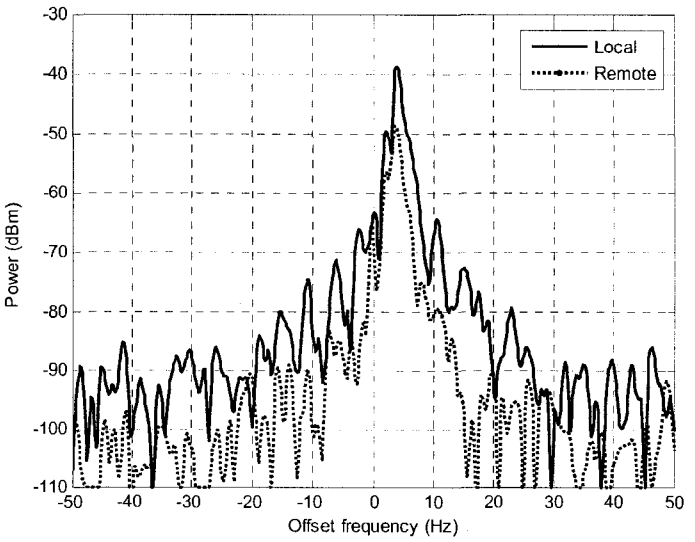

(b)

Fig. 11. Spectra of the 50-GHz signal generated locally and remotely. (a) Frequency span 10 kHz. (b) Frequency span 100 Hz.

Fig. 11 gives zoom-in views of the beating signal generated locally and remotely after transmission over 25-km signal mode fiber. The frequency of the electrical drive signal is tuned at 12.5 GHz; the generated mm-wave signal is at 50 GHz. As can be seen, the signal spectral purity of the remotely generated signal is maintained, which demonstrates that the signal is not seriously affected by the chromatic dispersion of the 25-km, single-mode fiber.

The lowest frequency of 32 GHz that can be generated by the proposed system is determined by the bandwidth of the FBG notch filter. With a narrower optical notch filter, this frequency could be much lower than 32 GHz. On the other hand, the highest frequency of the generated signal is only limited by the bandwidth of the optical intensity modulator. The intensity modulator used in the experiment can operate up to 15 GHz, so the highest frequency of the generated mm-wave signal can reach up to 60 GHz. Due to the bandwidth limitation of the photodetector and the electrical spectrum analyzer, the 60 GHz signal was not observed in electrical domain. However, optical spectrum observation supports the 60 GHz signal generation.

4. Conclusion

We have proposed and demonstrated a novel microwave-photonics system that could generate and distribute a broadband, frequency-tunable mm-wave signal using a low-frequency intensity modulator and a wavelength-fixed optical notch filter. The technique was based on the nonlinear response of the intensity modulator by properly biasing it to suppress the odd-order optical sidebands. The optical carrier was then removed by the optical notch filter. Since no tunable optical filter was used, the system was easy to implement. Theoretical analysis on the harmonic suppression with different modulation depths and filter attenuations was discussed. A system using a $LiNbO_3$ intensity modulator and an FBG filter was built. The results showed that a stable, high spectral purity mm-wave signal from 32 GHz to 50 GHz was directly observed on an electrical spectrum analyzer by tuning an electrical drive signal from 8 GHz to 12.5 GHz. The generated mm-wave signal was distributed over 25-km standard single mode fiber; the integrity of the generated mm-wave signal at the end of the fiber span was maintained after the transmission.

Acknowledgements

The authors would like to thank John Oldham, David Barlow, Fei Zeng and Xiangfei Chen for their assistance in setting up the experimental system.

References:

[1] A. J. Cooper, "Fiber/radio for the provision of cordless/mobile telephony services in the access network," *Electron. Lett.*, vol. 26, no. 24, pp. 2054-2056, Nov. 1990.

[2] A. J. Seeds, "Broadband wireless access using millimeter-wave over fiber systems," in *Tech. Dig. IEEE MTT-S Int. Microwave Symp.*, Jun. 1997, vol. 1, pp. 23-25.

[3] R. P. Braun, G. Grosskopf, D. Rohde, and F. Schmidt, "Optical millimetre-wave generation and transmission experiments for mobile 60 GHz band communications," *Electron. Lett.*, vol. 32, no. 7, pp. 626-628, Mar. 1996.

[4] H. Ogawa, D. Polifko, and S. Bamba, "Millimeter-wave fiber optics systems for personal radio communications," *IEEE Trans. Microwave Theory Tech.*, vol. 40, no. 12, pp. 2285-2293, Dec. 1992

[5] L. Nöel, D. Wake, D. G. Moodie, D. D. Marcenac, L. D. Westbrook, and D. Nesset, "Novel techniques for high capacity 60 GHz fiber-radio transmission systems," *IEEE Trans. Microwave Theory Tech.*, vol. 45, no. 8, pp. 1416-1423, Aug. 1997.

[6] H. Schmuck, "Comparison of optical millimeter-wave system concepts with regard to chromatic dispersion," *Electron. Lett.*, vol. 31, no. 21, pp. 1848-1849, Oct. 1995.

[7] U. Gliese, S. Nφrskov, and T. N. Nielsen, "Chromatic dispersion in fiber-optic microwave and millimeter-wave links," *IEEE Trans. Microwave Theory Tech.*, vol. 44, no. 10, pp. 1716-1724, Oct. 1996.

[8] G. H. Smith, D. Novak, and Z. Ahmed, "Overcoming chromatic-dispersion effects in fiber-wireless systems incorporating external modulators," *IEEE Trans. Microwave Theory Tech.*, vol. 45, no. 8, pp. 1410-1415, Aug. 1997.

[9] R. Hofstetter, H. Schmuck, and R. Heidemann, "Dispersion effects in optical millimeter-wave systems using self-heterodyne method for transport and generation," *IEEE Trans. Microwave Theory Tech.*, vol. 43, no. 9, pp. 2263-2269, Sept. 1995.

[10] L. Goldberg, H. F. Taylor, J. F. Weller, and D. M. Bloom, "Microwave signal generation with injection-locked laser diodes," *Electron. Lett.*, vol. 19, no. 13, pp. 491-493, Jun. 1983.

[11] T. Jung, J.-L. Shen, D. T. K. Tong, S. Murthy, M. C. Wu, T. Tanbun-Ek, W. Wang, R. Lodenkamper, R. Davis, L. J. Lembo, and J. C. Brock, "CW injection locking of a mode-locked semiconductor laser as a local oscillator comb for channelizing broad-band RF signals," *IEEE Trans. Microwave Theory Tech.*, vol. 47, no. 7, pp. 1225-1233, Jul. 1999.

[12] R. T. Ramos, and A.J. Seeds, "Fast heterodyne optical phase-lock loop using double quantum well laser diodes," *Electron. Lett.*, vol. 28, no. 1, pp. 82-83, Jan. 1992.

[13] M. Hyodo, K. S. Abedin, and N. Onodera, "High-purity, optoelectronic millimeter-wave signal generation by heterodyne optical phase-locking of external-cavity semiconductor lasers," *Lasers and Electro-Optics Europe*, Sept. 2000, pp. 1 pp.

[14] F. N. Timofeev, S. Bennett, R. Griffin, P. BayveL, A. J. Seeds, R. Wyatt, R. Kashyap, and M. Robertson, "High spectral purity millimetre-wave modulated optical signal generation using fibre grating lasers," *Electron. Lett.*, vol. 34, no. 7, pp. 668-669, Apr. 1998.

[15] J. J. O'Reilly, P. M. Lane, R. Heidemann, and R. Hofstetter, "Optical generation of very narrow linewidth millimetre wave signals," *Electron. Lett.*, vol. 28, no. 25, pp. 2309-2311, Dec. 1992.

[16] J. J. O'Reilly and P. M. Lane, "Remote delivery of video services using mm-wave and optics," *J. Lightwave Technol.*, vol. 12, no. 2, pp. 369-375, Feb. 1994.

[17] J. J. O'Reilly and P.M. Lane, "Fibre-supported optical generation and delivery of 60GHz signals," *Electron. Lett.*, vol. 30, no. 16, pp. 1329-1330, Aug. 1994.

[18] P. Shen, N. J. Gomes, P. A. Davies, W. P. Shillue, P. G. Huggard, and B. N. Ellison, "High-purity millimetre-wave photonic local oscillator generation and delivery," in *Proc. Microwave Photonics*, Sept. 2003, pp. 189-192.

[19] K. Okamoto, *Fundamentals of Optical Waveguides*. New York: Academic Press, 2000, pp. 72-72.

[20] W. K. Marshall, B. Crosignani, and A. Yariv, "Laser phase noise to intensity noise conversion by lowest-order group-velocity dispersion in optical fiber: exact theory," *Opt. Lett.*, vol. 25, no. 3, pp. 165-167, Feb. 2000.

3.2 Millimeter-wave signal generation using an optical phase modulator

In this Section, a millimeter-wave signal generation method based on the modulation of an optical phase modulator is proposed. Two wide bands of continuously tunable millimeter-wave signals are generated with an optical phase modulator and a fixed optical notch filter. Analysis shows that dispersion compensation is required in order to eliminate the power fluctuation of the generated electrical signal, and to maintain the suppression of the odd-order electrical harmonics when the optical signal is distributed using conventional single mode optical fiber. Experimentally, two bands of millimeter-wave signals from 37.6 GHz to 50 GHz and from 75.2 GHz to 100 GHz with high spectral purity are generated locally and remotely, when the electrical drive signal is tuned from 18.8 GHz to 25 GHz. As there is no DC bias needed in this method, this method does not have DC bias drifting problem observed when an optical intensity modulator is used.

Optical generation and distribution of continuously tunable millimeter-wave signals using an optical phase modulator[2]

Guohua Qi, Jianping Yao, *Senior Member, IEEE*, Joe Seregelyi*, Stéphane Paquet* and Claude Bélisle*

Microwave Photonics Research Laboratory

School of Information Technology and Engineering

University of Ottawa, Ottawa, Ontario, Canada K1N 6N5

(Email: jpyao@site.uottawa.ca)

* Communications Research Centre

Ottawa, Ontario, Canada K2H 8S2

Abstract

In this Section, we propose an approach to generate and distribute two wide bands of continuously tunable millimeter-wave (mm-wave) signals using an optical phase modulator and a fixed optical notch filter. We demonstrate theoretically that the odd-order electrical harmonics are cancelled and even-order electrical harmonics are generated at the output of a photodetector when the optical carrier is filtered out from the phase modulated optical spectrum. Analysis shows that dispersion compensation is required in order to eliminate the power fluctuation of the generated electrical signal and to maintain the suppression of the odd-order electrical harmonics when the optical signal is distributed using conventional single mode optical fiber. It is experimentally demonstrated that, when the electrical drive signal is tuned from 18.8- 25 GHz, two bands of millimeter-wave signals from 37.6 -50 GHz and from 75.2 -100 GHz with high spectral purity are generated locally and remotely. This approach does not suffer from the DC bias drifting problem observed when an optical intensity modulator is used.

Index term: Fiber Bragg grating (FBG), microwave photonics, millimeter-wave (mm-wave) generation, optical heterodyne, optical phase modulator.

1. Introduction

[2] Published in *J. Lightwave Technol.*, vol. 23, no. 9, pp. 2687-2695, Sept. 2005.

Optically generated microwave and mm-wave signals can find applications in many fiber-supported microwave and mm-wave systems. Examples of these include: carrier generation and distribution in broadband wireless access networks and antenna remoting; local oscillator creation in radar systems; signal synthesis in software defined radio; application of true-time delay in phased array antenna; and source generation for Brillouin scattering in optical sensors [1]. These systems take advantage of the extremely low transmission loss (0.2 dB/km) of the standard single mode fiber and the availability of erbium doped fiber amplifier (EDFA) at 1550 nm band for distributing microwave and mm-wave signals over long distances.

These microwave and mm-wave signal sources have been extensively investigated with most work to date focusing on high-frequency electrical signal generation - especially on mm-wave signal generation up to the 60 GHz band with narrow-bandwidth optical components. This is because high-frequency electrical signal generation using conventional electronics becomes less financially attractive for systems operating above about 26 GHz, and their distribution via wireless or co-axial methods is highly challenging when compared to optical methods. On the other hand, low-frequency electrical carriers can be generated by direct modulation of a laser diode (LD) or by external modulation using an optical intensity modulator. When compared to high-frequency signals, the power penalty and phase noise degradation induced on these low-frequency signals by chromatic dispersion of the fiber is less severe, even without dispersion compensation [2]-[4].

Many different approaches have been proposed to design mm-wave sources based on optical heterodyne techniques. They can be roughly classified into two types: one type is based on two stabilized lasers and the other is based on one laser plus an external optical modulator. Methods based on two stabilized lasers include the use of injection locking [5], and phase-locked loops [6]. Methods with one laser plus an external optical modulator have shown great potential for producing high-purity mm-wave signals [7]-[9]. These approaches are based on the inherent non-linearity of the phase modulator's response and, as a result, a high-frequency electrical signal can be optically generated with a low-frequency drive signal. Frequency doubling [7] or quadrupling [8], [9] becomes achievable. This dramatically lowers the bandwidth requirements for the optical modulator, the electrical drive signal source and the drive circuit itself. For the frequency quadrupling approaches [8], [9], additional components such as Mach-Zehnder-

modulator (MZM) based or Fabry-Perot (FP) filters are used to select the desired optical sidebands in order to obtain an electrical signal with a clean spectrum. The free spectral range (FSR) of these optical filters determines the frequency of the generated electrical signal. These methods work well for fixed frequency applications, but for systems with frequency reconfigurability, such as wideband surveillance radar, spread-spectrum or software defined radio, continuously tunable mm-wave signals are required.

Tunable optical filters would be required to realize a tunable mm-wave source using the methods mentioned in [8] and [9]. This adds extra complexity that can be avoided by exploring other approaches. The method described in [7] provides a solution to generate a tunable, frequency-doubled electrical signal. The DC bias is adjusted to suppress the even-order optical sidebands from the optical intensity modulator output spectrum. Therefore, an optical filter is not needed. However, biasing the intensity modulator to suppress the even-order optical sidebands suffers from a DC bias-drifting problem, which reduces the robustness of the system.

In this Section, we propose a robust method for the optical generation of two bands of continuously, tunable mm-wave signals using an optical phase modulator and a fixed optical notch filter. Frequency doubling and quadrupling of the electrical drive signal can be achieved without specific DC bias adjustment. A theoretical model of the proposed method and a mathematical analysis of the chromatic dispersion effect on the generated signal when distributed over optical fiber are presented. We successfully generate two bands of mm-wave signals_that can be tuned from 37.6 GHz to 50 GHz with frequency doubling, and from 75.2 GHz to 100 GHz with frequency quadrupling using a commercially available optical phase modulator and a fiber Bragg grating (FBG) serving as the fixed optical notch filter. We show that the spectral purity of the signal remains unchanged when remote generation is performed at the end of 60 km span of single-mode fiber with proper dispersion compensation.

2. Analysis

A. Principle of the proposed approach

A well-known method for optical generation of electrical signals is based on optical heterodyne technique. In our proposed approach, the two optical carriers used for heterodyning originate

from the same optical source. As a result, there is a high level of phase noise correlation between the two carriers. Therefore, the generated signal will have low phase noise and stable amplitude and frequency, a requirement for most system applications.

The operating principle of the proposed method is illustrated in Fig. 1.

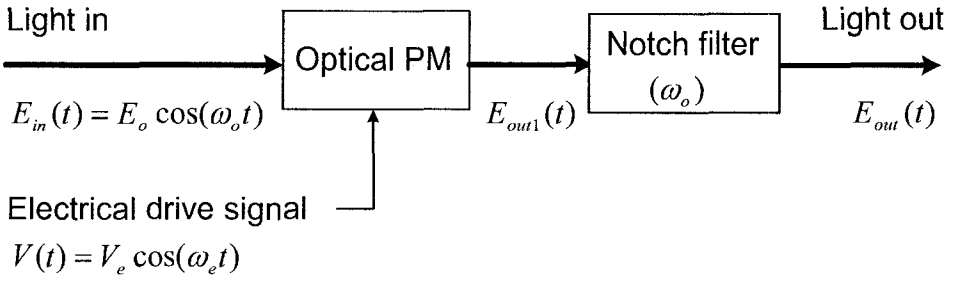

Fig. 1. Schematic diagram of the proposed mm-wave generation method. (Optical PM: optical phase modulator)

To simplify the analysis, we use pure sinusoidal signals to represent the electrical and optical sources without loss of generality. The waveform at the output of an optical phase modulator ($E_{out1}(t)$) driven by a pure sinusoidal electrical signal is given by

$$E_{out1}(t) = E_o \sum_{n=-\infty}^{\infty} J_n(\beta) \cos\left[(\omega_o + n\omega_e)t + n \cdot \frac{\pi}{2}\right], \tag{1}$$

where E_o and ω_o are the amplitude and angular frequency of the optical carrier; ω_e is the angular frequency of the electrical drive signal, $J_n(\beta)$ is a Bessel function of the first kind of order n with argument of β. $\beta = \frac{\pi}{V_\pi} \cdot V_e$ is related to the phase modulation depth, where V_π is the half-wave voltage of the optical phase modulator and V_e is the amplitude of the electrical drive signal.

Equation (1) shows that the power of the input optical carrier will be spread out to the first-, second-, third- and higher-order optical sidebands. The amplitude distribution of the sidebands is governed by the variation of the Bessel functions parameterized by β. Although equation (1) indicates that there are many optical sidebands at the output of the phase modulator, their beating at a photodetector will only generate a DC component. This is because all of the optical sidebands are related in amplitude and phase, and as a result, the beat products cancel. This

behavior is expected since the phase modulation does not alter the amplitude of the input optical carrier, and the square-law photodetector works like an envelope detector. Once converted to the electrical domain, the unfiltered optical output of the phase modulator can be mathematically expressed as

$$V_{out1}(t) = C\left[\sum_{n=-\infty}^{\infty} J_n(\beta)\cos\left[(\omega_o + n\omega_e)t + n\cdot\frac{\pi}{2}\right]\right]^2 = \frac{C}{2}\sum_{n=-\infty}^{\infty}[J_n(\beta)]^2 = \frac{C}{2}, \tag{2}$$

where C is a constant, which is related to E_o and the responsivity of the photodetector. The intrinsic insensitivity of the photodetector to the phase of the optical carrier means that only the amplitude is detected, and the DC component at its output will be proportional to that amplitude. Note that, in equation (2), all terms proportional to $\cos[2(\omega_o + n\omega_e)t + n\pi]$, $(n = -\infty, +\infty)$ are omitted because of the limited bandwidth of the receiving circuit.

Next, we filter out the optical carrier at the output of the phase modulator using a notch filter. The electric field at the output of the filter can be expressed as

$$E_{out}(t) = E_o\{\sum_{n=-\infty}^{\infty} J_n(\beta)\cos\left[(\omega_o + n\omega_e)t + n\cdot\frac{\pi}{2}\right] - J_0(\beta)\cos(\omega_o t)\}. \tag{3}$$

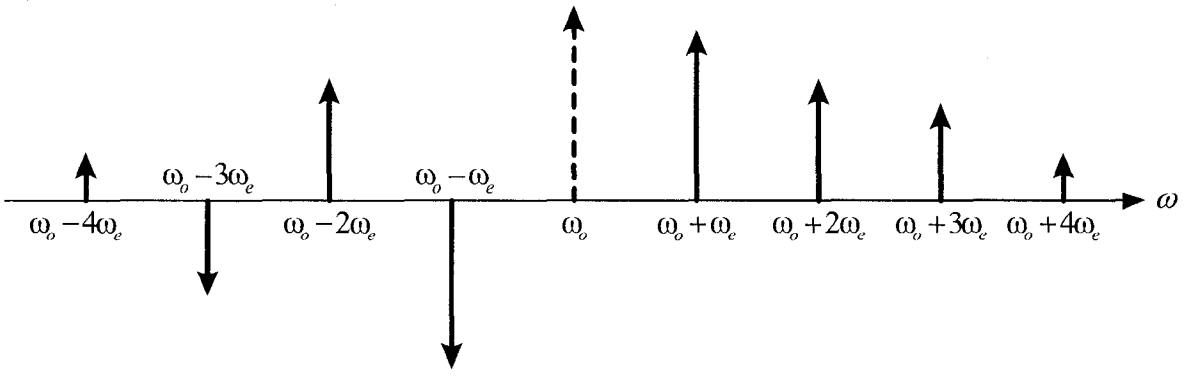

Fig. 2. Optical spectrum at the output of the notch filter. (The dashed line shows the removed optical carrier by the notch filter.)

The spectrum at the output of the notch filter consists of a series of impulses, each with their own amplitude and phase. An example of such a spectrum is shown in Fig. 2. Here the

additional $\frac{\pi}{2}$ phase shift between each impulse is not shown. The dashed line represents the optical carrier removed by the notch filter.

When these optical sidebands are fed to a photodetector, high-frequency electrical signals are generated. The voltage expression of the generated electrical signals $V_{out}(t)$ is

$$V_{out}(t) = C\{\left[\sum_{n=-\infty}^{\infty} J_n(\beta)\cos\left[(\omega_o + n\omega_e)t + n\cdot\frac{\pi}{2}\right]\right]^2 + [J_0(\beta)\cos(\omega_o t)]^2$$

$$-2\sum_{n=-\infty}^{\infty} J_n(\beta)\cdot J_0(\beta)\cos\left[(\omega_o + n\omega_e)t + n\cdot\frac{\pi}{2}\right]\cdot\cos(\omega_o t)\}$$

$$= C\{\frac{1}{2} + \frac{1}{2}\cdot[J_0(\beta)]^2 - \sum_{n=-\infty}^{\infty} J_n(\beta)\cdot J_0(\beta)\cos\left[n(\omega_e t + \frac{\pi}{2})\right]\}$$

$$= C\{\frac{1}{2} - \frac{1}{2}\cdot[J_0(\beta)]^2 - 2\sum_{n=1}^{\infty} J_{2n}(\beta)\cdot J_0(\beta)\cos\left[2n(\omega_e t + \frac{\pi}{2})\right]\}\cdot \quad (4)$$

Here the property of the Bessel function, $J_{-n}(\beta) = (-1)^n J_n(\beta)$, is used and the limited bandwidth of the receiving circuit is also taken into consideration.

In equation (4) the first two terms $\frac{C}{2}$ and $-\frac{C}{2}\cdot[J_0(\beta)]^2$ are DC components. The third term, $-2C\sum_{n=1}^{\infty} J_{2n}(\beta)\cdot J_0(\beta)\cos\left[2n(\omega_e t + \frac{\pi}{2})\right]$, represents an infinite number of even-order electrical harmonics of the electrical drive signal with the peak magnitude of each harmonic decaying according to the Bessel function distribution. Equation (4) clearly indicates that there are no odd-order harmonic terms in the optically generated electrical signals once the carrier is removed. This mathematically demonstrates that the proposed configuration is able to generate optically even-order harmonics of the electrical drive signal and suppress all odd-order harmonics.

By adjusting V_e, the modulation depth β is set such that the optical sidebands up to the fourth order dominate the optical power. As a result, the second- and fourth-order electrical harmonics

will be generated, and higher-order harmonics can then be ignored. The spectrum of the generated electrical signal is illustrated in Fig. 3.

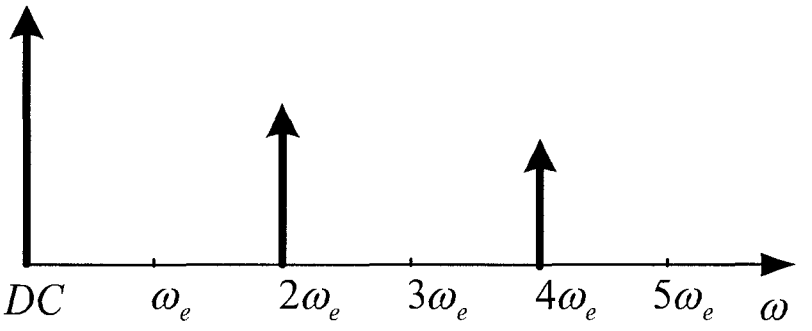

Fig.3. Electrical spectrum at the output of a photodetector.

For maximizing the power of the generated second- and fourth-order electrical harmonics, β can be adjusted in equation (4) to get the maximum value of $J_2(\beta)\cdot J_0(\beta)$ and $J_4(\beta)\cdot J_0(\beta)$.

Our signal generation scheme provides the possibility of generating tunable electrical signals by tuning the frequency of the electrical drive signal without changing the optical carrier frequency. Then a notch filter, with a fixed central wavelength, can be employed to remove the carrier. For example, if the optical phase modulator is driven by an 8-16 GHz signal two bands of electrical signals with frequency of 16-32 GHz and 32-64 GHz can be obtained.

B. Transmission effect analysis

A significant advantage of the optical generation of high-frequency electrical signals is the ease by which they can be distributed using optical fiber, without significant loss, over much greater distance than by using conventional electrical cables or waveguides. However, for propagation over many ten's of kilometers of standard single-mode fiber, fiber attenuation, chromatic dispersion and random polarization disturbances can affect the spectral purity of the generated signal. The fiber attenuation can be easily compensated for with the use of EDFA's. Random polarization disturbances do not affect signals generated by optical heterodyne as much as in optical coherent communication systems, where the polarization state of the local optical carrier needs to track the polarization state of the incoming signal. In our optical heterodyne-based systems, the optical carrier and sidebands used for creating the electrical carrier are sent

together. As a result, it is most likely that the polarization states of all the optical signal components will change in a similar way as they propagate in the fiber.

Although the chromatic dispersion of the standard single mode fiber is low, ($D = 17 ps/(nm \cdot km)$), it has to be considered when analyzing the quality of an electrical signal generated with our technique after the optical sidebands have traveled in a long fiber span. One key aspect is that odd-order electrical harmonics still have to be cancelled. To maintain the cancellation, the optical sidebands at the remote site must conserve the same amplitude and phase relations that existed at the beginning of the span. Cumulative effects from fiber chromatic dispersion will alter these relations, eventually resulting in a poor cancellation of the first- and third-order electrical harmonics and in some power penalty for the second- and fourth-order ones. We will now analyze the impact of chromatic dispersion on the resulting signal. Then we will show that dispersion compensation will eliminate these detrimental effects on the generated electrical carrier.

1). Dispersion effect: When fiber chromatic dispersion is taken into consideration, the propagation constant $\beta(\omega)$ of the fiber for an optical sideband at $\omega_o \pm n\omega_e$ can be approximately represented by a Taylor series around the center angular frequency ω_o [10]

$$\beta(\omega_o \pm n\omega_e) = \beta(\omega_o) + \beta'(\omega_o)(\pm n\omega_e) + \frac{1}{2}\beta''(\omega_o)(\pm n\omega_e)^2 + \ldots\ldots, \tag{5}$$

where the effect of higher-order dispersion is neglected [11].

We can now give the mathematical representation of the first-order electrical harmonic $V_{out,e1}$ after the optical signal has traveled through a fiber span of length L. After electro-optical conversion, we have

$$V_{out,e1}(t) = 2C\sum_{n=1}^{\infty} J_n(\beta)J_{n+1}(\beta)\sin\left[\frac{\beta''(\omega_o)}{2}(2n+1)\omega_e{}^2 L\right]\cdot\sin\left[\omega_e t + \frac{\pi}{2} - \beta'(\omega_o)\omega_e L\right], \tag{6}$$

where $\sum_{n=-1}^{-\infty} J_n(\beta)J_{n-1}(\beta) = -\sum_{n=1}^{\infty} J_n(\beta)J_{n+1}(\beta)$ is used. The widely used chromatic dispersion parameter D is related to $\beta''(\omega_o)$ by

$$D = -\frac{2\pi c}{\lambda_o^{\,2}}\beta''(\omega_o), \tag{7}$$

where c is the speed of light in free space and λ_o is the wavelength of the optical carrier. Therefore, equation (6) can be expressed in terms of D

$$V_{out,e1}(t) = C\left\{-2\sum_{n=1}^{\infty} J_n(\beta)J_{n+1}(\beta)\sin\left[(2n+1)\pi LcD(\frac{f_e}{f_o})^2\right]\right\}\cdot\cos[\omega_e t - \beta'(\omega_o)\omega_e L], \tag{8}$$

where f_e is the frequency of the electrical drive signal. Similarly, the second-order electrical harmonic $V_{out,e2}$ can be expressed as

$$V_{out,e2}(t) = C\left\{J_1^{\,2}(\beta) - 2\sum_{n=1}^{\infty} J_n(\beta)J_{n+2}(\beta)\cos\left[2(2n+2)\pi LcD(\frac{f_e}{f_o})^2\right]\right\}\cdot\cos[2\omega_e t - 2\beta'(\omega_o)\omega_e L], \tag{9}$$

where $\sum_{n=-1}^{-\infty} J_n(\beta)J_{n-2}(\beta) = \sum_{n=1}^{\infty} J_n(\beta)J_{n+2}(\beta)$ is used. The third- and the fourth-order electrical harmonics $V_{out,e3}$, $V_{out,e4}$ are

$$V_{out,e3}(t) = C\left\{2\sum_{n=1}^{\infty} J_n(\beta)J_{n+3}(\beta)\sin\left[3(2n+3)\pi LcD(\frac{f_e}{f_o})^2\right] - J_1(\beta)J_2(\beta)\sin\left[3\pi LcD(\frac{f_e}{f_o})^2\right]\right\}$$
$$\cdot\cos[3\omega_e t - 3\beta'(\omega_o)\omega_e L], \tag{10}$$

$$V_{out,e4}(t) = C\left\{J_2^{\,2}(\beta) + 2\sum_{n=1}^{\infty} J_n(\beta)J_{n+4}(\beta)\cos\left[4(2n+4)\pi LcD(\frac{f_e}{f_o})^2\right]\right.$$
$$\left. - 2J_1(\beta)J_3(\beta)\cos\left[8\pi LcD(\frac{f_e}{f_o})^2\right]\right\}\cdot\cos[4\omega_e t - 4\beta'(\omega_o)\omega_e L]\cdot \tag{11}$$

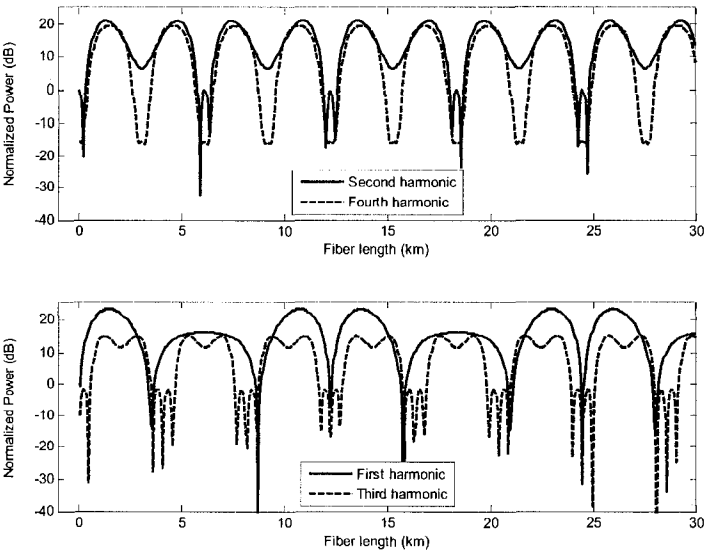

(a)

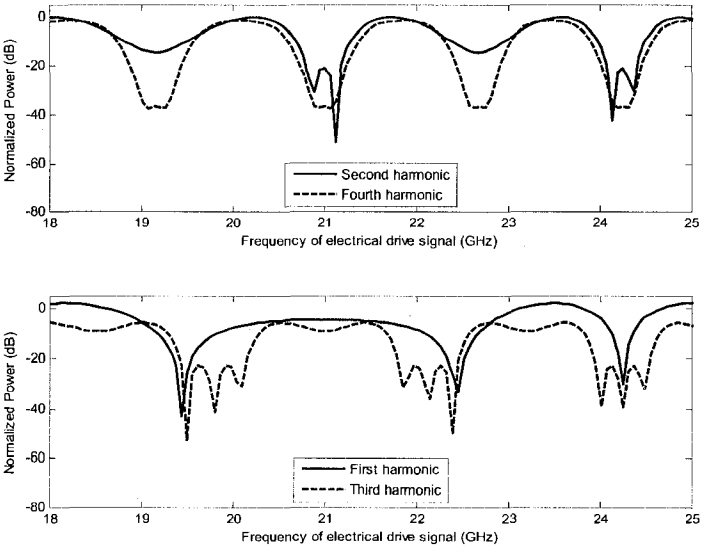

(b)

Fig. 4. Effects of the chromatic dispersion on the normalized power of generated electrical harmonics. (a) Normalized power versus fiber length. (b) Normalized power versus the frequency of the electrical drive signal.

Equations (8) to (11) show that the amplitudes of the first four electrical harmonics are determined by the value of $LcD(\frac{f_e}{f_o})^2$. The level of cancellation of the odd-order electrical

harmonics and the power penalty on the even-order harmonics at the other end of the fiber span depends on D and f_e. Hence, as the signal frequency is tuned, the cancellation and power penalty level will change. Obviously, this is not a desirable effect. To overcome these problems, dispersion compensation is required. The variation of the power in the four harmonics calculated using equations (8) to (11) is shown in Fig. 4. The power variation is plotted as a function of the fiber length (Fig. 4 (a)) and the frequency of the electrical signal that drives the modulator (Fig. 4 (b)). In Fig. 4 (a) all values are normalized to the power of the second harmonic when the fiber length is zero (local detection). The other parameters used in Fig. 4 (a) are set as followed: $D = 17 ps/(nm \cdot km)$, $\beta = 2.5$, $f_o = 1550 nm$, $c = 3 \times 10^8 m/s$ and $f_e = 24.5$ GHz. In Fig. 4 (b) all values are normalized to the power of the second harmonic when the frequency of the electrical drive signal is 18 GHz. All the parameters are the same in Fig. 4 (b), excepted for L, which is fixed at 25 km and f_e, which is varied between 18 GHz and 25 GHz.

2). With dispersion compensation: One way to compensate for fiber dispersion is to insert a length of dispersion compensating fiber (DCF) at the end of the span. Fig. 5 shows the dispersion compensation arrangement. A dispersion compensating fiber of chromatic dispersion parameter (D_c) and length (L_c) is connected after the transmission fiber, as shown in Fig. 5.

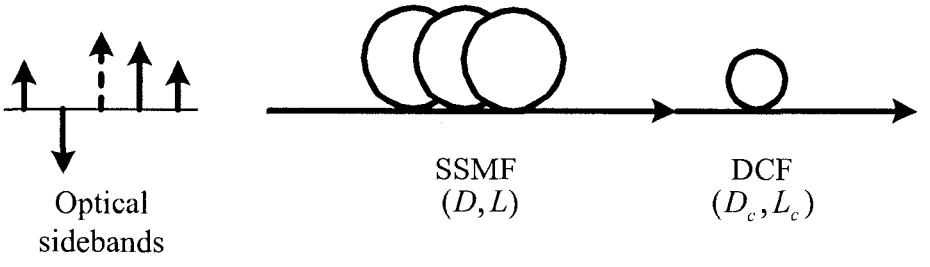

Fig. 5. Dispersion compensation using DCF for optical distribution of mm-wave signal. (SSMF: standard single mode fiber, DCF: dispersion compensating fiber)

The DCF will compensate for the phase shifts that are induced on the optical sidebands while they are traveling in the fiber span, bringing them back in phase as much as it is possible. Now, the phase delay $\Phi(\omega)$ of each of these optical sidebands is expressed in terms of the

propagation constant and fiber length of both the standard fiber and the dispersion compensation fiber, respectively.

$$\Phi(\omega) = \beta(\omega)L + \beta_c(\omega)L_c, \tag{12}$$

where $\beta_c(\omega)$ is the propagation constant of the dispersion compensating fiber. With the same analysis process as above, it is ready to get the result that when the dispersion parameter of the dispersion compensating fiber D_c is given, the required length L_c for proper compensation is calculated by

$$L_c = -\frac{D}{D_c}L. \tag{13}$$

3. Experiment

The experimental setup used to verify the performance of the proposed signal generation method is illustrated in Fig. 6.

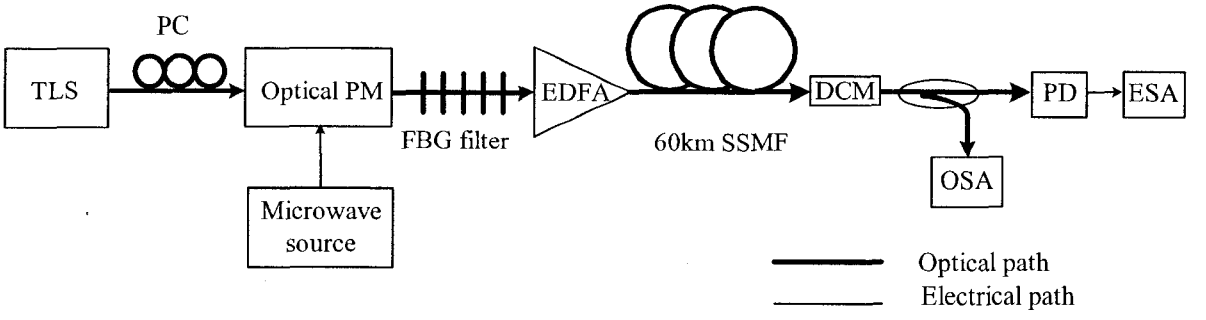

Fig. 6. Experimental setup for optical generation of mm-wave signals. (TLS: tunable laser source, PC: polarization controller, Optical PM: optical phase modulator, EDFA: erbium-doped fiber amplifier, SSMF: standard single mode fiber, DCM: dispersion compensation module, OSA: optical spectrum analyzer, PD: photodetector, ESA: electrical spectrum analyzer)

The optical phase modulator is a commercially available 1550-nm $LiNbO_3$ modulator. A tunable laser is used as the optical source. The optical carrier generated by the tunable laser source (TLS) is sent to the phase modulator through a polarization controller (PC). The wavelength of the optical carrier is set to match the maximum attenuation wavelength of the FBG notch filter. A microwave signal source tunable from 12.5 GHz to 25 GHz is applied to the

phase modulator. Optical sidebands at the output of the FBG filter are amplified with an EDFA, and then transmitted over 60 km of standard single mode fiber. The beating of these optical sidebands at a photodetector generates the required mm-wave signals.

The transmission spectrum of the FBG notch filter is shown in Fig. 7. The bandwidth from the minimum attenuation point at lower wavelengths to the minimum attenuation point at longer wavelengths is about 0.3 nm (≈37.5 GHz).

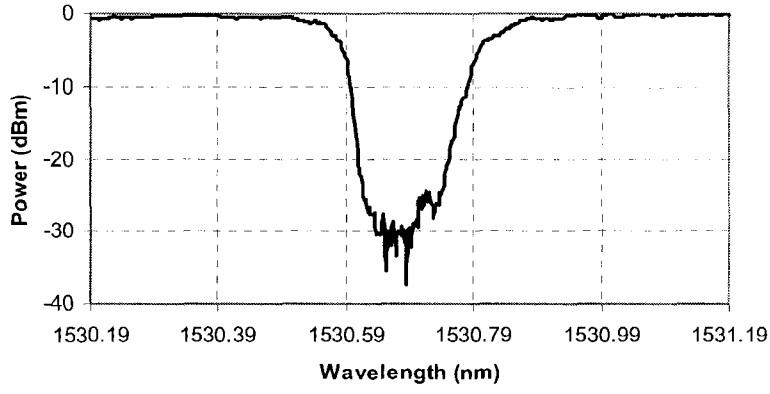

Fig. 7. Transmission spectrum of the FBG filter.

Measurements have been taken before and after transmission, with and without dispersion compensation in order to analyze and evaluate the performance of the system. Fig. 8 shows the typical optical spectra before and after the FBG filter. Here the optical phase modulator is driven by a 12.5-GHz signal. Fig. 8 (a) shows that optical sidebands are generated up to the fourth order. They are distributed symmetrically around the optical carrier. Fig. 8 (b) shows the optical spectrum after the FBG filter. It is clearly shown that the optical carrier power is attenuated about 40 dB. Due to the bandwidth of the FBG and its asymmetric attenuation characteristics, the first-order optical sidebands are not attenuated to the same level on each side of the carrier. This is an issue for drive frequencies up to about 19 GHz for this particular FBG, but the problem can be avoided by operating at higher frequencies or, in the future, by improving the spectrum symmetry of the FBG.

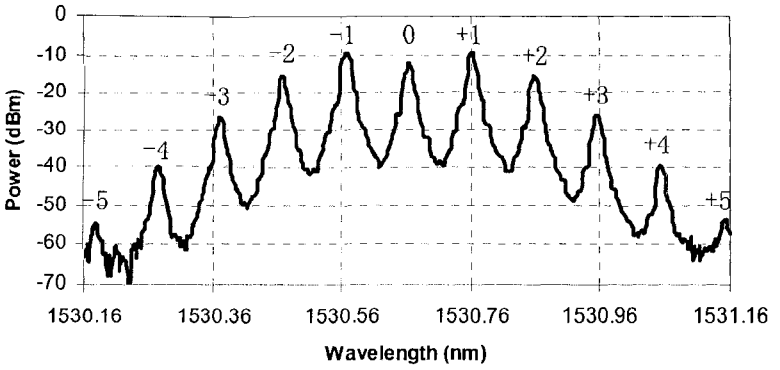

(a)

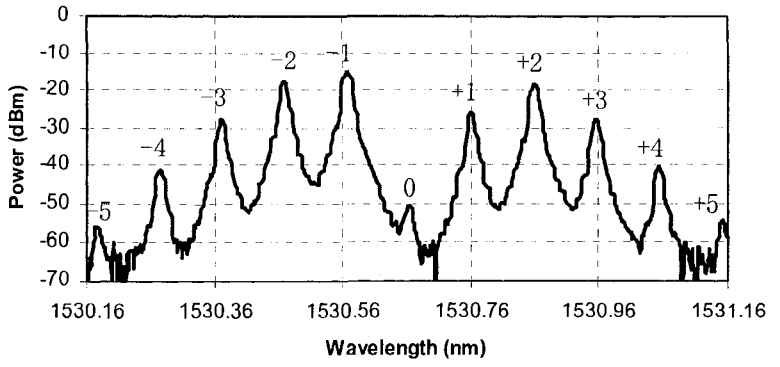

(b)

Fig. 8. Typical optical spectra before transmission. (+, -: optical sideband in upper frequency side and lower frequency side. 0: optical carrier. 1, 2, 3, 4, 5: first-, second-, third-, fourth-, and fifth-order optical sideband). (a) Before the FBG filter. (b) After the FBG filter.

Fig. 9 shows the spectrum of the optically generated electrical signal, measured at the output of the photodetector before transmission. The spectrum corresponds to a 24.5 GHz electrical drive signal – a frequency where the first-order optical harmonics are not attenuated by the FBG. It is easily seen that an mm-wave signal at twice the frequency of the drive electrical signal is generated. Signal components above 50 GHz are not visible due to the bandwidth limit of the photodetector and the electrical spectrum analyzer; however, they are present in the output when viewed on the OSA. When the electrical drive signal is tuned from 18.8 to 25 GHz, two bands of mm-wave signals from 37.6 to 50 GHz and from 75.2 to 100 GHz with high frequency

stability and narrow linewidth are generated. These observations agree well with the outcome of the mathematical analysis presented in the previous Section.

As can be seen in Fig. 7, the attenuation of the FBG filter on its lower and upper frequency slopes is not symmetrical with respect to the center of the notch. As such that the group delay is also not symmetrical. If the sidebands of the modulated optical signal fall in this Section of the filter bandwidth, the non-symmetrical characteristic will break down the intrinsic amplitude and phase relationship among the optical sidebands of a phase modulated signal. The power of the required mm-wave signal and the odd-order harmonic suppression will be affected. To avoid this, the electrical drive signal must have a low frequency criterion. The lowest frequency of the electrical drive signal should be equal or greater than half of the frequency bandwidth of the FBG. In this case, the generated mm-wave signal is only affected by the maximum attenuation at the center of the notch, and it is immunized from the imperfect characteristics of the FBG.

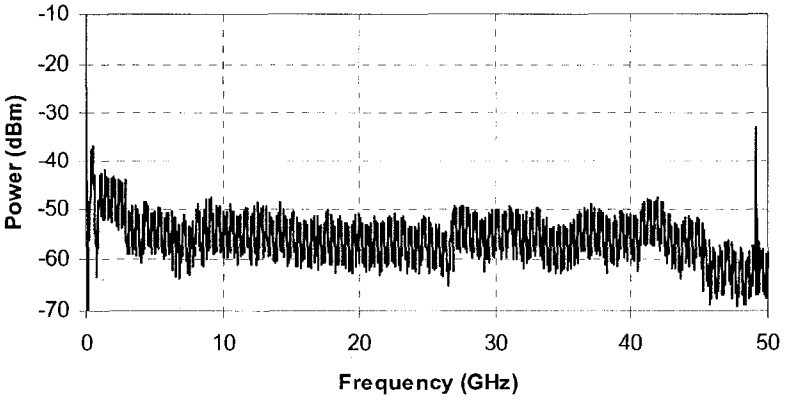

Fig. 9. Electrical spectrum of the generated mm-wave signals when the drive signal frequency is 24.5 GHz.

Fig. 10 shows the electrical spectra of the remotely generated electrical signals when the electrical drive signal is at 24.5 GHz, after propagation over 60 km single mode fiber. Fig. 10 (a) is an indication of the spectrum without dispersion compensation while Fig. 10 (b) is the spectrum when dispersion compensation is applied before photodetection. In Fig. 10 (a), the 24.5-GHz signal is not fully cancelled and the amplitude of the 49-GHz signal decreases due to a chromatic-dispersion-induced power penalty. Fig. 10 (b) clearly shows the cancellation of the 24.5-GHz signal and the elimination of the power penalty to the 49-GHz signal when chromatic

dispersion compensation is used. These measurements are in accordance with the analysis conclusion presented in Section 2.2.

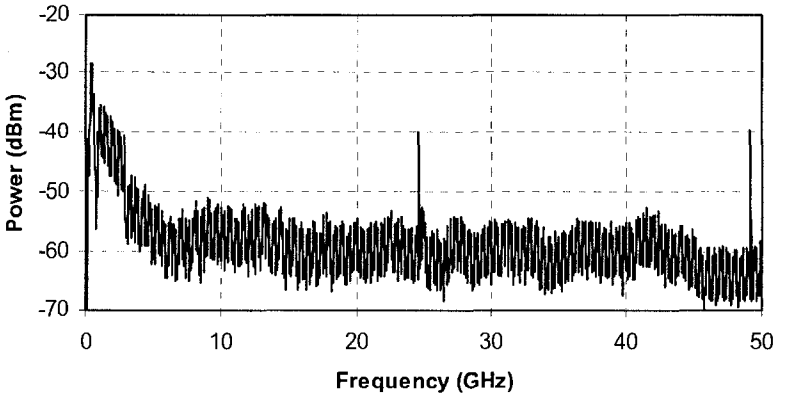

(a)

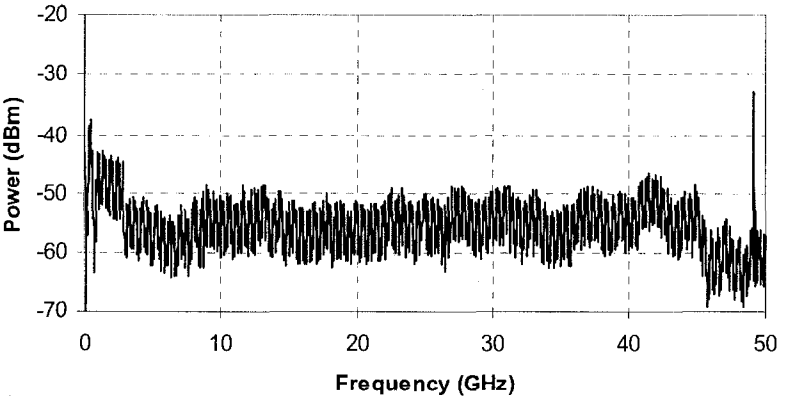

(b)

Fig. 10. Electrical spectra of the generated mm-wave signals after transmission over 60-km standard single mode fiber. (a) Without dispersion compensation module. (b) With dispersion compensation module.

Fig. 11 gives zoom-in views of the electrical spectra of the optically generated 49-GHz electrical signal before and after transmission with dispersion compensation. The resolution bandwidth of the electrical spectrum analyzer is 1 Hz and 100 Hz in Fig. 11 (a) and Fig. 11 (b), respectively. It can be seen that the 49-GHz electrical signal does not suffer from obvious phase noise degradation after the 60-km transmission. The quality of the signal is adequate for most practical applications.

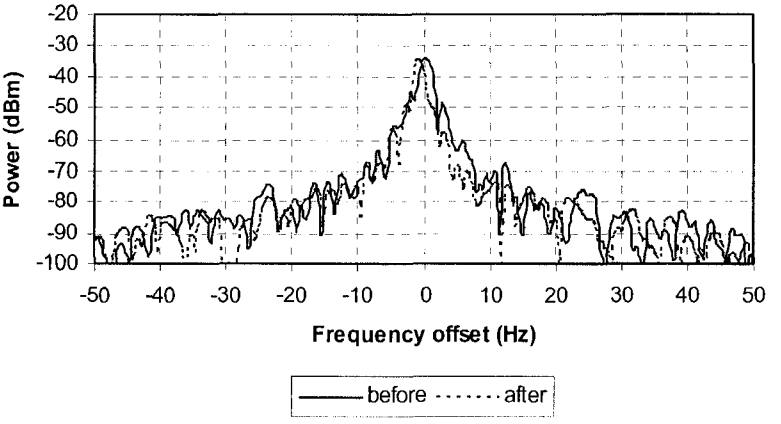

(a)

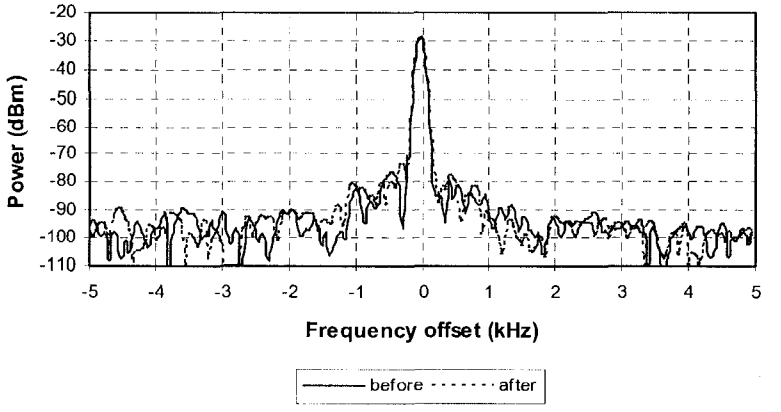

(b)

Fig. 11. Electrical spectra of the signal generated before and after transmission with dispersion compensation. (a) Span 100 Hz. (b) Span 10 kHz.

4. Conclusions

We have proposed a new and robust method for the optical generation of wideband, continuously tunable mm-wave signals. The mathematical foundations of the method have been detailed and an experimental verification of its performance has been performed. In the proposed configuration, an optical phase modulator and an FBG notch filter were used. The optical carrier was removed from the output of the optical phase modulator by the FBG notch filter. When the resulting optical sidebands were applied to a photodetector, only even-order electrical harmonics were generated and the odd-order harmonics were cancelled. The effect of

chromatic dispersion in the fiber used to distribute the signal on the generated electrical signal was also analyzed.

Experimental validation with an electrical drive signal tuned from 18.8 to 25 GHz has been conducted. Two bands of mm-wave signals from 37.6 - 50 GHz and 75.2 - 100 GHz (signal components above 50 GHz are only visible on the OSA) were generated locally and remotely. The generated signals had high frequency stability and narrow linewidth. It was verified that, after dispersion compensation, the integrity of the generated signals was maintained after transmission over a 60-km single mode fiber.

A major advantage of the proposed approach is that continuously tunable mm-wave signals over a wide frequency range can be generated using a fixed optical filter, which significantly simplifies the system configuration. Compared with the approaches based on an optical intensity modulator, the phase modulator does not need a DC bias, thus eliminating DC bias drifting related problems.

Acknowledgements

The authors would like to thank John Oldham and David Barlow of the Communications Research Centre of Canada, Fei Zeng and Xiangfei Chen of the University of Ottawa for their assistance in the experiments.

References:

[1] R. P. Braun, G. Grosskopf, D. Rohde, and F. Schmidt, "Optical millimetre-wave generation and transmission experiments for mobile 60 GHz band communications," *Electron. Lett.*, vol. 32, no. 7, pp. 626-628, Mar. 28, 1996.

[2] H. Schmuck, "Comparison of optical millimeter-wave system concepts with regard to chromatic dispersion," *Electron. Lett.*, vol. 31, no. 21, pp. 1848-1849, Oct. 1995.

[3] U. Gliese, S. Nφrskov, and T. N. Nielsen, "Chromatic dispersion in fiber-optic microwave and millimeter-wave links," *IEEE Trans. Microwave Theory Tech.*, vol. 44, no. 10, pp. 1716-1724, Oct. 1996.

[4] G. Qi, J. P. Yao, J. Seregelyi, S. Paquet, and J. C. Belisle, "Phase noise analysis of the optically generated and distributed millimeter wave signal using an external optical modulator," *Proceedings of SPIE*, vol. 5579C, pp. 598-606, Sept. 2004,

[5] L. Goldberg, H. F. Taylor, J. F. Weller, and D. M. Bloom, "Microwave signal generation with injection-locked laser diodes," *Electron. Lett.*, vol. 19, no. 13, pp. 491-493, Jun. 1983.

[6] R. T. Ramos and A.J. Seeds, "Fast heterodyne optical phase-lock loop using double quantum well laser diodes," *Electron. Lett.*, vol. 28, no. 1, pp. 82-83, Jan. 1992.

[7] J. J. O'Reilly, P. M. Lane, R. Heidemann, and R. Hofstetter, "Optical generation of very narrow linewidth millimetre wave signals," *Electron. Lett.*, vol. 28, no. 25, pp. 2309-2311, Dec. 1992.

[8] J. J. O'Reilly and P.M. Lane, "Fibre-supported optical generation and delivery of 60GHz signals," *Electron. Lett.*, vol. 30, no. 16, pp. 1329-1330, Aug. 1994.

[9] P. Shen, N. J. Gomes, P. A. Davies, W. P. Shillue, P.G. Huggard, and B. N. Ellison, "High-purity millimetre-wave photonic local oscillator generation and delivery," in *Proc. Microwave Photonics*, Sept. 2003, pp. 189-192.

[10] K. Okamoto, *Fundamentals of Optical Waveguides*, New York: Academic Press, 2000, pp. 72-72.

[11] W. K. Marshall, B. Crosignani, and A. Yariv, "Laser phase noise to intensity noise conversion by lowest-order group-velocity dispersion in optical fiber: exact theory," *Opt. Lett.*, vol. 25, no. 3, pp. 165-167, Feb. 2000.

3.3 Millimeter-wave signal generation and optical carrier recovery using an optical intensity modulator in a fiber ring laser

In this Section, an approach for millimeter-wave signal generation and optical carrier recovery using a single-longitudinal-mode, fiber ring laser incorporating an intensity modulator in the laser cavity is presented. The optically generated millimeter-wave signal tunable from 32 GHz to 50 GHz is obtained when the frequency of the electrical drive signal is tuned from 8 GHz to 12.5 GHz. In addition, an optical carrier at -5 dBm is recovered after a transmission over 25-km standard single mode optical fiber.

A single longitudinal mode fiber ring laser incorporating an intensity modulator for mm-wave signal generation and optical carrier recovery[3]

Guohua Qi, Xiangfei Chen, and Jianping Yao, *Senior Member, IEEE*

Microwave Photonics Research Laboratory,
School of Information Technology and Engineering
University of Ottawa, Ottawa, Ontario, Canada K1N 6N5

Abstract

A novel technique for millimeter-wave (mm-wave) signal generation and optical carrier recovery using a single- longitudinal-mode (SLM) fiber ring laser incorporating an intensity modulator in the laser cavity is presented. An mm-wave signal tunable from 32 GHz to 50 GHz is generated and an optical carrier of -5 dBm is recovered simultaneously at a base station.

1. Introduction

Distribution of microwave or millimeter-wave (mm-wave) signals over optical fiber has attracted great interest in the last few years. In a radio-over-fiber (RoF) system, one of the key techniques is to generate and distribute microwave and mm-wave signals optically. The optically generated and distributed electrical signal can be used at a base station either as a radio frequency carrier for downlink transmission or as a local oscillator signal for uplink transmission. The amplitude fluctuation, the long-term frequency stability and the short-term frequency stability are the three factors that are crucial to the RoF system performance. Among these factors, the amplitude fluctuation is relatively easy to control. For example, the saturation property of a buffer amplifier can be used to reduce the amplitude fluctuation. The frequency stabilities are hard to improve and a lot of efforts have been directed in the last few years to find solutions to generate stable mm-wave signals based on photonics technology.

Several techniques have been proposed to generate optically stable mm-wave signals, which include automatic frequency control loop [1], optical injection locking [2], optical phase-locked

[3] Published in *Proc. Microwave Photonics*, Oct. 2005, pp. 25-28.

loop (OPLL) [3], [4], and external modulation [5]-[9]. Among these signal generation methods, the technique using external modulation has shown great potential for producing electrical signals with high spectral purity [5]. The frequency of the generated electrical signal with external modulation techniques can be as high as four times of the frequency of the electrical drive signal; therefore a relatively low-speed low-cost intensity modulator can be used to generate an electrical signal with much higher frequency. However, the generated electrical signal is usually at a fixed frequency [6], [7]. For many applications, such as wideband surveillance radar, distributed antenna remoting network, spread-spectrum, and software defined radio, the systems are expected to be frequency reconfigurable. Therefore, a continuously frequency tunable signal is required. Since an optical filter would be used to select the two second-order sidebands [6], [7], to generate a tunable electrical signal, the optical filter must be tunable, which makes the system very complicated and costly. In addition, for a duplex communication system, a reliable optical carrier is needed at the remote site for carrying information back to the central office. The reuse of the downlink optical carrier is a cost-effective solution [10]. Therefore, at base stations the generation of a continuously tunable electrical signal and the recovery of an optical carrier are very attractive for system applications.

In this Section, we propose a novel and simple technique to generate a continuously tunable electrical signal and an optical carrier simultaneously at a base station. The system consists of a single longitudinal mode (SLM) fiber ring laser incorporating an intensity modulator in the ring cavity. The intensity modulator is driven by a low-frequency microwave signal. By properly biasing the intensity modulator, odd-order sidebands are suppressed, and an optical signal with only even-order sidebands is obtained. Considering that the higher even-order sidebands have much lower power than the second-order sidebands, the optical signal can be considered to consist of only two second-order sidebands and an optical carrier.

The optical signal is then distributed to a base station via a length of single mode fiber. By using a fiber Bragg grating (FBG) at the base station, the optical carrier is separated from the two second-order sidebands. An mm-wave signal of four times the frequency of the microwave drive signal is generated by beating the two sidebands at a photodetector. At the same time, an optical carrier is recovered at the output of the FBG. The recovered optical carrier can be used for in the base station for uplink transmission.

2. Principle

Recently we have proposed an approach to achieving SLM operation of a fiber ring laser by using an equivalent phase shift fiber Bragg grating (EFS FBG) [11].

In this Section, we propose to use the SLM fiber ring laser that incorporates an intensity modulator in the laser cavity to generate continuously tunable mm-wave signal and at the same time to recover the optical carrier at a base station. The schematic diagram of system is shown in Fig. 1.

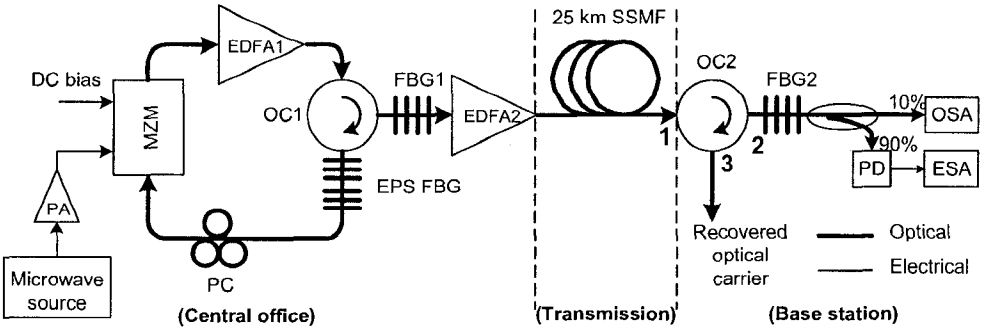

Fig. 1. Schematic diagram of the mm-wave generation and optical carrier recovery system. (PA: microwave power amplifier, MZM: Mach-Zehnder modulator, EDFA: Erbium doped fiber amplifier, OC: optical circulator, FBG: fiber Bragg grating, EPS FBG: equivalent phase shift fiber Bragg grating, SSMF: standard single mode fiber, PD: photodetector, OSA: optical spectrum analyzer, ESA: electrical spectrum analyzer.)

At the central office, an optical signal with two second-order sidebands and a carrier is generated by modulating the optical intensity modulator located in the cavity of the SLM fiber ring laser. The SLM fiber ring laser consists of an EDFA (EDFA1), an optical circulator (OC1), an apodized uniform FBG (FBG1), and an EPS FBG. The EDFA1 provides a broadband gain and the loop of the fiber forms the laser cavity. Because of the long cavity length of a fiber ring laser, many longitudinal modes would be found at laser output. By using a narrow band optical filter, the number of longitudinal modes will be greatly reduced. However, considering the small spacing between two adjacent longitudinal modes (several MHz), there are still thousands of longitudinal modes even a very narrow band optical filter is used. To restrict the number of longitudinal modes to one, recently we have proposed to use an EFS FBG in the laser cavity. Since the EFS FBG has an ultra narrow transmission bandwidth, only one longitudinal mode

can survive, stable SLM operation is realized. We should note that an EFS FBG is a sampled FBG with a π phase shift introduced to one of the many samples. Fig. 2 shows the transmission spectrum of an EFS FBG. In our application, a regular reflection FBG should be used to select the ultra-narrow transmission band. The combination of the EFS FBG and the regular reflection FBG via an optical circulator would lead to a true ultra-narrow transmission band filter.

For a general intensity modulation, when a single-frequency electrical drive signal is applied to an optical intensity modulator that is biased by a DC, optical sidebands with carrier are generated. Analysis shows that the power of the generated optical sidebands is governed by Bessel function coefficients of the first kind [12]; and the even-order or odd-order sidebands can be suppressed by adjusting the DC bias. To generate a frequency quadrupled electrical signal, the DC bias is tuned to suppress all odd-order optical sidebands. Then there will be an optical carrier and two second-order optical sidebands at the output of the modulator. Generally, the optical carrier is dominant in the generated optical signal. This dominance prevents the two small second-order sidebands from obtaining enough amplification from the optical amplifier because the amplifier is easily saturated by the presence of the large carrier. The use of an optical filter at the output of the intensity modulator may be able to equalize the powers of the carrier and the two sidebands. However, this would increase the complexity of the system.

This problem is solved by using the configuration shown in Fig. 1, in which an intensity modulator is incorporated in the laser ring cavity. The intensity modulator is properly biased to suppress the odd-order sidebands. When the modulator is driven by a microwave signal, an optical carrier and two second-order sidebands would be generated. In our design, the two second-order sidebands are located away from the center wavelength of FBG1 with low reflection, as shown in Fig. 2, and the carrier is located at the central reflection band of FBG1. Most of the optical carrier will be reflected into the laser cavity to maintain the lasing operation. While the two second-order sideband are transmitted. The optical signal generated with this specific design will generate an optical carrier and two second-order sideband with balanced power, which can be uniformly amplified by the optical amplifier after FBG1.

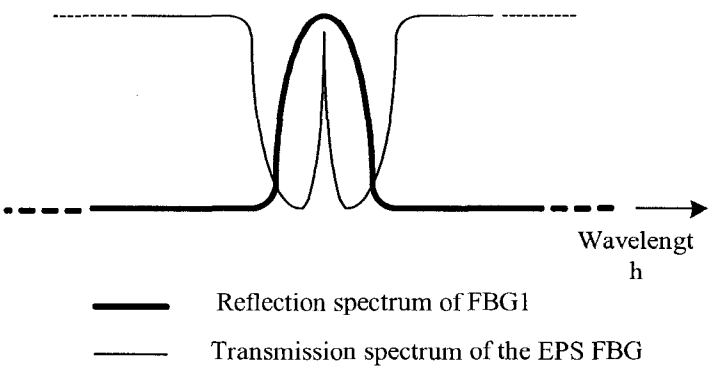

Fig. 2. An ultra-narrow band transmission filter built by using an EFS FBG and regular reflection FBG.

The amplified optical signal suffers from attenuation and chromatic dispersion when transmitted over a standard single mode fiber (SSMF) to a base station. If the optical signal is fed directly into a photodetector at the base station, the electrical signals will be composed of a second-order harmonic and a fourth-order harmonic of the electrical drive signal. The chromatic dispersion will not introduce a power penalty to the fourth-order harmonic because it is generated with only one beating between the upper and lower second-order optical sidebands. However, the second-order harmonic is formed by beating between the optical carrier and the upper and lower second-order optical sideband. The two beating signals will interfere with each other constructively or destructively depending on the phase difference caused by the chromatic dispersion. Since the phase difference varies with the transmission distance and the frequency of the electrical drive signal, the power of the second-order harmonic varies accordingly. The second-order harmonic is not useful in a frequency tunable system because of these fluctuations and the fact that it may cause interference to the fourth-order harmonic. Therefore, before the optical signal is fed to the photodetector, the optical carrier should be removed. On the other hand, at a base station, to send an uplink signal to the central office, an optical carrier is usually used to carry the uplink information. A cost-effective solution is to reuse the optical carrier from the downlink signal.

In addition, although the fourth-order harmonic does not suffer from a power penalty, transmission analysis shows that the phase noise of the generated electrical signal is related to the linewidth of the laser source and the time delay between the two second-order optical sidebands. As such, the much narrower linewidth of an SLM fiber ring laser source in the proposed configuration improves the spectral purity of the generated electrical signal.

At the base station, an optical circulator (OC2) and an FBG (FBG2) are used to recover the optical carrier. The transmission spectrum of FBG2 is shown in Fig. 3. FBG2 is a narrow-band optical notch filter which reflects the optical carrier back to OC2. Therefore, the recovered optical carrier is obtained from port 3 of OC2, and the two second-order optical sidebands are obtained at the output of FBG2. By beating the two second-order sidebands at the photodetector, an electrical signal with four times the frequency of the drive signal is generated. Since the optical carrier has a fixed wavelength, the removal of the carrier is easily accomplished by using a fixed FBG (FBG2). By varying the frequency of the electrical drive signal remotely at the central office, continuously tunable mm-wave signal can be generated.

3. Experimental results

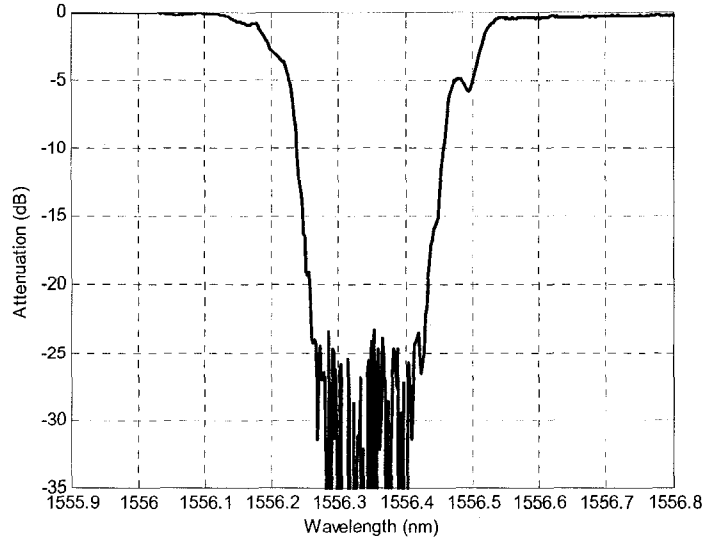

Fig. 3. Transmission spectrum of the FBG notch filter for optical carrier recovery.

The setup shown in Fig. 1 is experimented. The FBG's are custom designed and manufactured with a center wavelength of 1556 nm. FBG1 has a transmission attenuation of 20 dB and a transmission bandwidth of 0.2 nm of zero-to-zero attenuation. The transmission spectrum of FBG2 is shown in Fig. 3. Due to the limited dynamic range of the measurement system, attenuation over 25 dB can not be properly identified. Actually, FBG2 has a transmission attenuation over 40 dB at the center of the notch. In addition, the transmission bandwidth of the EPS FBG is very narrow and cannot be resolved using the available optical spectrum analyzer

(OSA). The Mach-Zehnder modulator (MZM) can operate up to 13.8 GHz with an optical loss smaller than 5 dB. The EDFA's are packed modules with a gain of around 20 dB in the band of interest.

The fiber ring laser is initially operating in the multi-longitudinal mode. This is confirmed by observing the beating signal at a photodetector, which shows an electrical signal of about 8 MHz which corresponds to the spacing between two adjacent longitudinal modes for a cavity length of about 25 m. When FBG1 is properly tuned to select the central transmission band of the EFS FBG, an ultra narrow gain profile is formed in the ring loop. Thus, only one longitudinal mode is supported and others are suppressed. No beating signal can be observed at the output of the photodetector.

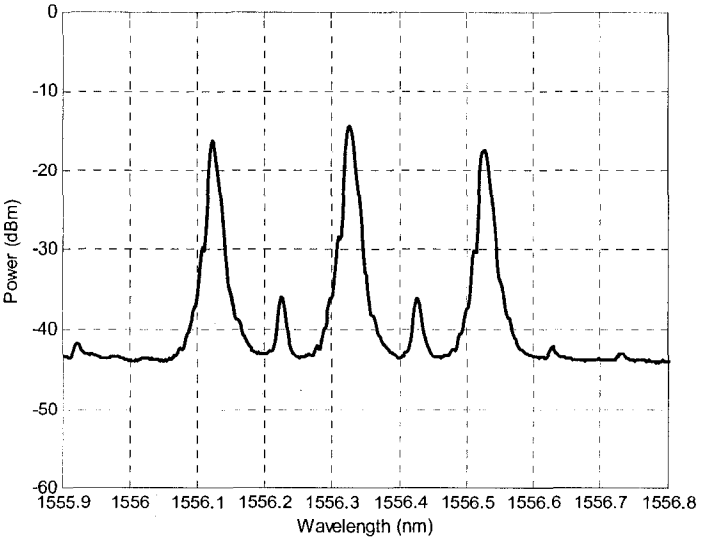

Fig. 4. Optical spectrum at the output of the SLM fiber ring laser when the intensity modulator is driven by a microwave signal at 12.5 GHz.

Then, a microwave signal tuned from 8 to 12.5 GHz is applied to the MZM. The MZM is biased by a DC voltage of 2.7 V to suppress the odd-order sidebands. A typical optical signal spectrum at the output of FBG1 is shown in Fig. 4. It can be seen that odd-order sidebands are suppressed. The two second-order sidebands have the same power level as that of the optical carrier. The optical carrier and the second-order sidebands are uniformly amplified by EDFA2 and sent to the base station over a 25 km SSMF.

Fig. 5 shows the spectrum of the optical signal at the output of the 10% port of the optical coupler. As can be seen the optical carrier and the odd-order optical sidebands are well suppressed. The power of the two second-order sidebands that are fed to the photodetector is 9.5 dB higher than that shown in Fig. 5 because it is obtained from the 90% port of the optical coupler. Fig. 6 shows the electrical spectra of the generated 32 GHz and 50 GHz signals when the frequency of the electrical drive signal tuned at 8 GHz and 12.5 GHz, respectively. The spectral purity of the generated signal is mainly affected by that of the electrical drive signal. The phase noise degradation contributed by the optical generation and distribution system is negligible because of the narrow linewidth of optical carrier generated by the SLM fiber ring laser.

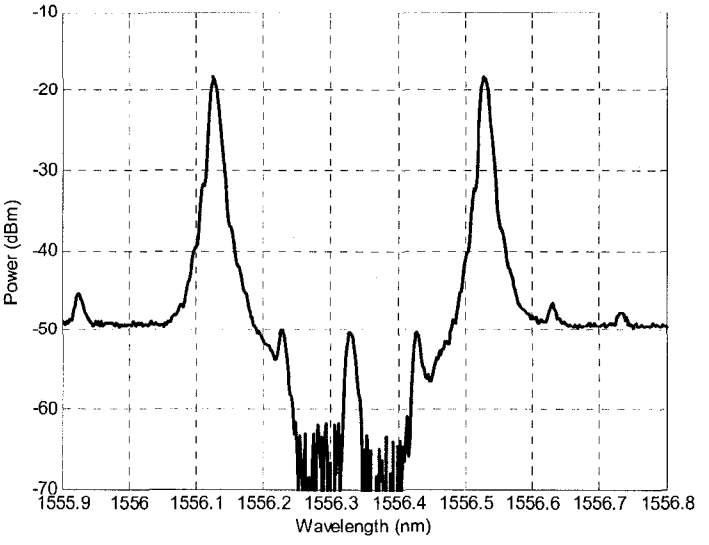

Fig. 5. Optical spectrum after optical carrier recovery. The intensity modulator is driven by a microwave signal at 12.5 GHz.

Fig. 7 shows the optical spectrum of the recovered optical carrier at port 3 of OC2 when the electrical drive signal is tuned at 12.5 GHz. The power of the recovered optical carrier is around -5 dBm. The second-order optical sidebands can also be observed, but over 20 dB lower than the recovered optical carrier. The power of the second-order optical sidebands can be further suppressed if a narrower bandwidth FBG is used.

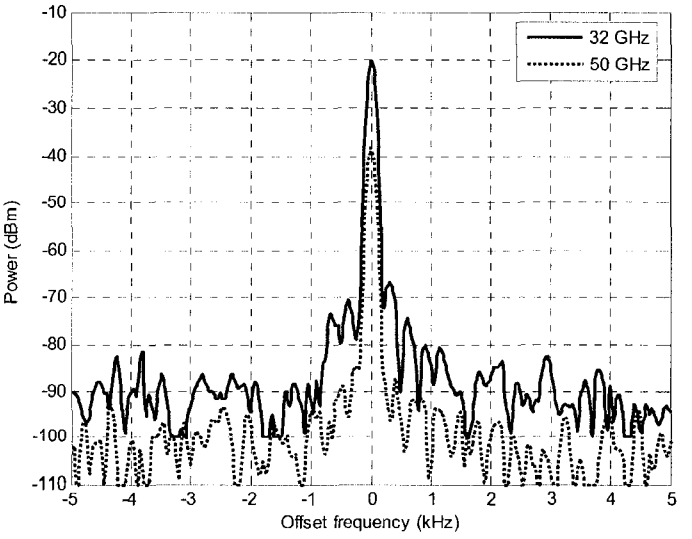

Fig. 6. Spectra of the generated mm-wave signals of 32 GHz and 50 GHz.

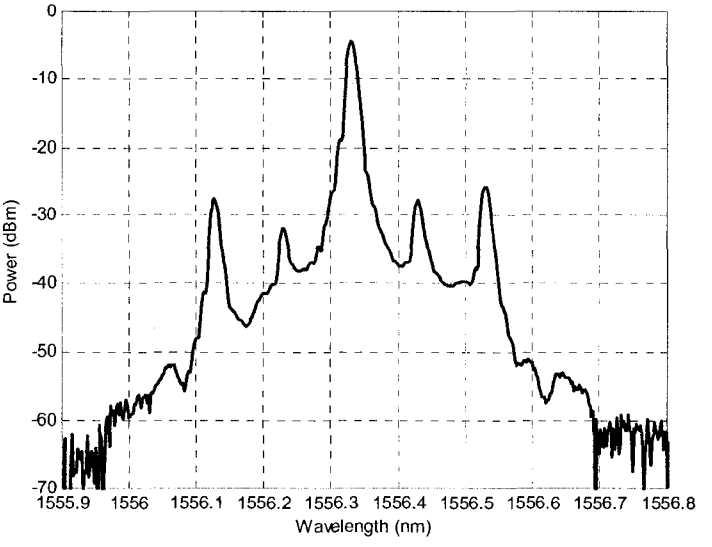

Fig. 7. Optical spectrum of the recovered carrier when the intensity modulator is driven by a 12.5 GHz microwave signal.

4. Conclusion

The generation of a continuously tunable mm-wave signal and the recovery an optical carrier based an SLM fiber ring laser incorporating an intensity modulator was proposed and demonstrated in this Section. An mm-wave signal from 32 GHz to 50 GHz with high spectral

purity was generated, and an uplink optical carrier of -5 dBm was recovered simultaneously at a base station after transmission over a 25 km standard single mode fiber.

Acknowledgements

The authors would like to thank John Oldham and David Barlow of the Communications Research Centre of Canada for their assistance in setting up the experimental system.

References:

[1] R. P. Braun, G. Grosskopf, D. Rohde, and F. Schmidt, "Optical millimetre-wave generation and transmission experiments for mobile 60 GHz band communications," *Electron. Lett.*, vol. 32, no. 7, pp. 626-628, Mar. 1996.

[2] L. Goldberg, H. F. Taylor, J. F. Weller, and D. M. Bloom, "Microwave signal generation with injection-locked laser diodes," *Electron. Lett.*, vol. 19, no. 13, pp. 491-493, Jun. 1983.

[3] R. T. Ramos and A. J. Seeds, "Fast heterodyne optical phase lock loop using double quantum well laser diodes," *Electron. Lett.*, vol. 28, no. 1, pp. 82-83, Jan. 1992.

[4] L. N. Langley, M. D. Elkin, C. Edge, M. J. Wale, U. Gliese, X. Huang, and A. J. Seeds, "Packaged semiconductor laser optical phase-locked loop (OPLL) for photonic generation, processing and transmission of microwave signals," *IEEE Trans. Microwave Theory Tech.*, vol. 47, no. 7, pp. 1257-1264, Jul. 1999.

[5] J. J. O'Reilly, P. M. Lane, R. Heidemann, and R. Hofstetter, "Optical generation of very narrow linewidth millimetre wave signals," *Electron. Lett.*, vol. 28, no. 25, pp. 2309-2311, Dec. 1992.

[6] J. J. O'Reilly and P. M. Lane, "Fibre-supported optical generation and delivery of 60 GHz signals," *Electron. Lett.*, vol. 30, no. 16, pp. 1329-1330, Aug. 1994.

[7] P. Shen, N. J. Gomes, P. A. Davies, W. P. Shillue, P.G. Huggard, and B. N. Ellison, "High-purity millimetre-wave photonic local oscillator generation and delivery," in *Proc. Microwave Photonics,* Sept. 2003, pp. 189-192.

[8] P. O. Hedekvist, B. E. Olsson, and A. Wiberg, "Harmonic generation of photonic microwave frequencies utilizing the properties of a phase modulator," in *Proc. Microwave Photonics,* Sept. 2003, pp. 193-196.

[9] G. Qi, J. P. Yao, J. Seregelyi, S. Paquet, and J. C. Bélisle, "Millimeter-wave carrier generation using an optical phase modulator and an optical notch filter," *Proceedings Of SPIE,* vol. 5579, pp. 673-679, Sept. 2004.

[10] A. Nirmalathas, D. Novak, C. Lim, and R. B. Waterhouse, "Wavelength reuse in the WDM optical interface of a millimeter-wave fiber-wireless antenna base station," *IEEE Trans. Microwave Theory Tech.* , vol. 49, no. 10, pp. 2006-2012, Oct. 2001.

[11] X. F. Chen, J. P. Yao, F. Zeng, and Z. Deng, "Single-longitudinal-mode fiber ring laser employing an equivalent-phase-shift fiber Bragg grating," *IEEE Photon. Tech. Lett.*, vol. 17, no. 7, pp. 1390-1392, Jul. 2005.

[12] G. Qi, J. P. Yao, J. Seregelyi, C. Belisle, and S. Paquet, "Generation and distribution of a wideband continuously tunable mm-wave signal with an optical external modulation technique," *IEEE Trans. Microwave Theory Tech.*, vol. 53, no. 10, pp. 3090-3097, Oct. 2005.

CHAPTER 4

QUALITY ANALYSES OF OPTICALLY GENERATED AND DISTRIBUTED MILLIMETER-WAVE SIGNALS

In this Chapter, the spectral purity of the optically generated electrical signals is analyzed using phase noise analysis. In Sec. 4.1, the phase noise performance of optically generated electrical signals based on external optical modulation techniques is investigated theoretically and experimentally. The effects of the phase fluctuation of the electrical drive signal, the phase fluctuation of the optical carrier, and the transmission effect of optical fiber on the spectral purity of generated electrical signals are taken into account in the theoretical analysis. The analysis is verified with an experimental setup with different linewidth of the optical source. In Sec. 4.2, a theoretical study of the effects of amplified spontaneous emission noise from optical amplifiers on the spectral purity of the optically generated electrical signals is performed. This is because applications of optical amplifiers, such as erbium-doped fiber amplifiers and semiconductor optical amplifiers, are inevitable in most optical millimeter-wave signal generation schemes. The result of the analysis gives a good explanation to experimental results observed in the earlier experimental studies to this subject.

4.1 Phase noise analysis of optically generated and distributed millimeter-wave signals

In this Section, the spectral purity of optically generated electrical signals based on external optical modulation techniques is investigated theoretically and experimentally. Effects caused by the phase fluctuation of the electrical drive signal applied to the external modulator and chromatic dispersion of optical fiber on the optically generated electrical signals are studied. With an experimental setup, spectra of optically generated mm-wave signals are measured for both locally and remotely generated electrical signals, and with optical carriers of different linewidths. The theoretical results agree with the experimental measurements.

Phase-noise analysis of optically generated millimeter-wave signals with external optical modulation techniques[4]

Guohua Qi, Jianping Yao, *Senior Member, IEEE*, Joe Seregelyi[*], Stéphane Paquet[*] and Claude Bélisle[*], Xiupu Zhang[**], *Member, IEEE*, Ke Wu[***], *Fellow, IEEE*, and Raman Kashyap[***]

Microwave Photonics Research Laboratory

School of Information Technology and Engineering

University of Ottawa, Ottawa, Ontario, Canada K1N 6N5

(Email: jpyao@site.uottawa.ca)

[*] Communications Research Centre

Ottawa, Ontario, Canada K2H 8S2

[**] Department of Electrical and Computer Engineering

Concordia Université, Montreal, Quebec, Canada

[***] École Polytechnique de Montréal, Québec, Canada.

Abstract

In this Section, we investigate theoretically and experimentally the phase noise performance of optically generated electrical signals based on external optical modulation techniques. Mathematical models are developed to represent perturbations on the transmitted optical signal caused by the phase fluctuations of the electrical drive signal applied to the external modulator and the optical carrier that feeds the external modulator. Closed form expressions of the power spectral density (PSD) for the electrical signals generated both locally and remotely are derived. The calculated PSD of the locally generated electrical signal indicates that its phase noise is determined only by the phase noise of the electrical drive signal. The PSD of the remotely generated signal shows that its spectral quality is also affected by chromatic dispersion of the fiber and the optical carrier linewidth. An experimental setup that can generate a millimeter-wave (mm-wave) signal continuously tunable from 32 GHz to 60 GHz using an electrical drive signal tunable from 8 GHz to 15 GHz is built. The spectra of the generated mm-wave signal are

[4] Published in *J. Lightwave Technol.*, vol. 24, no. 12, pp. 4861-4875, Dec. 2006.

measured for both locally and remotely generated electrical signals, with optical carriers of different linewidths. The theoretical results agree with the experimental measurements.

Index terms: Millimeter-wave generation, optical fiber dispersion, optical modulation, phase noise, spectral analysis, radio over fiber, microwave photonics

1. Introduction

Optical links have been widely used for the transmission of high-speed digital baseband signals because of the inherent low loss, low dispersion and wide bandwidth of single mode fibers, combined with the possibility of using optical amplifiers to compensate for the loss [1]. For similar reasons, use of optical links in wireless communication systems has increasingly attracted attention [2]-[5]. The advantages of optical links are even more noticeable when delivering radio frequency (RF), microwave, or mm-wave signals over long distances, for example, between a central office and base stations. They are particularly useful in applications like broadband wireless access networks [6], [7] and they have also found applications in military systems, such as antenna remoting, Doppler radar, and phased array antennas [8]-[10].

Key to this technology is the generation and distribution of microwave or mm-wave signals in the optical domain. In the past, extensive investigations of optical microwave generation systems have led to a variety of electrical signal generation methods. These methods employ techniques such as automatic frequency control loop [11], optical injection locking [12], optical phase-locked loop (OPLL) [13], [14], and external modulation [15]-[20]. The short- and long-term frequency stability of the optically generated mm-wave signals is critical because the resulting signal is generally used either as an RF carrier or a local oscillator signal in system applications. Optical frequency locking, optical injection locking and OPLL have all been used to improve the long-term frequency stability. An OPLL, when used in conjunction with a narrow linewidth optical source, can generate an mm-wave signal with high short-term frequency stability [21]. The short-term stability is directly related to the spectral purity of the generated signal and it can be characterized with phase noise measurement techniques.

Among the above mentioned signal generation methods, those using external modulation techniques have shown great potential for producing high-purity and frequency tunable

microwave or mm-wave signals [15], [19]. Thanks to the inherent nonlinearity of the external modulator, microwave generation techniques using external modulation enable the generation of microwave or mm-wave signals with a frequency that is two or four times that of the electrical drive signal, which makes the use of low-frequency, low cost external modulator possible. In 1994, O'Reilly applied such a method for the remote delivery of video services [22].

External-modulation-based signal generation schemes are built using a laser source, an electrical microwave source, an optical intensity or phase modulator, a photodetector and/or an optical filter. The microwave signals can be generated locally prior to fiber propagation and remotely after having propagated in a given length of optical fiber. For many applications, it is important to explore the quality of the generated electrical signal, especially its noise characteristics.

A number of previously published papers [23-29] have covered the modeling and measurement of signal phase noise in optical links within various contexts. For instance, phase noise caused by multiple reflections in an externally modulated optical link has been analyzed in [23]. A technique for measuring residual, single sideband (SSB) microwave phase noise added by an externally modulated fiber-optic link was reported in [24]. A model for calculating additive phase noise in direct-modulation optical links was presented in [25]. Chromatic dispersion effects on the phase noise of optical mm-wave systems were investigated in [26], [27] for direct and remote heterodyne detection. Effects of the amplified spontaneous emission (ASE) noise of an EDFA on the spectral broadening of optically generated electrical signals were experimentally examined in [28], [29]. However, no reports have covered the modeling of the phase noise in an external modulator-based generation system by considering the phase noise of the electrical drive signal.

In this Section, we present a theoretical and experimental investigation of the phase noise of an optically generated electrical signal by the external optical modulation technique. As part of this analysis, closed-form expressions for the PSD of the locally and remotely generated electrical signal are derived. An experimental setup is built to validate the theoretical analysis. The experimental setup can generate a continuously tunable mm-wave signal from 32 GHz to 60 GHz with the electrical drive signal tuned from 8 to 15 GHz. The experimental measurements

have verified that the phase noise of the locally generated mm-wave signal is independent of the effect of active optical components used in the system. In effect, the phase noise deterioration of the locally generated mm-wave signal can be modeled using the same theory employed for electronic frequency multipliers. Experimental results also showed that the phase noise of a remotely generated mm-wave signal has no noticeable phase noise deterioration compared with the locally generated electrical signal for transmission distances of 25 km and 50 km over standard single mode fiber (SSMF). These results are valid for an optical source at the spectral width of 700 kHz and 50 MHz. All these experimental results agree well with the theoretical PSD analysis. However, based on our theoretical analysis, using a low coherence optical source or extending the transmission length of the fiber will bring noticeable phase noise deterioration to the remotely generated mm-wave signal since the phase correlation between the optical sidebands is reduced. Optical carrier of a sliced ASE source with a 3-dB linewidth of 33 GHz is examined over different transmission distances over SSMF.

The paper is organized as follows. In Section II, mathematical models representing the generation of local and remote electrical signal using an external modulator are presented. Then, phase noise analysis of the electrical drive signal using the PSD of its phase fluctuation is performed in Section III. A review of the circuit theory representation of phase noise as a fractional power series of frequency is also presented in this Section. Phase noise of the locally generated electrical signal is analyzed in Section IV. Phase noise of the remotely generated electrical signal is analyzed in Section V. Experimental results and the validation of the theoretical models are detailed in Section VI. Lastly, conclusions are given in Section VII.

2. Optical microwave generation based on external optical modulation techniques

Systems used for generating mm-wave signals based on external modulation techniques [15]-[20] can be generally classified into two types: phase modulator and intensity modulator based configurations. They are shown in Fig. 1.

The configuration using an intensity modulator can be designed with or without an optical filter. For example, references [15], [19] presented a design that did not use an optical filter. A design that includes an optical filter was demonstrated in [16]. By properly biasing the intensity modulator, the odd-order sidebands were suppressed. The optical carrier was then removed with

the inclusion of a narrow-band, optical notch filter. A fourth-order harmonic of the electrical drive signal was thus generated. In the configuration using a phase modulator, the creation of the electrical signal requires the use of an optical filter [17], [20]. This is because the beating between the optical carrier and the optical sidebands at a photodetector will cancel completely the harmonics, and only a DC component is generated at the photodetector. This is understandable because phase modulation will not alter the amplitude of the modulated optical signal and a photodetector acts as an envelope detector. The use of an optical filter after the phase modulator to remove the optical carrier will lead to the generation of 2nd and 4th order harmonics. References [18], [20] discusses various filtering configurations, such as cascading the optical phase modulator with an optical polarizer, or incorporating the optical phase modulator in an optical loop mirror or a Faraday mirror, or the use of a narrow-band fiber Bragg grating (FBG) notch filter. In the remainder of this paper, we will use the configuration shown in Fig. 1 for our theoretical analysis and experimental verifications.

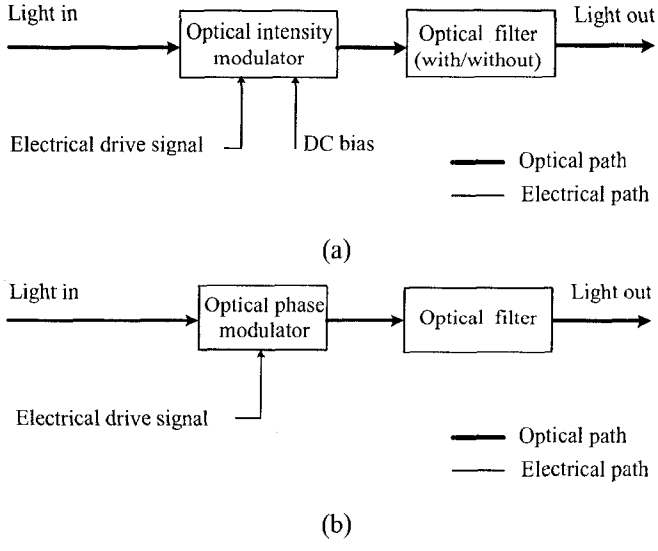

Fig. 1. Diagrams of systems for electrical signal generation based on external optical modulation techniques. (a) Optical intensity modulator-based system. (b) Optical phase modulator-based system.

Both the electrical signal and optical signal in Fig. 1 have a finite spectral width due to the phase fluctuations of the signal. Phase fluctuations for a single-frequency laser can be caused by, for example, refractive index variation in the laser due to temperature changes and carrier concentration effects. For the electrical source, the phase fluctuation comes from the thermal noise, the shot noise, and the $1/f$ noise [30]. All these phase fluctuations bear random characteristics. The phase noise statistics of the optical carrier and the electrical drive source are

treated as two independent random processes, which will define the spectral quality of the generated electrical signal. Phase fluctuations of a signal can be interpreted as a parasitic phase modulation of an ideal sinusoidal signal [30], [31]. This interpretation is valid for both the electrical drive signal and optical carrier in Fig. 1. It is assumed that both the optical carrier and the electrical drive signal are continuous wave (CW) in nature. Therefore, they can be expressed as

$$E(t) = E_o \cos[\omega_o t + \phi_o(t)], \tag{1}$$

and

$$V(t) = V_e \cos[\omega_e t + \phi_e(t)], \tag{2}$$

where $E(t)$ is the electric field of the optical carrier in scalar form (scalar form is used based on the assumption that the light is linearly polarized and it is aligned with the corresponding polarization state axis of the modulator), and $V(t)$ is the voltage of the electrical drive signal. E_o and ω_o are the electric field amplitude and angular frequency ($\omega_o = 2\pi f_o$) of the optical carrier. V_e and ω_e are the voltage amplitude and angular frequency ($\omega_e = 2\pi f_e$) of the electrical drive signal. Finally, $\phi_o(t)$ and $\phi_e(t)$ are two independent random processes that introduce phase fluctuations to the optical and electrical signals, respectively. It must be emphasized that we are studying a case where the phase noise is dominant and amplitude or intensity noise can be neglected due to the presence of limiting mechanisms in the electrical and optical source. It is true for most quality electrical and optical sources. Thus, E_o and V_e are assumed to be constant. For many fiber links, amplitude modulation (AM) noise of the link can be dominant and even exceed the phase noise contribution of the link, especially after many stages of optical amplification. But in an optical source, not a link, the link noise is much smaller than the phase noise of the source. Many experimental reports have verified that there is no obvious spectral broadening observed due to the link AM noise [28], [29].

A. Optical microwave generations based on an external optical intensity modulator

The optical signal at the output of an intensity modulator, shown in Fig. 1 (a), is given by [32]

$$E_I(t) = E_o \cos\left\{\frac{\phi_{DC}}{2} + \beta_i \cos[\omega_e t + \phi_e(t)]\right\} \cdot \cos[\omega_o t + \phi_o(t)], \quad (3)$$

where ϕ_{DC} is the constant phase shift determined by the DC bias voltage, β_i is a modulation index expressed as

$$\beta_i = \frac{\pi}{V_{\pi i}} \cdot \frac{V_e}{2}, \quad (4)$$

where $V_{\pi i}$ is the half-wave voltage of the intensity modulator. Expanding equation (3), we have

$$E_I(t) = E_o \cos(\frac{\phi_{DC}}{2}) J_0(\beta_i) \cos[\omega_o t + \phi_o(t)]$$

$$+ E_o \cos(\frac{\phi_{DC}}{2}) \sum_{n=1}^{\infty} J_{2n}(\beta_i)$$

$$\times \{\cos[\omega_o t - 2n\omega_e t + \phi_o(t) - 2n\phi_e(t) + n\pi] + \cos[\omega_o t + 2n\omega_e t + \phi_o(t) + 2n\phi_e(t) - n\pi]\}$$

$$+ E_o \sin(\frac{\phi_{DC}}{2}) \sum_{n=1}^{\infty} J_{2n-1}(\beta_i)$$

$$\times \{\cos[\omega_o t - (2n-1)\omega_e t + \phi_o(t) - (2n-1)\phi_e(t) + n\pi] + \cos[\omega_o t + (2n-1)\omega_e t + \phi_o(t) + (2n-1)\phi_e(t) - n\pi]\}, \quad (5)$$

where J_n is the Bessel function of the first kind, of order n. Equation (5) shows that the power of the input optical carrier spreads to the first-, second-, third- and higher-order optical sidebands. The amplitude of these sidebands is governed by the corresponding order of Bessel function parameterized by β_i. Their amplitude is also affected by ϕ_{DC}. Fig. 2 (a) shows a general optical spectrum obtained from (5).

Different values of ϕ_{DC} can be obtained by adjusting the DC bias. There are two sets of important values: $\phi_{DC} = 2k\pi$ and $\phi_{DC} = (2k-1)\pi$, where k is an integer. When $\phi_{DC} = (2k-1)\pi$, all even-order optical sidebands disappear. Fig. 2 (b) shows the optical spectrum when even-order optical sidebands are suppressed by tuning the DC bias. With an appropriate power level of the electrical drive signal, the 2nd and higher-order optical sidebands can be ignored. The beating

between the two 1st-order sidebands will lead to the generation of a microwave signal that has two times the frequency of the electrical drive signal. An optical filter is not required for this configuration [15]. In this specific scenario, equation (5) is reduced to

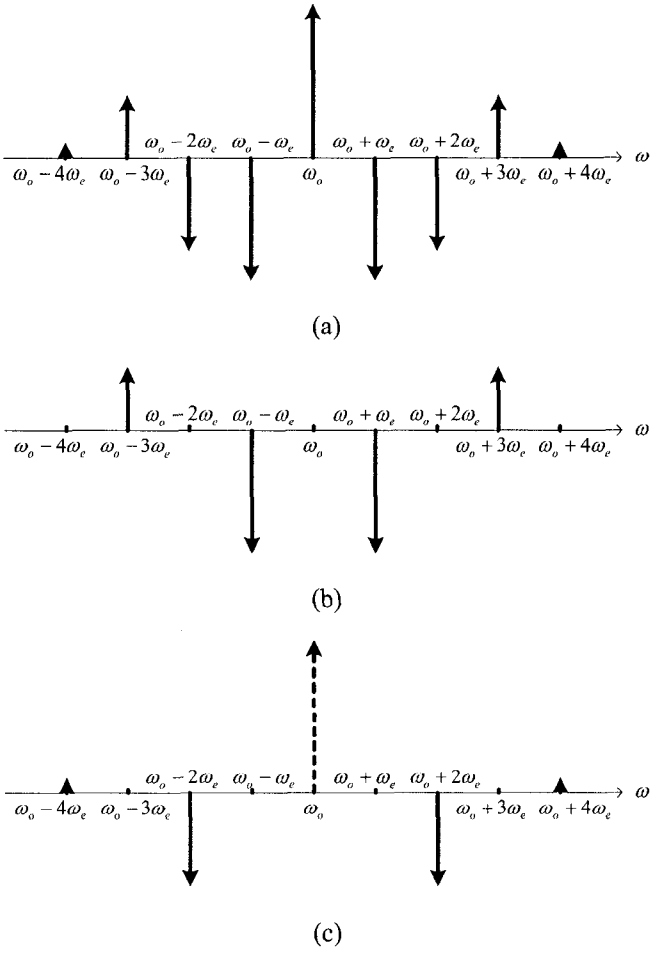

Fig. 2. Typical optical spectra generated by an optical intensity modulator. The arrow direction shows the relationship between the phase of the sidebands and the phase of the optical carrier. (a) A general spectrum. (b) Even-order optical sidebands suppressed. (c) Odd-order optical sidebands and the optical carrier suppressed.

$$E_{I1}(t) = -E_o J_1(\beta_i)\{\cos[(\omega_o - \omega_e)t + \phi_o(t) - \phi_e(t)] + \cos[(\omega_o + \omega_e)t + \phi_o(t) + \phi_e(t)]\}. \quad (6)$$

O'Reilly et al. proposed another approach by biasing the intensity modulator to meet the $\phi_{DC} = 2k\pi$ condition, which can be used to generate an electrical signal having four times the frequency of the electrical drive signal [16]. In their system, they used an unbalanced Mach-Zehnder interferometer with a specific free spectral range (FSR) to select the second-order

optical sidebands and, therefore, improve the suppression of the unwanted optical sidebands. In this approach, the optical intensity modulator is biased at zero volts. In the experimental Section of this paper, we will demonstrate a simplified approach to generating a microwave frequency that has 4 times the frequency of the electrical drive signal. A key device in our approach is a narrow-band FBG notch filter. The optical intensity modulator is biased to have a constant optical phase of $\phi_{DC} = 2k\pi$ to suppress the odd-order optical sidebands. The optical notch filter is placed at the output of the optical intensity modulator to filter out the optical carrier (the zero order in (5)). Fig. 2 (c) shows the optical spectrum when the odd-order optical sidebands are suppressed and the optical carrier (the dashed line) is removed. Using an appropriate power level for the electrical drive signal, optical sidebands of orders higher than the second have very low power and can be ignored. Then, an optical microwave generation system having a similar optical spectrum as in [16] is obtained. Since we use a fixed FBG notch filter, the frequency separation of the two optical sidebands in our approach can be continuously tuned by changing the frequency of the electrical drive signal. Therefore, a continuously frequency tunable mm-wave signal can be generated. In our configuration and the one described in [16], equation (5) is reduced to

$$E_{I2}(t) = E_o J_2(\beta_I)\{\cos[(\omega_o - 2\omega_e)t + \phi_o(t) - 2\phi_e(t)] + \cos[(\omega_o + 2\omega_e)t + \phi_o(t) + 2\phi_e(t)]\}. \quad (7)$$

B. Optical microwave generation based on an external optical phase modulator

When the optical carrier and electrical drive signal in equations (1) and (2) are applied to an optical phase modulator (case shown in Fig. 1 (b)), the optical field at its output is given by

$$E_P(t) = E_o \cos[\omega_o t + \phi_o(t) + \beta_p \cos[\omega_e t + \phi_e(t)]]$$

$$= E_o \sum_{n=-\infty}^{+\infty} J_n(\beta_p) \cos\left[(\omega_o + n\omega_e)t + \phi_o(t) + n\phi_e(t) + n\frac{\pi}{2}\right], \quad (8)$$

where $\beta_p = \frac{\pi}{V_{\pi p}} \cdot V_e$, $V_{\pi p}$ is the half-wave voltage of the optical phase modulator. J_n is defined as before. A typical spectrum calculated from (8) is shown in Fig. 3 (a).

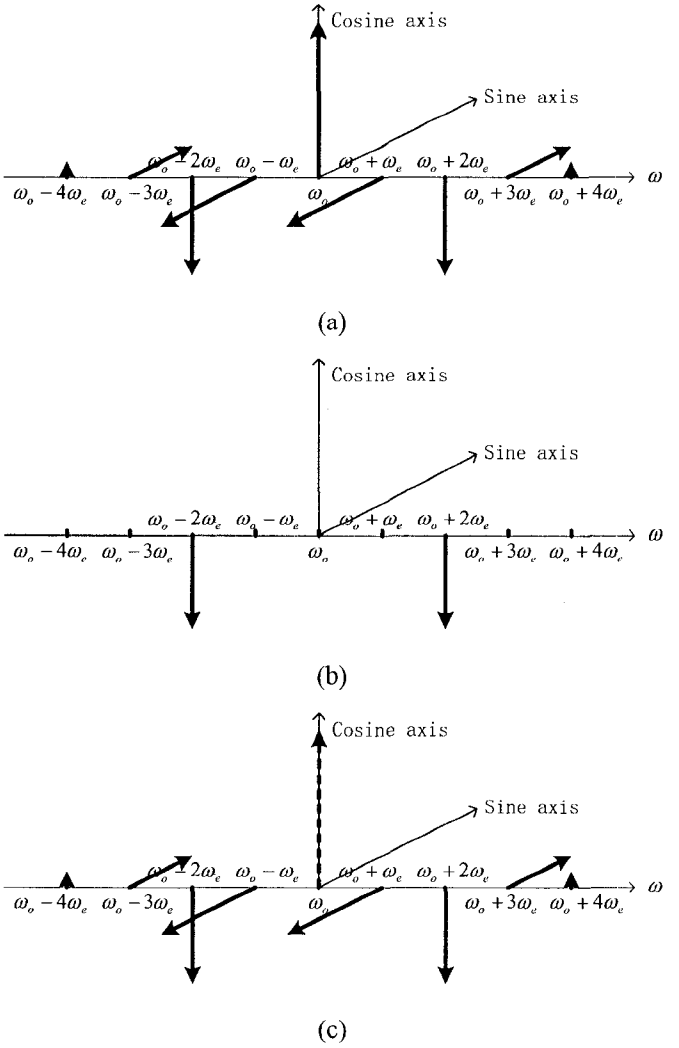

Fig. 3. Typical optical spectra generated by an optical phase modulator. (a) A general spectrum. (b) Filtered spectrum with an F-P filter. (c) Filtered spectrum with an FBG notch filter.

Various configurations have been suggested using a phase modulator. The approach in [17] used a Fabry-Perot filter to select the second-order optical sidebands at the output of the phase modulator. The corresponding optical spectrum is shown in Fig. 3 (b). For this configuration, equation (8) is reduced to

$$E_{P1}(t) = -E_o J_2(\beta_p)\{\cos[(\omega_o - 2\omega_e)t + \phi_o(t) - 2\phi_e(t)] + \cos[(\omega_o + 2\omega_e)t + \phi_o(t) + 2\phi_e(t)]\}. \quad (9)$$

In another approach [20], an optical notch filter is used to eliminate the optical carrier at the output of the optical phase modulator. The resulting spectrum is shown in Fig. 3 (c). The dashed arrow signifies the removal of the optical carrier. Using (8), the optical signal after the notch filter is then given by

$$E_{P2}(t) = E_o \sum_{n=-\infty}^{+\infty} J_n(\beta_p) \cos\left[(\omega_o + n\omega_e)t + \phi_o(t) + n\phi_e(t) + n\frac{\pi}{2}\right] - E_o J_0(\beta_p)\cos(\omega_o t + \phi_o(t)). \quad (10)$$

Comparing (6), (7), and (9), we obtain a general expression for the optical signal produced by the configurations based on i) an intensity modulator alone, ii) an intensity modulator with a notch filter to eliminate the optical carrier and iii) a phase modulator with a Fabry-Perot filter

$$E_{out}(t) = E_o J_n(\beta)\{\cos[(\omega_o - n\omega_e)t + \phi_o(t) - n\phi_e(t)] + \cos[(\omega_o + n\omega_e)t + \phi_o(t) + n\phi_e(t)]\}, \quad (11)$$

where β is a general representation of the modulation index β_i or β_p. n is a positive integer with $n = 1$ or $n = 2$. Optical signals expressed in (10) and (11) represent all reported approaches for harmonically generated electrical signals based on external optical modulation techniques. In the following, we will discuss the phase noise performance of the optically generated microwave signals.

3. Phase noise representation of the electrical drive signal

A. Low-index approximation of the electrical drive signal

Due to the intrinsic properties of the noise and the central limit theorem, the phase fluctuation $\phi_e(t)$ of the electrical signal $V(t)$ expressed by (2) is classically treated as a stationary zero - mean Gaussian random process [33]. This allows the existence of the autocorrelation function $R_{\phi e}(\tau)$ of $\phi_e(t)$ as

$$R_{\phi e}(\tau) = \langle \phi_e(t+\tau)\phi_e(t) \rangle, \quad (12)$$

where τ is a time shift and $\langle\ \rangle$ represents the ensemble average. Using the Wiener-Khintchine theorem [34], the double sideband (DSB) PSD $S_{\phi e}(f)$ of $\phi_e(t)$ can be obtained as

$$S_{\phi e}(f) = F[R_{\phi e}(\tau)], \quad (13)$$

where F denotes the Fourier transform operation. Although $S_{\phi e}(f)$ has theoretical pertinence, it is not a quantity that can be directly measured. In contrast, the SSB PSD of $V(t)$, where $V(t)$ is a random process built up from $\phi_e(t)$, can be measured by a spectrum analyzer.

Using a noise model that assumes the low-index phase modulation of $\phi_e(t)$ [35], the DSB PSD $S_{\phi e}(f)$ of $\phi_e(t)$ has a simple relation with the measurable SSB PSD of $V(t)$. This condition is met in most practical applications in which the electrical drive signal is created by an electrical source with a high spectral quality. Under this condition, the electrical drive signal has a small phase fluctuation and $R_{\phi e}(0) << 1$, i.e. the mean power of the phase fluctuation $\phi_e(t)$ is much smaller than 1 rad^2. In the remainder of this paper, our analysis is developed under the low phase modulation index condition.

In order to obtain the expression giving the SSB PSD of $V(t)$, we have to first find the expression for its autocorrelation function. It is found that $V(t)$ is not stationary in a wide sense (WSS) although $\phi_e(t)$ is stationary [35]. However, $V(t)$ has a defined time-averaged autocorrelation function. If $R_V(\tau)$ and $S_V(f)$ are denoted as the time-averaged autocorrelation function and the SSB PSD of the electrical drive signal $V(t)$, respectively, then $R_V(\tau)$ can be obtained by using

$$R_V(\tau) = \overline{\langle V(t+\tau)V(t)\rangle}$$

$$= \frac{V_e^2}{2}\cos(\omega_e\tau)\exp\left\{-\left[R_{\phi e}(0) - R_{\phi e}(\tau)\right]\right\}, \tag{14}$$

where $\overline{f(t)}$ represents time average of $f(t)$ and τ is a time shift. Equation (14) makes use of the fact that $\phi_e(t)$ is a stationary zero-mean Gaussian random process. With the condition that $R_{\phi e}(0) << 1$ generally, $R_V(\tau)$ can be further simplified as

$$R_V(\tau) \cong \frac{V_e^2}{2}\cos(\omega_e\tau)\left[1 - R_{\phi e}(0) + R_{\phi e}(\tau)\right] \tag{15}$$

Using the Wiener-Khintchine theorem, the SSB $S_V(f)$ is found to be

$$S_V(f) \cong F\left[R_V(\tau)\right]$$

$$= \frac{V_e^2}{2}\left[1 - R_{\phi e}(0)\right]\delta(f - f_e) + \frac{V_e^2}{2}S_{\phi e}(f - f_e), \tag{16}$$

where $\delta(f)$ is the impulse function and $S_{\phi e}(f)$ is the DSB PSD of $\phi_e(t)$). Equation (16) indicates that $S_V(f)$ is an exact replica of the DSB $S_{\phi e}(f)$ around f_e except that it is multiplied by the constant linear factor $V_e^2/2$. Therefore, one can use the measurable function $S_V(f)$ to represent $S_{\phi e}(f)$ for characterizing the phase fluctuation of an electrical drive signal with high spectral quality.

B. SSB PSD and phase noise measurement of the electrical drive signal

Based on circuit theory, the SSB PSD of an electrical signal produced by an oscillator can be expressed as a power series of offset frequencies [30], [33]. The overall noise of the oscillator is contributed from various types of noise, such as $1/f$ noise, shot noise, and thermal noise. Considering these, the SSB PSD of the electrical signal can be expressed as

$$S(f) = \frac{A}{|f - f_c|^2} + \frac{B}{|f - f_c|^3}, \tag{17}$$

where f_c is the center frequency of the electrical signal, A and B are two constants, f is an arbitrary frequency around f_c and $f \neq f_c$. Again, we would like to assess the relationship between the measured function $S_V(f)$ and the expression defined in (17).

To do so, we introduce another technique to evaluate the phase noise. It is based on the ratio of the power in one phase modulation sideband (on a per-Hertz basis) to the total power of the signal [36]. This new quantity is denoted as $L_V(f_m)$ and called the phase noise of the signal, where f_m represents a frequency shift from the carrier frequency f_e. It can be demonstrated that $L_V(f_m)$ can be expressed as a function of $S_V(f)$ by using

$$L_V(f_m) = \frac{P_{SSB}(f_e + f_m, 1Hz)}{P_e}$$

$$\cong \frac{S_V(f_e + f_m)}{P_e} = \frac{1}{P_e}\left[\frac{A}{f_m^2} + \frac{B}{f_m^3}\right], \tag{18}$$

where $P_e = V_e^2/2$ is the average power of the electrical signal expressed in (2) and $f_m > 0$. Therefore, $L_V(f_m)$ is proportional to $S_V(f)$, the proportionality constant being the inverse of the average power in $V(t)$. A typical plot of $L_V(f_m)$ is shown in Fig. 4. Finally, we conclude that the PSD of $V(t)$ completely describes the phase noise of the electrical signal. Hence, in the remainder of the paper, the analysis will be focused on the evaluation of the PSDs of the optically generated electrical signals.

The singularity of the SSB PSD expressed in (17) does not allow us to perform an inverse Fourier transform to obtain its autocorrelation function. However, based on (13), (16) and (17), we can loosely denote that

$$S_{\phi\phi}(f) = F[R_{\phi\phi}(\tau)] \cong \frac{1}{P_e}\left[\frac{A}{|f|^2} + \frac{B}{|f|^3}\right], \tag{19}$$

where $f \neq 0$.

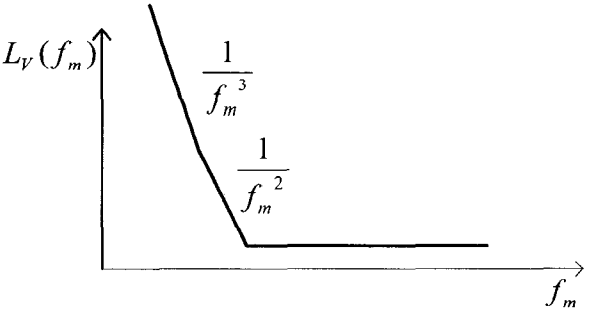

Fig. 4. Phase noise $L_V(f_m)$ in the approximation of a power of offset frequency.

4. Phase noise analysis of the locally generated microwave signals

When the optical signal expressed in (10) or (11) is fed into a square-law photodetector, electrical signals will be generated. For the optical signal defined in (10), the generated high-frequency electrical signal, $V_{P2}(t)$, can be written as

$$V_{P2}(t) = C_1 \sum_{n=1}^{+\infty} J_0(\beta_p) J_{2n}(\beta_p) \cos[2n\omega_e t + 2n\phi_e(t) + n\pi], \tag{20}$$

where C_1 is a constant related to the value of E_o and the responsivity of the photodetector, and the property of the Bessel function, $J_{-n}(\beta_p) = (-1)^n J_n(\beta_p)$ is used. Equation (20) clearly indicates that only even-order harmonics of the electrical drive signal are generated [20]. Equation (20) also shows that the phase fluctuation of the generated electrical harmonics is not affected by the phase fluctuation $\phi_o(t)$ of the optical carrier. This is because there is a complete correlation between the noises presented at the sidebands defined by (10), since the light feeding the modulator comes from a single light source. Therefore, complete noise cancellation occurs after photodetection. Thus, the phase fluctuation of the optical source will not contribute to the phase noise of the generated electrical signal. Similarly, for optical signal expressed in (11), the generated high-frequency electrical signal is

$$V_{out}(t) = C_1 J_n^{\,2}(\beta)\cos[2n\omega_e t + 2n\phi_e(t)], \tag{21}$$

where C_1 is defined as before.

Concentrating on one of the harmonics defined in (20) and (21) enables us to use a common mathematical expression for $V_{P2}(t)$ and $V_{out}(t)$:

$$V_L(t) = C_L \cos[2n\omega_e t + 2n\phi_e(t)], \tag{22}$$

where C_L is a constant.

Applying the theory developed in Section III A, the autocorrelation function of $V_L(t)$ is found to be

$$R_{V_L}(\tau) \cong \frac{C_L^{\,2}}{2}\cos(2n\omega_e\tau)\left[1 - (2n)^2 R_{\phi e}(0) + (2n)^2 R_{\phi e}(\tau)\right], \tag{23}$$

and the SSB PSD of $V_L(t)$ is

$$S_{V_L}(f) = F[R_{V_L}(\tau)]$$

$$\cong \frac{C_L^{\,2}}{2}\left[1 - (2n)^2 R_{\phi e}(0)\right]\delta(f - 2nf_e) + \frac{C_L^{\,2}}{2}(2n)^2 S_{\phi e}(f - 2nf_e)\cdot \tag{24}$$

Using (19) to express $S_{\phi e}(f)$ in the form of $L_V(f_m)$, we obtain a closed-form expression of the SSB PSD of the locally generated electrical signal.

$$S_{V_L}(f) \cong \frac{C_L^{\,2}}{2}\left[1-(2n)^2 R_{\phi e}(0)\right]\delta(f-2nf_e) + \frac{C_L^{\,2}}{2}(2n)^2 \frac{1}{P_e}\left[\frac{A}{|f-2nf_e|^2}+\frac{B}{|f-2nf_e|^3}\right]. \tag{25}$$

Because the total average power of $V_L(t)$ is $C_L^{\,2}/2$, the SSB phase noise $L_{V_L}(f_m)$ of $V_L(t)$ is then given by

$$L_{V_L}(f_m) = \frac{S_{V_L}(2nf_e+f_m)}{C_L^{\,2}/2}$$

$$\cong (2n)^2 \frac{1}{P_e}\left[\frac{A}{|f_m|^2}+\frac{B}{|f_m|^3}\right], \tag{26}$$

where f_m is the offset frequency away from $2nf_e$.

It is clear that $L_{V_L}(f_m)$ in (26) is $(2n)^2$ times $L_V(f_m)$ in (18). It shows that the phase noise of the locally generated electrical signal has a $20\log(2n)$ (dB) degradation with respect to the phase noise of the electrical drive signal, where $2n$ is the frequency multiplication number. This is exactly the same result as would be obtained for an electronic frequency multiplier [37]. Due to the absence of the transmission fiber, in the optical sidebands, the phase noises originated from the optical source are fully correlated. They cancelled in the beating process. So the phase noise of the locally generated electrical is immunized to the phase noise of the optical source.

5. Phase noise analysis of the remotely generated electrical signals

The phase noise present in the side bands of the optical carrier is fully correlated. Therefore, the phase noise of the locally generated electrical signal can be much lower that that of the optical source. However, when these optical signals, as expressed in (10) and (11), are transmitted over SSMF, different time delays will be introduced to the various optical sidebands at the output of the system because of chromatic dispersion. If the frequency of an optical sideband is nf_e, the

time delay difference (τ_D) between the nth-order sideband and the optical carrier at the end of the span is given by: ,

$$\tau_D = DL\delta\lambda = -n\tau_d, \tag{27}$$

where

$$\tau_d = \frac{DL\lambda_0^2 f_e}{c}, \tag{28}$$

τ_d is the fundamental time delay difference between the 1st-order sideband and the optical carrier, D is the chromatic dispersion parameter of the fiber (typically 17 ps/(nm·km) at 1550 nm for SSMF), L is the length of the fiber, $\delta\lambda$ is the wavelength difference between the optical carrier and the nth-order optical sideband, λ_o is the center wavelength of the optical source, c is the speed of light in free space, and n is the sideband order.

For the optical signal defined in (11), the expression for the optical signal at the end of the link is

$$E_2(t) = \alpha E_o J_n(\beta)\cos[(\omega_o - n\omega_e)(t - n\tau_d) + \phi_o(t - n\tau_d) - n\phi_e(t - n\tau_d)]$$

$$+ \alpha E_o J_n(\beta)\cos[(\omega_o + n\omega_e)(t + n\tau_d) + \phi_o(t + n\tau_d) + n\phi_e(t + n\tau_d)], \tag{29}$$

$E_2(t)$ represents the output signal when the input signal is $E_{out}(t)$ in (11). Also, α is the attenuation of the fiber.

We now express the electrical signal generated from the optical signal defined in (29)

$$V_R(t) = C_R \cos\{2n\omega_e t + 2n\omega_o\tau_d + n[\phi_e(t + n\tau_d) + \phi_e(t - n\tau_d)] + \phi_o(t + n\tau_d) - \phi_o(t - n\tau_d)\}, \tag{30}$$

where C_R is a constant, which is related to values α, E_o, $J_n(\beta)$, and the responsivity of the photodetector. Equation (30) shows that the phase fluctuation of the remotely generated electrical signal depends on the fiber chromatic dispersion and the phase fluctuations of the electrical drive signal and optical carrier.

$V_R(t)$, like $V(t)$, is not a WSS random process. The time-averaged autocorrelation function of $V_R(t)$, denoted by $R_{V_R}(\tau)$, is given by

$$R_{V_R}(\tau) = \overline{\langle V_R(t+\tau)V_R(t)\rangle}$$

$$= \frac{C_R^{\,2}}{2}\cos(2n\omega_e\tau) \times \left\langle \cos\left\{n\left[\phi_e(t+n\tau_d+\tau) - \phi_e(t+n\tau_d) + \phi_e(t-n\tau_d+\tau) - \phi_e(t-n\tau_d)\right]\right\}\right\rangle$$

$$\times \left\langle \cos\left[\phi_o(t+n\tau_d+\tau) - \phi_o(t+n\tau_d) - \phi_o(t-n\tau_d+\tau) + \phi_o(t-n\tau_d)\right]\right\rangle, \tag{31}$$

where $\overline{f(t)}$, $\langle\ \rangle$, and τ are defined as before. The independent property of $\phi_o(t)$ and $\phi_e(t)$, and the zero-mean Gaussian property of $\phi_o(t)$ and $\phi_e(t)$ are used in obtaining (31). To better understand the contribution of each factor to the phase noise of the remotely generated electrical signal, $R_{V_R}(\tau)$ can be rewritten as

$$R_{V_R}(\tau) = \frac{C_R^{\,2}}{2}\cos(2n\omega_e\tau)R_{e,R}(\tau)R_{o,R}(\tau), \tag{32}$$

where

$$R_{e,R}(\tau) = \left\langle \cos\left\{n\left[\phi_e(t+n\tau_d+\tau) - \phi_e(t+n\tau_d) + \phi_e(t-n\tau_d+\tau) - \phi_e(t-n\tau_d)\right]\right\}\right\rangle, \tag{33}$$

and

$$R_{o,R}(\tau) = \left\langle \cos\left[\phi_o(t+n\tau_d+\tau) - \phi_o(t+n\tau_d) - \phi_o(t-n\tau_d+\tau) + \phi_o(t-n\tau_d)\right]\right\rangle. \tag{34}$$

$R_{e,R}(\tau)$ and $R_{o,R}(\tau)$ are the electrical and optical autocorrelation functions of $R_{V_R}(\tau)$, respectively. If $S_{V_R}(f)$ is denoted as the SSB PSD of $V_R(t)$, $S_{e,R}(f)$ and $S_{o,R}(f)$ are denoted as the Fourier transforms of $R_{e,R}(\tau)$ and $R_{o,R}(\tau)$, respectively, then

$$S_{V_R}(f) = F[R_{V_R}(\tau)]$$

$$= \frac{C_R^{\,2}}{2}\delta(f-2nf_e) * S_{e,R}(f) * S_{o,R}(f), \tag{35}$$

where * is the convolution operator. $S_{e,R}(f)$ and $S_{o,R}(f)$ are the DSB PSD of the electrical and optical contributions to $S_{V_R}(f)$, respectively. They are investigated separately in the following two Subsections.

A. Electrical driving signal contribution to the SSB PSD of the remotely generated electrical signal

Based on the assumption that $\phi_e(t)$ is stationary and on the spectral quality of the electrical drive signal discussed in Section III A, the low phase modulation index approximation is used again to simplify the expression of $R_{e,R}(\tau)$ in (33). $R_{e,R}(\tau)$ can then be expressed as a function of $R_{\phi e}(\tau)$:

$$R_{e,R}(\tau) \cong 1 - 2n^2[R_{\phi e}(0) + R_{\phi e}(2n\tau_d)] + n^2\left[2R_{\phi e}(\tau) + R_{\phi e}(\tau + 2n\tau_d) + R_{\phi e}(\tau - 2n\tau_d)\right]. \tag{36}$$

Then $S_{e,R}(f)$ is found to be

$$S_{e,R}(f) = F[R_{e,R}(\tau)]$$

$$\cong \left\{1 - 2n^2[R_{\phi e}(0) + R_{\phi e}(2n\tau_d)]\right\}\delta(f) + (2n)^2 \cos^2(2n\pi\tau_d f)\frac{1}{P_e}\left[\frac{A}{|f|^2} + \frac{B}{|f|^3}\right]. \tag{37}$$

We have used the expression for $S_{\phi e}(f)$ given in (19) to obtain (37).

Note that when $\tau_d = 0$, equation (37) becomes identical to (25) if the constant amplitude and frequency shift are ignored. That means that the DSB PSD expression in (37) is more general for characterizing the phase noise of the optically generated electrical signal.

Typical plots of $S_{e,R}(f)/S_{\phi e}(f)$ in dB for frequency greater than zero are shown in Fig. (5).

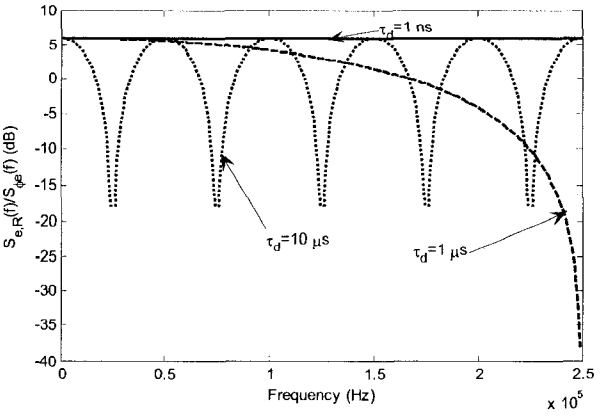

(a)

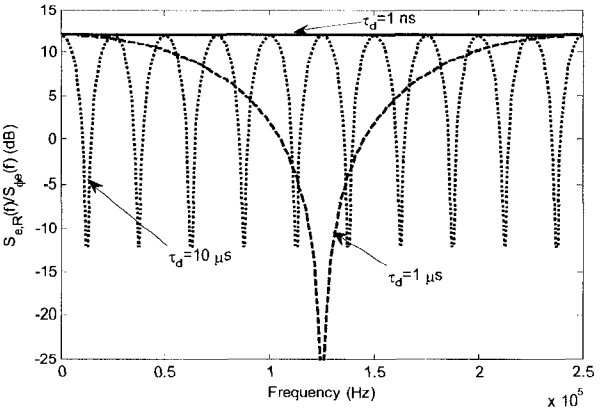

(b)

Fig. 5. Plots of $S_{e,R}(f)/S_{\phi e}(f)$ (a) $n=1$. (b) $n=2$.

B. Optical carrier contribution to the SSB PSD of the remotely generated electrical signal

The phase fluctuation of the optical carrier expressed in (1) is characterized by a Wiener-Lèvy process [39], i.e.

$$\phi_o(t) = 2\pi \int_0^t F(\tau)d\tau\,, \tag{38}$$

where $F(t)$ is a white Gaussian random process characterizing the frequency noise in a laser source. The power spectral density of $F(t)$ is a constant N_0. The PSD of the noisy carrier $E(t) = \exp[j\phi_o(t)]$, denoted $S_E(f)$, turns out to be Lorenzian in shape [39],

$$S_E(f) = \frac{2}{\pi B} \frac{1}{1+\left(\frac{2f}{B}\right)^2}, \tag{39}$$

where $B = 2\pi N_0$ denotes the two-sided half-power bandwidth.

It is clear that the Wiener-Lèvy process $\phi_o(t)$ expressed in (38) is a non-stationary zero-mean Gaussian process and is not periodic with respect to time. Hence, the time average technique that we used earlier for obtaining the autocorrelation functions of $V(t)$ and $V_L(t)$ cannot be used here. Without the autocorrelation function of $\phi_o(t)$, the low-index approximation treatment cannot be used for the analysis of $S_{o,R}(f)$.

However, one interesting property of the statistical distribution given in (38) is that all phase fluctuations over non-overlapping time periods are statistically independent [34]. This allows us to obtain an expression of $S_{o,R}(f)$ from $R_{o,R}(\tau)$ in (35). $S_{o,R}(f)$ is

$$S_{o,R}(f) = \exp\left[-\frac{4n\tau_d}{\tau_c}\right]\left\{\delta(f) + \frac{\tau_c}{1+(\pi f\tau_c)^2} \times \left\{\exp\left[\frac{4n\tau_d}{\tau_c}\right] - \cos(4n\pi f\tau_d) + \pi f\tau_c \sin(4n\pi f\tau_d)\right\}\right.$$

$$\left. - \frac{\sin(4n\pi f\tau_d)}{\pi f}\right\}, \tag{40}$$

where τ_c is the coherence time of the optical carrier [40], and

$$\tau_c = \frac{1}{\pi B}. \tag{41}$$

The derivation of (40) is given in the Appendix A.

Typical plots of $S_{o,R}(f)$ in dBm are shown in Fig. 6, where the 3-dB linewidth of the laser source is 10 MHz.

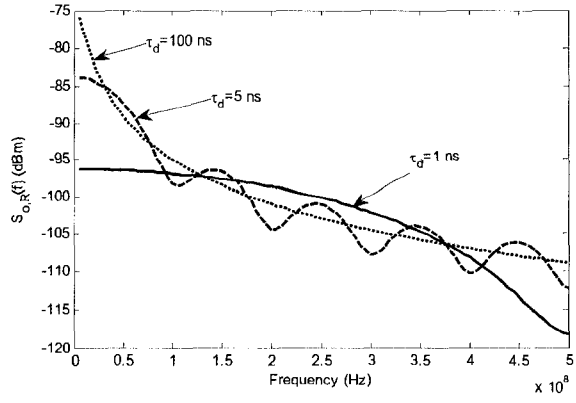

(a)

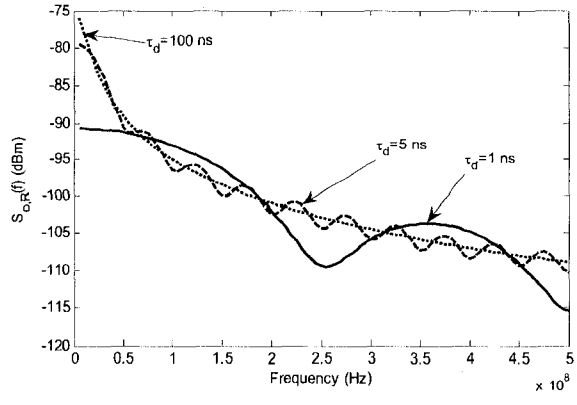

(b)

Fig. 6. Plots of $S_{o,R}(f)$ for $B = 10$ MHz. (a) $n = 1$. (b) $n = 2$.

Substitute (37) and (40) into (35), we obtain the closed-form expression of $S_{V_R}(f)$.

$$S_{V_R}(f) = \frac{C_R^{\,2}}{2}\exp\left[-\frac{4n\tau_d}{\tau_c}\right]\delta(f - 2nf_c)$$

$$* \left\{\left\{1 - 2n^2[R_{\phi e}(0) + R_{\phi e}(2n\tau_d)]\right\}\delta(f)\right.$$

$$+ (2n)^2\cos^2(2n\pi\tau_d f)\frac{1}{P_e}\left[\frac{A}{|f|^2} + \frac{B}{|f|^3}\right] + \left\{1 - 2n^2[R_{\phi e}(0) + R_{\phi e}(2n\tau_d)]\right\}\left\{\frac{\tau_c}{1 + (\pi\tau_c f)^2}\right.$$

$$\left.\times\left\{\exp\left[\frac{4n\tau_d}{\tau_c}\right] - \cos(4n\pi\tau_d f) + \pi\tau_c f\sin(4n\pi\tau_d f)\right\} - \frac{\sin(4n\pi\tau_d f)}{\pi f}\right\}$$

$$+(2n)^2\cos^2(2n\pi\tau_d f)\frac{1}{P_e}\left[\frac{A}{|f|^2}+\frac{B}{|f|^3}\right]*\left\{\frac{\tau_c}{1+(\pi\tau_c f)^2}\right.$$

$$\left.\times\left\{\exp\left[\frac{4n\tau_d}{\tau_c}\right]-\cos(4n\pi\tau_d f)+\pi f\tau_c\sin(4n\pi\tau_d f)\right\}-\frac{\sin(4n\pi\tau_d f)}{\pi f}\right\}, \tag{42}$$

where $*$ is the convolution operator. If the SSB phase noise of the remotely generated electrical signal is denoted as $L_{V_R}(f_m)$, the expression of $L_{V_R}(f_m)$ obtained from $S_{V_R}(f)$ is

$$L_{V_R}(f_m)\approx$$

$$(2n)^2\cos^2(2n\pi\tau_d f_m)\frac{1}{P_e}\left[\frac{A}{|f_m|^2}+\frac{B}{|f_m|^3}\right]$$

$$+\frac{\tau_c}{1+(\pi\tau_c f_m)^2}\times\left\{\exp\left[\frac{4n\tau_d}{\tau_c}\right]-\cos(4n\pi\tau_d f_m)+\pi\tau_c f_m\sin(4n\pi\tau_d f_m)\right\}$$

$$-\frac{\sin(4n\pi\tau_d f_m)}{\pi f_m}$$

$$+(2n)^2\cos^2(2n\pi\tau_d f_m)\frac{1}{P_e}\left[\frac{A}{|f_m|^2}+\frac{B}{|f_m|^3}\right]*\left\{\frac{\tau_c}{1+(\pi\tau_c f_m)^2}\right.$$

$$\left.\times\left\{\exp\left[\frac{4n\tau_d}{\tau_c}\right]-\cos(4n\pi\tau_d f_m)+\pi\tau_c f_m\sin(4n\pi\tau_d f_m)\right\}-\frac{\sin(4n\pi\tau_d f_m)}{\pi f_m}\right\}, \tag{43}$$

where f_m is the offset frequency away from $2nf_e$, and $f_m\neq 0$. In (43), the approximation of $1-2n^2[R_{\phi e}(0)+R_{\phi e}(2n\tau_d)]\approx 1$ is used.

Because of the singularity of (42) and (43) at f and f_m = 0, their convolution cannot be conducted analytically. This problem can be alleviated by using the processed data from an electrical spectrum measurement of the drive signal $V_e(t)$ to represent $\frac{1}{P_e}\left[\frac{A}{|f_m|^2}+\frac{B}{|f_m|^3}\right]$ in (42) and (43). Then, based on (16), $S_{Ve}(f)$ can be changed to $S_{\phi e}(f)$. Here the resolution bandwidth

of the spectrum analyzer has to be set to 1 Hz or converted to the 1 Hz basis when obtaining the SSB PSD of $V_e(t)$.

For the optical signal expressed by (10), analyses showed that a dispersion compensation module (DCM) is needed to alleviate the power variation problem of the generated electrical signal [38]. With the deployment of the DCM, the time delay difference caused by the chromatic dispersion is fully compensated. Then the phase noise of the remotely generated electrical signals is exactly the same as that of the signal generated locally.

6. Experiment

A. Experiment with a tunable laser source

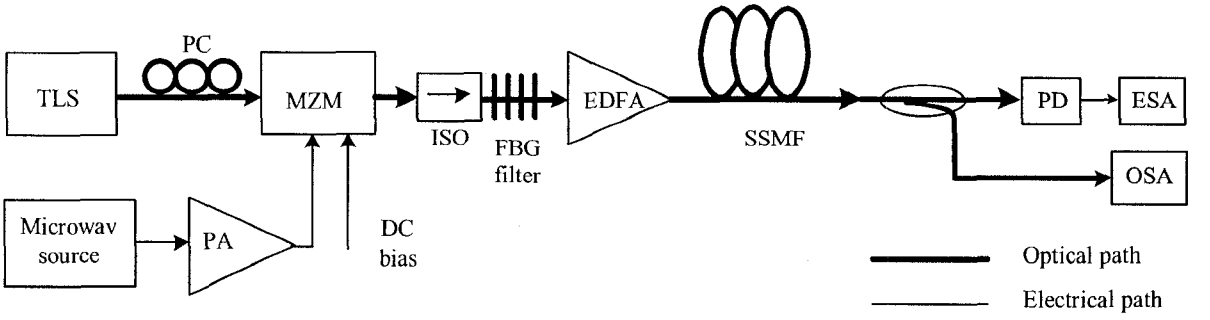

Fig. 7. Experimental setup for optical generation and transmission of mm-wave signals. (TLS: tunable laser source, PC: polarization controller, MZM: Mach-Zehnder modulator, ISO: isolator, EDFA: erbium-doped fiber amplifier, PA: power amplifier, OSA: optical spectrum analyzer, PD: photodetector, ESA: electrical spectrum analyzer, SSMF: standard single mode fiber)

To validate the above analysis, an experimental setup shown in Fig. 7 is built. In the setup, a tunable laser source with two linewidth settings is used, to investigate the phase noise performance of the generated electrical signals, with different optical carrier linewidths.

The electrical signal is generated by externally modulating the optical carrier with an electrical drive signal via an optical intensity modulator. Odd-order optical sidebands are suppressed with a constant DC bias. The optical carrier is filtered out with a narrow-band optical FBG filter. Two second-order optical sidebands remain at the output of the FBG filter when the power of the electrical drive signal is balanced with the attenuation of the FBG filter. This experimental setup supports the generation of a continuously-tunable mm-wave signal with a frequency of four times that of the electrical drive signal. The advantage of this configuration is that the

wavelength of the optical carrier is fixed; therefore a tunable optical notch filter is not required to remove the optical carrier.

The tunable laser source used in Fig. 7 is an Anritsu MG9637A. It has two optical linewidth settings of 700 kHz and 50 MHz, corresponding to coherence times of $\tau_{c1} = 455$ ns and $\tau_{c2} = 6.37$ ns, respectively. The SSMF used in Fig. 7 has a chromatic dispersion of 17 ps/(nm·km). Fibers with a length of 25 km and 50 km are used in the experiment. When the wavelength of the optical carrier is 1543 nm and the frequency of the electrical drive signal is 12.5 GHz, from (28) the fundamental time delay differences of the 25 km and 50 km fibers are $\tau_{d1} = 0.04216$ ns and $\tau_{d2} = 0.08432$ ns, respectively. The spectrum of the electrical drive signal at 12.5 GHz is shown in Fig. 8. The spectral measurement is performed with an HP8565E electrical spectrum analyzer, which is set to a resolution bandwidth (RBW) of 1 Hz and a frequency span of 100 Hz. The phase noise is measured to be -48 dBc/Hz @ 10 Hz.

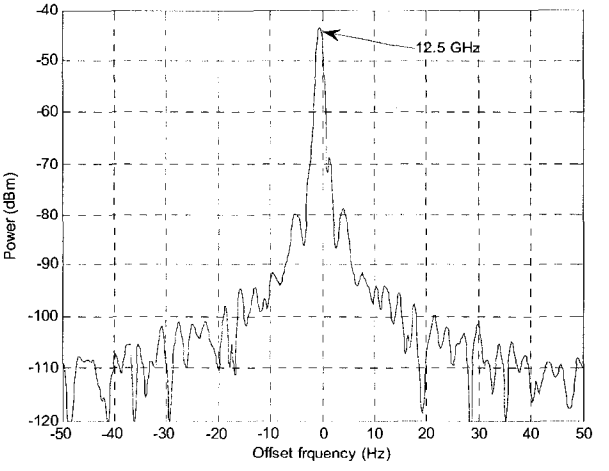

Fig. 8. Electrical spectrum of the electrical drive signal at 12.5 GHz.

Fig. 9 shows the spectra of the locally and remotely generated electrical signals at 50 GHz when the linewidths of the optical carrier are respectively set at 700 kHz and 50 MHz, with fiber lengths of 0 km, 25 km and 50 km. For locally generated 50-GHz signals, the phase noises are -35.5 dBc/Hz @ 10 Hz for the two different carrier linewidths, as shown in Fig. 9 (a) and Fig. 9 (b). Compared with the phase noise of the drive signal shown in Fig. 8, the phase noise degradation is very close to the theoretical value of 12 dB. The measurement agrees with the prediction given by (26) in Section IV. For remotely generated 50-GHz signals, negligible

phase noise degradation is observed for the two different carrier linewidths with two different transmission distances, as shown in Fig. 9 (a) and Fig. 9 (b). This is in good agreement with the analytical predictions of (43), as shown in the simulated spectral plots in Fig. 10.

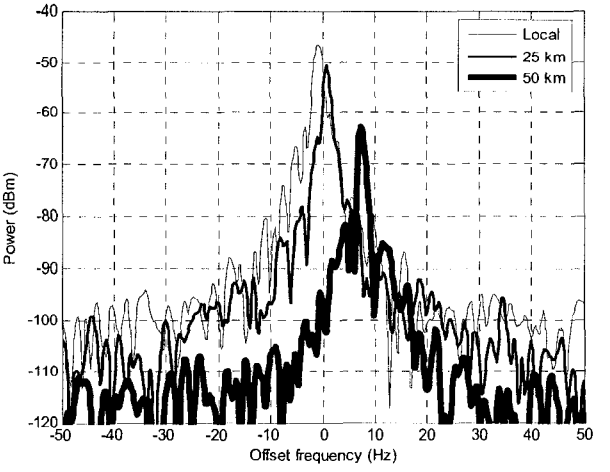

(a)

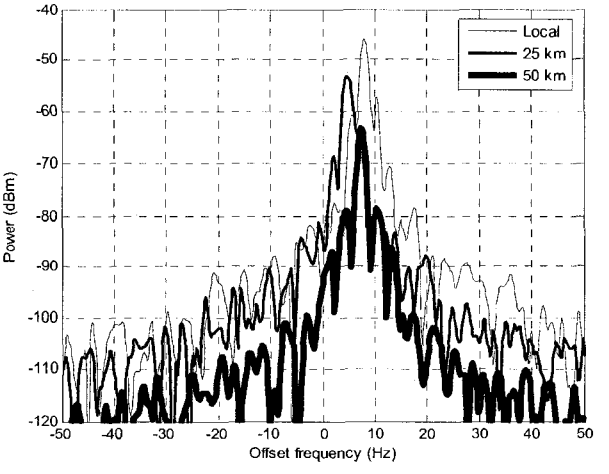

(b)

Fig. 9. Spectra of the locally and remotely generated electrical signals at 50 GHz. (a) The linewidth of the optical signal is set at 700 kHz. (b) The linewidth of the optical signal is set at 50 MHz.

In Fig. 10, line (a) is the normalized spectrum of the 12.5-GHz electrical drive signal obtained from the experimental measurement. Line (b) consists of five simulated spectra of the 50 GHz signals generated locally and remotely. For the locally generated signal, the spectrum in line (b) is obtained from (26). For the remotely generated signals, the spectra in line (b) are obtained from (43). In the simulation of (43), the phase noise of the electrical drive signal

$\frac{1}{P_e}\left[\frac{A}{|f_m|^2}+\frac{B}{|f_m|^3}\right]$ is substituted with the experimental data obtained from spectrum measurement; and the coherence time of the optical source of 700 kHz and 50 MHz and the delay time difference of the transmission fiber of 25 km and 50 km are simulated. All five spectra overlap on line (b) showing that there is negligible phase noise degradation for the five different situations. The experimental measurement shown in Fig. 9 agrees with the theoretical prediction given by (43) in Fig. 10.

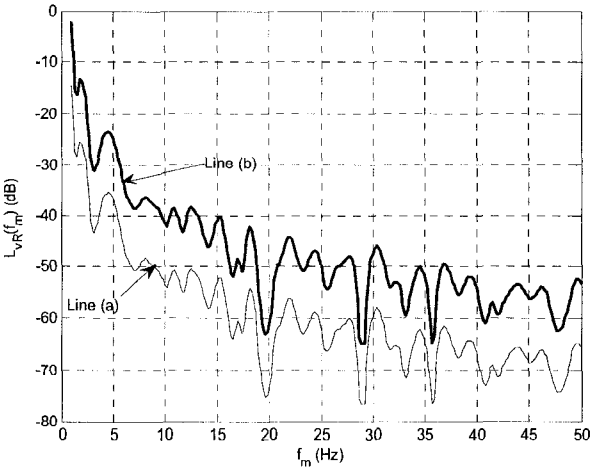

Fig.10. Electrical spectrum of the 12.5 GHz electrical drive signal (line a) and simulated spectra of the locally and remotely generated electrical signals at 50 GHz (line b). There is no visible deviation in the simulated results.

Note that the deviation in the peak frequency offset in Fig. 9 is caused by the frequency fluctuations of the electrical drive signal at 12.5 GHz. The amplitude offset is attributed to the fiber loss. In addition, using an electrical spectrum analyzer (Agilent 8565E) to measure phase noise is an approximate technique and the total frequency span is limited when using a 1-Hz resolution bandwidth. Phase noise at larger offset frequencies will decrease monotonically.

B. Experiment with a sliced ASE source

To further investigate the impact of the linewidth of the optical carrier and the transmission distance on the phase noise performance of the remotely generated electrical signal, the tunable laser source in Fig. 7 is replaced by a sliced ASE source obtained by slicing an EDFA ASE noise with an FBG. The FBG has a 3-dB bandwidth of 33 GHz. As a rough approximation, the linewidth of the sliced ASE source is assumed to equal to the bandwidth of the FBG. It should

be noted that the PSD of the sliced ASE source does not follow a Lorenzian shape, the experimental results obtained are an approximation of the analysis.

The experiment using the sliced ASE source is performed with fiber transmission lengths of 0 km, 8.8 km and 12.6 km. Their spectra are shown in Fig. 11. As can be seen, there is negligible phase noise difference between the generated electrical signals after 0 km and 8.8 km transmission. But to the 12.6-km spectrum, due to the large power drops of the generated electrical signal, the signal power at the offset frequency of 10 Hz is within the system noise floor. Adequate phase noise measurement can not be conducted. The power drop of the generated electrical signal over SSMF transmission is indicated by the first term of (42).

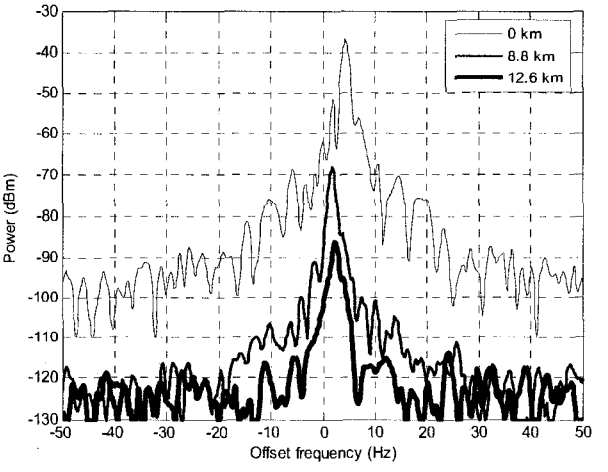

Fig. 11. Electrical spectra of the locally and remotely generated electrical signal at 50 GHz using a sliced ASE source with a linewidth of 33 GHz.

To further study the phase noise degradation versus the fiber transmission length with the sliced ASE source, we simulate the spectra of the generated electrical signal using (43) for fiber transmission lengths of 0, 10, 12, 14, 16, and 18 km. The simulation results are shown in Fig. 12. As can be seen, when the transmission distance is below 10 km, there is negligible phase noise degradation, which is consistent with the experimental result in Fig. 11. When the transmission distance is over 12 km, phase noise degradation starts at the offset frequency of 10 Hz.

Note that there is some discrepancy between the experimental result and the simulation result, which may be caused by the limitation of the approximation of the sliced ASE source as a laser

source, the inaccuracy of the 3-dB linewidth of the slicing FBG, and the inaccuracy of the fiber transmission distance.

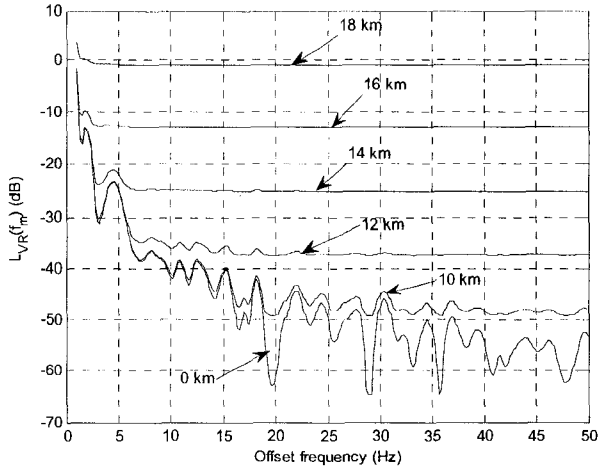

Fig. 12. Simulated spectra of the generated electrical signal at 50 GHz for different transmission lengths using the sliced ASE source with a linewidth of 33 GHz.

7. Conclusion

In this Section, we have investigated theoretically and experimentally the phase noise performance of optically generated electrical signals based on optical external modulation techniques. Mathematical expressions for the optical signals before photodetection have been developed which incorporate the phase fluctuations of both the electrical drive signal and the optical carrier. Closed form expressions of the power spectral density of the electrical signals generated both locally and remotely have been developed. It is shown that the power spectral density of the locally generated electrical signal is only determined by the phase noise of the electrical drive signal and the order of frequency multiplication. The phase noise degradation of the locally generated electrical signal follows the same rule as in a standard electronic frequency multiplier. The power spectral density of the remotely generated electrical signal is additionally affected by the linewidth of the optical carrier, and the chromatic dispersion effect of the transmission fiber. Outcomes of the analysis have been validated by the experiments using a tunable laser source with optical linewidths of 700 kHz and 50 MH, and a sliced ASE source with a linewidth of 33 GHz. For the experiment using a tunable laser source with 700-kHz and 50-MH linewidths, the phase noise of the locally generated electrical signal has a 12.5 dB degradation compared with that of the electrical drive signal. There was no significant

degradation of the phase noise when this signal is generated after a 50-km SSMF transmission. For the experiment using a sliced ASE source with a linewidth of 33 GHz, no phase noise degradation was observed when the transmission distance was within 8.8 km. When the transmission distance is 12.6 km, due to the large power drop and system sensitivity limitation, adequate phase noise measurement can not be conducted. However, its power degradation can be predicted by the analysis result.

The results obtained here provide a model in predicting the effect of the fiber chromatic dispersion and the linewidth of the optical source on the spectral quality of the generated electrical signal. In addition, the experimental results show when the linewidth of the optical source is within 50 MHz and transmission distance is within 50 km, the fiber chromatic dispersion and the linewidth of the light source will cause negligible degradation to the phase noise of the optically generated electrical signal.

Appendix

In this appendix, we develop the expression for $S_{o,R}(f)$ used in Section V. B from the function $R_{o,R}(\tau)$.

For a laser source, the DSB PSD of its noisy carrier $E(t) = \exp[j\phi_o(t)]$ is Lorenzian [39]. Its normalized DSB PSD is given by (39). If the autocorrelation function of $E(t)$ is denoted as $R_E(\tau)$. From (39) $R_E(\tau)$ can be obtained by the inverse Fourier transform of $S_E(f)$ as

$$R_E(\tau) = F^{-1}[S_E(f)]$$

$$= \exp\left[-\frac{|\tau|}{1/(\pi B)}\right] = \exp\left[-\frac{|\tau|}{\tau_c}\right], \tag{45}$$

where F^{-1} denotes the inverse Fourier transform operation. In addition, from the expression of $E(t)$, $R_E(\tau)$ can be obtained as

$$R_E(\tau) = \left\langle E(t+\tau)E(t)^* \right\rangle$$

$$= \left\langle \exp\{j[\phi_o(t+\tau) - \phi_o(t)]\} \right\rangle, \tag{46}$$

where $E(t)^*$ is the conjugate of $E(t)$. If the increment process of $\phi_o(t)$ is denoted as $\Phi_o(t)$, i.e.

$$\Phi_o(t) = \phi_o(t_1 + t) - \phi_o(t_1). \tag{47}$$

Obviously, $\Phi_o(t)$ is a zero mean Gaussian processes and random variables of $\Phi_o(t)$ are statistically independent for variables t generated by non-overlapping time periods of $\phi_o(t)$ [34]. Using the property of Gaussian processes, (46) can be further written as

$$R_E(\tau) = \exp\left[-\frac{1}{2}\left\langle [\Phi_o(\tau)]^2 \right\rangle\right]. \tag{48}$$

From (45) and (48) the variance of the phase change process $\Phi_o(t)$ at time difference τ is

$$\left\langle [\Phi_o(\tau)]^2 \right\rangle = \frac{2|\tau|}{\tau_c}. \tag{49}$$

We rewrite $R_{o,R}(\tau)$ from (34) as

$$R_{o,R}(\tau) = \left\langle \cos[\phi_o(t + n\tau_d + \tau) - \phi_o(t + n\tau_d) - \phi_o(t - n\tau_d + \tau) + \phi_o(t - n\tau_d)] \right\rangle. \tag{50}$$

When $|\tau| \le 2n\tau_d$,

$$R_{o,R}(\tau) = \left\langle \cos[\phi_o(t + n\tau_d + \tau) - \phi_o(t + n\tau_d)] \right\rangle \times \left\langle \cos[\phi_o(t - n\tau_d + \tau) - \phi_o(t - n\tau_d)] \right\rangle$$

$$= \left\langle \cos[\Phi_o(\tau)] \right\rangle^2$$

$$= \exp\left[-\left\langle [\Phi_o(\tau)]^2 \right\rangle\right]$$

$$= \exp\left[-\frac{2|\tau|}{\tau_c}\right]. \tag{51}$$

When $|\tau| > 2n\tau_d$,

$$R_{o,R}(\tau) = \langle \cos[\phi_o(t + n\tau_d + \tau) - \phi_o(t - n\tau_d + \tau)] \rangle \times \langle \cos[\phi_o(t + n\tau_d) - \phi_o(t - n\tau_d)] \rangle$$

$$= \langle \cos[\Phi_o(2n\tau_d)] \rangle^2$$

$$= \exp\left[- \langle [\Phi_o(2n\tau_d)]^2 \rangle \right]$$

$$= \exp\left[-\frac{4n\tau_d}{\tau_c} \right]. \tag{52}$$

In the above calculations, the following relations are used [41]. If X is a zero mean Gaussian random variable, then

$$\langle \cos(X) \rangle = \exp\left[-\frac{1}{2} \langle X^2 \rangle \right]. \tag{53}$$

$$\langle \sin(X) \rangle = 0 . \tag{54}$$

Then $S_{o,R}(f)$ can be obtained as

$$S_{o,R}(f) = \int_{-\infty}^{+\infty} R_{o,R}(\tau) \exp(-j2\pi f\tau) d\tau$$

$$= \int_{-\infty}^{-2n\tau_d} \exp(-\frac{4n\tau_d}{\tau_c}) \exp(-j2\pi f\tau) d\tau + \int_{-2n\tau_d}^{0} \exp(\frac{2\tau}{\tau_c}) \exp(-j2\pi f\tau) d\tau$$

$$+ \int_{0}^{2n\tau_d} \exp(-\frac{2\tau}{\tau_c}) \exp(-j2\pi f\tau) d\tau + \int_{n\tau_d}^{+\infty} \exp(-\frac{4n\tau_d}{\tau_c}) \exp(-j2\pi f\tau) d\tau$$

$$= \exp(-\frac{4n\tau_d}{\tau_c}) \left[\int_{-\infty}^{+\infty} \exp(-j2\pi f\tau) d\tau - \int_{-2n\tau_d}^{+2n\tau_d} \exp(-j2\pi f\tau) d\tau \right]$$

$$+ \int_{-2n\tau_d}^{0} \exp\left[(\frac{2}{\tau_c} - j2\pi f)\tau \right] d\tau + \int_{0}^{2n\tau_d} \exp\left[(-\frac{2}{\tau_c} - j2\pi f)\tau \right] d\tau$$

$$= \exp(-\frac{4n\tau_d}{\tau_c}) \left[\delta(f) - \frac{\sin(4n\pi\tau_d f)}{\pi f} \right]$$

$$+\frac{\tau_c}{1+(\pi f\tau_c)^2}\times\left\{1-\exp\left[-\frac{4n\tau_d}{\tau_c}\right]\left[\cos(4n\pi f\tau_d)-\pi f\tau_c\sin(4n\pi f\tau_d)\right]\right\}. \quad (55)$$

Acknowledgment

The authors would like to thank John Oldham and David Barlow of the Communications Research Centre, Canada, and Fei Zeng and Xiangfei Chen of the University of Ottawa, Canada, for their assistance in setting up the experimental system.

References:

[1] B. Mukherjee, "WDM optical communication networks: progress and challenges," *IEEE J. Select. Areas Commun.,* vol. 18, no. 10, pp. 1810-1824, Oct. 2000.

[2] A. J. Cooper, "Fibre/Radio for the provision of cordless/mobile telephony services in the access network," *Electron. Lett.,* vol. 26, no. 24, pp. 2054-2056, Nov. 1990.

[3] H. Ogawa, D. Polifko, and S. Banba, "Millimeter-wave fiber optics systems for personal radio communication," *IEEE Trans. Microwave Theory Tech.,* vol. 40, no. 12, pp. 2285-2293, Dec. 1992.

[4] A. J. Seeds, "Broadband wireless access using millimetre-wave over fibre systems," in *Tech. Dig. IEEE MTT-S Int. Microwave Symp.,* Jun. 1997, vol. 1, pp. 23–25.

[5] D. Novak, "The merging of the wireless and fiberoptic worlds," in *Tech. Dig. Lasers and Electro-Optics Conf. (CLEO'02),* 2002, vol. 1, pp. 276-276.

[6] L. Nöel, D. Wake, D. G. Moodie, D. D. Marcenac, L. D. Westbrook, and D. Nesset, "Novel techniques for high capacity 60 GHz fiber-radio transmission systems," *IEEE Trans. Microwave Theory Tech.*, vol. 45, no. 8, pp. 1416-1423, Aug. 1997.

[7] M. Goloubkoff, E. Pénard, D. Tanguy, P. Legaud, D. Mathoorasing, F. Devaux, and C. Minot, "Outdoor and indoor applications for broadband local loop with fibre supported mm-wave radio systems," in *Tech. Dig. IEEE MTT-S Int. Microwave Symp.,* Jun. 1997, vol. 1, pp. 31-34.

[8] J. E. Román, L. T. Nichols, K. J. Williams, R. D. Esman, G. C. Tavik, M. Livingston, and M. G. Parent, "Fiber-optic remoting of an ultrahigh dynamic range radar," *IEEE Trans. Microwave Theory Tech.*, vol. 46, no. 12, pp. 2317-2323, Dec. 1998.

[9] E. C. Niehenke and P. Hercafeld, "An optical link for W-band transmit/receive applications," in *Tech. Dig. IEEE MTT-S Int. Microwave Symp.,* Jun. 1997, vol. 1, pp. 35-38.

[10] J. L. Corral, J. Marti, J. M. Fuster, R. Laming, and M. J. Cole, "Continuously variable true time-delay optical feeder for phased-array antenna employing chirped fiber gratings," *IEEE Trans. Microwave Theory Tech.*, vol. 45, no. 8, pp. 1531-1536, Aug. 1997.

[11] R. P. Braun, G. Grosskopf, D. Rohde, and F. Schmidt, "Optical millimetre-wave generation and transmission experiments for mobile 60 GHz band communications," *Electron. Lett.*, vol. 32, no. 7, pp. 626-628, Mar. 1996.

[12] L. Goldberg, H. F. Taylor, J. F. Weller, and D. M. Bloom, "Microwave signal generation with injection-locked laser diodes," *Electron. Lett.*, vol. 19, no. 13, pp. 491-493, Jun. 1983.

[13] R. T. Ramos and A. J. Seeds, "Fast heterodyne optical phase lock loop using double quantum well laser diodes," *Electron. Lett.*, vol. 28, no. 1, pp. 82-83, Jan. 1992.

[14] L. N. Langley, M. D. Elkin, C. Edge, M. J. Wale, U. Gliese, X. Huang, and A. J. Seeds, "Packaged semiconductor laser optical phase-locked loop (OPLL) for photonic generation, processing and transmission of microwave signals," *IEEE Trans. Microwave Theory Tech.*, vol. 47, no. 7, pp. 1257-1264, Jul. 1999.

[15] J. J. O'Reilly, P. M. Lane, R. Heidemann, and R. Hofstetter, "Optical generation of very narrow linewidth millimetre wave signals," *Electron. Lett.*, vol. 28, no. 25, pp. 2309-2311, Dec. 1992.

[16] J. J. O'Reilly and P.M. Lane, "Fibre-supported optical generation and delivery of 60 GHz signals," *Electron. Lett.*, vol. 30, no. 16, pp. 1329-1330, Aug. 1994.

[17] P. Shen, N. J. Gomes, P. A. Davies, W. P. Shillue, P.G. Huggard, and B. N. Ellison, "High-purity millimetre-wave photonic local oscillator generation and delivery," in *Proc. Microwave Photonics,* Sept. 2003, pp. 189-192.

[18] P. O. Hedekvist, B. E. Olsson, and A. Wiberg, "Harmonic generation of photonic microwave frequencies utilizing the properties of a phase modulator," in *Proc. Microwave Photonics,* Sept. 2003, pp. 193-196.

[19] X. J. Meng and J. Menders, "Optical generation of microwave signals using SSB-based frequency-doubling scheme," *Electron. Lett.*, vol. 39, no. 1, pp. 103–105, Jan. 2003.

[20] G. Qi, J. P. Yao, J. Seregelyi, S. Paquet, and J. C. Bélisle, "Millimeter-wave carrier generation using an optical phase modulator and an optical notch filter," *Proceedings of SPIE,* vol. 5579, pp. 673-679, Sept. 2004.

[21] F. N. Timofeev, S. Bennett, R. Griffin, P. Bayvel, A. J. Seeds, R. Wyatt, R. Kashyap, and M. Robertson, "High spectral purity millimetre-wave modulated optical signal generation using fibre grating lasers," *Electron. Lett.*, vol. 34, no. 7, pp. 668-669, Apr. 1998.

[22] J. J. O'Reilly, and P. M. Lane, "Remote delivery of video services using mm-wave and optics," *J. Lightwave Technol.*, vol. 12, no. 2, pp. 369-375, Feb. 1994.

[23] W. Shieh and L. Maleki, "Phase noise of optical interference in photonic RF systems," *IEEE Photon. Tech. Lett.*, vol. 10, no. 11, pp. 1617–1619, Nov. 1998.

[24] P. J. Matthews and R. D. Esman, "Intrinsic microwave phase noise of fiber-optic links," in *Tech. Dig. IEEE MTT-S Int. Microwave Symp.,* Jun. 1998, vol. 3, pp. 1517–1520.

[25] M. Bibey, F. Deborgies, M. Krakowski and D. Mongardien, "Very low phase-noise optical links - experiments and theory," *IEEE Trans. Microwave Theory Tech.*, vol. 47, no. 12, pp. 2257–2262, Dec. 1999.

[26] R. Hofstetter, H. Schmuck, and R. Heidemann, "Dispersion effects in optical millimeter-wave systems using self-heterodyne method for transport and generation," *IEEE Trans. Microwave Theory Tech.*, vol. 43, no. 9, pp. 2263-2269, Sept. 1995.

[27] U. Gliese, S. Norskov, and T. N. Nielsen, "Chromatic dispersion in fiber-optic microwave and millimeter-wave links," *IEEE Trans. Microwave Theory Tech.*, vol. 44, no. 10, pp. 1716-1724, Oct. 1996.

[28] B. Pourbahri, P. A. Davies, D. S. George, and D. Wake, "The effects of fiber amplifier phase noise on radio over fibre signals," in *Proc. Broadband Communications,* Feb. 2000, pp. 89-91.

[29] G. J. Cowle, P. R. Morkel, R. I. Laming, and D. N. Payne, "Spectral broadening due to fibre amplifier phase noise," *Electron. Lett.,* vol. 26, no. 7, pp. 424-425, Mar. 1990.

[30] J. Rogers, and C. Plett, *Radio Frequency Integrated Circuit Design.* Artech House, 2003, pp. 283-287.

[31] A. G. Armada and M. Calvo, "Phase noise and sub-carrier spacing effects on the performance of an OFDM communication system," *IEEE Commun. Lett.*, vol. 2, no. 1, pp. 11–13, Jan. 1998.

[32] K. Okamoto, *Fundamentals of Optical Waveguides*. New York: Academic Press, 2000, pp. 159-161.

[33] J. Rutman and F. L. Walls, "Characterization of frequency stability in precision frequency sources," *Proc. IEEE*, vol. 79, no. 7, pp. 952-960, Jul. 1991.

[34] A. Papoulis, *Probability, Random Variables, and Stochastic Processes*. New York: McGraw-Hill, 1984.

[35] H. E. Rowe, *Signals and Noise in Communication Systems*. New York: Van Nostrand, 1965. pp. 130-130

[36] Product Note 11729B-1, *Phase Noise Characterization of Microwave Oscillators -Phase Detector Method*, Hewlett Packard.

[37] W. P. Robins, *Phase Noise in Signal Sources*. London: Peter Peregrinus, 1982, pp. 77-78.

[38] G. Qi, J. P. Yao, J. Seregelyi, C. Bélisle, and S. Paquet, "Optical generation and distribution of continuously tunable millimeter-wave signals using an optical phase modulator," *J. Lightwave Technol.*, vol. 23, no. 9, pp. 2687-2695, Sept. 2005.

[39] E. Costa and S. Pupolin, "M-QAM-OFDM system performance in the presence of a nonlinear amplifier and phase noise," *IEEE Trans. Commun.*, vol. 50, no. 3, pp. 462-472, Mar. 2002.

[40] J. W. Goodman, *Statistical Optics*. New York: John Wiley & Sons, 1985, pp. 167-168.

[41] L. E. Richter, H. I. Mandelberg, M. S. Kruger, and P. A. McGrath, "Linewidth determination from self-heterodyne measurements with subcoherence delay times," *IEEE J. Quantum Electron.*, vol. QE-22, no. 11, pp. 2070–2074, Nov. 1986.

4.2 Effects of amplified spontaneous emission noise on the phase noise of optically generated electrical signals

In most optical millimeter-wave signal generation schemes, optical amplifiers like erbium-doped fiber amplifiers or semiconductor optical amplifiers are always deployed to compensate optical losses. These optical amplifiers not only amplify the optical signal but also add amplified spontaneous emission noise to the amplified optical signal at the same time. In this Section, the effects of the amplified spontaneous emission noise of optical amplifiers on the spectral purity of the optically generated electrical signals are theoretically studied. The result of the analysis gives a good explanation to those experimental results observed in the earlier experimental studies to this subject.

Effects of amplified spontaneous emission noise of optical amplifiers on the phase noise of optically generated electrical signals[5]

Guohua Qi, Jianping Yao, *Senior Member, IEEE,* Joe Seregelyi*, Stéphane Paquet* and Claude Bélisle*

Microwave Photonics Research Laboratory

School of Information Technology and Engineering

University of Ottawa, Ottawa, Ontario, Canada K1N 6N5

(Email: jpyao@site.uottawa.ca)

* Communications Research Centre

Ottawa, Ontario, Canada K2H 8S2

Abstract

The applications of optical amplifiers, such as erbium-doped fiber amplifiers (EDFAs) and semiconductor optical amplifiers (SOAs), are inevitable in most optical transmission links. These optical amplifiers augment both the optical signal and the amplified spontaneous emission (ASE) noise. In radio-over-fiber systems, optical links are used to distribute high spectral purity radio frequency (RF) signal, microwave signal or millimeter-wave (mm-wave) signal over optical fiber for low-loss distant transmission. In this Section, the effects of amplified spontaneous emission (ASE) noise of optical amplifiers on the spectral purity of the optically generated electrical signals are theoretically studied.

Keywords: Optical generation of electrical signals, erbium-doped fiber amplifier (EDFA), amplified spontaneous emission (ASE) noise, phase noise.

1. Introduction

The distribution of RF, microwave and mm-wave signals over optical fiber has attracted a lot of interest because of advantages such as inherent low-loss, low dispersion and wide bandwidth

[5] Published in *Proceedings of SPIE*, vol. 5971, pp. 59712D-1-59712D-8, Sept. 2005.

offered by single-mode optical fiber. Potential applications include broadband wireless access networks, sensor networks, antenna remoting, Doppler radar, and phased-array antenna [1], [2].

One of the key technologies in a radio-over-fiber system is the optical generation and distribution of a high spectral purity microwave signal or mm-wave signal. It is well known that the beating of two wavelengths from two free-running semiconductor laser diodes can only generate a low spectral purity electrical signal. The low spectral purity of the generated electrical signal is reflected by the broad spectrum caused by the wide linewidths of the laser diodes. Generally, the linewidth of a commercially available semiconductor laser diode is around tens of MHz. The broad spectrum of the beat signal in the electrical domain will be on the same order, making it useless for most applications. This is because the optically generated electrical signal is usually used either as an RF carrier or as a local oscillator signal in system applications, and these applications always require their transmitter carrier and local oscillator signal to have good long-time and short-time frequency stability. Theoretical and experimental studies shows that good phase correlation of the two beating wavelengths can overcome this broad linewidth problem [3]. Therefore, the generation of two phase-correlated wavelengths is crucial to the optical generation of high spectral purity electrical signals. In the past, different approaches to implementing these optical signals have been proposed, such as automatic frequency control loop [4], optical injection locking [5], optical phase-locked loop (OPLL) [6], and external modulation [7]. The techniques of optical frequency locking, optical injection locking, and OPLL have been used to improve the long-time frequency stability of the generated electrical signal. The short-time frequency stability of an electrical signal translates to the spectral purity in frequency domain (can also be characterized by phase noise measurement) and can be improved by OPLL and external modulation techniques.

Although state-of-the-art optical fiber has very low loss, distributing microwave or mm-wave signals over long-distance optical fiber still requires optical amplification to compensate for power loss. EDFA's and SOA's are two types of optical amplifiers that are widely used for amplifying optical signals at the 1550-nm band. These optical amplifiers not only bring power amplification to the optical signal, but also add ASE noise. Obviously, the effects of the ASE noise on the spectral purity of the optically generated electrical signal needs to be studied.

A few experimental studies have been reported to date; these studies were focused on the spectral broadening of an optical signal passing through an EDFA [8]-[11]. In 1990 Cowle et al. first reported that the spectral linewidth broadening of an optical signal was less than 20 kHz with an EDFA of 17 dB gain at 1.5 μm region [8]. Later in the same year, Okamura et al. published their experimental results that less than 1.4 kHz spectral linewidth broadening at the 3 dB down point was found with two types of EDFA [9]. In 1992 Simeonidou et al. examined the spectral linewidth broadening of EDFA's and Raman fiber amplifiers (RFA) and found that the amplification process did not introduce any significant broadening to the 3 dB down point of the signal linewidth [10]. These experimental results show that EDFA's can be used to amplify optical signals with negligible degrading the phase noise of the optical signals. In 2000 Pourbahri et al. reported their experimental results about the effects of fiber amplifier phase noise on radio-over-fiber signals [11]. A single optical carrier and a pair of optical carriers produced by optical side-band injection locking were examined, the spectral linewidth broadening caused by passing the optical signals through an EDFA was found to be down to a few Hz. These reports showed experimentally the effects of EDFA or RFA on the spectral linewidth broadening of the amplified optical signal and its generated electrical signal. They did not reveal the mechanism of the added phase noise of the generated electrical signal caused by the ASE noise. This paper will analyze theoretically the ASE noise effects on the phase noise of the generated electrical signal for radio-over-fiber applications.

2. Analysis

2.1 Phase Noise and ASE Noise Models

In those approaches for optical electrical signal generation, a high spectral purity electrical signal is often needed as a reference for generating high spectral purity microwave or mm-wave signals; in the reported experimental studies for evaluating the ASE noise effects on optical linewidth broadening, an electrical signal is also employed to facilitate the examination of the broadening effect in electrical domain. In both cases, the electrical signal is needed to compare with the optically generated electrical signal to evaluate the optical effects. That means that the phase noise of the electrical reference signal must also be taken into account. Its phase fluctuations come mainly from thermal noise, shot noise, and $1/f$ noise. The optical signal

originated from a distributed feedback (DFB) laser diode has a finite linewidth in the optical domain. That means continuous phase fluctuation exists in the optical signal. The cause of the phase fluctuations in a laser output can be, for example, refractive index variation in the laser cavity due to temperature changes and carrier concentration effects. The phase noises (or fluctuations) of the electrical reference signal and the optical signal are two independent random processes.

The phase fluctuations of the electrical signal and optical signal can be interpreted as a parasitic phase modulation of an ideal sinusoidal signal [12]. As the electrical signal and the optical signal used are all continuous wave (CW) signals, so they can be modeled as

$$V_r(t) = V_e \cos[\omega_e t + \phi_e(t)], \tag{1}$$

and

$$E_s(t) = E_o \cos[\omega_o t + \phi_o(t)], \tag{2}$$

where $V_r(t)$ is the voltage of the reference electrical signal, $E_s(t)$ is the electric field of the optical source in scalar form. For simplicity, we assume that the linear polarization state of the optical signal is controlled and the vector characteristic can be ignored. V_e and ω_e are the voltage amplitude and angular frequency ($\omega_e = 2\pi f_e$) of the electrical reference signal. E_o and ω_o are the electric field amplitude and angular frequency ($\omega_o = 2\pi f_o$) of the optical carrier. Finally, $\phi_e(t)$ and $\phi_o(t)$ are two random processes that introduce phase fluctuations to the electrical and optical signals. It should be noted that the phase noise is dominant and amplitude or intensity noise can be neglected due to the presence of the limiting mechanisms in the electrical and optical source. That is the reason that V_e and E_o are regarded as constants here.

In general, the electric field of the generated optical signal consisting of two phase-correlated optical wavelengths, $E_{sig}(t)$, can be generally expressed as

$$E_{sig}(t) = E_{o1} \cos[\omega_o t + \phi_o(t)] + E_{o2} \cos[(\omega_o + m\omega_e)t + \phi_o(t) + m\phi_e(t)], \tag{3}$$

where E_{o1} and E_{o2} are the amplitudes of the two wavelengths, which are constants, m is a non-zero integer.

The ASE noise of an EDFA and SOA has been well documented in literatures [13], [14]. Conventionally, the ASE noise is treated as an additive Gaussian noise due to the large number of independent spontaneous emission; and its power spectral density at a single polarization $S_{ASE}(f)$ is given

$$S_{ASE}(f) = n_{sp} hf(G-1), \tag{4}$$

where n_{sp} is the spontaneous emission factor, h is Planck's constant, f is the optical frequency, G is the power gain of the optical amplifier. It is clearly seen from (4) that the ASE noise is not white since $S_{ASE}(f)$ varies with the optical frequency f. Usually the 3-dB gain bandwidth of an EDFA is around 30 nm and that of an SOA is in the range of 30 to 50 nm, and the center optical frequency of both optical amplifiers is around 1550 nm. That means the ASE noise bandwidth of an optical amplifier is much smaller the center frequency of the amplifier. So the power spectral density $S_{ASE}(f)$ can be approximated to a constant across the valid gain bandwidth of the optical amplifier. If S_{ASE} is used to denote the constant power spectral density of an ASE noise, we have

$$S_{ASE} = n_{sp} hf_l(G-1), \tag{4.1}$$

where f_l is the lower 3-dB optical frequency of the optical amplifier. Equation (4.1) is valid in the frequency bandwidth, B_o, of an optical amplifier. Fig. 1 shows the unfiltered power spectral density of the ASE noise of an optical amplifier.

Based on the fact that the time of a filtered noise that keeps a sinusoidal waveform in time domain is inversely proportional to the bandwidth of the filter [15]. Then the ASE noise in (4.1) can be expressed in the electric field form as

$$E_{ASE}(t) = \sum_{i=0}^{M} \sqrt{2S_{ASE}\Delta B}\cos[2\pi(f_l + i\Delta B)t + \phi_i], \tag{5}$$

where $E_{ASE}(t)$ is the electric field of the ASE noise, ΔB is a small frequency interval, $M = B_o / \Delta B$, ϕ_i is a random phase having a uniform probability distribution in $[-\pi,+\pi]$. ϕ_i in (5) represents the random property of the ASE noise.

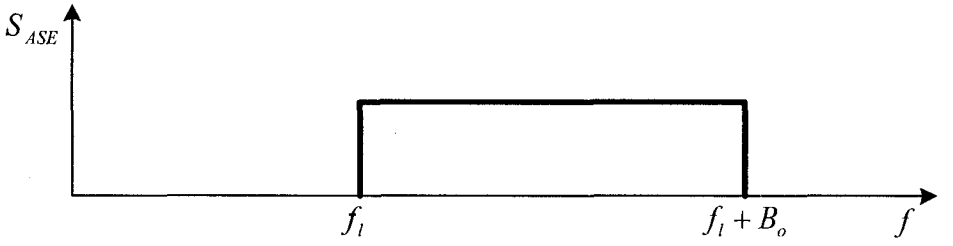

Fig. 1. Power spectral density of the unfiltered ASE noise of an optical amplifier.

2.2 The current of the electrical signal and noise current after photodetection

In radio-over-fiber links, regardless of what technique is used to generate it, the optical signal needs to be amplified by one or a few optical amplifiers to compensate for the losses in the transmission link. In the experimental reports studying the EDFA phase noise effects [8]-[11], an optical frequency shifter is used to shift the frequency of an optical signal. Then the frequency shifted optical signal passes through an EDFA and is combined with an un-shifted optical signal. In general, the electric field at the output of the optical amplifier is a combination of the amplified optical signal and the additive ASE noise. From (3) and (5) the electric field, $E_{out}(t)$, at the output of the optical amplifier is

$$E_{out}(t) = E_1 \cos[\omega_o t + \phi_o(t)] + E_2 \cos[(\omega_o + m\omega_e)t + \phi_o(t) + m\phi_e(t)]$$

$$+ \sum_{i=0}^{M} \sqrt{2S_{ASE}\Delta B} \cos[2\pi(f_l + i\Delta B)t + \phi_i], \qquad (6)$$

where E_1 and E_2 are amplitudes of the two amplified wavelengths.

It is known that photodetection follows a square law. When the amplified signal and ASE noise $E_{out}(t)$ are fed into a photodetector with a responsivity of R, the resulting photodetecting current $i_d(t)$ is then

$$i_d(t) = RE_{out}^2(t)$$

$$= I_{DC} + i_e(t) + i_{sig-ASE}(t) + i_{ASE-ASE}(t), \tag{7}$$

where I_{DC} is the generated DC current, $i_e(t)$ is the instantaneous current of the generated electrical signal, $i_{sig-ASE}(t)$ is the noise current generated by the cross beating between the optical signal and the ASE noise, $i_{ASE-ASE}(t)$ is the noise current generated by cross beatings among ASE noise. They are respectively expressed as

$$I_{DC} = \frac{1}{2}R(E_1^2 + E_2^2) + RS_{ASE}B_o, \tag{7.1}$$

$$i_e(t) = RE_1E_2\cos[m\omega_e t + m\phi_e(t)], \tag{7.2}$$

$$i_{sig-ASE}(t) = R\sqrt{2S_{ASE}\Delta B}\left\{E_1\sum_{i=0}^{M}\cos[2\pi(f_l + i\Delta B - f_o)t + \phi_i - \phi_o(t)]\right.$$

$$\left. + E_2\sum_{i=0}^{M}\cos[2\pi(f_l + i\Delta B - f_o - mf_e)t + \phi_i - \phi_o(t) - m\phi_e(t)]\right\}, \tag{7.3}$$

$$i_{ASE-ASE}(t) = RS_{ASE}\Delta B\sum_{i=0}^{M}\sum_{\substack{j=0 \\ j\neq i}}^{M}\cos[2\pi(i-j)\Delta Bt + \phi_i - \phi_j]\cdot \tag{7.4}$$

Here, the terms with a frequency of $2f_o$, and equal or higher than $2f_l$ cannot be detected by the photodetector and are omitted.

When a DC current flows through the potential barrier of a photodetector, a shot noise current is generated. In our analysis, when the DC current I_{DC} in (7.1) goes through the photodiode, the spectral density σ_{shot}^2 of the generated shot noise current $i_{shot}(t)$ is

$$\sigma_{shot}^2 = qR(E_1^2 + E_2^2) + 2qRS_{ASE}B_o, \tag{8}$$

where q is the electron charge. The shot noise is white.

To evaluate the spectral density $\sigma^2_{sig-ASE}$ of the variance of the noise current $i_{sig-ASE}(t)$ in (7.3), an approximation can be made to simplify the analysis without affecting the validity of the results. In most cases, the frequency offset of the two wavelengths of the optical signal in (3) is below 100 GHz, which corresponds to a wavelength spacing between the two wavelengths smaller than 0.8 nm. The ASE noise bandwidth is around 30-50 nm. Therefore, the two wavelengths can be considered identical, that is, $\lambda_1 \approx \lambda_2 = \lambda_0$, or in frequency, we have $f_1 \approx f_2 = f_o$, as shown in Fig. 2.

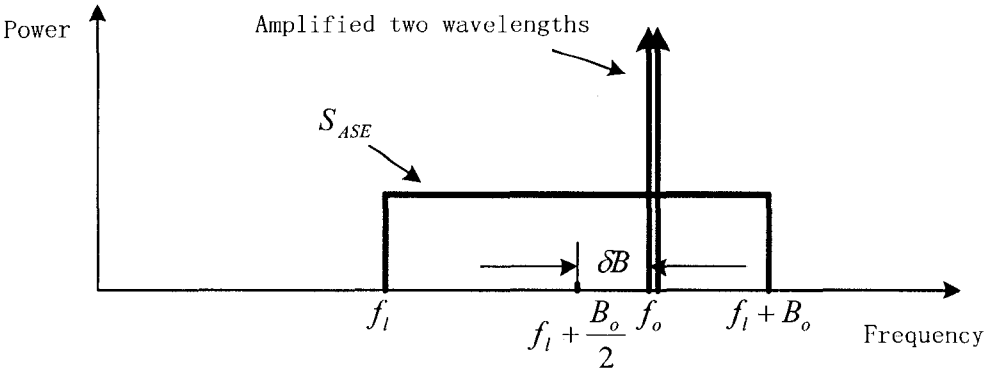

Fig. 2. Power spectral density of the unfiltered ASE noise of an optical amplifier.

If the frequency offset δB, defined as the absolute value from f_o to the center frequency of the ASE noise, is

$$\delta B = \left| f_l + \frac{B_o}{2} - f_o \right|, \tag{9}$$

then the spectral density $\sigma^2_{sig-ASE}$ of $i_{sig-ASE}(t)$ is

$$\sigma^2_{sig-ASE}(f) = 2R^2 S_{ASE}(E_1^2 + E_2^2), \text{ for } f \in \left[0, \frac{B_o}{2} - \delta B\right], \tag{10}$$

and

$$\sigma^2_{sig-ASE}(f) = R^2 S_{ASE}(E_1^2 + E_2^2), \text{ for } f \in \left[\frac{B_o}{2} - \delta B, \frac{B_o}{2} + \delta B\right]. \tag{11}$$

The spectral density of $i_{sig-ASE}(t)$ can be schematically plotted, as shown in Fig. 3.

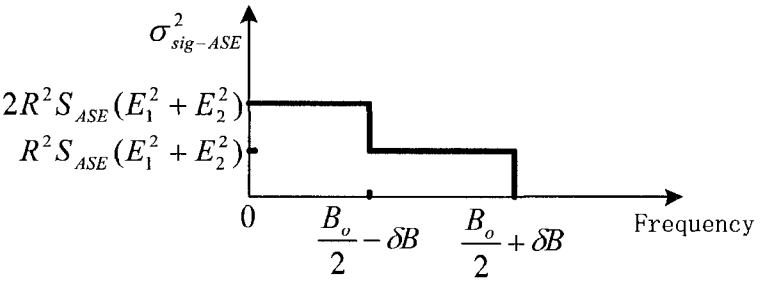

Fig. 3. Spectral density of $i_{sig-ASE}(t)$.

For the noise current $i_{ASE-ASE}(t)$ generated by cross beatings among ASE noise, its spectral density $\sigma^2_{ASE-ASE}$ varies with frequency.

$$\sigma^2_{ASE-ASE}(f) = R^2S^2_{ASE}(B_o - f), \text{ for } f \in (0, B_o]. \tag{12}$$

The spectral density of $i_{ASE-ASE}(t)$ can be schematically plotted, as shown in Fig. 4.

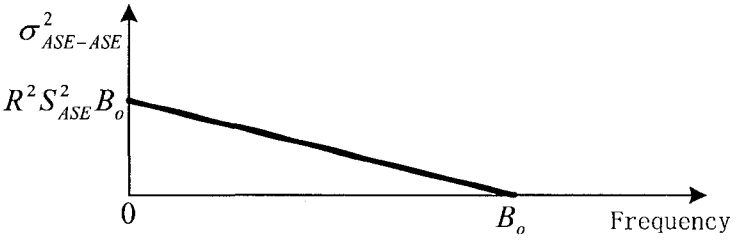

Fig. 4. Spectral density of $i_{ASE-ASE}(t)$.

In summary, after photodetection, the current of the generated electrical signal $i_e(t)$ in (7.2) is rewritten as

$$i_e(t) = RE_1E_2\cos[m\omega_e t + m\phi_e(t)], \tag{13}$$

and the root mean square value of the generated noise current $\overline{i_n}$ per $\sqrt{Hz}$ can be obtained by

$$\overline{i_n} = \sqrt{\sigma^2_{shot} + \sigma^2_{sig-ASE}(f) + \sigma^2_{ASE-ASE}(f)}. \tag{14}$$

2.3 Induced phase variation

Equation (14) shows that the generated electrical noise is not white in a strict sense. This is because the amplitude of the noise current varies with frequency. In the components of $\overline{i_n}$, $\sigma^2_{sig-ASE}$ has two step changes with frequency; while $\sigma^2_{ASE-ASE}$ decreases linearly from DC to B_o. In most of the cases, the wavelength of the amplified optical signal is displaced from the wavelength of the 3-dB optical amplification bandwidth of an optical amplifier. Under these circumstances, the spectral density $\sigma^2_{sig-ASE}$ of $i_{sig-ASE}(t)$ in (14) should use (10) instead if (11), i.e. $\sigma^2_{sig-ASE}(f) = 2R^2 S_{ASE}(E_1^2 + E_2^2)$. Because we are only interested in the noise characteristic within a small frequency range around mf_e, say a few tens of MHz, compared to the value of B_o, the linear variation of $\sigma^2_{ASE-ASE}$ can be approximated as white within a few tens of MHz. All of these allow $\overline{i_n}$ to be approximated as white within a few tens of MHz around mf_e. If $\overline{i_{ne}}$ is used to denote the value of $\overline{i_n}$ in (14) in a small frequency range around mf_e, then

$$\overline{i_{ne}} = \sqrt{qR(E_1^2 + E_2^2) + 2qRS_{ASE}B_o + 2R^2 S_{ASE}(E_1^2 + E_2^2) + R^2 S^2_{ASE}(B_o - mf_e)}\ , \ [A/\sqrt{Hz}]. \qquad (15)$$

Now after photodetection, the current of the generated electrical signal $i_e(t)$ and the root mean square (rms) value of the spectral density of the noise current $\overline{i_n}$ are obtained. To evaluate the effects of the white noise on the electrical signal, a small frequency interval of noise at an offset frequency is generally studied. In [15], the phase jitter caused by the superimposed double sideband white noise to an ideal sinusoidal signal is analyzed. Here if the results in [15] are used in our case, the phase fluctuation $m\phi_e(t)$ of $i_e(t)$ has to be neglected by assuming that the linewidth caused by $m\phi_e(t)$ is infinitely narrow, as shown in Fig. 5.

With the above approximation, assuming the offset frequency from mf_e is f_m, and defining a small frequency interval around $mf_e \pm f_m$ to be ΔB_e, the spectral density of the phase fluctuation caused by the noise power of these two small frequency intervals at f_m is

$$\overline{\phi_{ne}}^2 = \frac{qR(E_1^2 + E_2^2) + 2qRS_{ASE}B_o + 2R^2 S_{ASE}(E_1^2 + E_2^2) + R^2 S^2_{ASE}(B_o - mf_e)}{R^2 E_1^2 E_2^2 / 2}, \qquad (16)$$

where $\overline{\phi_{ne}}^2$ is the spectral density of the variance of the phase fluctuation. Equation (16) shows $\overline{\phi_{ne}}^2$ is white.

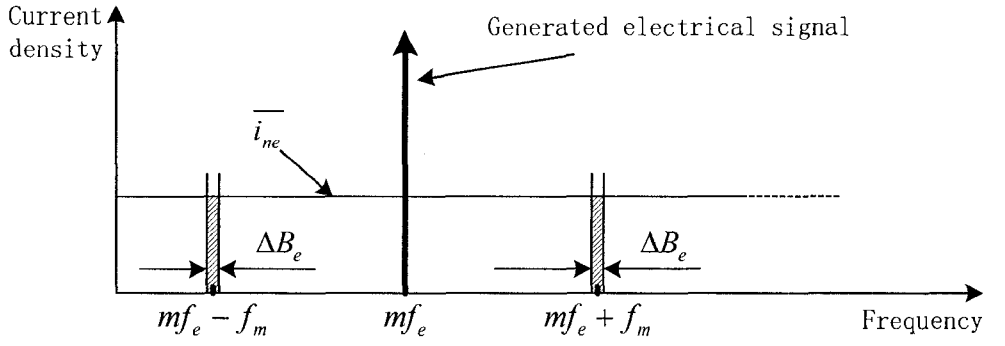

Fig. 5. Current spectral density of the generated electrical signal and noise.

Unfortunately, $\overline{\phi_{ne}}^2$ cannot be measured with an electrical spectrum analyzer. This is because the time averaging of the compound signal is used to show the power spectral density (PSD) of the signal, instead of showing the PSD of the phase fluctuation, with an electrical spectrum analyzer. When the ergodic property of the signal and the small phase modulation assumption are valid, then an electrical spectrum analyzer can be used to display the approximate PSD of the phase fluctuation. But in our case, the noise power of these two small frequency intervals also induces amplitude fluctuation at f_m [15]. Without a perfect limiter, it is hard to distinguish the phase fluctuation from amplitude fluctuation with an electrical spectrum analyzer. Furthermore, as $\overline{\phi_{ne}}^2$ is far below the power level of the signal at a 3-dB or 30-dB linewidth, it is hard to examine the noise effect by the spectral width measurement, which is widely used in the experimental studies [8]-[11].

3. Conclusion

In this Section, the effects of ASE noise of optical amplifiers on the spectral purity of the optically generated electrical signal were theoretically studied. Models representing the phase noise of the optical signal and the phase noise of the electrical reference signal were constructed. The ASE noise of an EDFA or a SOA was modeled as the summation of narrow band sinusoidal signals with random phases. The shot noise, the noise generated by cross beating

between the optical signal and ASE noise, and the noise generated by cross beating between ASE noise components at different frequencies were derived after photodetection. The spectral density of the phase fluctuations caused by the generated noise on the optically-generated electrical signal was obtained.

Acknowledgement

The work was supported by the Canadian Institute for Photonic Innovations (CIPI).

References

[1] L. Nöel, D. Wake, D. G. Moodie, D. D. Marcenac, L. D. Westbrook, and D. Nesset, "Novel techniques for high capacity 60 GHz fiber-radio transmission systems," *IEEE Trans. Microwave Theory Tech.*, vol. 45, no. 8, pp. 1416-1423, Aug. 1997.

[2] J. E. Román, L. T. Nichols, K. J. Williams, R. D. Esman, G. C. Tavik, M. Livingston, and M. G. Parent, "Fiber-optic remoting of an ultrahigh dynamic range radar," *IEEE Trans. Microwave Theory Tech.*, vol. 46, no. 12, pp. 2317-2323, Dec. 1998.

[3] U. Gliese, S. Norskov, and T. N. Nielsen, "Chromatic dispersion in fiber-optic microwave and millimeter-wave links," *IEEE Trans. Microwave Theory Tech.*, vol. 44, no. 10, pp. 1716-1724, Oct. 1996.

[4] R. P. Braun, G. Grosskopf, D. Rohde, and F. Schmidt, "Optical millimetre-wave generation and transmission experiments for mobile 60 GHz band communications," *Electron. Lett.*, vol. 32, no. 7, pp. 626-628, Mar. 1996.

[5] L. Goldberg, H. F. Taylor, J. F. Weller, and D. M. Bloom, "Microwave signal generation with injection-locked laser diodes," *Electron. Lett.*, vol. 19, no. 13, pp. 491-493, Jun. 1983.

[6] R. T. Ramos and A. J. Seeds, "Fast heterodyne optical phase lock loop using double quantum well laser diodes," *Electron. Lett.*, vol. 28, no. 1, pp. 82-83, Jan. 1992.

[7] J. J. O'Reilly, P. M. Lane, R. Heidemann, and R. Hofstetter, "Optical generation of very narrow linewidth millimetre wave signals," *Electron. Lett.*, vol. 28, no. 25, pp. 2309-2311, Dec. 1992.

[8] G. J. Cowle, P. T. Morkel, R. I. Laming, and D. N. Payne, "Spectral broadening due to fibre amplifier phase noise," *Electron. Lett.*, vol. 26, no. 7, pp. 424-425, Mar. 1990.

[9] H. Okamura, and K. Iwatsuki, "Spectral linewidth broadening in Er-doped-fibre amplifiers measured with less than 1.4 kHz linewidth light source," *Electron. Lett.*, vol. 26, no. 23, pp. 1965-1967, Nov. 1990.

[10] D. Simeonidou, S. Hamidi, and A. S. Siddiqui, "Spectral linewidth broadening in Erbium-doped and Raman fibre amplifiers," *Electron. Lett.*, vol. 28, no. 18, pp. 1965-1966, Aug. 1992.

[11] B. Pourbahri, P. A. Davies, D. S. George, and D. Wake, "The effects of fibre amplifier phase noise on radio over fibre signals," in *Pro. Broadband Communications*, Feb. 2000, pp. 89-91.

[12] J. Rogers, and C. Plett, *Radio Frequency Integrated Circuit Design.* Artech House, 2003, pp. 283-283.

[13] E. Desurvire, "Analysis of noise figure spectral distribution in erbium doped fiber amplifiers pumped near 980 and 1480 nm," *Appl. Opt.*, vol. 29, no. 21, pp. 3118-3125, Jul. 1990.

[14] M. J. Connelly, *Semiconductor Optical Amplifiers.* Boston: Kluwer academic publishers, 2002.

[15] W. P. Robins, *Phase Noise in Signal Sources.* London: Peter Peregrinus, 1982, pp. 6-8, 20-26.

PART 2

CHAPTER 5
OPTICAL UP-CONVERSION

As discussed in Chapter 2, the technology of optical up-conversion is important for radio-over-fiber applications. In this Chapter, techniques of optical up-conversion are studied. In Sec. 5.1, an approach for optically up-converting an electrical subcarrier from a low-frequency band to the millimeter-wave band is proposed with optical signals generated in Chapter 3 for millimeter-wave signal generation. One of these optical signals is generated using an optical intensity modulator with an optical notch filter, as detailed in Sec. 3.1. Another is generated using an optical phase modulator with an optical notch filter, as detailed in Sec. 3.2. In order to incorporate information in the up-converted signal, an optical intensity modulator is used to directly modulate these optical signals by a low-frequency electrical subcarrier. Analysis confirms that the data information carried by the low-frequency electrical subcarrier is up-converted to the millimeter-wave band. Data transmission experiments and simulations of BPSK and QPSK signals validate the proposed optical up-conversion approach. In Sec. 5.2, nonlinear effects of an electro-optic intensity modulator used in optical up-conversion schemes for radio-over-fiber applications are studied. Harmonic and inter-modulation distortions generated in an optical up-conversion approach are analyzed. One-tone and two-tone measurements are performed to validate the analyses.

5.1 Optical up-conversion of an electrical subcarrier from a low-frequency band to the millimeter-wave band

In this Section, an optical up-conversion approach for millimeter-wave-over-fiber applications is proposed. This approach uses external optical intensity modulation to superimpose a low-frequency electrical subcarrier on the up-converted, optically-generated carrier. Analyses show that the data information carried by the low-frequency electrical subcarrier is up-converted to the millimeter-wave band. Data transmission experiments and simulations of BPSK and QPSK signals are performed to verify the proposed approach.

1. Introduction

The technology of millimeter-wave (mm-wave) over fiber is very attractive for applications such as next-generation broadband wireless access networks, sensor networks, radar and software defined radio systems, and has been intensively investigated in the past few years [1]-[10].

In millimeter-wave-over-fiber systems, millimeter-wave signals are usually generated at a base station by beating two phase-correlated optical carriers. This is essential since the optical carriers can be easily distributed over optical fiber with very low loss. In addition, the millimeter-wave signal is easy to obtain at the base stations by beating the two optical carriers at a photodetector, which significantly reduces the complexity and cost of the base stations. Many approaches have been proposed in the past few years for optical generation and distribution of millimeter-wave signals, which include automatic frequency control [3], optical phase locking of two laser diodes [4], optical injection locking of two laser diodes [5], and a combination of phase locking and injection locking [6]. The two phase-correlated optical wavelengths can also be generated using external modulation techniques [7]-[9]. By modulating an optical carrier with a microwave drive signal using an external intensity modulator, a millimeter-wave signal that has 2 or 4 times the frequency of the microwave drive signal can be generated. In these schemes, an optical filter is usually required to select two optical sidebands. Recently, we have proposed two approaches for generating millimeter-wave signals of large frequency tunability with external optical modulation and a fixed notch optical filter [10], [11]. With a two-laser

approach, data information or an RF subcarrier can be superimposed on the wavelength of one of the two lasers before combining and sending them to a base station. In schemes based on external modulation [7]-[11], however, the two wavelengths are generated within one fiber. If a data signal or an RF subcarrier is to be superimposed on one of the carriers, the two optical wavelengths must be physically separated [7], [9]. This separation is usually implemented using a narrowband optical filter, which complicates the system and limits its versatility.

2. Principle and analysis

The proposed optical up-conversion approach is shown in Fig. 1. The input optical signal can be two phase-correlated optical carriers with a frequency difference located in the millimeter-wave band. It can be generated by an optical phase lock loop [4], an optical phase modulator and an optical filter [9], or an optical intensity modulator with an optical notch filter [10]. The optical signal can also be a series of optical harmonics generated by an optical phase modulator processed by an optical notch filter [11]. The Mach-Zehnder modulator (MZM), which is biased at its linear region, is driven by a low-frequency electrical subcarrier.

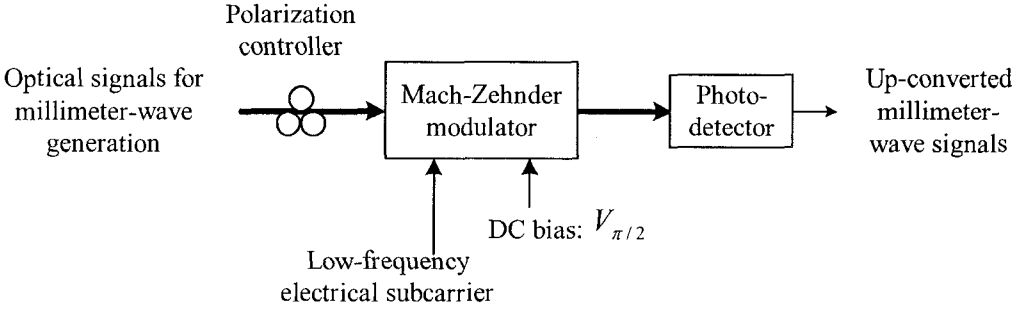

Fig. 1. Proposed subcarrier frequency up-conversion approach.

Before we proceed with the complete analysis of the optical up-conversion, we perform a brief analysis of the intensity modulation of a one-wavelength optical carrier to simplify the optical up-conversion analysis. For typical LiNbO3 MZM's, the refractive index change with respect to the applied voltage is dominated by the linear electro-optic effect of the material. When an optical carrier with a wavelength λ passes through a MZM driven by a signal of voltage $V(t)$, the voltage induced phase difference between the two arms of the modulator is given by

$$\Phi[V(t)]=\frac{2\pi}{\lambda}r_1 V(t)L, \tag{1}$$

where r_1 is a constant reflecting the linear electro-optic effect of the LiNbO3 and L is the physical length of the modulator electrode. If, with the same applied voltage $V(t)$, there is a wavelength offset $\Delta\lambda$ with respect to λ, then the corresponding phase offset will be

$$\Delta\Phi[V(t)] = \Phi[V(t)] \times (-\frac{\Delta\lambda}{\lambda}) . \tag{2}$$

For radio-over-fiber systems operating at 1550 nm window, a 50-GHz millimeter-wave offset corresponds to a $\Delta\lambda$ of 0.4 nm, which leads to $\Delta\lambda/\lambda_o \approx 2.6\times10^{-4}$, where $\lambda_o = 1550$ nm. Therefore, the phase offset $\Delta\Phi[V(t)]$ variation between the two wavelengths is very small and can be neglected. Therefore, when two optical carriers have a frequency offset in the millimeter-wave band, their voltage induced phase shifts are about the same. This allows us to treat the modulation of these optical carriers the same way as the modulation of one optical carrier.

In addition, as is often found in the literature, a sinusoidal signal can be used to represent a low-frequency electrical subcarrier to simplify the analysis. This is because the small amplitude modulation (AM), phase modulation (PM) or frequency modulation (FM) does not significantly perturb the original signal. The modulated low-frequency electrical subcarrier, $V_s(t)$, can then be written as $V_s(t) = A_s \cos(\omega_s t + \phi_s)$; where A_s, ω_s and ϕ_s are the amplitude, angular frequency and phase of the low-frequency electrical subcarrier. They are time invariant under the assumption of narrow band modulation. Then the voltage applied to the optical modulator can be written as

$$V_e(t) = V_{DC} + V_s(t) , \tag{3}$$

where V_{DC} is the DC bias voltage.

When an optical carrier with an electrical field defined as $E_o \cos(\omega_o t)$ passes through the MZM, and the modulator is driven by a low-frequency electrical subcarrier biased at a DC voltage as expressed in (3), the electrical field of the output optical signal is approximately given by [12]

$$E_{out}(t) = E_o \cos[\frac{\phi_{DC}}{2} + C_1 V_s(t)]\cos(\omega_o t), \tag{4}$$

where $\phi_{DC} = \frac{\omega}{c} r_1 V_{DC} L$, $C_1 = \frac{\omega}{2c} r_1 L$, and c is light speed in free space. When $\phi_{DC} = \pi/2$, equation (4) can be rewritten as

$$E_{out}(t) = \frac{E_o}{\sqrt{2}}\{\cos[C_1 V_s(t)] - \sin[C_1 V_s(t)]\}\cos(\omega_o t) = \frac{E_o}{\sqrt{2}}[1 - C_1 V_s(t) - \cdots]\cos(\omega_o t), \tag{5}$$

Here Taylor series expressions of $\sin(x)$ and $\cos(x)$ are used; higher-order terms of $V_s(t)$ are ignored when modeling weak modulation.

A. Optical up-conversion with two phase correlated optical carriers

In general the electrical field, $E_{in1}(t)$, of an optical signal of two phase correlated optical carriers can be simply expressed as

$$E_{in1}(t) = E_1 \cos[(\omega_o - \frac{\omega_{mm}}{2})t] + E_2 \cos[(\omega_o + \frac{\omega_{mm}}{2})t], \tag{6}$$

where E_1 and E_2 are the field amplitudes of the two wavelengths with angular frequencies $\omega_o - \omega_{mm}/2$ and $\omega_o + \omega_{mm}/2$, and ω_{mm} is the frequency difference between the two carriers. If this optical signal is fed into the MZM shown in Fig. 1, driven by a signal expressed by (3), the electric field of the optical signal at the output of the MZM is given by

$$E_{out1}(t) = \frac{E_1}{\sqrt{2}}\cos[(\omega_o - \frac{\omega_{mm}}{2})t] - \frac{E_1 C_1}{2\sqrt{2}} A_s \left\{\cos[(\omega_o - \frac{\omega_{mm}}{2} - \omega_s)t - \phi_s] + \cos[(\omega_o - \frac{\omega_{mm}}{2} + \omega_s)t + \phi_s]\right\}$$

$$+ \frac{E_2}{\sqrt{2}}\cos[(\omega_o + \frac{\omega_{mm}}{2})t] - \frac{E_2 C_1}{2\sqrt{2}} A_s \left\{\cos[(\omega_o + \frac{\omega_{mm}}{2} - \omega_s)t - \phi_s] + \cos[(\omega_o + \frac{\omega_{mm}}{2} + \omega_s)t + \phi_s]\right\}. \tag{7}$$

When this modulated optical signal is fed into a photodetector, beatings among the spectral terms will occur. If the DC term is blocked and the limited bandwidth of the photodetector is taken into account, the voltage expression of the electrical signal at the output of the photodetector is

$$V_{out1}(t) \propto \frac{E_1 E_2}{2}\left\{(1+\frac{C_1^{\,2} A_s^{\,2}}{2})\cos(\omega_{mm} t)\right.$$

$$-C_1 A_s \cos[(\omega_{mm}-\omega_s)t-\phi_s] - C_1 A_s \cos[(\omega_{mm}+\omega_s)t+\phi_s]$$

$$\left.+\frac{C_1^{\,2} A_s^{\,2}}{4}\cos[(\omega_{mm}-2\omega_s)t-2\phi_s] + \frac{C_1^{\,2} A_s^{\,2}}{4}\cos[(\omega_{mm}+2\omega_s)t+2\phi_s]\right\}. \qquad (8)$$

In (8), the first term is a pure millimeter-wave carrier sinusoidal signal at the frequency ω_{mm}; the second and third terms are the two required up-converted millimeter-wave signals at the frequency of $\omega_{mm}-\omega_s$ and $\omega_{mm}+\omega_s$, respectively; the fourth and fifth terms are amplitude distorted signals at the frequency of $\omega_{mm}-2\omega_s$ and $\omega_{mm}+2\omega_s$, respectively. As the pure millimeter-wave carrier at the frequency of ω_{mm} and the amplitude distorted terms at frequency of $\omega_{mm}-2\omega_s$ and $\omega_{mm}+2\omega_s$ are one subcarrier frequency, ω_s, away from the required signals, these unwanted beating terms will not cause interference to the required up-converted millimeter-wave signals at the frequency of $\omega_{mm}-\omega_s$ and $\omega_{mm}+\omega_s$. With proper filtering and amplification techniques, an up-converted millimeter-wave signal $V_{mm1}(t)$ or $V_{mm2}(t)$ can be obtained and is ready for radiation at base stations,

$$V_{mm1}(t) \propto \frac{E_1 E_2 C_1}{2} A_s \cos[(\omega_{mm}-\omega_s)t-\phi_s], \qquad (9.1)$$

$$V_{mm2}(t) \propto \frac{E_1 E_2 C_1}{2} A_s \cos[(\omega_{mm}+\omega_s)t+\phi_s]. \qquad (9.2)$$

The millimeter-wave signals $V_{mm1}(t)$ in (9.1) and $V_{mm2}(t)$ in (9.2) clearly show that the low-frequency electrical subcarrier, $V_s(t) = A_s \cos(\omega_s t + \phi_s)$, is successfully up-converted to the millimeter-wave band. Information contained in the amplitude A_s or the phase ϕ_s of $V_s(t)$ has been transferred to the new millimeter-wave signals.

B. Optical up-conversion with a series of optical harmonics generated by an optical phase modulator and an optical notch filter

The electric field, $E_{in2}(t)$, of an optical signal generated by using an optical phase modulator and an optical notch filter can be expressed as [11]

$$E_{in2}(t) = E_o\{\sum_{n=-\infty}^{\infty} J_n(\beta)\cos[(\omega_o + n\omega_e)t + n\cdot\frac{\pi}{2}] - J_0(\beta)\cos(\omega_o t)\}, \tag{10}$$

where: E_o and ω_o are the amplitude and angular frequency of the input optical carrier fed into the optical phase modulator, ω_e is the angular frequency of the electrical drive signal that drives the optical phase modulator, $J_n(\beta)$ is a Bessel function of the first kind of order n with argument of β, the phase modulation depth.

If this optical signal $E_{in2}(t)$ is fed into the optical intensity modulator shown in Fig. 1, and modulated by the electrical signal expressed by (3), based on (5) its electric field at the output of the MZM becomes

$$E_{out2}(t) =$$

$$\frac{E_o}{\sqrt{2}}\left\{\sum_{n=-\infty}^{\infty} J_n(\beta)\left\{\cos[(\omega_o + n\omega_e)t + n\cdot\frac{\pi}{2}]\right.\right.$$

$$\left.-\frac{C_1}{2}A_s\left\{\cos[(\omega_o + n\omega_e - \omega_s)t + n\cdot\frac{\pi}{2} - \phi_s] + \cos[(\omega_o + n\omega_e + \omega_s)t + n\cdot\frac{\pi}{2} + \phi_s]\right\}\right\}$$

$$\left.-J_0(\beta)\left\{\cos(\omega_o t) - \frac{C_1}{2}A_s\{\cos[(\omega_o - \omega_s)t - \phi_s] + \cos[(\omega_o + \omega_s)t + \phi_s]\}\right\}\right\}, \tag{11}$$

When these modulated optical sidebands are fed to a photodetector, up-converted millimeter-wave signals are generated. If the DC and low-frequency products are ignored and the limited bandwidth of the photodetector is taken into account, the voltage expressions of the high-frequency electrical signals, $V_{out2}(t)$, is

$$V_{out2}(t) \propto -E_o{}^2\sum_{n=1}^{\infty} J_0(\beta)J_{2n}(\beta)\left\{(1 + \frac{C_1{}^2 A_s{}^2}{2})\cos(2n\omega_e t + n\pi)\right.$$

$$\left.- C_1 A_s\cos[(2n\omega_e - \omega_s)t + n\pi - \phi_s] - C_1 A_s\cos[(2n\omega_e + \omega_s)t + n\pi + \phi_s]\right.$$

$$+\frac{C_1^2 A_s^2}{4}\cos[(2n\omega_e - 2\omega_s)t + n\pi - 2\phi_s] + \frac{C_1^2 A_s^2}{4}\cos[(2n\omega_e + 2\omega_s)t + n\pi + 2\phi_s]\Big\}. \quad (12)$$

Equation (12) shows a series of electrical signals are generated at frequency of $2n\omega_e$, $2n\omega_e - \omega_s$, $2n\omega_e + \omega_s$, $2n\omega_e - 2\omega_s$, and $2n\omega_e + 2\omega_s$. In (12), the first term is a pure carrier; the last two terms are amplitude distortion products. They are one subcarrier frequency, ω_s, away from the useful up-converted electrical signals, the second and third terms in (12). With appropriate filtering, useful up-converted electrical signal $V_1(t)$ or $V_2(t)$ is obtained without distortion. They are

$$V_1(t) \propto E_o^2 C_1 A_s \sum_{n=1}^{\infty} J_0(\beta) J_{2n}(\beta) \cos[(2n\omega_e - \omega_s)t + n\pi - \phi_s], \quad (13.1)$$

$$V_2(t) \propto E_o^2 C_1 A_s \sum_{n=1}^{\infty} J_0(\beta) J_{2n}(\beta) \cos[(2n\omega_e + \omega_s)t + n\pi + \phi_s]. \quad (13.2)$$

Again, it is clearly shown that the low-frequency electrical subcarrier $[V_s(t) = A_s \cos(\omega_s t + \phi_s]$ is successfully up-converted to the frequency of $2n\omega_e - \omega_s$ and $2n\omega_e + \omega_s$. Note that the analysis assumes that the amplitude and phase of the optical harmonics are maintained before photodetection. That means a dispersion compensation module is needed if this optical signal is distributed with standard single mode fiber. A discussion of the effect of the chromatic dispersion of standard single mode fiber can be found in [11].

In summary, the above analyses show that optical signals generated with approaches for millimeter-wave signals generation can be used directly in the above proposed optical up-conversion approach. This makes the optical up-conversion setup simple, and reduces polarization uncertainty existing if the optical signal is separated and put back.

3. Experiment

To validate approaches to optically generating millimeter-wave signals for radio-over-fiber applications [10], [11] and validate the above proposed optical up-conversion approach, experiments and simulation are performed. Their results are as follows.

A. Experiments with two phase correlated optical carriers generated with an optical intensity modulator and an optical notch filter

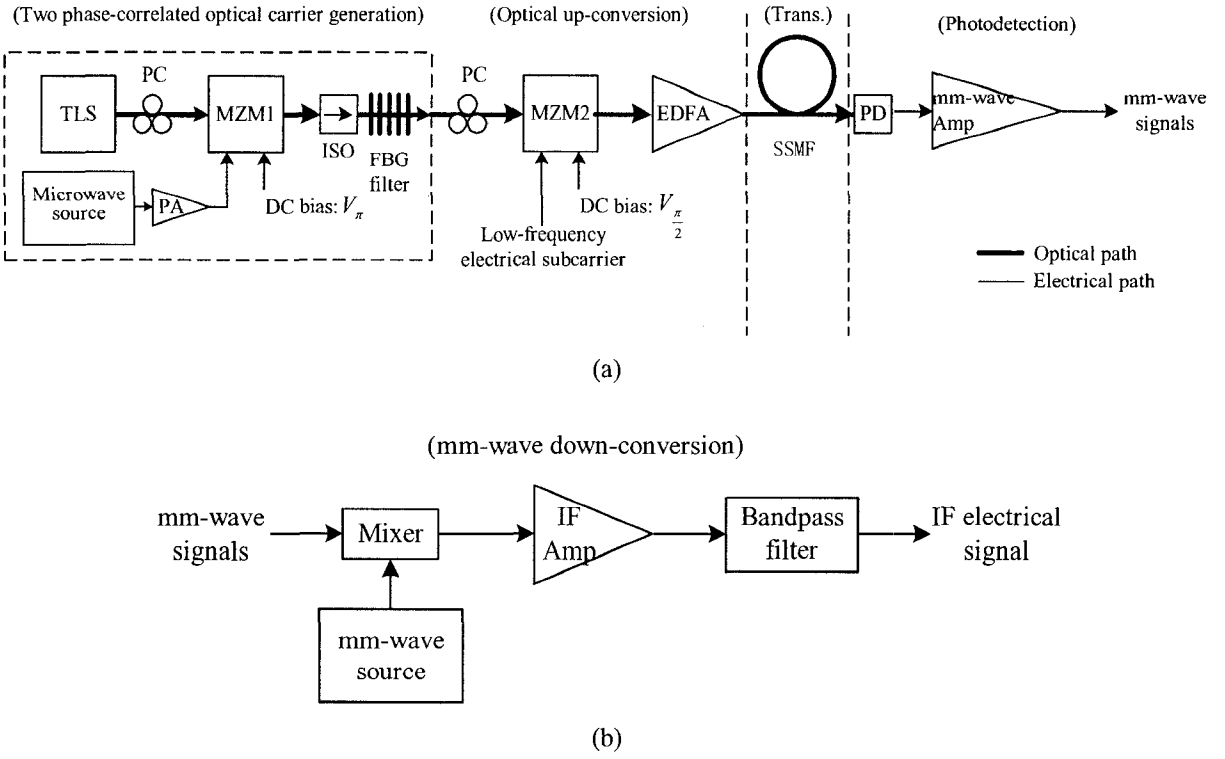

Fig. 2. Experimental setups. (a) The setup of the generation of two correlated optical carriers and the optical up-conversion. (b) The setup of a millimeter-wave down-conversion . Thick line indicates optical path. (TLS: tunable laser source, PC: polarization controller, MZM: Mach-Zehnder modulator, ISO: isolator, EDFA: erbium-doped fiber amplifier, PA: power amplifier, SSMF: standard single mode fiber, PD: photodetector, Amp.: amplifier, IF: intermediate frequency)

An experimental optical up-conversion setup is built with two correlated optical carriers as shown in Fig. 2. Fig. 2 (a) shows the optical up-conversion scheme with two phase-correlated optical carriers. The two phase-correlated optical carriers are generated using an intensity modulator and a fixed optical filter [10]. The two optical carriers have a frequency separation of 4 times the frequency of the microwave drive signal obtained from a microwave source. By tuning the microwave drive signal, tunable wavelength separation between the two carriers is realized. The generated optical carriers are then applied to a second MZM to which a low-frequency electrical subcarrier and a DC bias are applied. Up-converted millimeter-wave

signals are generated after photodetection. Fig. 2 (b) shows a setup of a standard frequency down-conversion configuration.

A1. Experiment with an un-modulated low-frequency electrical subcarrier

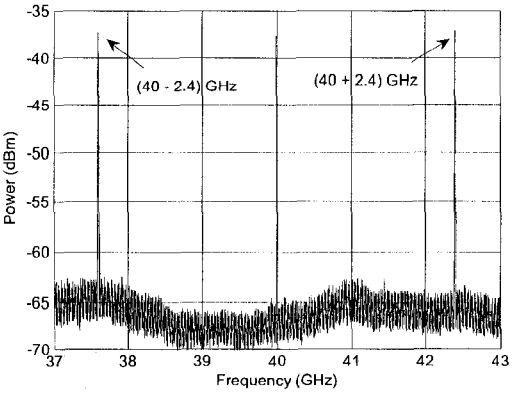

(a)

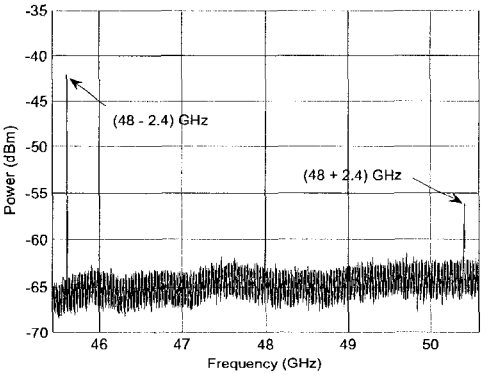

(b)

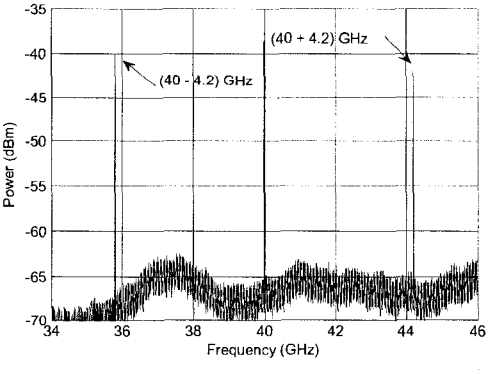

(c)

Fig. 3. Electrical spectra of the up-converted millimeter-wave signals. (a) 40 ± 2.4 GHz. (b) 48 ± 2.4 GHz. (c) 40 ± 4.2 GHz.

An un-modulated low-frequency electrical subcarrier is used to characterize the frequency tunable ability of the optical up-conversion part with an electrical spectrum analyzer to examine the output millimeter-wave signals in Fig. 2 (a). The frequency of the microwave source is tuned between 10 GHz and 12 GHz, which leads to an optical carrier separation from 40 GHz to 48 GHz. Fig. 3 shows the electrical spectra of the up-converted millimeter-wave signals. Fig. 3 (a) and Fig. 3 (b) show the spectra of the up-converted millimeter-wave signals with the optical carrier separations of 40 and 48 GHz, respectively. Since the frequency of the low-frequency electrical subcarrier is 2.4 GHz, up-converted signals with frequencies at 37.6 GHz and 42.4 GHz in Fig. 3 (a) and 45.6 GHz and 50.4 GHz in Fig. 3 (b) are observed. The asymmetric power levels of the spectral peaks in Fig. 3 (b) are due to the limited bandwidth of the 45 GHz photodetector. Fig 3 (c) shows the spectrum of the up-converted millimeter-wave signal when the optical carrier separation is at 40 GHz. In this case the frequency of the low-frequency electrical subcarrier is 4.2 GHz and the up-converted signals are at 35.8 GHz and 44.2 GHz. These results show the versatility of the proposed approach.

A2. Experiment and simulation with a BPSK modulated low-frequency electrical subcarrier

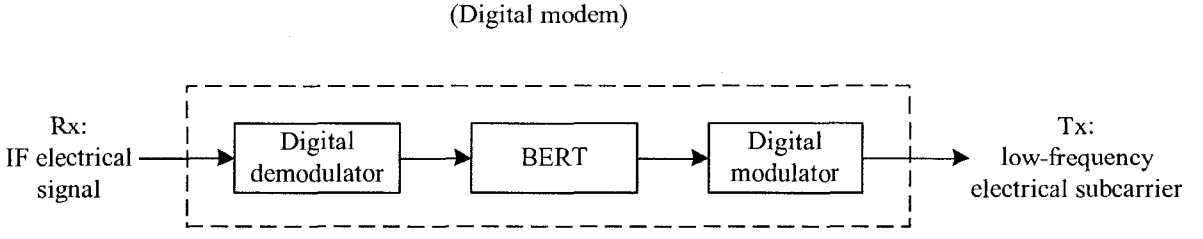

Fig. 4. Digital modem. (Rx: receive, Tx: transmit, BERT: BER tester)

As a proof of concept, a commercially available instrument with functions of standard digital modem and BERT shown in Fig. 4 is used with the setup of optical up-conversion shown in Fig. 2 (a) and the setup of millimeter-wave down-conversion shown in Fig. 2 (b) to perform a data transmission experiment to a BPSK modulated signal.

In the experiment, the instrument can transmit (Tx) and receive (Rx) a 2.048 Mbps BPSK modulated 70 MHz subcarrier, and calculate BER. In Fig. 2 (a), the frequency of the microwave drive signal is set to 7 GHz, and the length of the standard single mode fiber is 25 km. So the BPSK modulated 70 MHz signal is up-converted to 27.93GHz (28 GHz - 70 MHz) and 28.07 GHz (28 GHz + 70 MHz). Then in Fig. 2 (b) the frequency of the millimeter-wave local signal

is set to 28 GHz to down-convert the up-converted signal back to 70 MHz. Note that choosing the frequency of 7 GHz of the microwave drive signal is a compromise to the bandwidth and conversion loss of the millimeter-wave mixer in Fig. 2 (b); and the bit rate of BSPK signal is limited by the modem used.

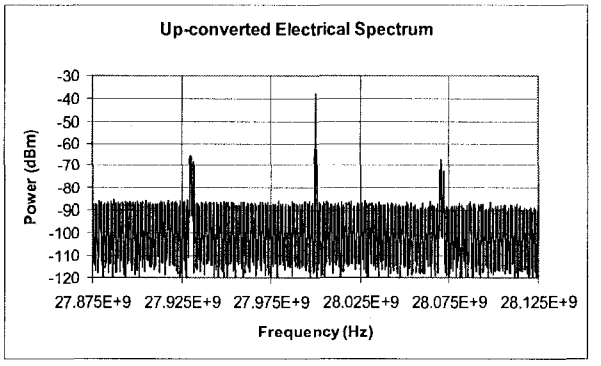

(a)

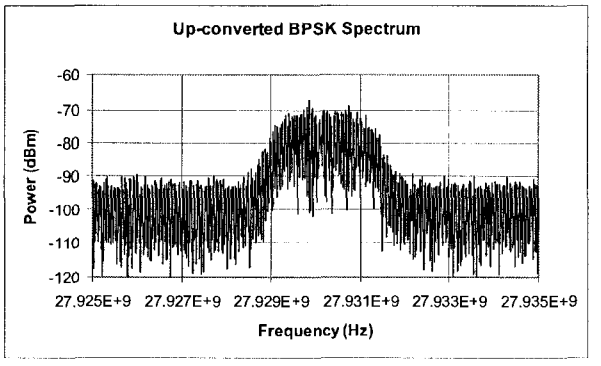

(b)

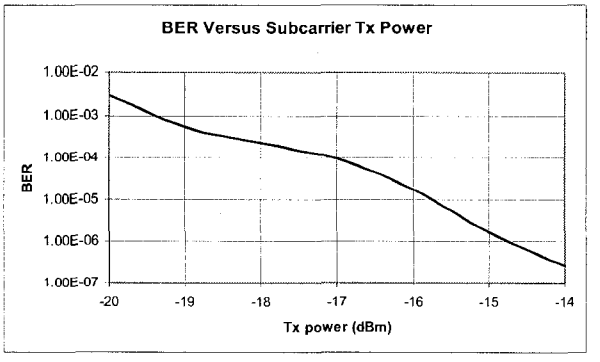

(c)

Fig. 5. Experimental results of the BPSK signal transmission experiment. (a) Up-converted electrical spectrum with a span of 250 MHz. (b) Up-converted BPSK spectrum at a span of 10 MHz. (c) BER versus subcarrier Tx power.

Fig. 5 shows results of the BPSK signal transmission experiment. Fig. 5 (a) and Fig. 5 (b) show the electrical spectra of the up-converted millimeter-wave signals at the output of the millimeter-wave amplifier. Fig. 5 (a) shows the spectrum of the up-converted BPSK signals when the span of the electrum spectrum analyzer is 250 MHz. There are up-converted BPSK signals at the frequency of 27.93 GHz and 28.07 GHz respectively and there is also a 28 GHz signal. Fig. 5 (b) shows a detailed spectrum of the up-converted BPSK signal centered at 27.93 GHz when the span of the electrum spectrum analyzer is 10 MHz. Fig. 5 (c) shows the curve of BER versus the output power of the digital modem.

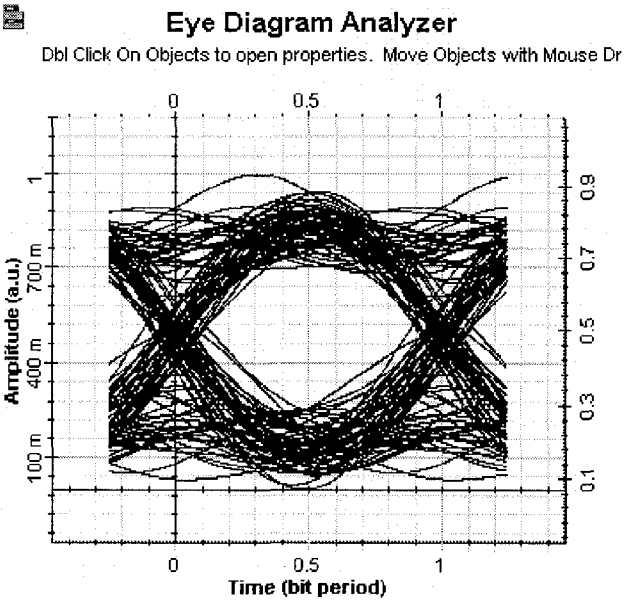

(a)

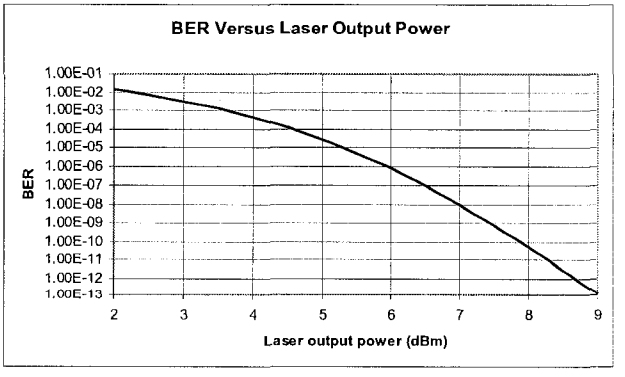

(b)

Fig. 6. Simulation results of the BPSK signal transmission with a bit rate of 1 Gbps. (a) A typical eye diagram at a BER of 9.37×10^{-9}. (b) BER versus laser output power.

An experimental simulation based on the setup shown in Fig. 2 and Fig. 4 is performed with a high bit rate digital signal. In the simulation, parameters are set the same as above experiment except that the bit rate of the digital signal is set to 1 Gbps, and the frequency of the subcarrier is set to 3 GHz. Fig. 6 shows simulation results. Fig. 6 (a) shows an eye diagram corresponding to a BER of 9.37×10^{-9}. Fig. 6 (b) shows the curve of BER versus laser output power.

A3. Experiment with a QPSK modulated low-frequency electrical subcarrier

A data transmission experiment of 500 Mbps QPSK signal is performed with the setup of the QPSK signal generation and analysis shown in Fig. 7, along with the setup of optical up-conversion scheme shown in Fig. 2 (a) and the setup of millimeter-wave down-conversion scheme shown in Fig. 2 (b). In Fig. 7 an arbitrary waveform generator and a vector signal generator are used for QPSK signal generation, and a vector signal analyzer is used for QPSK signal analysis.

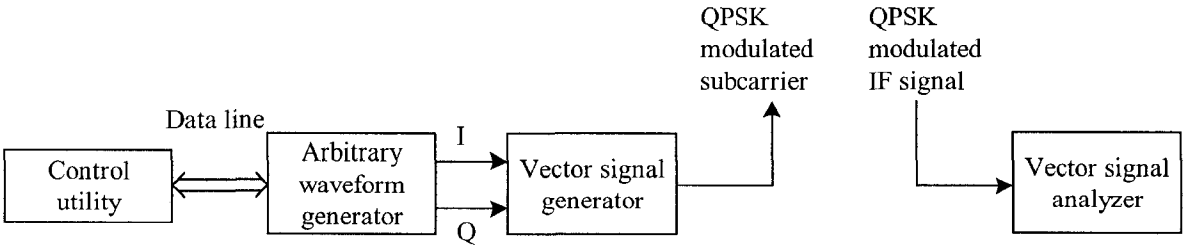

Fig. 7. The setup of QPSK modulated signal generation and analysis.

In the experiment, the arbitrary waveform generator generates 250 Mbps I and Q digital signals. These digital signals are fed to the vector signal generator, where the frequency of the carrier is set to 11 GHz. In Fig. 2 (a), the frequency of the microwave drive signal is set to 8 GHz, and the length of the standard, single-mode fiber is 25 km. Then the 500 Mbps QPSK modulated 11 GHz signal is up-converted to 21GHz (32 GHz - 11 GHz) and 43 GHz (32 GHz + 11 GHz). In Fig. 2 (b) the frequency of the millimeter-wave local signal is set to 25 GHz to down-convert the up-converted signal at 21 GHz to 4 GHz. Note that choosing the frequency of 8 GHz of the microwave drive signal in Fig. 2 (a) and the frequency of 11 GHz of the QPSK carrier in Fig. 7 is a compromise to the bandwidth and conversion loss of the millimeter-wave mixer in Fig. 2 (b).

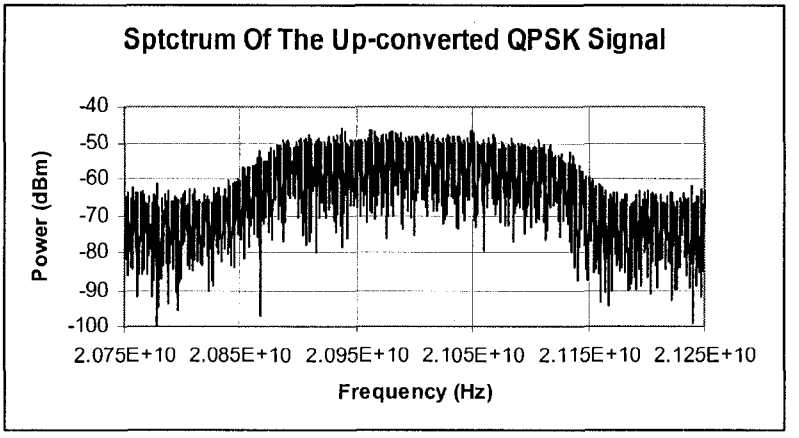
Sptctrum Of The Up-converted QPSK Signal
Power (dBm)
-40
-50
-60
-70
-80
-90
-100
2.075E+10
2.085E+10
2.095E+10
2.105E+10
2.115E+10
2.125E+10
Frequency (Hz)

(a)

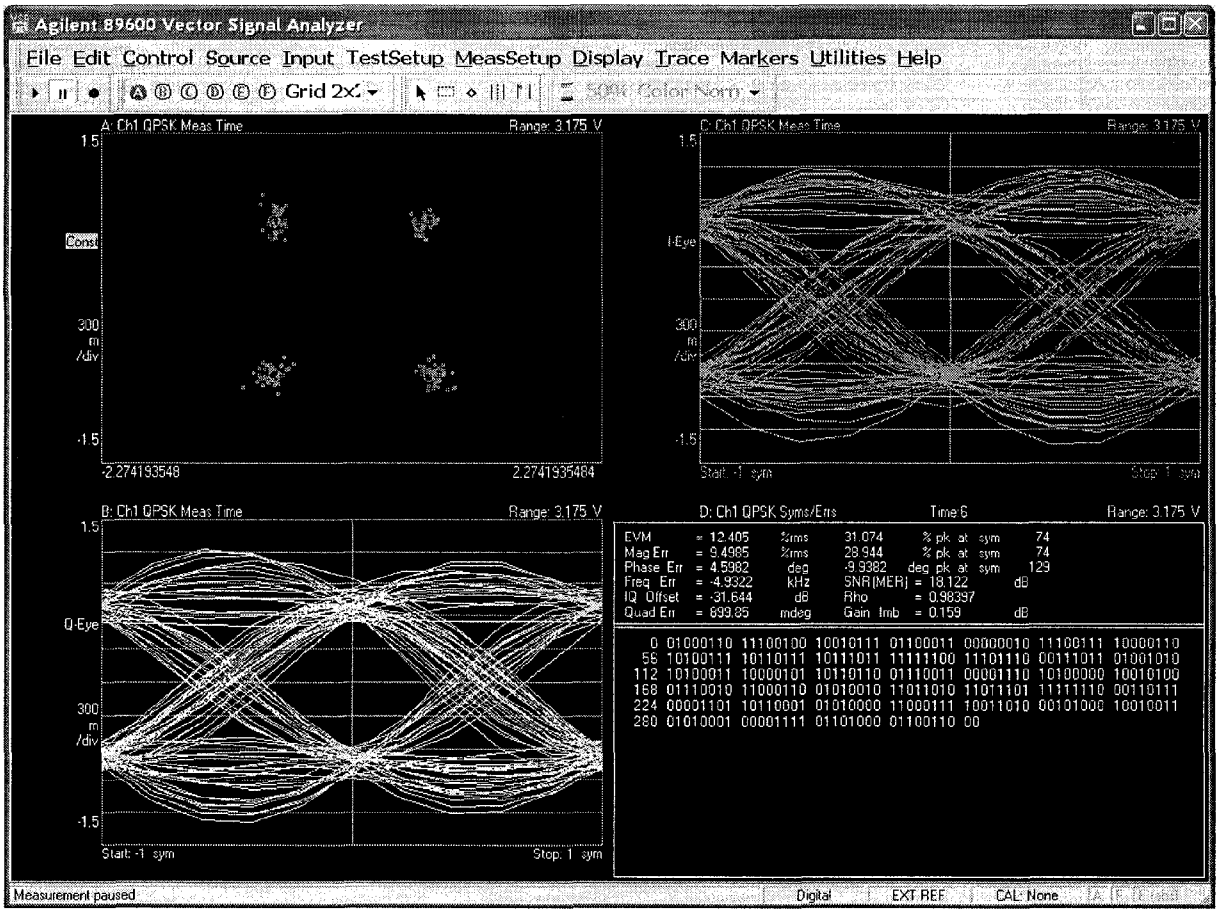
Agilent 89600 Vector Signal Analyzer
File Edit Control Source Input TestSetup MeasSetup Display Trace Markers Utilities Help
A: Ch1 QPSK Meas Time
Range: 3.175 V
Const
-2.274193548
2.274193484
C: Ch1 QPSK Meas Time
Range: 3.175 V
I-Eye
B: Ch1 QPSK Meas Time
Range: 3.175 V
Q-Eye
Start: -1 sym
Stop: 1 sym
D: Ch1 QPSK Syms/Errs
Time 6
Range: 3.175 V
EVM = 12.405 %rms 31.074 % pk at sym 74
Mag Err = 9.4985 %rms 28.944 % pk at sym 74
Phase Err = 4.5982 deg -9.9382 deg pk at sym 129
Freq Err = -4.9322 kHz SNR(MER) = 18.122 dB
IQ Offset = -31.644 dB Rho = 0.98397
Quad Err = 899.85 mdeg Gain Imb = 0.159 dB
0 01000110 11100100 10010111 01100011 00000010 11100111 10000110
56 10100111 10110111 10111011 11111100 11101110 00111011 01001010
112 10100011 10000101 10110110 01110011 00001110 10100000 10010100
168 01110010 11000110 01010010 11011010 11011101 11111110 00110111
224 00001101 10110001 01010000 11000111 10011010 00101000 10010011
280 01010001 00001111 01101000 01100110 00
Measurement paused
Digital
EXT REF
CAL: None

(b)

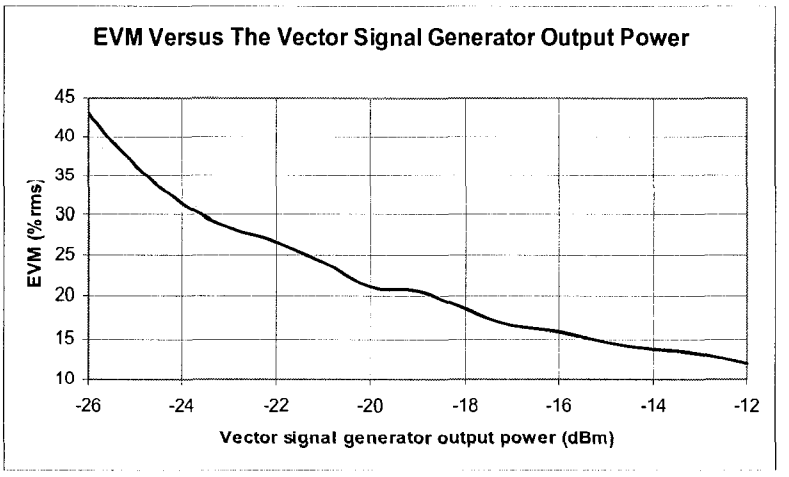

(c)

Fig. 8. Results of the QPSK signal transmission experiment. (a) Spectrum of the up-converted QPSK signal at 21 GHz. (b) A typical picture of constellation diagram, I eye diagram, Q eye diagram at EVM of 12.405 %rms. (c) EVM versus the output power of the vector signal generator.

In the experiment, error-vector magnitude (EVM) is used to evaluate the quality of the received QPSK signal [13]. Results of the 500 Mbps QPSK signal transmission experiment are shown in Fig. 8. Fig. 8 (a) shows the spectrum of the up-converted QPSK signal of 21 GHz at the output of the millimeter-wave amplifier in Fig. 2 (a). Fig. 8 (b) shows a typical picture of the vector signal analyzer at an EVM of 12.405 %rms, which includes the constellation diagram, the eye diagram of I signal, and the eye diagram of Q signal. Wide opening of I and Q eye diagrams can be obtained. Fig. 8 (c) shows the curve of EVM versus the output power of the vector signal generator.

B. Experiment and simulation of the transmission of BPSK modulated signals with an optical signal generated by an optical phase modulator and an optical notch filter

As a proof of concept, a data transmission experimental setup is built with the optical signal generated with an optical phase modulator and an optical notch filter as shown in Fig. 9 [11]. Fig. 9 shows the optical part of the experiment. The digital modem and the millimeter-wave down conversion are the same as those shown in Fig. 4 and Fig. 2 (b), respectively. In Fig. 9 the generated optical carriers are applied to the MZM to which a low-frequency electrical subcarrier and a DC bias are applied. Up-converted millimeter-wave signals at even frequencies of the microwave drive signal of the optical phase modulator are generated after photodetection. In Fig.

9 an optical attenuator is used to simulate the transmission effect of the standard single mode optical fiber with the corresponding dispersion compensation module.

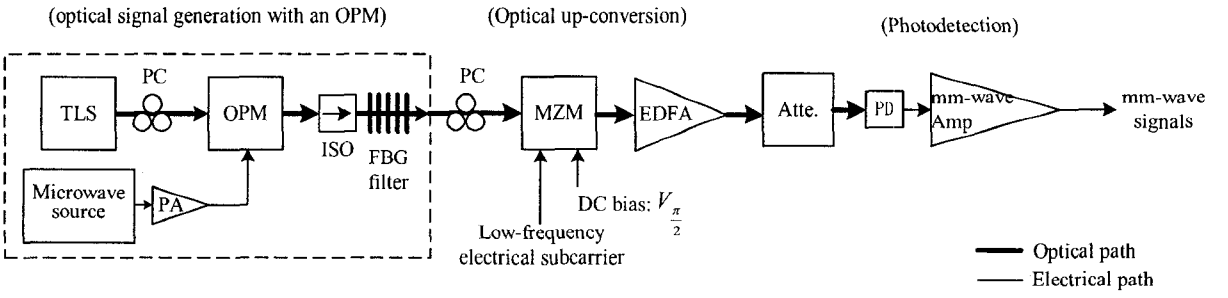

Fig. 9. System experimental setup with an optical signal generated by an optical phase modulator and an optical notch filter. (TLS: tunable laser source, PC: polarization controller, OPM: optical phase modulator, ISO: isolator, PA: power amplifier, MZM: Mach-Zehnder modulator, EDFA: erbium-doped fiber amplifier, Atte.: optical attenuator, PD: photodetector, Amp.: amplifier)

In the experiment, the digital modem shown in Fig. 4 is set to have a 2.048 Mbps BPSK modulated 70 MHz subcarrier. The frequency of the microwave drive signal in Fig. 10 is set to 7 GHz. The BPSK modulated 70 MHz signal is up-converted to 13.93GHz (14 GHz - 70 MHz) and 14.07 GHz (14 GHz + 70 MHz), and 27.93GHz (28 GHz - 70 MHz) and 28.07 GHz (28 GHz + 70 MHz) after photodetection. The frequency of the millimeter-wave local signal in Fig. 2 (b) is set to 14 GHz to down-convert the up-converted signal back to 70 MHz.

Fig. 10 shows the curve of BER versus the output power of the digital modem.

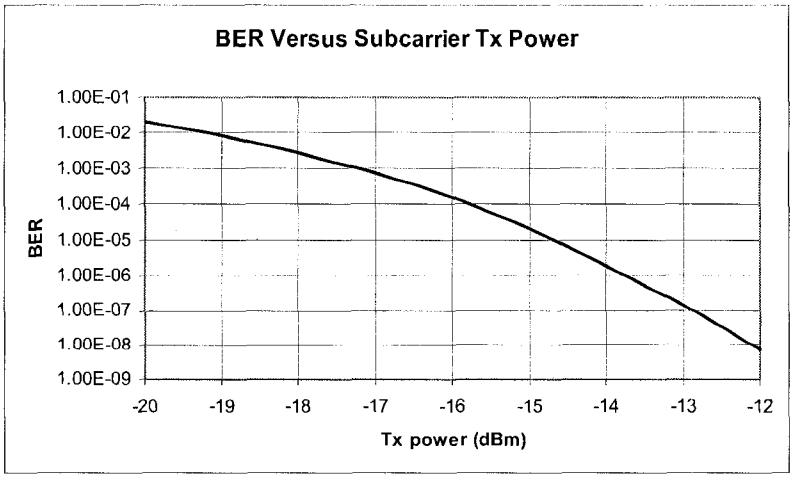

Fig. 10. BER versus the output power of the modem in the BPSK transmission experiment.

An experimental simulation based on the setup shown in Fig. 9 and Fig. 2 (b) is performed with a high bit rate digital signal. In the simulation, the bit rate of the digital signal is set to 1 Gbps; the frequency of the subcarrier is set to 3 GHz; digital modulation scheme is BPSK; the frequency of the microwave drive signal is set to 7 GHz; the frequency of the millimeter-wave local signal is set to 14 GHz. Fig. 11 shows simulation results. Fig. 11 (a) shows an eye diagram corresponding to a BER of 6.36×10^{-10}. Fig. 11 (b) shows the curve of BER versus the output power of the BPSK modulated subcarrier.

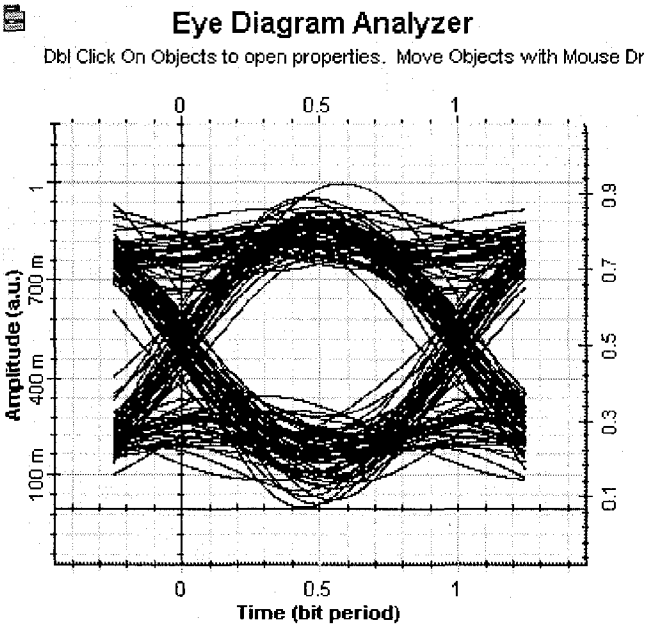

(a)

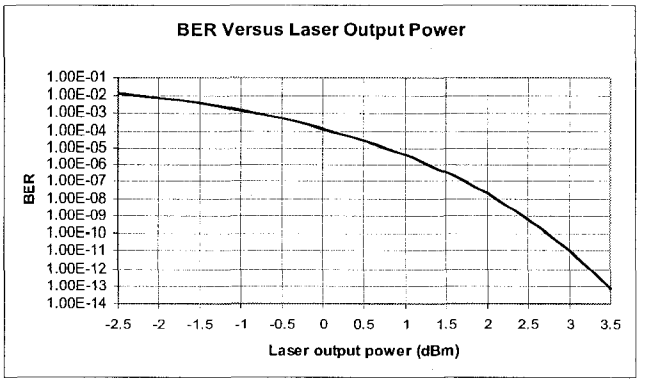

(b)

Fig. 11. Simulation results of the BPSK signal transmission with a bit rate of 1 Gbps. (a) A typical eye diagram at a BER of 6.36×10^{-10}, (b) BER versus laser output power.

4. Conclusion

An approach to realizing optical up-conversion implemented using an optical intensity modulator was proposed. Principles of the proposed approach were analyzed with respect to two optical signals for millimeter-wave signal generation. One optical signal is composed of two phase-correlated optical carriers; another optical signal is a series of optical sidebands generated with an optical phase modulator and an optical notch filter. Analyses showed that information carried by the amplitude, frequency and phase of the low-frequency subcarrier have been up-converted to the millimeter-wave band. Data transmission experiments and experimental simulations of BPSK and QPSK signals have validated the proposed approach. The attractive point of this optical up-conversion approach is that no treatment is needed to the optical signal before modulation. This makes the optical up-conversion setup simple, and reduces polarization uncertainty existing if the optical signal is separated and put back.

References

[1] A. J. Seeds, "Microwave photonics," *IEEE Trans. Microwave Theory Tech.*, vol. 50, no. 3, pp. 877-887, Mar. 2002.

[2] L. Nöel, D. Wake, D. G. Moodie, D. D. Marcenac, L. D. Westbrook, and D. Nesset, "Novel techniques for high capacity 60 GHz fiber-radio transmission systems," *IEEE Trans. Microwave Theory Tech.*, vol. 45, no. 8, pp. 1416-1423, Aug. 1997.

[3] R. P. Braun, G. Grosskopf, D. Rohde, and F. Schmidt, "Optical millimetre-wave generation and transmission experiments for mobile 60 GHz band communications," *Electron. Lett.*, vol. 32, no. 7, pp. 626-628, Mar. 1996.

[4] K. J. Williams, L. Goldberg, and R. D. Esman, "6–34 GHz offset phase locking of Nd :YAG nonplanar ring lasers," *Electron. Lett.*, vol. 25, no. 18, pp. 1242–1243, Aug. 1989.

[5] A.C. Bordonalli, C. Walton, A. J. Seeds, "High-performance phase locking of wide linewidth semiconductor lasers by combined use of optical injection locking and optical phase-lock loop," *J. Lightwave Technol.*, vol. 17, no. 2, pp. 328 – 342, Feb. 1999.

[6] L. A. Johansson and A. J. Seeds, "36-GHz 140-Mb/s radio-over-fiber transmission using an optical injection phase-lock loop source," *IEEE Photon. Tech. Lett.*, vol. 13, no. 8, pp. 893–895. Aug. 2001.

[7] J. O'Reilly and P. Lane, "Remote delivery of video services using mm-waves and optics," *J. Lightwave Technol.*, vol. 12, no. 2, pp. 369-375. Feb. 1994.

[8] P. Shen, N. J. Gomes, P. A. Davies, W. P. Shillue, P.G. Huggard, and B. N. Ellison, "High-purity millimetre-wave photonic local oscillator generation and delivery," in *Proc. Microwave Photonics,* Sept. 2003, pp. 189-192.

[9] R. Hofstetter, H. Schmuck, and R. Heidemann, "Dispersion effects in optical millimeter-wave systems using self-heterodyne method for transport and generation," *IEEE Trans. Microwave Theory Tech.*, vol. 43, no. 9, pp. 2263-2269, Sept. 1995.

[10] G. Qi, J. P. Yao, J. Seregelyi, C. Bélisle, and S. Paquet, "Generation and distribution of a wide-band continuously tunable millimeter-wave signal with an optical external modulation technique," *IEEE Trans. Microwave Theory Tech.*, vol. 53, no. 10, pp. 3090-3097, Oct. 2005.

[11] G. Qi, J. P. Yao, J. Seregelyi, C. Bélisle, and S. Paquet, "Optical generation and distribution of continuously tunable millimeter-wave signals using an optical phase modulator," *J. Lightwave Technol.*, vol. 23, no. 9, pp. 2687-2695, Sept. 2005.

[12] K. Okamoto, *Fundamentals of Optical Waveguides*. New York: Academic Press, 2000, pp. 159-161.

[13] P. Hartmann, X. Qian, A. Wonfor, R. V. Penty, and I. H. White, "1-20 GHz directly modulated radio over MMF link," in *Proc. Microwave Photonics,* Oct. 2005, pp. 95-98.

5.2 Nonlinear effects of an optical intensity modulator on the performance of an optically up-converted millimeter-wave signal

In this Section, nonlinearity of an optical intensity modulator used in an optical up-conversion system for millimeter-wave over fiber applications is studied. Electrical fields of the up-converted optical signal are expressed in power series form to analyze harmonic distortion and inter-modulation distortion in the up-converted electrical domain. One-tone and two-tone measurements are performed to validate the analyses.

Nonlinear effects of an external intensity modulator on the performance of an optical up-conversion system for millimeter-wave over fiber applications[6]

Guohua Qi, Jianping Yao, *Senior Member, IEEE*, Joe Seregelyi*, Stéphane Paquet* and Claude Bélisle*

Microwave Photonics Research Laboratory

School of Information Technology and Engineering

University of Ottawa, Ottawa, Ontario, Canada K1N 6N5

(Email: jpyao@site.uottawa.ca)

* Communications Research Centre

Ottawa, Ontario, Canada K2H 8S2

Abstract

The nonlinear effects of an electro-optic intensity modulator in an optical up-conversion system for millimeter-wave (mm-wave) over fiber applications are investigated in this Section. In the analysis, general nonlinearities caused by the Mach-Zehnder modulator used for optical up-conversion are analyzed and discussed. Electrical fields of the up-converted optical signal are expressed in power series form, which are widely used in electronics in expressing memoryless nonlinearity. Harmonic distortion and inter-modulation distortion generated in an optical up-conversion, a scheme recently proposed for mm-wave over fiber applications, are analyzed in detail. One-tone and two-tone measurements are performed to validate the analyses based on our newly proposed optical up-conversion configuration.

Keywords: Millimeter-wave over fiber, electro-optic modulator, optical up-conversion, nonlinearity.

1. Introduction

The concept of fiber radio is being investigated for numerous applications, such as wideband

[6] Published in *Proceedings of SPIE*, vol. 5971, pp. 597126-1-597126-10, Sept. 2005.

wireless access networks and intelligent transport system (ITS). In a broadband wireless access network, this concept is very appealing since high frequency signals (up to 60 GHz) are required to obtain the high data rates required by modern multi-media applications. Fiber radio allows a unique millimeter-wave generation technique, located in a central office, to produce and optically distribute a signal to the proper base station. The same distribution network is also used on the return path, forming a bi-directional wireless access network.

Optical links have the potential to reduce the installation and operation cost, and also to increase the flexibility of network administration and dynamic resource allocation [1], [2]. However, the technique used to generate the modulated optical signal has been significantly bearing on the practical application of the technology.

Conventional intensity modulation (IM) using a one-wavelength optical carrier modulated by an mm-wave subcarrier is not practical due to the many difficulties such as the power penalty caused by the chromatic dispersion of the single-mode fiber [3], the relaxation oscillation frequency limitation of a laser diode in direct modulation [4], or the high half-wave voltage of a Mach-Zehnder modulator in an external modulator [4].

Ideally, the optical signal distributed from a central office to various base stations is modulated by an mm-wave subcarrier. This allows a direct-detection (DD) technique to recover the mm-wave electrical signal from the optical signal received at the remote site. After appropriate electrical amplification, this mm-wave signal is ready to be feed to an antenna for transmission. Hence, there is no need to have a high-quality local oscillator at each base station. The advantages of optical links are particularly obvious when the radio-over-fiber system is operating at the mm-wave band, where conventional techniques for distributing mm-wave signals are expensive and inefficient.

In the past, extensive investigation has been focused on optical mm-wave generation techniques. The goal was to generate an optical signal that contains two optical carriers, which are phase correlated and in the same polarization state, with a fixed mm-wave wavelength separation. The many approaches reported can generally be classified into two categories. In the first category, two laser sources are optically phase locked [5] or injection locked [6]. In the second category, one laser source is externally modulated [7]-[9] by a microwave signal, by using an optical filter

or by properly biasing the external modulator, only two sidebands are obtained. The latter approach has an advantage in generating mm-wave signals of high spectral purity because of the inherently high degree of phase correlation when the two optical carriers are generated by the same source.

Once the two-carrier optical signal is generated, it can be used for optical up-conversion. Two techniques for optical frequency up-conversion have been reported, with each corresponding to one of the two categories of optical signal generation discussed above. They are the direct modulation of one laser diode in a two-laser diodes scheme [10], and the external modulation of one of the two optical carriers in a one-laser diode scheme [4], [11]. The inherent non-linearity of the laser diode or external optical intensity modulator leads to signal distortion and cross-talk problems, both of which affect the system performance. The analysis and understanding of these nonlinearities becomes a means of mitigating their influence on a system.

In this Section, the nonlinearity an external modulator on the performance of an optical up-conversion system is analyzed and characterized. The electrical-field expression of the output optical signal for two different Mach-Zehnder intensity modulator topologies is reviewed. The electrical-field expressions are derived for an up-converted optical signal obtained by externally modulating a one-wavelength optical carrier with a Mach-Zehnder intensity modulator at three typical DC bias voltages. Finally, the nonlinearity of our newly proposed optical up-conversion scheme for mm-wave over fiber applications are analyzed and discussed; the voltage expression of the up-converted mm-wave signal generated after photodetection is given. One-tone and two-tone measurements are performed to validate the analysis.

2. Analysis of optical up-conversion with Mach-Zehnder modulators

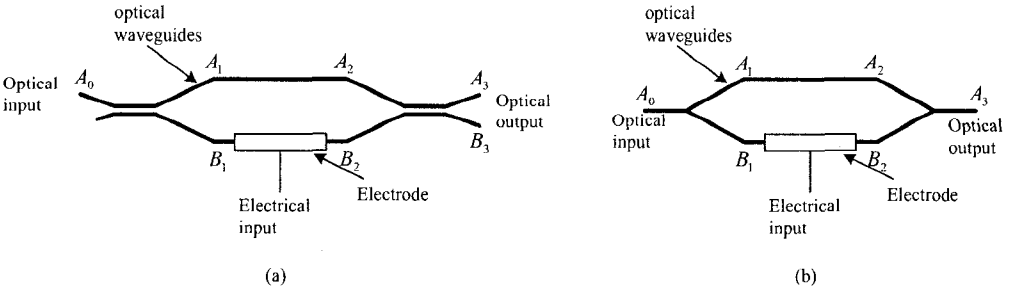

Fig. 1. Mach-Zehnder interferometric modulators. (a) 3-dB directional coupler type modulator. (b) Y junction type modulator.

Optical up-conversion based on external modulation techniques rely primarily on the use of LiNbO3 Mach-Zehnder optical intensity modulators. Fig. 1 shows two types of Mach-Zehnder interferometer constructed using 3-dB integrated directional couplers and Y junctions, respectively.

The Mach-Zehnder modulator shown in Fig. 1 (a) has been thoroughly analyzed in [12]. The electrical-field expression of the input optical signal, $A_o(t)$, can be expressed as

$$A_o(t) = A_0 \cos(\omega_o t), \tag{1}$$

where A_0 is the field amplitude of the input optical signal and $\omega_o = 2\pi f_o = \frac{2\pi c}{\lambda_o}$ is its angular frequency, f_o and λ_o are the frequency and wavelength of the input optical signal, respectively; c is light speed in free space. The electrical field expressions of the output optical signals can be written as [13]

$$A_3(t) = A_0 \sin(\frac{\phi}{2}) \cos(\omega_o t - \beta L + \frac{\phi}{2} - \frac{\pi}{2}), \tag{2a}$$

$$B_3(t) = A_0 \cos(\frac{\phi}{2}) \cos(\omega_o t - \beta L + \frac{\phi}{2} - \frac{\pi}{2}), \tag{2b}$$

where ϕ is the excess phase shift caused by the electrical input in the lower arm, β is the propagation constant of the optical waveguide, and L is the physical length of the two modulator arms. For the Y junction modulator of Fig. 1 (b), if the input optical signal is denoted in a phasor notation as A_0, then $A_1 = B_1 = \frac{A_0}{\sqrt{2}}$, and $A_2 = \frac{A_0}{\sqrt{2}} \exp(-j\beta L)$, $B_2 = \frac{A_0}{\sqrt{2}} \exp(-j\beta L + \phi)$. The phasor of the output optical signal A_3 is then

$$A_3 = \frac{A_0}{2} \exp(-j\beta L) + \frac{A_0}{2} \exp(-j\beta L + j\phi) = A_0 \cos(\frac{\phi}{2}) \exp(-j\beta L + j\frac{\phi}{2}). \tag{3}$$

As a result, the output optical signal of the Y junction type modulator can be written as

$$A_3(t) = A_0 \cos(\frac{\phi}{2}) \cos(\omega_o t - \beta L + \frac{\phi}{2}). \tag{4}$$

It can be seen that there are two output ports in the interferometer of Fig. 1 (a). However, only port B_3 is relevant in a one-in/one-out modulator because when no voltage is applied, $\phi = 0$, the output power at this port is at a maximum. Comparing (2b) with (4), it is found that the amplitude varies as a function of ϕ in the same way for both modulator types. In addition, because square-law photodetection is insensitive to phase and phase variation, the phase terms in (2b) and (4) can be ignored without loss of the generality in the following analysis. So the electrical field of the output signal of a Mach-Zehnder interferometric modulator is generally given as

$$E_o(t) = A_0 \cos(\frac{\phi}{2}) \cos(\omega_o t) \cdot \tag{5}$$

When a Mach-Zehnder modulator is used to perform an optical frequency up-conversion, it is generally driven by both a DC biasing voltage, V_{DC}, and a baseband or modulated subcarrier information signal. The voltage of electrical input applied to the optical modulator, $V_e(t)$, can be written as

$$V_e(t) = V_{DC} + V_s(t). \tag{6}$$

When the optical carrier expressed in (1) passes through a Mach-Zehnder modulator driven by an electrical signal expressed in (6). From (5), the electrical field of the output optical signal of the Mach-Zehnder modulator can be rewritten as

$$E_o(t) = A_0 \cos[\frac{\phi_{DC}}{2} + \frac{C_1 V_s(t)}{2}] \cos(\omega_o t)$$

$$= A_0 \left\{ \cos(\frac{\phi_{DC}}{2}) \cos[\frac{C_1 V_s(t)}{2}] - \sin(\frac{\phi_{DC}}{2}) \sin[\frac{C_1 V_s(t)}{2}] \right\} \cos(\omega_o t), \tag{7}$$

where $\phi_{DC} = \frac{2\pi}{\lambda_o} n_1 V_{DC} L$, $C_1 = \frac{2\pi}{\lambda_o} n_1 L$ and n_1 is a constant reflecting the linear electro-optic effect of LiNbO3. The expression of the up-converted optical signal in (7) can be evaluated at three typical DC bias cases.

When $\phi_{DC} = 0$, with a corresponding electrical field denoted as $E_{o0}(t)$, we obtain from (7)

$$E_{o0}(t) = A_0 \cos[\frac{C_1 V_s(t)}{2}]\cos(\omega_o t)$$

$$= A_0\left\{1-\frac{[C_1 V_s(t)]^2}{2^2\times 2!}+\frac{[C_1 V_s(t)]^4}{2^4\times 4!}-\ldots\right\}\cos(\omega_o t)\cdot \tag{8}$$

Here the Taylor series expression of $\cos(x)$ is used. It can be seen that there are only even-order power terms of $V_s(t)$, and no linear term of $V_s(t)$, in the amplitude of the optical carrier in (8). That means that without a DC bias, the Mach-Zehnder modulator cannot be used to realize linear optical up-conversion of $V_s(t)$.

When $\phi_{DC} = \frac{\pi}{2}$, with a corresponding electrical field denoted as $E_{o\frac{\pi}{2}}(t)$, we obtain from (7)

$$E_{o\frac{\pi}{2}}(t) = \frac{A_0}{\sqrt{2}}\{\cos[\frac{C_1 V_s(t)}{2}]-\sin[\frac{C_1 V_s(t)}{2}]\}\cos(\omega_o t)$$

$$= \frac{A_0}{\sqrt{2}}\left\{1-\frac{C_1 V_s(t)}{2}-\frac{[C_1 V_s(t)]^2}{2^2\times 2!}+\frac{[C_1 V_s(t)]^3}{2^3\times 3!}+\ldots\right\}\cos(\omega_o t)\cdot \tag{9}$$

Here Taylor series expressions for $\cos(x)$ and $\sin(x)$ are used, with the fourth- and higher order terms being ignored when $V_s(t)$ is moderate. In the amplitude of the optical carrier in (9), the first two terms form a typical expression for amplitude modulation of the input optical signal, and the third and fourth terms generate harmonic distortion and inter-modulation distortion of $V_s(t)$ in the optical domain. Since the information signal $V_s(t)$ can be recovered from $E_{o\frac{\pi}{2}}(t)$ with a square-law photodetector, a $\pi/2$ biasing can be used to analyze the nonlinear performance of the intensity modulated and direct detection (IM/DD) optical link. It should be pointed out that the information signal $V_s(t)$ can also be recovered from $E_{o\frac{\pi}{2}}(t)$ with heterodyne photodetection techniques, especially the remote heterodyne detection techniques that are widely used in mm-wave over fiber systems.

When $\phi_{DC} = \pi$, with a corresponding output electrical field denoted as $E_{o\pi}(t)$, from (7) we obtain

$$E_{o\pi}(t) = A_0 \sin[\frac{C_1 V_s(t)}{2}]\cos(\omega_o t)$$

$$= A_0\left\{\frac{C_1 V_s(t)}{2} - \frac{[C_1 V_s(t)]^3}{2^3 \times 3!} + \frac{[C_1 V_s(t)]^5}{2^5 \times 5!} - \ldots\right\}\cos(\omega_o t) \cdot \qquad (10)$$

Here the Taylor series expression of $\sin(x)$ is used and a π phase shift of the optical carrier is omitted. The first linear term $A_0 \frac{C_1 V_s(t)}{2}$ in the amplitude of the optical carrier in (10) clearly shows that the information signal $V_s(t)$ has been linearly up-converted to the optical domain. This term builds up a double sideband modulation to the optical carrier. The remaining terms $A_0\left\{-\frac{[C_1 V_s(t)]^3}{2^3 \times 3!} + \frac{[C_1 V_s(t)]^5}{2^5 \times 5!} - \ldots\right\}$ generate harmonic distortion and inter-modulation distortion of $V_s(t)$. Note that the information signal $V_s(t)$ cannot be recovered from $E_{o\pi}(t)$ with a square-law photodetection technique. Instead, heterodyne photodetection is needed. Comparing (10) with (9), the power of the linear term of $V_s(t)$ in (10) is 3 dB higher than that in (9) and there is no second-order harmonic distortion of $V_s(t)$ in (10).

In an mm-wave over fiber system, an mm-wave signal can be generated using external modulation technique [7-9], by using either an optical filter to select two optical sidebands or by biasing the modulator to generate only two sidebands. The wavelength difference between the two sidebands is equivalent to the mm-wave frequency required by the mm-wave over fiber system. With the generated two optical sidebands, the baseband or the subcarrier signal can be modulated to one of the wavelengths after they are separated using an optical filter [4, 11]. The above results can be used to characterize the distortion of the information signal in the optical domain. However, the use of an optical filter to separate the two wavelengths makes the system complicated with a poor reconfigurability. Here, we proposed a simple approach for optical subcarrier up-conversion without the need of an optical filter to separate the two wavelengths. It is realized by externally modulating the two wavelengths without separating them with a Mach-Zehnder modulator biased at the quadrature, as shown in Fig. 2.

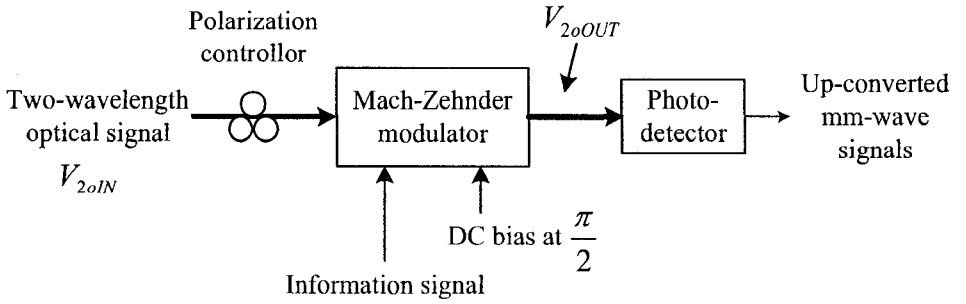

Fig. 2. Principle of our newly proposed optical subcarrier frequency up-conversion approach.

From (9) it can be seen that the up-converted optical signal $E_{o\frac{\pi}{2}}(t)$ of the information signal $V_s(t)$ includes even- and odd-order harmonics of $V_s(t)$ in the optical domain. We can use this expression to analyze the distortions in the mm-wave band.

The two wavelengths of the optical signal are assumed to be phase correlated, in the same linear polarization state, and their frequency separation is in the mm-wave frequency range, then the electrical field, $E_{2oIN}(t)$, of this optical signal can be written as

$$E_{2oIN}(t) = A_1 \cos[(\omega_o - \frac{\omega_{mm}}{2})t] + A_2 \cos[(\omega_o + \frac{\omega_{mm}}{2})t], \tag{11}$$

where A_1 and A_2 are field amplitudes of the two wavelengths, ω_o is the optical angular frequency and ω_{mm} is the mm-wave angular frequency. Because the two wavelengths have a wavelength difference less than a few nanometers, phase change by an applied voltage for the two wavelengths can be considered identical, from (9) the optical signal at the output of the Mach-Zehnder modulator can be expressed as

$$E_{2oOUT}(t) = \frac{A_1}{\sqrt{2}}\left\{\cos[\frac{C_1 V_s(t)}{2}] - \sin[\frac{C_1 V_s(t)}{2}]\right\}\cos[(\omega_o - \frac{\omega_{mm}}{2})t] + \frac{A_2}{\sqrt{2}}\left\{\cos[\frac{C_1 V_s(t)}{2}] - \sin[\frac{C_1 V_s(t)}{2}]\right\}\cos[(\omega_o + \frac{\omega_{mm}}{2})t]. \tag{12}$$

When this optical signal is fed into a square law photodetector, an up-converted mm-wave signal is generated. Let $V_{mm}(t)$ denote the generated mm-wave signal, we have

$$V_{mm}(t) = KA_1A_2\left\{\cos[\frac{C_1 V_s(t)}{2}] - \sin[\frac{C_1 V_s(t)}{2}]\right\}^2 \cos[(\omega_o - \frac{\omega_{mm}}{2})t]\cos[(\omega_o + \frac{\omega_{mm}}{2})t]$$

$$= K\frac{A_1 A_2}{2}\{1 - \sin[C_1 V_s(t)]\}\cos(\omega_{mm} t)$$

$$= K\frac{A_1 A_2}{2}\left\{1 - C_1 V_s(t) + \frac{[C_1 V_s(t)]^3}{3!} - \ldots\right\}\cos(\omega_{mm} t), \quad (13)$$

where K is a constant which is determined by the responsivity of the photodetector. The term with a frequency at $2\omega_o$ will not be detected by the photodetector and is ignored in the equation. It is clearly shown in (13) that the information signal $V_s(t)$ is successfully up-converted to the mm-wave band. It is interesting to note that there is no even-order power term of $V_s(t)$ in (13). That means, although even-order harmonic distortions of $V_s(t)$ are generated in the optical domain as shown in (9), these distortions do not contribute to the distortions of the up-converted mm-wave signal. The nonlinearity of the Mach-Zehnder modulator generates odd-order harmonic distortion of $V_s(t)$ with our proposed optical up-conversion approach, as expressed in (13). The most serious distortion is the inter-modulation distortion generated by the term $\frac{[C_1 V_s(t)]^3}{3!}$ when $V_s(t)$ has more than one frequency.

If the information signal, $V_s(t)$, is a narrow band modulated subcarrier, all of its odd-order harmonics will be far from the first-order sidebands of interest and can be filtered out. On the contrary, the third-order inter-modulation distortion (IMD3) generated by the term, $\frac{[C_1 V_s(t)]^3}{3!}$, will fall in band and cause interference to the original signal. Estimating the power ratio of IMD3 over the base band signal becomes important in evaluating the overall system performance. If we use V_π to denote the half-wave voltage of the modulator, then C_1 can be alternatively expressed as $C_1 = \frac{\pi}{V_\pi}$. In the widely used two-tone test for characterizing IMD3, $V_s(t)$ is composed of two sinusoidal signals with an identical amplitude A_s and angular frequency ω_{s1} and ω_{s2}, respectively, i.e. $V_s(t) = A_s\cos(\omega_{s1} t) + A_s\cos(\omega_{s2} t)$. Substituting C_1 and $V_s(t)$ into (13), the voltage amplitude of IMD3 is

$$V_{IMD3} = K\frac{A_1 A_2}{2} \times \frac{\pi^3}{8} \times \left(\frac{A_s}{V_\pi}\right)^3, \quad (14)$$

and the voltage amplitude of the linear term can be obtained as

$$V_{LT} = K\frac{A_1 A_2}{2}\left[-\pi\times\frac{A_s}{V_\pi}+\frac{3\times\pi^3}{8}\times\left(\frac{A_s}{V_\pi}\right)^3\right]. \tag{15}$$

Then the power ratio of IMD3 over the linear term, $\frac{IMD3}{LT}$, can be expressed in dB as

$$\frac{IMD3}{LT} = 20\log\frac{\frac{\pi^3}{8}\times\left(\frac{A_s}{V_\pi}\right)^3}{\left|-\pi\times\frac{A_s}{V_\pi}+\frac{3\times\pi^3}{8}\times\left(\frac{A_s}{V_\pi}\right)^3\right|}. \tag{16}$$

When $A_s << V_\pi$, equation (16) can be further approximated as

$$\frac{IMD3}{LT} = 40\log\frac{A_s}{V_\pi}+1.824dB. \tag{17}$$

Equation (17) can be used to evaluate the maximum voltage amplitude of the information signal to meet the specific requirement of $\frac{IMD3}{LT}$ in applying the optical up-conversion scheme shown in Fig. 2 to system applications. The value of $\frac{IMD3}{LT}$ with respect to $\frac{A_s}{V_\pi}$ is plotted in Fig. 3.

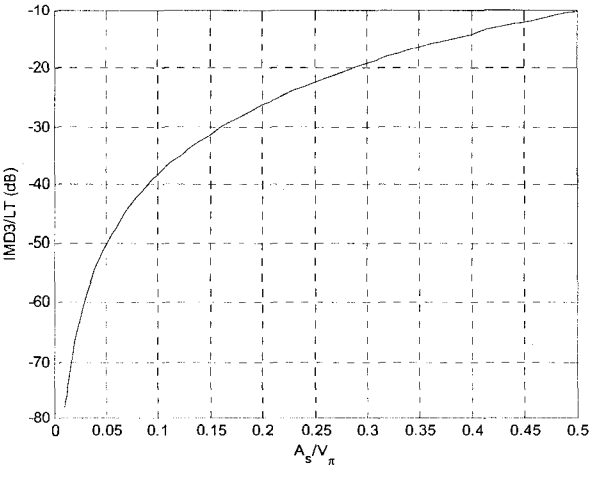

Fig. 3. Power ratio of IMD3 over the linear term versus the amplitude of the applied voltage.

3. Experiment

The nonlinearity of the up-converted mm-wave information signal is experimentally characterized in the setup shown in Fig. 4.

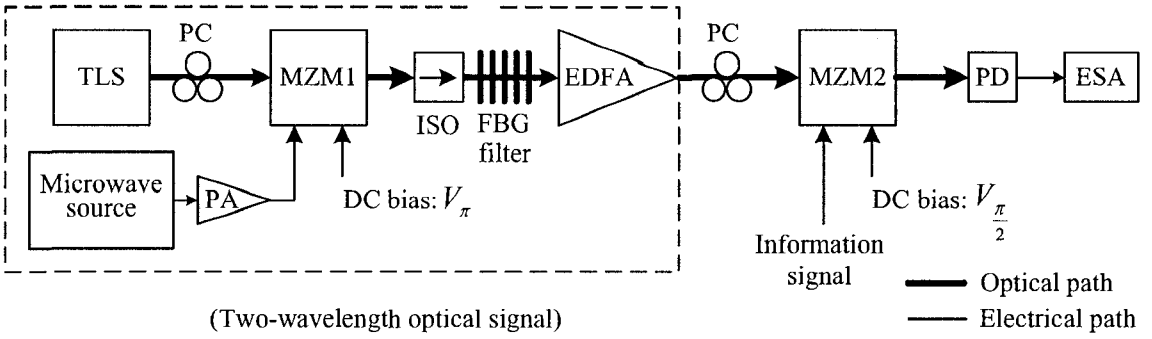

Fig. 4. Experimental setup. (TLS: tunable laser source, PC: polarization controller, MZM: Mach-Zehnder modulator, ISO: isolator, EDFA: erbium-doped fiber amplifier, PA: power amplifier, PD: photodetector, ESA: electrical spectrum analyzer)

In this setup, a two-wavelength optical signal is generated with the external modulation technique reported in [9]. The optical signal has two wavelengths that have a frequency separation of four times the frequency of the electrical drive signal. At the output of the photodetector, a continuously tunable mm-wave carrier of high spectral purity over the frequency range of 32 to 50 GHz can be generated, when the electrical drive signal is varied from 8 to 12.5 GHz. One-tone and two-tone tests are used to characterize the nonlinear distortions of the optical up-conversion approach.

The one-tone test is for characterizing the harmonic distortion of the optical up-conversion. During the one-tone test, the information signal is substituted by a sinusoidal electrical signal. Here a 2.4 GHz and a 4.2 GHz electrical signal are measured, respectively. By appropriately tuning the DC bias voltage of MZM2, it is observed that the second-order sidebands are well suppressed. Fig. 5 shows typical electrical spectra of the up-converted mm-wave signal, generated around 40 GHz, when the information signal is at 2.4 GHz and 4.2 GHz, respectively. It is seen that the second-order sidebands are under the noise floor. This result agreed well with the expression of (13).

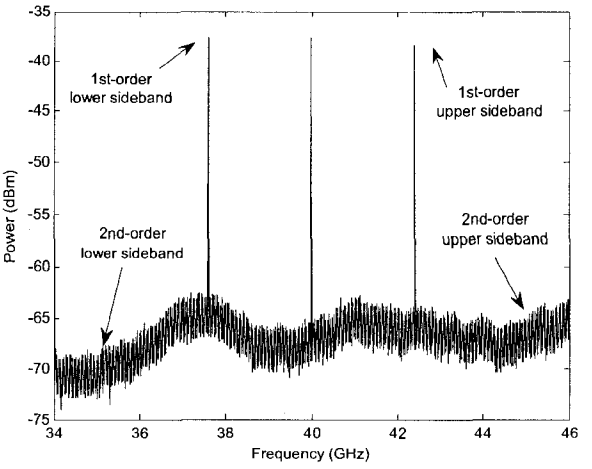

(a)

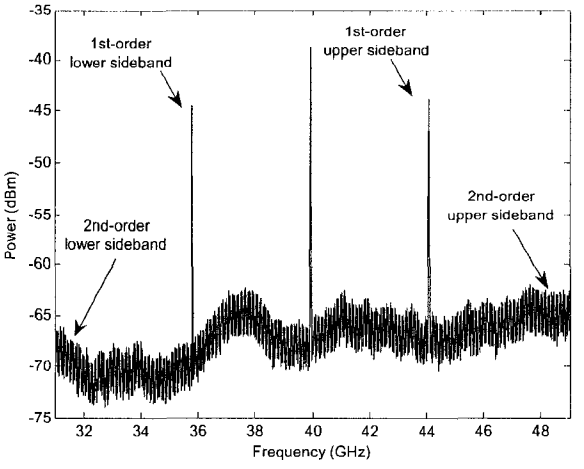

(b)

Fig. 5. Spectra of the one-tone test of the up-converted mm-wave signals at 40 GHz to (a) 2.4 GHz (b) 4.2 GHz electrical signals.

Since the second-order sidebands of the up-converted mm-wave signal are well suppressed or are far from the information-carrying first-order sidebands, the inter-modulation distortion becomes the predominant interference source. Fig. 6 shows typical electrical spectra of the two-tone test with a 95 MHz and a 105 MHz sinusoidal drive signal. Fig. 6 (a) shows the spectrum of the up-converted signal when the 95 MHz drive signal is at the power of 15 dBm It can be seen under this situation the third-order inter-modulation distortion is below the noise floor of the spectrum analyzer. But the power of the third-order inter-modulation distortion is above the noise floor when the power of the 95 MHz drive signals is increased to 19 dBm, as shown in Fig. 6 (b).

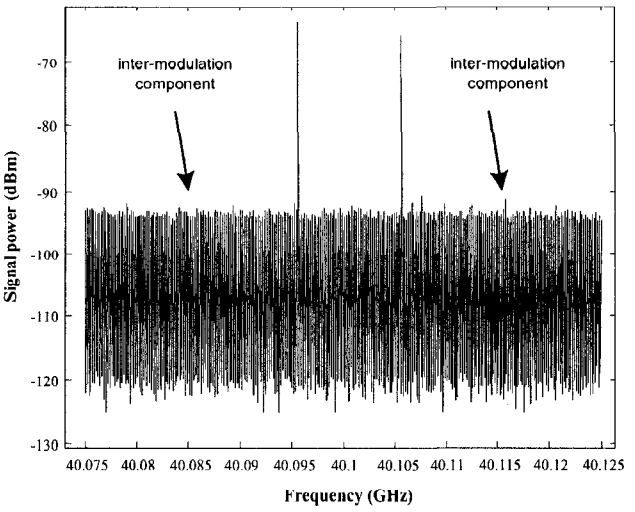

(a)

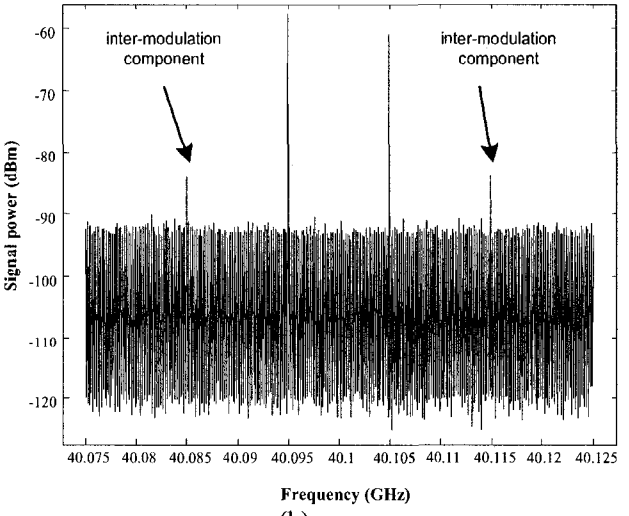

(b)

Fig. 6. Typical spectrum of the two-tune test of the up-converted mm-wave signals at 40 GHz. (a) The power of the 95 MHz drive signal at 15 dBm. (b) The power of the 95 MHz drive signal at 19 dBm.

4. Conclusions

In this Section, the nonlinearity effects of an external intensity modulator used in our newly proposed optical up-conversion scheme for mm-wave over fiber applications have been analyzed and discussed. The voltage expression of the up-converted mm-wave signal generated after photodetection was given. One-tone and two-tone measurements were performed to validate the analyses. The results of the analysis can be used to evaluate the maximum voltage

of the information signal to meet a specific power ratio between IMD3 and the linear term, for system applications.

Acknowledgement

The work was supported by the Canadian Institute for Photonic Innovations (CIPI). The authors would like to thank David Barlow and John Oldham of the Communications Research Centre Canada for their assistance in setting up the experimental systems.

References

[1] H. Ogawa, D. Polifko, and S. Banba, "Millimeter-wave fiber optics systems for personal radio communication," *IEEE Trans. Microwave Theory Tech.*, vol. 40, no. 12, pp. 2285-2293, Dec. 1992.

[2] D. Wake, "Trends and prospects for radio over fibre picocells," in *Proc. Microwave Photonics*, Nov. 2002, pp. 21-24.

[3] H. Schmuck, "Comparison of optical millimeter-wave system concepts with regard to chromatic dispersion," *Electron. Lett.*, vol. 31, no. 21, pp. 1848-1849, Oct. 1995.

[4] J. O'Reilly and P. Lane, "Remote delivery of video services using mm-waves and optics," *J. Lightwave Technol.*, vol. 12, no. 2, pp. 369-375. Feb. 1994.

[5] M. Hyodo, K. S. Abedin, and N. Onodera, "High-purity, optoelectronic millimeter-wave signal generation by heterodyne optical phase-locking of external-cavity semiconductor lasers," *Lasers and Electro-Optics Europe*, Sept. 2000, pp. 1 pp.

[6] L. Goldberg, H. F. Taylor, J. F. Weller, and D. M. Bloom, "Microwave signal generation with injection-locked laser diodes," *Electron. Lett.*, vol. 19, no. 13, pp. 491-493, Jun. 1983.

[7] J. J. O'Reilly and P. M. Lane, "Fibre-supported optical generation and delivery of 60GHz signals," *Electron. Lett.*, vol. 30, no. 16, pp. 1329–1330, Aug. 1994.

[8] P. Shen, N. J. Gomes, P. A. Davies, W. P. Shillue, P. G. Huggard, and B. N. Ellison, "High-purity millimetre-wave photonic local oscillator generation and delivery," in *Proc. Microwave Photonics*, Sept. 2003, pp. 189-192.

[9] G. Qi, J. P. Yao, J. Seregelyi, C. Bélisle, and S. Paquet, "Generation and distribution of a wide-band continuously tunable millimeter-wave signal with an optical external modulation

technique," *IEEE Trans. Microwave Theory Tech.*, vol. 53, no. 10, pp. 3090-3097, Oct. 2005.

[10] L. A. Johansson and A. J. Seeds, "36-GHz 140-Mb/s radio-over-fiber transmission using an optical injection phase-lock loop source," *IEEE Photon. Tech. Lett.*, vol. 13, no. 8, pp. 893–895, Aug. 2001.

[11] R. Hofstetter, H. Schmuck, and R. Heidemann, "Dispersion effects in optical millimeter-wave systems using self-heterodyne method for transport and generation," *IEEE Trans. Microwave Theory Tech.*, vol. 43, no. 9, pp. 2263-2269, Sept. 1995.

[12] K. Okamoto, *Fundamentals of Optical Waveguides*. New York: Academic Press, 2000, pp. 159-161.

CHAPTER 6
SUMMARY AND FUTURE WORK

6.1 Summary

In this thesis, two subsystems required for radio-over-fiber applications were studied in detail. These include optical generation and distribution of millimeter-wave signals and optical up-conversion. Optical carrier recovery at remote sites was also experimentally demonstrated.

In Chapter 1, radio-over-fiber systems were introduced and reviewed. The concept of radio-over-fibers was presented and the necessity of building radio-over-fiber systems was detailed. Objectives of the study were drawn.

In Chapter 2, a detailed literature review was conducted to identify previously reported work on both optical techniques for generating and distributing microwave and millimeter-wave signals, and optical up-conversion techniques.

In Chapter 3, three different techniques to optically generate and distribute millimeter-wave signals were proposed. These optically generated millimeter-wave signals were all continuously tunable and wideband. In the first approach, an optical source and low-frequency electrical source were used in combination with an optical intensity modulator and an optical notch filter to generate a continuously tunable, wide-band millimeter-wave signal at a photodetector. In addition, this optical signal could be distributed over long-distances with an optical fiber, so this millimeter-wave signal could be generated remotely. Harmonic suppression of the generated signal was also analyzed. In the second approach, the combination of an; optical phase modulator, optical notch filter, optical source and a low-frequency electrical source generated an optical signal with two wide bands of continuously tunable millimeter-wave signals after photodetection. The dispersion effects of standard single mode fiber on the performance of a

millimeter-wave signal after transmission was analyzed. In the third approach, an optical intensity modulator and an optical notch filter were incorporated into a single-longitudinal-mode, fiber ring laser to realize the generation of a wideband, continuously-tunable, millimeter-wave signal, and the simultaneous recovery of an optical carrier at remote sites.

In Chapter 4, analyses of the phase noise of the optically generated electrical signal were presented. In one analysis, the phase noise of the optical and electrical sources, and the dispersion effect of a standard single-mode fiber were taken into account for the phase noise analysis of an optically generated electrical signal based on optical external modulation techniques. In another analysis, the effect of the amplified spontaneous emission of an optical amplifier on the phase noise of a generated electrical signal was theoretically analyzed.

In Chapter 5, techniques of optical up-conversion for radio-over-fiber systems were studied. An optical up-conversion was proposed based on external intensity modulation of optical signals for millimeter-wave generation, which were proposed in Chapter 3. Principle analyses show that information carried by a low-frequency subcarrier was up-converted to the millimeter-wave band. Experimental demonstrations and simulations of BPSK and QPSK signal transmission were performed to verify the proposed approach. Nonlinear effects of an optical intensity modulator on the performance of the up-converted millimeter-wave signal were also analyzed.

6.2 Future work

When generating a millimeter-wave signal with an optical intensity modulator, it is observed that the suppression of unwanted optical harmonics around the optical carrier is not symmetrical when setting a DC bias on the modulator. In addition, although it has been proven mathematically that the optical intensity modulator can completely suppress even-order or odd-order harmonics at its output with appropriate DC biases, practically the suppression of the unwanted optical harmonics is not complete. There is always residual unwanted harmonics remaining. Since unsymmetrical harmonic suppression and residual harmonics in the output spectrum of the optical signal will increase the power level of spurs in the generated millimeter-wave signal, further study of these problems is warranted. In this approach, another problem

that needs further study is the suppression of the unwanted harmonics generated by the temperature and DC bias drift of the modulator. The temperature stability and long-term stability of a fixed DC bias is crucial to the practical application of this method. Special optical intensity modulators designed for the purpose of generating millimeter-wave signals may be developed based on these findings.

In the fiber ring laser scheme, further theoretical analysis and experimental study need to be conducted. By appropriate modeling of the components in the loop of the fiber ring laser, conditions for a single longitudinal mode lasing could be investigated theoretically, and conditions for a stable lasing versus temperature and vibration should also be studied.

Finally, linearization techniques such as pre-distortion and feed-forward need to be investigated for compensating the nonlinearity existing in the optical up-conversion process based on the modulation of an optical intensity modulator.

PUBLICATIONS

1 G. Qi, J. P. Yao, J. Seregelyi, S. Paquet, C. Bélisle, X. Zhang, K. Wu, and R. Kashyap, "Phase-noise analysis of optically generated millimeter-wave signals with external optical modulation techniques," *J. Lightwave Technol.*, vol. 24, no. 12, pp. 4861-4875, Dec. 2006.

2 G. Qi, J. P. Yao, J. Seregelyi, C. Bélisle, and S. Paquet, "Generation and distribution of a wide-band continuously tunable millimeter-wave signal with an optical external modulation technique," *IEEE Trans. Microwave Theory Tech.*, vol. 53, no. 10, pp. 3090-3097, Oct. 2005.

3 G. Qi, J. P. Yao, J. Seregelyi, C. Bélisle, and S. Paquet, "Optical generation and distribution of continuously tunable millimeter-wave signals using an optical phase modulator," *J. Lightwave Technol.*, vol. 23, no. 9, pp. 2687-2695, Sept. 2005.

4 G. Qi, X. Chen, and J. P. Yao, "A single longitudinal mode fiber ring laser incorporating an intensity modulator for mm-wave signal generation and optical carrier recovery," in *Proc. Microwave Photonics*, Oct. 2005, pp. 25-28.

5 G. Qi, J. P. Yao, J. Seregelyi, S. Paquet, and C. Bélisle, "Effects of amplified spontaneous emission noise of optical amplifiers on the phase noise of optically generated electrical signals," *Proceedings of SPIE*, vol. 5971, pp. 59712D-1-59712D-8, Sept. 2005.

6 G. Qi, J. P. Yao, J. Seregelyi, S. Paquet, and C. Bélisle, J. Oldham, "Nonlinear effects of an external intensity modulator on the performance of an optical up-conversion system for millimeter-wave over fiber applications," *Proceedings of SPIE*, vol. 5971, pp. 597126-1-597126-10, Sept. 2005.

7 G. Qi and J. P. Yao, J. Seregelyi, S. Paquet, and C. Bélisle, "Millimeter-wave carrier generation using an optical phase modulator and an optical notch filter," *Proceedings of SPIE*, vol. 5579, pp. 673-679, Sept. 2004.

8 G. Qi and J. P. Yao, J. Seregelyi, S. Paquet, and C. Bélisle "Phase noise analysis of the optically generated and distributed millimeter wave signal using an external optical modulator," *Proceedings of SPIE*, vol. 5579, pp. 598-606, Sept. 2004.

9 S. Paquet, G. Qi, J. Seregelyi, J. P. Yao, C. Bélisle, and J. Oldham, "An all-optical software defined radio prototype platform," *Proceedings of SPIE*, vol. 5971, pp. 59712E-1-59712E-11, Sept. 2005.

10 C. Bélisle, S. Paquet, J. Seregelyi, G. Qi, and J. P. Yao, "All-optical microwave front end for SDR," presented at 2005 Software Defined Radio Technical Conference, Nov. 2005, California, USA.

LIST OF ACRONYMS

A

AFC Automatic Frequency Control
AM Amplitude Modulation
ASE Amplified Spontaneous Emission

B

BS Base Station

C

CIPI Canadian Institute for Photonic Innovations
CO Central Office
CW Continuous Wave

D

DC Direct Current
DCM Dispersion Compensation Module
DD Direct Detection
DFB Distributed Feedback
DCF Dispersion Compensating Fiber
DSB Double Sideband

E

EDFA Erbium Doped Fiber Amplifier
EFS FBG Equivalent Phase Shift Fiber Bragg Grating
EOM Electro-Optic Modulator
EOIM Electro-Optic Intensity Modulator
EOPM Electro-Optic Phase Modulator
ESA Electrical Spectrum Analyzer
EVM Error-Vector Magnitude

F

FBG Fiber Bragg Grating
FM Frequency Modulation
FP Fabry Perot
FSR Free Spectral Range

G

GHz Giga Hertz

I

IF Intermediate Frequency
IM Intensity Modulation
IMD3 3rd-order Inter-Modulation Distortion

IM/DD Intensity Modulated and Direct Detection

ISO Isolator

ITS Intelligent Transport System

L

LD Laser Diode

LED Light Emission Diode

$LiNbO_3$ Lithium Niobate

M

MHz Mega Hertz

mm-Wave Millimeter-Wave

MoF Millimeter-wave over Fiber

MZI Mach-Zehnder Interferometer

MZM Mach-Zehnder modulator

O

OC Optical Circulator

OPLL Optical Phase-Locked Loop

OPM Optical Phase Modulator

OSA Optical Spectrum Analyzer

P

PA Power Amplifier

PC Polarization Controller

PD Photodetector

PM Phase Modulation

PSD Power Spectral Density

R

RBW Resolution Bandwidth

RF Radio Frequency

RMS Root Mean Square

RoF Radio over Fiber

S

SLM Single Longitudinal Mode

SOA Semiconductor Optical Amplifier

SSB Single Sideband

SSMF Standard Single Mode Fiber

T

TLS Tunable Laser Source

V

VCSEL Vertical-cavity surface-emitting laser

W

WSS Wide-Sense Stationary